Final Report

IMPLEMENTATION OF SHRPP INDIRECT TENSION TESTER TO MITIGATE CRACKING IN ASPHALT PAVEMENTS AND OVERLAYS

UF Project: No.: 4910450457912

WPI No.: 0510755

Contract No.: BA-546

State Job No.: 99700-3311-010

Submitted to:

Research Center
Florida Department of Transportation
605 Suwannee Street, MS 30
Tallahassee, FL 32399-0450

by

Principal Investigator: Reynaldo Roque, Professor
Co-Principal Investigator: Bjorn Birgisson, Assistant Professor
Researchers: Zhiwang Zhang
Boonchai Sangpetngam
Thomas Grant

Department of Civil and Coastal Engineering
College of Engineering
University of Florida
124 Yon Hall
P.O. Box 116580
Gainesville, FL 32611-6580
Tel: (352) 392-9537 Extension 1458
Fax: (352) 392-3394

UNIVERSITY OF FLORIDA

May 2002

ACKNOWLEDGMENTS

The authors would like to acknowledge and thank the Florida Department of Transportation (FDOT) for providing technical and financial support and materials for this project. Special thanks go to engineers and technicians of the Bituminous Section of the State Materials Office for their contributions in terms of their expert knowledge, experience, and constructive advice throughout the course of this work. Their efforts are sincerely appreciated and clearly made a positive impact on the quality of the research.

EXECUTIVE SUMMARY

The SuperPave™ Indirect Tension Test (IDT) was originally developed as part of the Strategic Highway Research Program (SHRP) as one of the key tools for evaluation of thermal cracking. Additional research sponsored by the Florida Department of Transportation (FDOT) resulted in further evaluation and development of the SuperPave™ IDT for use in the evaluation of load-associated cracking (fatigue and/or top-down cracking), because the test offers many important advantages over conventional fatigue testing, as well as the fact that the relationship between conventional fatigue test results and field cracking performance has been questionable at best. The FDOT effort culminated in the development of testing and data reduction procedures and software to reliably obtain tensile properties of asphalt mixtures. The key recommendations of this work were to use the SuperPave™ IDT and the systems developed to achieve a better understanding of how cracks initiate and grow in mixtures, with the ultimate goal of establishing guidelines for using properties determined from the test in mixture design procedures and specifications that would mitigate cracking in pavements and overlays.

Therefore, this research project focused on the following goals:

- Use the SuperPave™ IDT to achieve a better understanding of how cracks initiate and propagate in asphalt mixtures. This required the development of testing and data reduction procedures and software to determine fracture resistance from SuperPave™ IDT tests.
- Based on this understanding identify the key mixture properties that are necessary to control cracking performance of mixtures and pavements.
- To develop a framework and/or model for using these properties to evaluate the cracking performance of mixtures, and a framework for an asphalt mixture specification based on these same properties.
- To provide recommendations for the development of asphalt mixture specification criteria.

All goals were met.

It was determined that only five mixture properties, which are easily obtained from the SuperPave™ IDT, are needed to control the cracking performance of asphalt mixtures subjected to any loading condition:

1. The m-value, which was determined to be directly related to the rate of micro-crack development in asphalt mixtures.
2. The dissipated creep strain energy to fracture ($DCSE_f$), which was determined to be the threshold energy above which macro-cracks develop under repeated loading conditions.
3. The total energy to fracture (FE_f), which was determined to be the threshold energy above which macro-cracks will develop under a single critical load.
4. The resilient modulus (M_R), which affects the stress level for a given load and pavement structure, and is needed to determine $DCSE_f$.
5. The creep compliance (D(t)), which affects the thermal stress level for a given cooling condition.

Testing and data reduction procedures and software were developed to determine these properties simply and reliably from the following tests using the SuperPave™ IDT:

1. A 100-second creep test (m-value and creep compliance).
2. A 10-second tensile strength test ($DCSE_f$ and FE_f).
3. A 5-second resilient modulus test (M_R).

In addition, a fundamental crack initiation and growth law that can predict the cracking performance of asphalt mixtures subjected to any generalized loading condition was developed and evaluated. The test procedures and crack growth law developed in this study provide FDOT, as well as the pavement community in general, with the tools needed to design and specify

asphalt mixtures and pavements that resist cracking. It was recommended that FDOT now proceed with the development of mixture and pavement design guidelines and specifications based on these tools. It was also determined that the rate of micro-damage healing may play a role in cracking performance, and that its significance and measurement should be the subject of future research.

TABLE OF CONTENTS

Page

LIST OF TABLES

TABLES Page

LIST OF FIGURES

CHAPTER 1

INTRODUCTION

1.1 BACKGROUND

Fatigue cracking due to repeated traffic loading is one of the major distresses in asphalt concrete pavements. These cracks may start as microcracks that later coalesce to form macro-cracks that propagate due to tensile or shear stress or combinations of both. Pavement service-ability is reduced as these cracks propagate. A mixture's resistance to crack development and propagation affects the cracking performance of asphalt pavement. Therefore, it is necessary to acquire more insight into the crack behavior of asphalt concrete mixture, to obtain a better understanding of the cracking mechanism of asphalt pavements, and to have a practical and reliable system to determine a mixture's resistance to crack development and propagation.

The SuperPave™ Indirect Tension Test (IDT) was originally developed as part of the Strategic Highway Research Program (SHRP) as one of the key tools for evaluation of thermal cracking. Additional research sponsored by the Florida Department of Transportation (FDOT) resulted in further evaluation and development of the SuperPave™ IDT for use in the evaluation of load-associated cracking (fatigue and/or top-down cracking), because the test offers many important advantages over conventional fatigue testing, as well as the fact that the relationship between conventional fatigue test results and field cracking performance has been questionable at best. The FDOT effort culminated in the development of testing and data reduction proce-dures and software to reliably obtain tensile properties of asphalt mixtures.

Investigations of field sections sponsored by FDOT (Sedwick, 1998) indicated that frac-ture energy can be a good indicator of the cracking performance of asphalt pavements in the

field. However, it was recognized that the cracking mechanisms of pavements are still not fully understood. So, the key recommendations from these projects were to use the SuperPave™ IDT and the systems developed to achieve a better understanding of how cracks initiate and grow in mixtures, with the ultimate goal of establishing guidelines for using properties determined from the test in mixture design procedures and specifications that would mitigate cracking in pavements and overlays.

1.2 OBJECTIVE

The objectives of this research are summarized below:

- Use the SuperPave™ IDT to achieve a better understanding of how cracks initiate and propagate in asphalt mixtures. This required the development of testing and data reduction procedures and software to determine fracture resistance from SuperPave™ IDT tests.
- Based on this understanding identify the key mixture properties that are necessary to control cracking performance of mixtures and pavements.
- To develop a framework and/or model for using these properties to evaluate the cracking performance of mixtures, and a framework for an asphalt mixture specification based on these same properties.
- To provide recommendations for the development of asphalt mixture specification criteria.

The practical aim of this work was to provide the insight necessary to specify asphalt mixtures and help to produce more crack-resistant mixtures.

1.3 SCOPE

To develop an understanding of crack development of asphalt concrete, two SuperPave™ coarse mixtures (aged and unaged), two SuperPave™ fine mixtures (aged and unaged), and mixtures from eight field sections were examined. The eight field sections are located within a 75-mile radius in north-central Florida and have high traffic volumes. Seven of the eight sections had surface layers that were between 10 to 14 years old. The other section was 5 years old (Sedwick, 1998).

CHAPTER 2

LITERATURE REVIEW

2.1 INTRODUCTION

A literature review was undertaken to obtain a better understanding of the mechanism of crack development and propagation in asphalt concrete pavements. As a starting point, traditional fatigue approach, conventional fracture mechanics approach, and viscoelasticity and continuum damage mechanics approach to cracking performance were examined.

Fatigue is the process of damage accumulation and eventual failure due to repeated loading at stress levels below a material's ultimate strength. In general, there are two approaches to analyze and design against fatigue failure: conventional approach, which bases on the analysis on the nominal (average) stresses in the region of the component being analyzed; and fracture mechanics approach, which specifically treats growing cracks using the methods of fracture mechanics (Dowling, 1993).

It is noted that, in recent years, continuum damage mechanics (Kim, Lee and Little, 1997) has found increasing use in the analysis and evaluation of asphalt mixtures and pavements. Each approach offers advantages and disadvantages with respect to the type of failure mechanism that can be considered.

Through this review, a basic knowledge of development and propagation of cracks in asphalt pavements was obtained, and the reliability and practicality of these theories for use in asphalt pavement were examined.

2.2 TRADITIONAL FATIGUE APPROACH

Several fatigue models have been developed using conventional strain-based equations.

Monismith et al. (1981) proposed one of the first fatigue models:

$$N_f = c(1/\varepsilon_t)^d \quad (2.1)$$

where N_f is the number of cycles to failure, ε_t is the tensile strain applied, and c and d are coefficients determined from strain-controlled laboratory beam fatigue tests.

An improved equation used by several organizations (Monismith, Epps and Finn, 1985) today includes the mixture stiffness and a factor that accounts for asphalt content and degree of compaction:

$$N_f = K\,(1/\varepsilon_t)^a\,(1/S_{mix})^b \quad (2.2)$$

where S_{mix} is the mixture stiffness, K is the mixture-related factor accounting for the influence of asphalt content and degree of compaction, a and b are coefficients determined from beam fatigue at 25C. Failure is defined as the point at which S_{mix} is one-half the initial stiffness.

The following equation was proposed as a result of work performed in the SHRP program (Sousa, 1996):

$$N_f = S_f * 2.738*10^5 * e^{0.077VFB} * \varepsilon_o^{-3.624} * S_0^{-2.720} \quad (2.3)$$

where S_f is a factor converting laboratory measurements to the field results, *e* is the base of the natural logarithm, VFB is the voids filled with bitumen, and S_0 is the loss stiffness.

Besides the strain-dependent models described above, several researchers have also used energy-dependent models for predicting the fatigue behavior of asphalt mixtures. The cumulative dissipated energy versus the number of cycles to failure could be characterized as follows (Chomton and Valayer, 1972, van Dijk, 1975, van Dijk and Visser, 1977, Pronk and Hopman, 1990, Tayebali, Rowe, and Sousa, 1992):

$$W_{Nf} = A\,(N_f)^z \quad (2.4)$$

Where W_{Nf} is the cumulative dissipated strain energy to failure (J/m^3), N_f is the number of load cycles to failure, and A and z are experimentally derived mix coefficients.

Recent work conducted by Tseng and Lytton (1990), and Harvey and Tsai (1996) demonstrated that the predictive equations had become more complex because the fracture behavior of asphalt mixtures was complex and there was no simple hard-fast rule that would guarantee accurate results for all conditions.

2.3 CONVENTIONAL FRACTURE MECHANICS APPROACH

2.3.1 Conventional Fracture Mechanics

The science of fracture mechanics, first published in the 1920s by Griffith, sets out to describe the propagation of cracks through materials. Figure 2.1 is a schematic log-log plot of da/dN versus ΔK, which illustrates typical fatigue crack growth behavior in metals. The sigmoidal curve contains three distinct regions: in Region I, da/dN approaches zero at a threshold ΔK_{th}; in Region II, the crack growth rate deviates from the linear trend at high and low ΔK levels; in Region III, the crack growth rate accelerates as K_{max} approaches K_{crit}, the fracture toughness of the material (Anderson, 1993).

Paris and Erdogan (1963) first discovered the power law relationship for fatigue crack growth in Region II, which is commonly known as Paris law:

$$\frac{da}{dN} = A(\Delta K)^n \tag{2.5}$$

where da/dN is the crack growth rate (mm/cycle), ΔK is the range of stress intensity factor ($Mpa\text{-}mm^{0.5}$) during repeated loading condition, and A and n are mixture parameters determined from laboratory data.

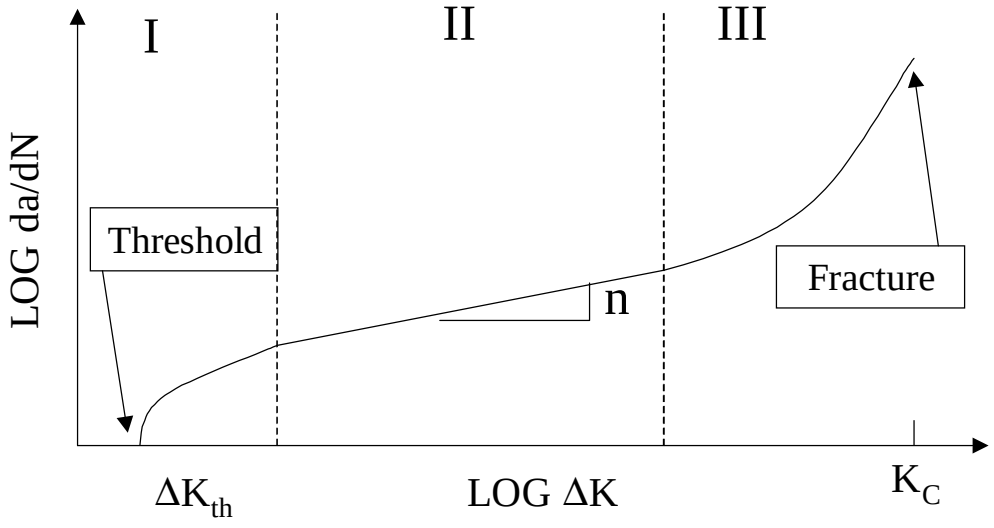

Figure 2.1 Typical Fatigue Crack Growth Behavior in Metals

In addition, a number of researchers have developed equations that model all or part of the sigmoidal da/dN - ΔK relationship. For example, Forman (1967) proposed the following equation for Region II and III:

$$\frac{da}{dN} = \frac{C\Delta K^{m-1}}{\frac{K_{crit}}{K_{max}} - 1} \tag{2.6}$$

where c and m are the material constants, K_{max} is the maximum stress and K_{crit} is the fracture toughness of a material.

In 1966, Weertman developed an alternative semiempirical equation for Regions II and III:

$$\frac{da}{dN} = \frac{C\Delta K^4}{K_{crit}^2 - K_{max}^2} \tag{2.7}$$

Klesnil and Lukas (1972) modified Paris law to account for a threshold:

$$\frac{da}{dN} = C\left(\Delta K^m - \Delta K_{th}^m\right) \tag{2.8}$$

where the threshold (ΔK_{th}) is a fitting parameter to be determined experimentally. Further investigation on the threshold, which is generally defined in fracture mechanics, is not related to our research work. Therefore, no additional description about this concept will be included in the literature review.

In 1988, McEvily developed another equation to fit the entire growth curve, which is based on a simple physical model:

$$\frac{da}{dN} = C\left(\Delta K - \Delta K_{th}\right)^2 \left(1 + \frac{\Delta K}{K_{crit} - K_{max}}\right) \tag{2.9}$$

As Paris law became widely used for prediction of fatigue crack growth, it was realized that this simple expression was not universally applicable. Therefore, further research work led to insight into crack performance (e.g., introduction of crack closure and the fatigue threshold). For example, Elber (1970) proposed a modified Paris law:

$$\frac{da}{dN} = C\Delta K_{eff}^{m} \tag{2.10}$$

where ΔK_{eff} is the effective stress intensity range, defined as $K_{max} - K_{op}$ (K_{op} is the stress intensity factor at which the crack opens).

Furthermore, Dowling and Begley (1976) applied the J integral for fatigue crack growth under large-scale yielding conditions where K is no longer valid. They developed the following equation:

$$\frac{da}{dN} = C(\Delta J)^{m} \tag{2.11}$$

The literature review presented above is based on the classical fracture mechanics, which focuses on predicting crack growth behavior presented in Figure 2.1 (i.e., typical crack growth behavior in metals). Asphalt concrete is a viscoelastic material, therefore, Paris law presented above cannot be applied in asphalt concrete directly. In 1984, Schapery developed the theoretical analyses for the time-dependent fracture of nonlinear viscoelastic media based on his previous work (1973 and 1975). In his analysis, the emphasis was on predicting mechanical work available at the crack tip for initiation and continuation of growth. He noted that stress intensity factor is the primary characterizing parameter for fracture initiation and crack growth rate.

2.3.2 Application of Conventional Fracture Mechanics in Asphalt Mixtures

During the 1970s, several researchers began to apply fracture mechanics to analyze the fatigue behavior in asphalt concrete. Majidzadeh et al. (1971) and Salam et al. (1972) studied

the fatigue performance of asphalt mixture by bending beams under repeated loading conditions. They noticed the increase in compliance resulting from crack growth. They concluded that fatigue life can be expressed as the number of load applications which caused an initial flaw (a_o) to grow, according to Paris law, until it reached a critical size (a_c), corresponding to failure state.

In 1991, Ramsamooj researched the prediction of fatigue life from fracture tests. In his study, he derived a general expression of the crack growth rate, which is related to a critical stress intensity factor (K_{IC}), yield stress in flexural tension (σ_t), and an initial stress intensity factor (K_{Io}). He obtained the number of cycles to failure by integrating the equation of crack growth rate from crack initiation (a_o) to failure state (a_c). In his conclusion, he stated that there is no significant difference between the experimental data and the theoretical predictions. Therefore, fatigue life can be predicted from simple fracture tests.

Jacobs et al. (1996) analyzed the crack growth process in asphalt concrete mixtures using fracture mechanics principles. In their research, 50-mm x 50-mm x 150-mm specimens, were subjected to tension-compression tests under repeated loading conditions. The crack growth parameters, A and n, were determined by analyzing the Crack Opening Displacement (COD) measurements. According to their research results, they concluded that: (1) Schapery's theoretical derivations for A and n for viscoelastic materials appears to be valid; (2) the exponent in Paris law can be estimated from the slope of the compliance curve; (3) the constant A in Paris law can be estimated from a combination of the maximum tensile strength, the fracture energy and the mixture stiffness.

In 1997, Read and Collop evaluated the Indirect Tensile Fatigue Test (ITFT) for fatigue cracking and introduced a Linear Elastic Fracture Mechanics (LEFM) approach to characterize crack propagation in bituminous paving mixtures using ITFT. In their study, cylindrical

specimens with a mode I crack in the center were subjected to repeated loading along the vertical diameter. The load point deflections, associated with the number of load application, were measured. The crack length was evaluated numerically based on the relationship between the crack length and the load point deflection. At the final stage, the crack growth parameters, A and n, were determined from the relationship between crack length and the number of repeated loading. After a comprehensive evaluation of the Indirect Tensile Fatigue Test (ITFT) and the methodology proposed, they stated that the Indirect Tensile Fatigue Test (ITFT) is able to characterize the fatigue performance of asphalt concrete mixtures.

2.4 VISCOELASTICITY AND CONTINUUM DAMAGE APPROACH

In recent years, it has been noted that the loading conditions are different between laboratory and field. Continuous cycles of loading at a constant strain or stress amplitude, which are generally applied in laboratory tests, do not realistically simulate actual traffic conditions to which pavements are subjected. One of the major differences between laboratory and field loading conditions is the rest period between loading applications which occurs in the field with random length but normally not in the laboratory (Kim, Little, Benson, 1990).

There are two different mechanisms occurring in a partially cracked asphalt concrete pavement during rest periods. One is the relaxation of stresses in the system due to the viscoelastic nature of asphalt concrete, and the other is the chemical healing across microcrack and macrocrack faces. Both of these mechanisms enhance the fatigue life of asphalt concrete pavements (Kim, Little, Benson, 1990).

One of the first papers evaluating the chemical healing potential of asphalt concrete was published in 1967 (Bazin and Saunier). They introduced rest periods to asphalt concrete beam samples, which were previously damaged under uniaxial tensile testing. They reported that an

ordinary dense mix could recover 90 percent of its initial resistance with only 3 days of rest at 77F.

In 1987, Little et al. reported that an increase in work was needed to open the crack after rest periods in controlled-displacement crack propagation testing of asphalt concrete mixes modified with various additives. They evaluated relaxation and chemical healing separately by analyzing the behavior of asphalt concrete using nonlinear viscoelasticity theory developed by Shapery (1984). The further chemical and mechanical evaluation of healing mechanics of asphalt concrete was done by Kim et al. (Kim, Little and Benson, 1990). They concluded that the chemical healing is of a significant magnitude and can have an overpoweringly important influence on the ultimate fatigue life of asphalt concrete pavements.

A mechanics approach to fatigue characterization of asphalt concrete using viscoelasticity and continuum damage theory was introduced by Kim et al. (Kim, Lee, and Little, 1997). In their study, damage accumulation, which is assumed to grow continuously under uniaxial tensile cyclic loading, and microdamage healing during rest periods, were modeled using the elastic-viscoelastic correspondence principle and work potential theory. The fatigue life of asphalt mixtures under realistic cyclic loading conditions was determined from the relationship between pseudo-stiffness and the number of loading cycles. In conclusion, they stated that this constitutive model can successfully predict the damage growth as well as recovery for load conditions with different loading rates and rest periods.

Little et al. (Little, Lytton, Williams, and Kim, 1999) researched fatigue performance in asphalt concrete pavements using micromechanics approach. In their study, they noticed that two opposing components of the fatigue process, fracture and healing, must be considered for an accurate accounting of the fatigue process. They assumed average microcrack length as a mean

crack length, and determined the crack growth rate, which includes fracture and healing, based on first principles of fracture mechanics. They stated that this micromechanics model verifies crack growth is the mechanism of damage in the samples. At the final step, the rate of fracture and rate of healing calculated, which are related to the surface energy measured from the laboratory, were used to evaluate the fatigue behavior of the different mixtures.

2.5 FATIGUE FAILURE CRITERIA

In the traditional fatigue approach, fatigue failure criterion is defined as the number of load applications, N_f, from the beginning of loading to failure, for both strain-dependent models (Monismith, Epps, and Finn, 1985) and energy-dependent models (van Dijk and Visser, 1977).

In the conventional fracture approach, there are two failure criteria used in a asphalt concrete pavement. One is the number of load applications, N_f, from the initial crack length, a_o, to the critical crack length, a_c (Majidzadeh., Kaufmann and Ramsamooj, 1971). The other criterion is fracture energy. Irwin (1977) stated that since fracture energy is a function of the initial crack size and the specific surface energy, which is also a scalar invariant, it is fundamental to the rate of crack propagation and it should be a reliable fatigue failure criterion for pavement design. This result was also confirmed by Sedwick's work (1998), which showed that fracture energy is a good indicator to represent the crack performance of asphalt pavement in the field: high fracture energy, high resistance to crack growth.

In the viscoelasticity and continuum damage approach, the failure criterion is defined as 50 percent reduction in pseudo-stiffness to represent the damage state of the material (Kim, Lee and Little, 1997).

2.6 SUMMARY OF KEY POINTS IN THE LITERATURE REVIEW

From the literature, several conclusions can be drawn that relate to crack performance in asphalt concrete pavements:

2.6.1 Traditional Fatigue Approach:

- Traditional models for predicting fatigue life may not be reasonable to predict the fatigue life of asphalt concrete pavements.
- Conventional strain-based fatigue approach does not consider the effects of flaws or microcracks in asphalt concrete mixtures. In other words, geometry changes are not considered in this approach.
- Accumulated damage is treated in a linear fashion; realistic cyclic loading conditions and healing are not considered in conventional strain-based approach.

2.6.2 Conventional Fracture Mechanics Approach:

Recent work has shown that the fracture mechanics approach seems to be a rational approach to describe fatigue behavior in asphalt concrete pavements.

- Conventional Fracture Approach considers flaws or microcracks in a material, which changes the geometry of a material.
- The basic concept in this approach is the stress redistribution near the crack tip. In defining stress intensity factor, K, the material is assumed to behave in a linear-elastic manner (linear-elastic fracture mechanics (LEFM)).
- The number of cycles to failure is determined by integrating the proposed equations from initial crack length a_o to critical crack length a_c, where initial crack length a_o is assumed based on laboratory data, and critical crack length a_c is obtained from fracture test.

- Crack growth is assumed to be continuous, and crack growth rate is determined by Paris law.
- Paris law is based on linear-elastic fracture mechanics principles, however, asphalt mixture is a time-dependent material (viscoelastic material).

2.6.3 Viscoelasticity and Continuum Damage Approach:

- Viscoelasticity and Continuum Damage Approach considers realistic loading conditions and healing in asphalt pavements.
- All microcracking and macrocracking are represented by an appropriate number of internal state variables in the model.
- It defines 50 percent reduction in pseudo-stiffness as a failure criterion, so failure has no physical meaning.
- It assumes that cracks grow continuously, but in fact, cracks in asphalt mixtures grow in a discontinuous manner.
- Crack length, *a*, is not determined in the approach.
- The approach is fairly complex, since it is based on the equations derived from micro-damage theory.

2.7 IDENTIFICATION OF AN APPROPRIATE CRACKING MODEL

Given the literature review presented above, it is believed that a more appropriate model for analyzing cracking performance of asphalt concrete pavements is needed. Because laboratory measured crack growth rate does not correlate well with field performance, the mechanism of cracking in laboratory may significant different from in field, current material cracking model is not fundamental enough to address both of these mechanisms.

As indicated earlier, in recent years, fracture mechanics and continuum damage mechanics have gained increasing applications in analysis and evaluation of asphalt mixtures and asphalt pavements. However, each approach offers advantages and disadvantages in mechanics. Even though the advantages and disadvantages in each approach are described in Section 2.6, it is thought to be important to emphasize the key features in this section for helping to identify an appropriate cracking model.

Conventional fracture mechanics begins with the assumption that there are inherent flaws or cracks in a material. Therefore, fracture mechanics is incapable of properly addressing the mechanism of crack initiation. Initial crack length must generally be selected for analysis and evaluation. However, fracture mechanics provides a physical interpretation of damage (i.e., crack length has a physical meaning). Some research has been done based on linear-elastic fracture mechanics (LEFM: i.e., application of stress intensity and Paris law), but there is little data to support the validity of fracture mechanics and/or application to cracking mechanics of asphalt pavement in the field. Furthermore, it must be noted that there are several disadvantages in conventional fracture mechanics approach, which influences its application (at least in present form) in asphalt mixtures and asphalt pavements. First, the concept of K_{th} (threshold of stress intensity) is not applicable to asphalt mixtures. Based on this concept, cracks will not grow if stress intensity is smaller than K_{th}. However, cracks can propagate even at small K values in asphalt mixtures because of creep effects. Secondly, according to Paris law, cracks propagate in a continuous manner, but in reality, cracks grow in a discontinuous manner in asphalt mixtures. Finally, as mentioned previously, the determination of K_{th} and Paris law is based on linear-elastic fracture mechanics, however, behavior of asphalt mixtures is viscoelastic (time-dependent).

Continuum damage mechanics offers a much more fundamental explanation of damage than conventional fatigue approaches. However, given the fact that only a continuum can be modeled, continuum damage mechanics is incapable of properly addressing the mechanism of crack propagation (i.e., once a crack is introduced, the system is no longer a continuum). In addition, damage mechanics does not provide a physical meaning of failure. It defines 50 percent reduction in pseudo-stiffness, which is not applicable to the field, as a failure criterion.

Furthermore, another difficulty associated with the current fracture testing is the measurements of crack growth rate during the test. Cracks are difficult to see in asphalt mixture. Use of crack foils or coatings can help, but it may be difficult to match the properties of these materials exactly with those of different asphalt mixtures at different temperature.

The discussion presented above leads back to the fracture mechanic as the most promising approach. Fracture mechanics has the potential of providing a more fundamental approach; which can reasonably and practically capture the failure and mechanisms observed in the laboratory and in the field. Therefore, further investigation includes: (1) developing a model, based on fracture mechanics, to indirectly measure crack growth rate in the laboratory and evaluate if crack growth rate measured in laboratory matches field performance; (2) identifying the factors, defined in classical fracture mechanics, that need to be changed for this model to work; (3) identifying the improvements that may be necessary to address model deficiencies.

CHAPTER 3

MATERIALS AND EXPERIMENTAL PROGRAM

3.1 INTRODUCTION

Field cores from eight field test sections, two SuperPave™ coarse mixtures (aged and unaged), and two SuperPave™ fine mixtures (aged and unaged) were used to obtain a better understanding of cracking behavior of asphalt concrete. A total of 225 field cores were obtained. The cores were sliced to obtain a specimen from directly under the friction course, which is herein referred to as the test specimen. Resilient modulus, creep compliance, strength, and fracture tests were performed using the SuperPave™ Indirect Tensile Test (IDT) with the systems developed by Roque et al. (1997). The results of resilient modulus, creep compliance, and strength tests of the field cores were summarized in Sedwick's work (1998), and the results of resilient modulus, creep compliance, strength tests and fracture tests of four SuperPave™ mixtures (aged and unaged) were summarized in Honeycutt's work (2000).

Field test specimens were submitted to the Florida Department of Transportation (FDOT) Materials Office for extraction and binder testing. The binder tests performed include the Bending Beam Rheometer, Dynamic Shear Rheometer, and Brookfield Viscosity. Rice gravity, asphalt content, coarse aggregate specific gravity and absorption, fine aggregate specific gravity, and aggregate grading were also determined for the submitted test specimens (Sedwick, 1998).

3.2 PREPARING SPECIMENS FOR THE TEST PROGRAMS

Forty-eight cores from eight field sections were used to perform fracture tests. Four SuperPave™ mixtures were also chosen for the resilient modulus, creep compliance, strength and fracture tests.

Two of the four SuperPave™ mixtures were on the fine side of the restricted zone; the other two were on the coarse side of the restricted zone. Both mixtures were 12.5 mm nominal maximum size mixtures produced with oolitic limerock obtained from South Florida. Specimens were compacted using a SuperPave™ Gyratory compactor to produce a 4500 g, 150-mm diameter Gyratory-compacted specimen with an air void content of 7 percent (±0.5 percent). Both mixtures met all SuperPave™ requirements, including all aggregate and volumetric requirements. Gyratory compacted specimens were sliced to obtain test specimens that were approximately 50-mm thickness for resilient modulus, creep compliance, and strength tests. Two 50-mm thick specimens were obtained from each Gyratory-compacted specimen. Twenty-five-mm-thick test specimens were used for fracture tests, so up to three specimens were obtained from each Gyratory-compacted specimen (Honeycutt, 2000).

Additional information about the test specimens is as follows:

- Resilient modulus, creep compliance, and strength tests:

  Three test specimens from each section were selected to perform the tests at the given temperature (three different temperatures: -10C, 0C, and +10C). The dimensions of these specimens were 150-mm diameter and 50-mm thickness. Two sets of gage points were glued on each side of the specimen. After the gage points were placed, the specimens were placed in a low relative humidity (about 40%) chamber for 72 hours to reduce moisture effects prior to testing (Sedwick, 1998).

- Fracture tests:

  Four test specimens were selected from each field section and Superpave mixture. The dimensions of these specimens were 150 mm diameter and 25 mm thick with an 8 mm hole in the center of the specimen. Two sets of gage points were placed on both of the

smooth, sliced faces of the specimen. All fracture tests were performed at 10C. A masonry bit was used to drill an 8 mm diameter hole at the center of each specimen. The specimens were placed on a specially designed template that assured that the hole was drilled at the exact center of the specimen. The template was composed of two aluminum plates that were used to hold the specimen securely on the drill press. The specimens were positioned with the help of a series of concentric circles inscribed on the surface of the bottom plate. It is important to drill the hole with the specimen's center positioned on a hole on the support plate (bottom plate) that is just slightly greater than 8 mm. This prevents damage from occurring when the drill bit exits the specimen.

3.3 EXPERIMENTAL PROGRAM

An experimental program was carried out to obtain crack growth characteristics for asphalt mixtures. This program resulted in a characterization of the resistance to crack propagation.

The experimental program consisted of:

(1) Resilient Modulus Test

- Before the resilient modulus test, specimens were initially cooled for about 8 hours to achieve stabilization.
- The resilient modulus was performed first with a peak load resulting in approximately 300 microstrain being applied. The harversine loading cycle was repeated five times with one-tenth of a second loading time and a rest period of nine-tenth of a second.

(2) Creep Test

- After re-stabilizing, a 1000-second creep compliance test was conducted. At 30 seconds during the test, the two horizontal deformation measurements were recorded and checked to make sure that they were within 60 and 180 microstrain.

(3) Strength Test

- Strength test was performed with a constant stroke of 50 mm per minute until the specimen failed.

(4) Fracture Test

- Before the fracture test, specimens were initially cooled for about 8 hours to achieve stabilization.
- The fracture test was conducted at higher deformation levels in order to determine crack growth characteristics of the mixes in this study.
- Fracture test was performed at 10C with a constant repeated haversine load of one-tenth of a second, which corresponds to a vehicle speed of about 60 Km/h, and then resting for nine-tenth of a second.
- Two horizontal deformation measurements, two vertical deformation measurements, applied load and the corresponding time were recorded at a rate of 150 points per seconds (pps) for 5 second every 60 seconds until the specimen failed.

CHAPTER 4

DETERMINATION OF CRACK GROWTH RATE PARAMETERS

4.1 INTRODUCTION

As mentioned in the literature review, traditional fatigue approach, conventional fracture mechanics approach, and viscoelasticity and continuum damage approach have limitations related to analyzing cracks in asphalt concrete. Therefore, a new approach, termed the HMA (Hot-Mix-Asphalt) Fracture Mechanics approach was introduced in this study. As a beginning, a testing and data acquisition, reduction, and analysis system to determine crack growth rate parameters using the SuperPave™ indirect tension test (IDT) was developed in this study.

It is known that cracks in asphalt mixtures are difficult to see. Use of crack foils or coatings can help, but it may be difficult to match the properties of those materials exactly with those of different asphalt mixtures at different temperatures. Therefore, the crack length determined from crack foils or coatings is an estimate.

Therefore, the system developed not only has the capability to determine fracture parameters using the SuperPave™ IDT, but it also meets the following criteria:

- The system does not require the direct measurement of crack growth during testing.
- The system is a stand-alone system. In other words, the interpretation of the test data does not require the use of properties (e.g., stiffness or Poisson's ratio) that have to be determined independently from other tests on the mixture.

4.1.1 Scope

The system developed for the determination of fracture parameters that represent a mixture's resistance to crack propagation is presented in this chapter. The concept of effective crack length is defined as the crack length that results in a specified change in material response. The

use of the effective crack length concept assumes that all damage is a result of crack growth. In reality, the change in mixture response results not only from crack growth, but also from heat and damage in the form of micro-cracking. A procedure, separating the effect of heat and micro-cracking induced during crack initiation, was developed to determine effective crack length and associated fracture parameters.

4.1.2 Research Approach

The development of the system to determine crack growth rate parameters from SuperPave™ IDT involved the following steps:

1. Determination of the best specimen geometry, including specimen thickness and proper notching procedures for the most accurate determination of fracture parameters.
2. Development of the theoretical relationships between crack length and stress intensity factor from load and horizontal deformation measurements obtained from the SuperPave™ IDT.
3. Establishment of proper data acquisition procedures to assure that sufficient data is obtained to define crack growth rate precisely enough to determine fracture parameters.
4. Establishment of proper data reduction procedures to consistently and reliably determine fracture parameters.
5. Evaluation of fracture test data to determine the reasonableness of the results. This was accomplished in several ways: (a) by determining whether the crack lengths determined from the test data were reasonable; (b) by comparing the measured fracture parameters to values published in the literature for similar mixtures; (c) by evaluating the repeatability of the test results; (d) by evaluating the reasonableness of the trends in the fracture test results.

4.2 SPECIMEN THICKNESS AND NOTCH GEOMETRY

The SuperPave™ IDT is shown in Figure 4.1. Based on Roque and Buttlar (1992) and Hugo (1993)'s work, if a relatively thin (approximately 25 mm) specimen thickness is used for indirect tension tests, plane stress conditions are approximated fairly closely. Therefore, uniform stress intensity factor can be achieved by using a specimen thickness of approximately 25 mm, which was used in fracture test for determining fracture parameters.

Fracture tests are generally performed on notched specimens. The notch serves to concentrate the stress so that the crack initiates and propagates along a predetermined path. There are two considerations that need to be made in selecting notch size and shape: (1) the notch must be large enough to assure the crack will initiate and propagate along the desired path; (2) the effect of the notch must be interpretable such that stress intensity factors can be accurately determined. The latter requirement can be achieved in one of two ways: (1) the notch can be produced with such a sharp instrument that it essentially represents a true crack and its effect can be ignored; or (2) a well-defined shape notch can be produced, such that the effects of the shape can be analyzed theoretically.

After numerous unsuccessful attempts to produce a sharp notch in the center of the specimen, the latter approach was selected in this investigation. A circular hole was first drilled in the center of the specimen through which the blade was inserted and a notch was made. Further attempts at notching were abandoned, because it was difficult to accomplish and provided little, if any, benefit over the use of a simple hole. Based on these preliminary tests, the decision was made to use an 8-mm diameter hole at the center of the specimen.

As shown in the following section, two analysis procedures were developed: one assumed a crack at the center of the specimen; and the other considered the stress states in the

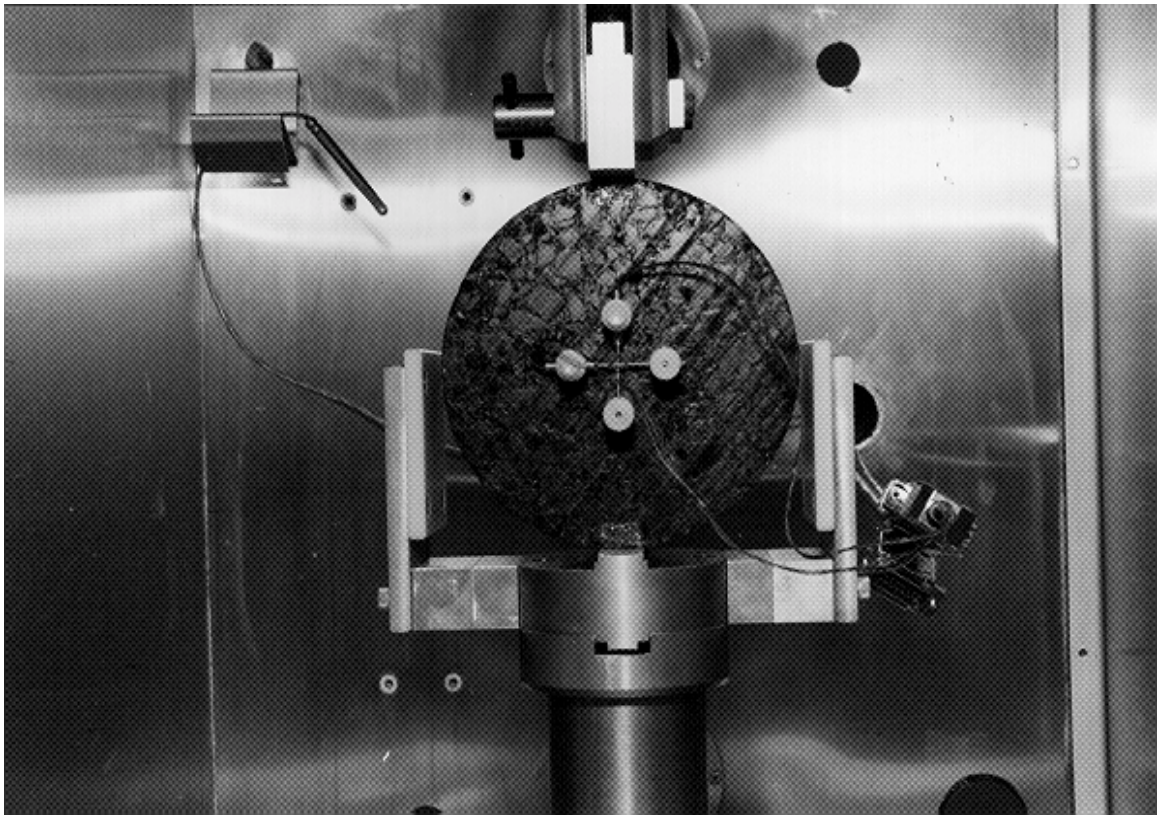

Figure 4.1 The SuperPave™ Indirect Tension Test (IDT)

vicinity of the hole in the determination of stress intensity factors. The two approaches were compared for evaluation and illustration of the effects of ignoring notch geometry in the determination of stress intensity factors and fracture parameters.

4.3 DETERMINATION OF CRACK LENGTH AND STRESS INTENSITY FACTOR

As mentioned earlier, it is difficult to measure crack length of asphalt concrete accurately and reliably. Therefore, it was necessary to develop a system where the measurement of crack length would not be required during the test. This implies that crack length could be determined using the measured response(s), load, and dimensions of the specimen. Two theoretical approaches were developed to accomplish this:

- An energy-based approach
- A compliance-based approach

4.3.1 Energy-Based Approach

An energy-based approach is based on the concept that the change of total energy caused by externally applied load is equal to the energy used to create new surface of the crack. The above statement can be described by the following equation:

$$U_B - U_A = \frac{1}{2} P(\Delta\delta) \tag{4.1}$$

where U_B and U_A are the potential energy in the whole body of the specimen corresponding to the number of load replications N+ΔN and N (or crack length a+Δa and a), respectively. P is the externally applied load, Δδ is the difference in the deformations at the steel loading platens corresponding to the number of load replications N+ΔN and N (or crack length a+Δa and a), respectively. In order to make the calculation simple, it was assumed that all of the damage was near the crack tip and was in the form of crack growth. The results published in the literature show

that cracks influence stress distribution within the process zone, causing extremely high stresses; while beyond this zone, stresses are close to the so-called the far away stress. Based on definition of stress intensity factor (K), K is valid within 0.1*a* (*a* is half of crack length), therefore, the size of this process zone was selected to be 0.1*a* away from crack tip in this approach.

The procedure of calculating crack length using the energy-based approach involves the following steps:

1. The change of total energy density was determined from the externally applied load and the external deformation measurement at the loading platens caused by this load. The following equation was used to calculate the change of the total energy density:

$$\Delta \quad \text{Total Energy} \quad = \quad \frac{1}{2} P(\Delta\delta)/V \qquad (4.2)$$

where P is the maximum applied load, V is the volume of the specimen, $\Delta\delta$ is the difference in the deformations at the steel loading platens corresponding to crack length (*a*) and crack length ($a+\Delta a$), respectively, which were obtained from the vertical deformation measurements from the SuperPave™ IDT, since the deformations measured at the loading platens were known to include the effects of significant damage that causes in this area.

2. The energy used to create new crack surface was determined from measurements of the crack opening after a specified number of load cycles were applied.

   (1) Determination of average stress

   Based on the definition of stress intensity factor, the stress distribution near the crack tip was assumed to be $\sigma_{FA}(a/2\pi r)^{0.5}$ within the range of r=0.1*a* (*a* is half of crack length, corresponding to the number of load replications N) (Figure 4.2).

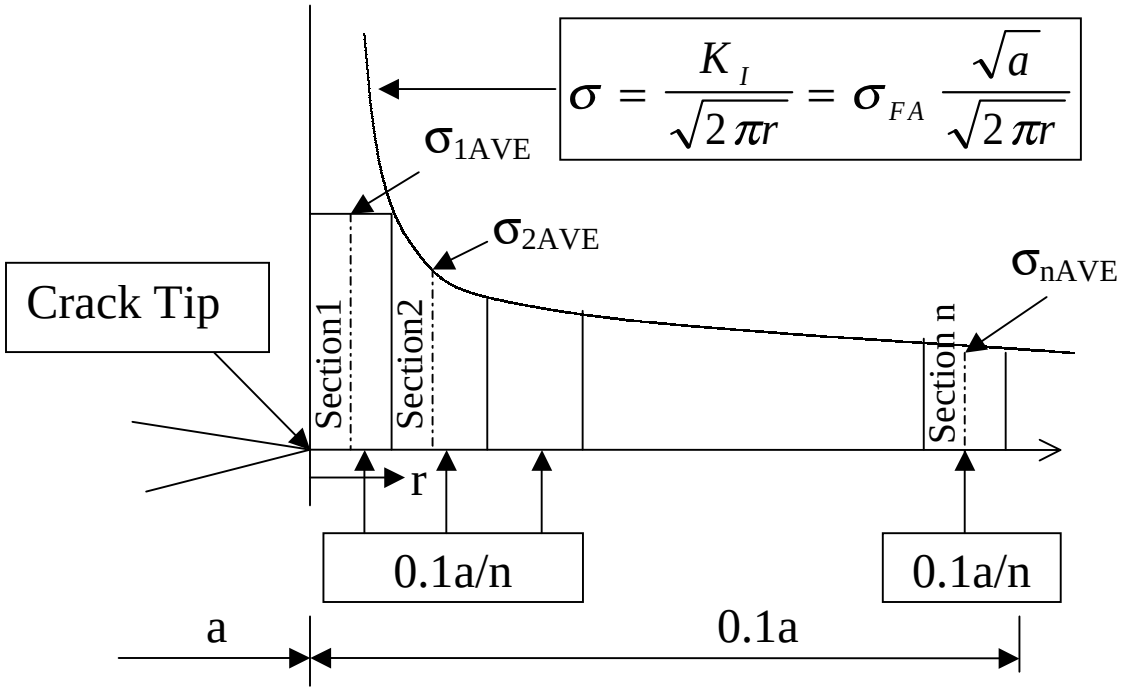

Figure 4.2 Calculation of Average Stress Using the Energy-Based Approach

Dividing the range, r, into n sections (e.g., n=10), the average stress in each section was determined:

$$\sigma_{1AVE} = \sigma_1 = \frac{\sigma_{FA}\sqrt{a}}{\sqrt{2\pi(0.1a/n)}}$$

$$\sigma_{2AVE} = \frac{1}{2}(\sigma_1 + \sigma_2) = \frac{1}{2}\left(\frac{\sigma_{FA}\sqrt{a}}{\sqrt{2\pi(0.1a/n)}} + \frac{\sigma_{FA}\sqrt{a}}{\sqrt{2\pi(0.1a/n)*2}}\right)$$

..... (4.3)

$$\sigma_{nAVE} = \frac{1}{2}(\sigma_{n-1} + \sigma_n) = \frac{1}{2}\left(\frac{\sigma_{FA}\sqrt{a}}{\sqrt{2\pi(0.1a*(n-1)/n)}} + \frac{\sigma_{FA}\sqrt{a}}{\sqrt{2\pi(0.1a*(n)/n)}}\right)$$

(2) Determination of average strain

The horizontal measurement obtained from the SuperPave™ IDT was used to determine the strains. After several trials of selecting the deformation distribution, an elliptical function was chosen since it was thought to be the most accurate representation of the real deformation distribution (Figure 4.3) within the range of 0.1*a*. Dividing this range (0.1*a*) into n sections, the average deformation in each section was determined from the equation shown in Figure 4.3 (e.g., the value of y_{1AVE} corresponding to x = (*a*+(0.1*a*/n)(1/2)), the value of y_{nAVE} corresponding to x=(*a*+(0.1*a*/n)(n-1/2)). The average strain was obtained by using the values of y divided by the gage length (GL)

(3) The energy within the range of 0.1*a* at crack length *a*, corresponding to the number of load replications, was:

$$\text{Energy}_{(a)} = \sum_{i=1}^{n} \sigma_{AVEi} * \varepsilon_{AVEi} \quad (4.4)$$

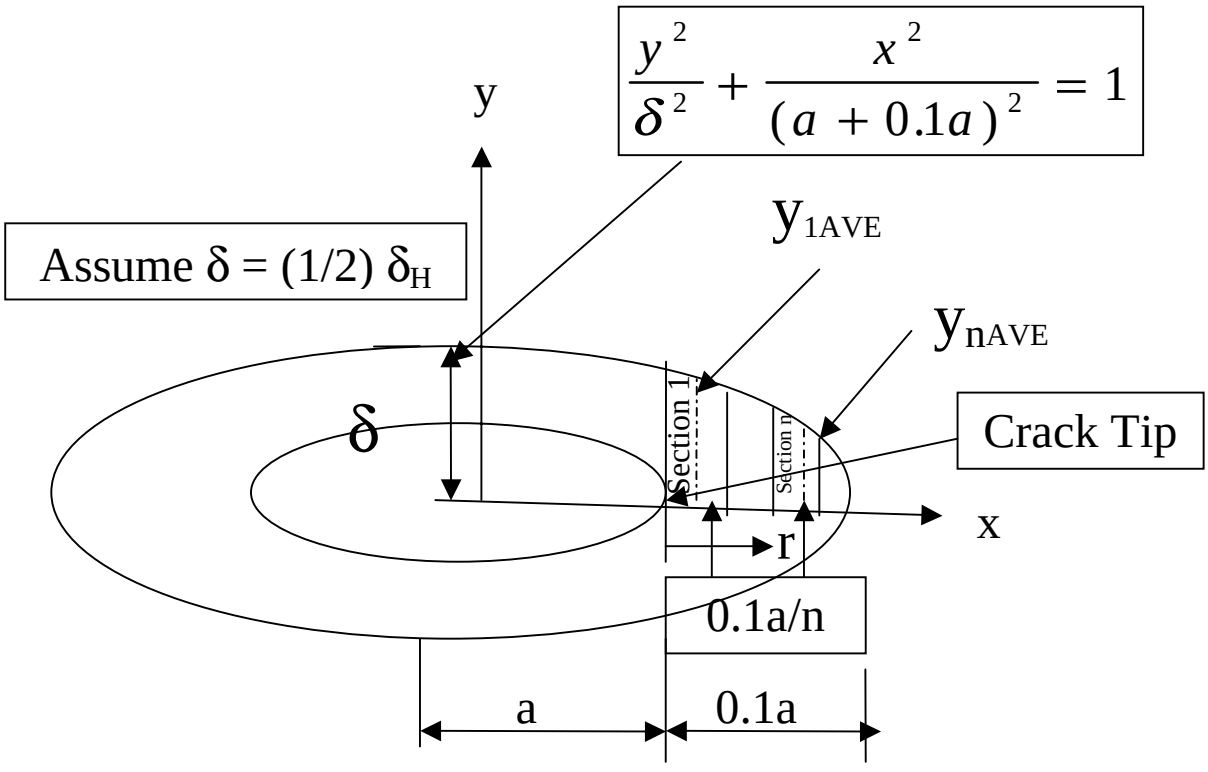

Figure 4.3 Calculation of Average Strain Using the Energy-Based Approach

(4) Repeat steps (1) and (2), calculate the energy within the range of 0.1(a+Δa) at crack length (a+Δa), corresponding to the number of load replications (N+ΔN)

$$\text{Energy}_{(a+\Delta a)} = \sum_{i=1}^{n} \sigma_{AVEi} * \varepsilon_{AVEi} \quad (4.5)$$

(5) The difference in deformation before and after the specified number of load cycles was used to compute the energy associated with crack growth Δa. Therefore, the total energy to create the crack length Δa was determined as follows:

$$\Delta U = \text{Energy}_{(a+\Delta a)} - \text{Energy}_{(a)} \quad (4.6)$$

3. Check the values obtained from step 1 (ΔTotalEnergy) and step 2-(5) (ΔU). If these two values were equivalent, Δa was assumed to be correct. Otherwise, another Δa would be assumed, and the steps, 2-(4), 2-(5), and 3, were repeated.

In summary, since the crack length was unknown, an iterative procedure was developed to solve for crack length. In this procedure, the crack length was varied until the dissipated energy associated with the creation of new crack surface was equal to the total energy absorbed by the specimen.

It was noticed that a significant amount of damage, and consequently, energy dissipation would occur in the vicinity of the steel loading platens. Therefore, it was determined that the external energy should be estimated from the internal vertical deformation measurements from the SuperPave™ IDT. In reality, this determination may have resulted in significant inaccuracy. Furthermore, the assumption that all of the damage in the asphalt specimen was near the crack tip, may also cause inaccuracy for the different mixtures for two reasons: (1) for some asphalt mixtures, damage may occur throughout the whole specimen; (2) the size of the process zone near the crack tip may vary for the different mixtures. However, even though the range of this

process zone was chosen from 0.1a to 0.2a, no significant improvement was achieved in this approach.

In spite of the great deal of time and care that was taken to set up this energy-based system and associated software, the results were generally poor. Crack lengths determined from this system were not considered to be reasonable. Sensitivity analyses indicated that the system was excessively sensitive to the stress distributions predicted near the crack tip. Meanwhile, the stress limit that asphalt concrete can tolerate was not considered in this approach. In addition, the deformation distribution (an elliptical function) predicted near the crack tip may have also introduced the significant inaccuracy because: (1) the deformation distribution was estimated while the real deformation distribution was unknown; and (2) the values of δ on the deformation distribution curve was assumed to be half of the horizontal measurements obtained at a gage length of 37.5 mm (1.5 in).

Finally, a constant load was assumed in the calculation whereas the actual load was a harversine load.

Based on these preliminary results and observations, the decision was made to not pursue this approach any further.

4.3.2 Compliance-Based Approach

The compliance-based approach is based on the concept that the specimen will become more compliant as the crack length increases. The key in this approach is to establish a definitive relationship between crack length and measured deformation for the specified specimen geometry and measurement system being used.

(1) Approximate Approach

As an approximate approach, the system was modeled as shown in Figure 4.4, which shows the indirect tensile specimen with a vertical crack length c (2*a*). The following relationship was developed between the crack length and the horizontal measurements obtained from the SuperPave™ IDT:

$$\frac{\delta}{\delta_o} = 2\sqrt{1 + \frac{c^2}{L^2}} - \frac{(1 + \nu)}{\sqrt{1 + \frac{c^2}{L^2}}} + \nu \qquad (4.7)$$

where δ is the resilient horizontal deformation across the crack length, δ_o is the resilient horizontal deformation of the uncracked specimen (this corresponds to the deformation measured on the first cycle of loading), L is the gage length over which deformation is measured, c (2*a*) is the crack length, and ν is Poisson's ratio.

Note that the equation was set up in dimensionless terms by dividing the measured deformation (δ) for any crack length by the deformation measured at the start of the test before any crack growth had occurred (δ_o). This is a very powerful technique because it had the effect of eliminating the stiffness of the mixture as a variable in the equation (i.e., stiffness dropped out in the development and does not appear in the equation above). The implication is that mixture stiffness does not need to be measured or even estimated to determine crack length and crack growth rate parameters.

Unfortunately, Poisson's ratio did not drop out of the equation. However, the sensitivity analysis presented in Figure 4.5 shows that varying Poisson's ratio from 0.0 to 0.5 (the typical range of asphalt mixtures) had a relatively small effect on the relationship between normalized deformation (δ/δ_o) and normalized crack length (c/L).

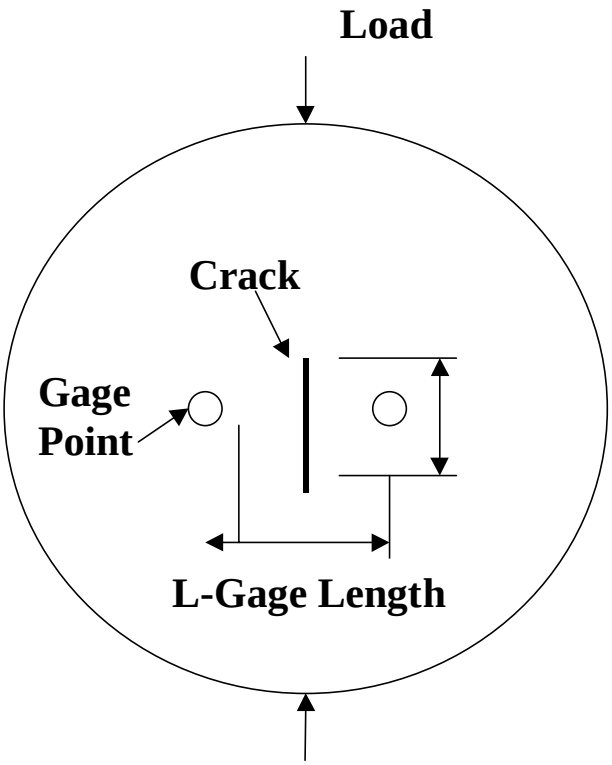

Figure 4.4 Model of SuperPave™ IDT With Vertical Crack

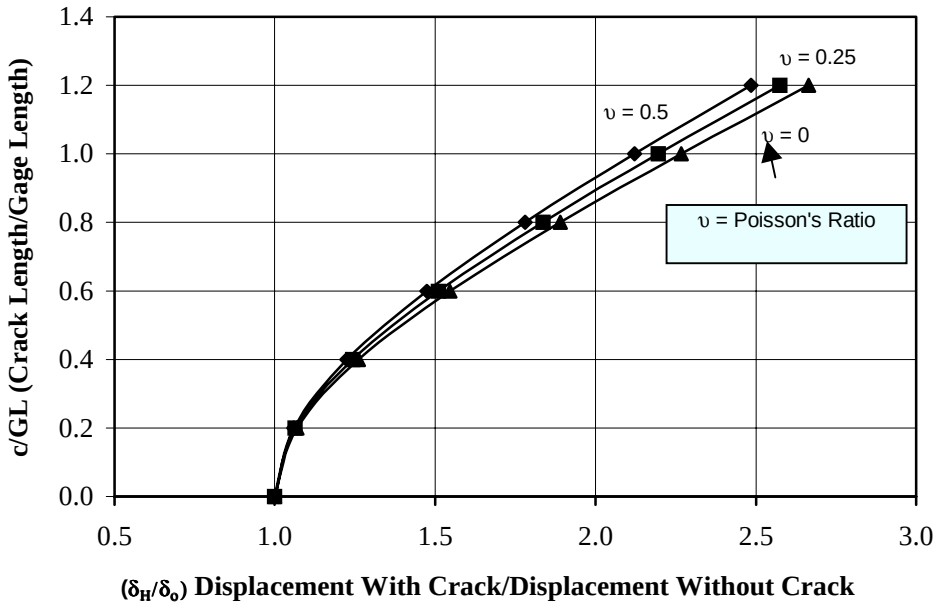

Figure 4.5 Effect of Poisson's Ratio on Predicted Crack Length Using Displacement from SuperPave™ IDT

It is well known that horizontal tensile stresses are highly uniform along the vertical axis of a diametrally loaded cylindrical specimen. For a relatively thin specimen (e.g., 25 mm thickness), where plane stress conditions are approximated, the magnitude of the tensile stress may be calculated as follows:

$$\sigma = \frac{2P}{\pi t D} \tag{4.8}$$

where σ is the horizontal stress along the vertical axis, P is the total load applied to the diametrally loaded specimen, t is the specimen thickness, and D is the specimen diameter.

The stress intensity factor (K) for the crack and specimen geometry illustrated in Figure 4.4 can be approximated with the following equation:

$$K = \sigma\sqrt{\pi\alpha} \tag{4.9}$$

where K is the stress intensity factor, σ is the horizontal stress along the vertical axis, and *a* is half the crack length. Although this is the solution for a crack of length 2*a* within an infinitely large body subjected to a uniform stress, comparisons to the rigorous solutions presented later in this chapter indicated that this equation reasonably approximates K for this problem. This approximate approach was used to make an initial evaluation to determine the viability of the system.

(2) Rigorous Solution (Finite Element Method Analysis)

The obvious limitation of the approximate solution presented above is that it does not account for the effect of the hole at the center of the specimen. Although the approximate solution does represent the opening created by the hole as a crack, a round hole distributes stress much differently than a crack. Therefore, it was necessary to develop a more accurate solution and determine the effect of the hole on determining fracture parameters.

The finite element computer program ABAQUS was used to model the diametrally-loaded specimen with an 8 mm diameter hole at its center. Numerous finite element meshes were generated to represent specimens with different crack length, including the case of a specimen without a crack (i.e., only an 8 mm diameter hole). The goal was to obtain a matrix of solutions from which relationships could be developed to determine crack lengths from measured deformation, and stress intensity factors for known crack length, load, and specimen dimensions.

A preliminary evaluation was conducted to determine the most accurate method of determining stress intensity factor from the ABAQUS code. Two methods of determining stress intensity factor were evaluated. The first makes use of the definition of stress intensity factor:

$$K = \lim_{r \to 0} \left(\sigma_r \sqrt{2\pi r} \right) \tag{4.10}$$

where K is the stress intensity factor, r is the distance from the crack tip, and σ_r is the stress at distance r from the crack tip.

Therefore, K can be determined in practice by plotting $\sigma_r(2\pi r)^{1/2}$ as a function of r and determining the intercept of the relation at r=0 (Figure 4.6). It is noted that, near r=0, the shape of the function ($\sigma_r(2\pi r)^{1/2}$) is unusual. It is known that this phenomenon is caused by inaccuracies in numerical solutions and is not representative of the true stress distribution in front of the crack tip. Therefore, K was determined by the trend of the function approaching r=0.

As an example, Single Edge Notched Tension (SENT) models were selected to illustrate the use of this method to determine K (Figure 4.7). It was observed that in order to achieve an accurate K, use of very refined meshes, especially near the crack tip, was required. An evaluation of this approach to determine K revealed that the solutions were within 10% difference of published closed-form solutions for which K is known.

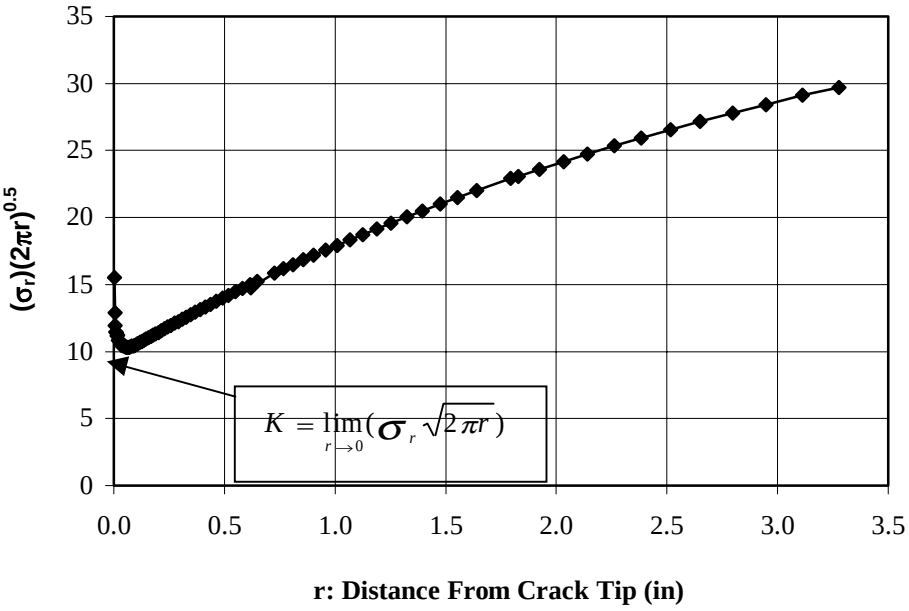

Figure 4.6 Determination of Stress Intensity Factor from Predicted Stress

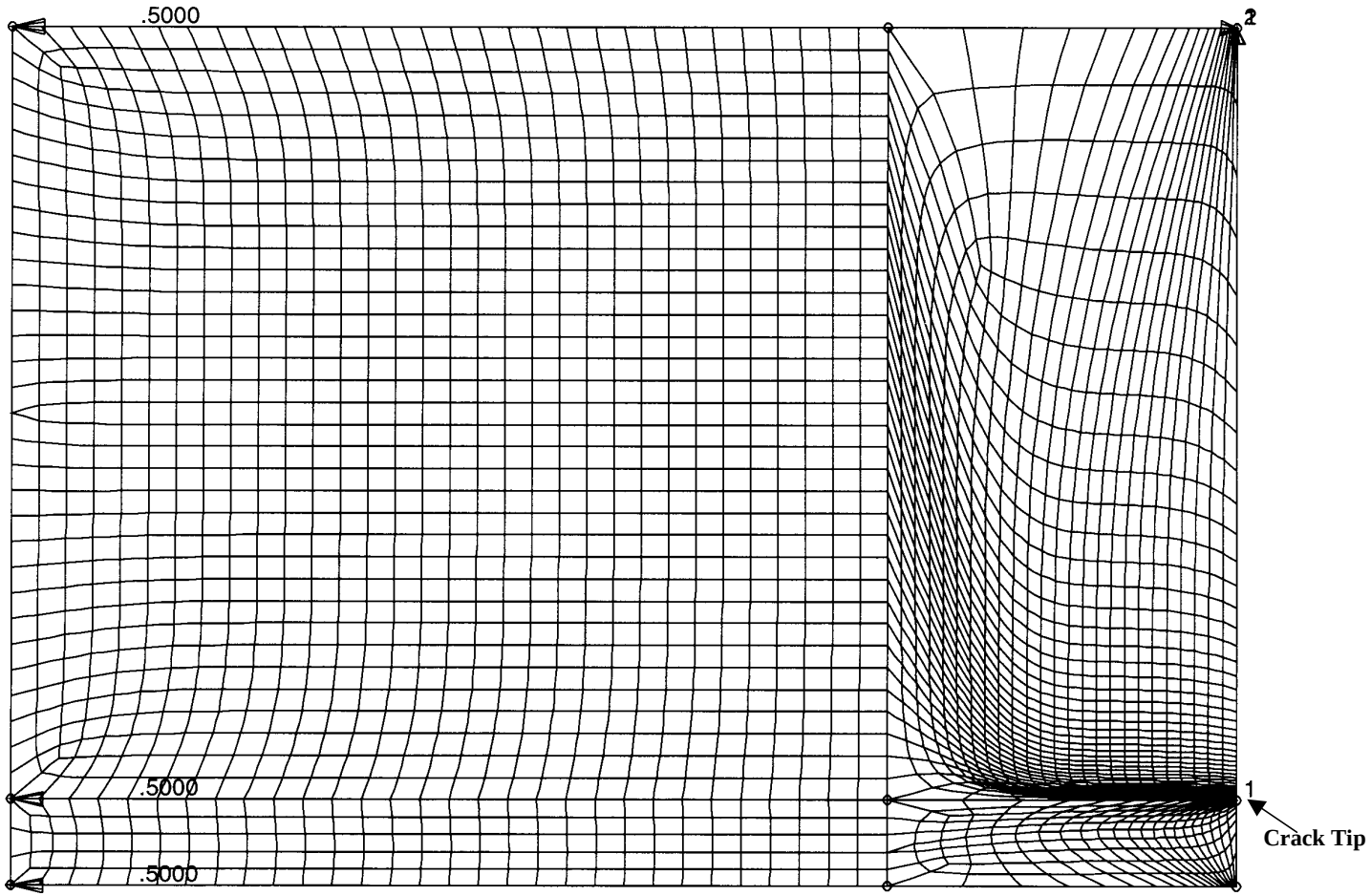

Figure 4.7 Single Edge Notched Tension (SENT) Model With Fine Mesh Near Crack Tip

Stress intensity factor can also be determined by using the J-integral approach, since:

$$K = \sqrt{JE} \tag{4.11}$$

where K is the stress intensity factor, J is the potential energy in the entire specimen, and E is the Young's modulus.

It should be noted that although the J-integral method theoretically requires knowledge of Young's modulus for determination of K, it could be easily shown that K is practically independent of Young's modulus. The reason is that the J-integral is also a function of Young's modulus, such that the effect of Young's modulus cancels in the determination of K.

The ABAQUS computer program has an automated routine that can be used to determine the J-integral and K. It is important to note that ABAQUS will apparently not calculate the J-integral if there are any triangular elements anywhere in the finite element mesh. The "isomesh" feature in ABAQUS, which automatically generates a mesh composed strictly of quadratic elements near the crack tip, was found to be very useful in this regard.

An example of calculation of K using J-integral is shown in Figure 4.8. A Single Edge Notched Tension (SENT) model was also chosen in this approach. From this model, it is easy to find the "isomesh" feature near the crack tip with fairly rough finite element meshes. An evaluation of stress intensity factors determined using the J-integral approach resulted in solutions are within 2% of published closed-form solutions for which K is known. Therefore, the J-integral method was selected to be used in the development of relationship to determine stress intensity factor, K.

A typical finite element mesh used for the analyses of the SuperPave™ IDT is shown in Figure 4.9. Given the symmetrical nature of this problem it was only necessary to model one

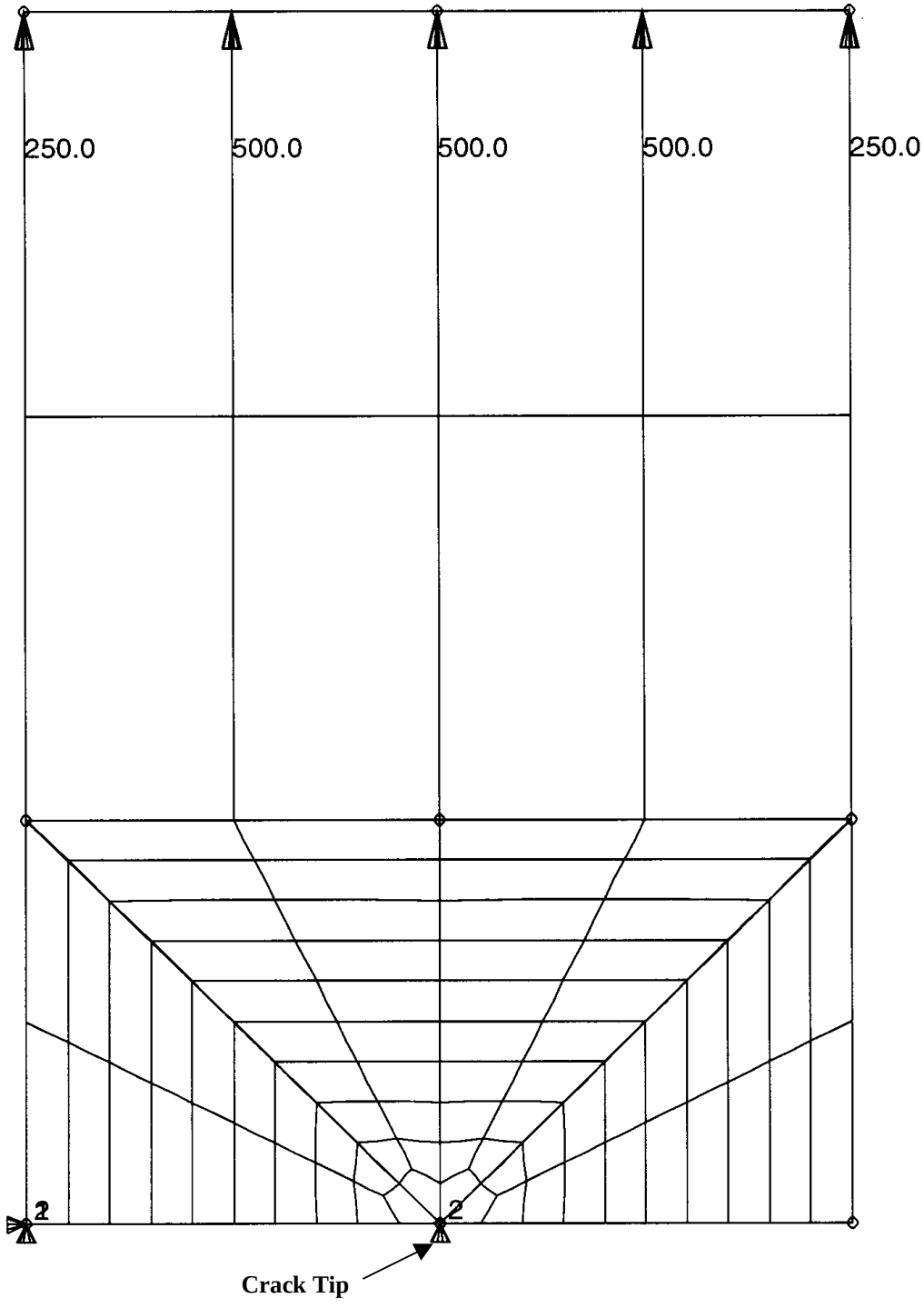

Figure 4.8 Single Edge Notched Tension (SENT) Model With Isomesh Near Crack Tip

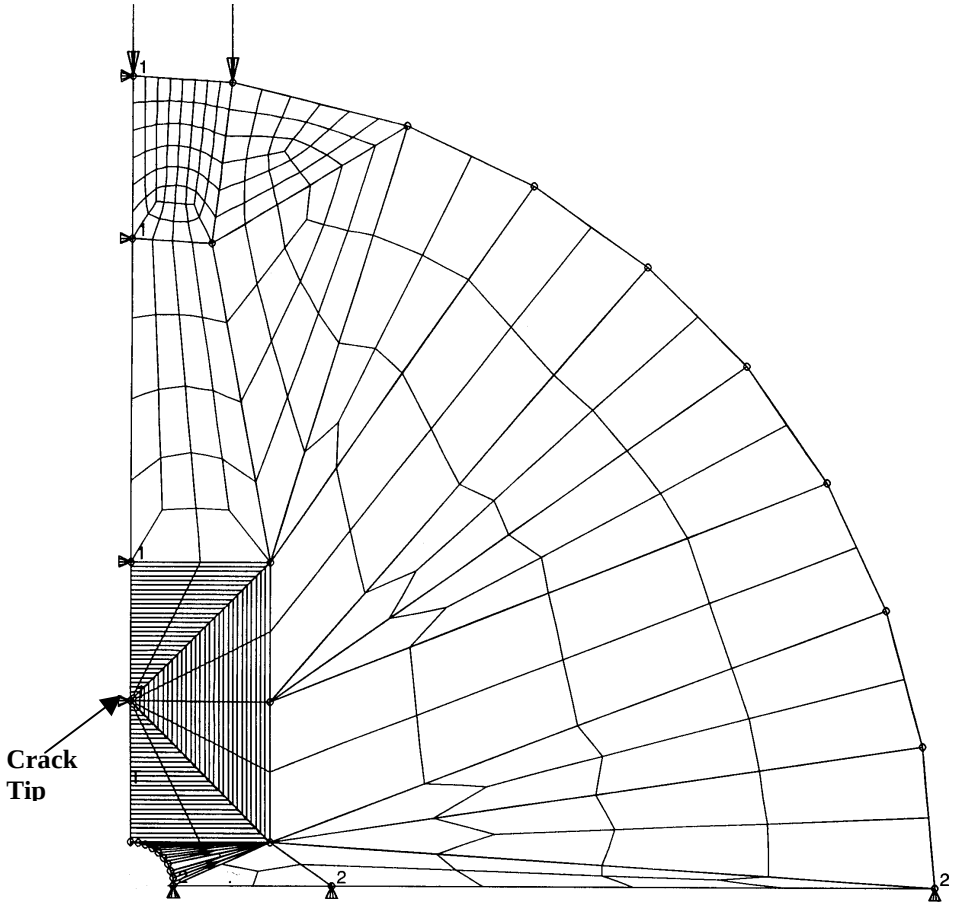

Figure 4.9 Finite Element Mesh of SuperPave™ IDT With Hole and Vertical Crack

quarter of the specimen for analysis. In addition, specimens without the presence of a hole were also modeled (Figure 4.10, one quarter of the specimen).

A matrix of finite element analyses were conducted to develop the relationship between horizontal displacement measured with the SuperPave™ IDT and crack length. The relationship is shown in Figure 4.11, which also shows the relationship based on the approximate solution which did not consider the presence of a circular hole in the analysis. This relationship was developed in dimensionless terms, which eliminates the effect of mixture stiffness. It is clear from Figure 4.11 that the approximate solution would lead to significant errors in the determination of crack length and fracture parameters.

Figure 4.12 shows the relationship developed between crack length and stress intensity factor based on results of the finite element analyses. This relationship was also developed in dimensionless terms, such that K can be obtained for specimens of different diameter, thickness, load or gage length. Figure 4.12 also shows that there is a significant difference between the stress intensity factor determined with the approximate solution and the one from the finite element method analysis.

4.4 MATERIAL AND TESTING PROCEDURES

Two SuperPave™ mixtures were tested as part of this investigation: one designed on the fine side of the restricted zone, the other designed on the coarse side of the restricted zone. Specimens with 150 mm diameter and 25 mm thickness were selected for the fracture tests. Detailed information about the mixtures and specimens was described in Chapter 3.

All fracture tests were conducted at 10C with a load consisting of a 0.1-second harversine load followed by a 0.9 second rest period. Two horizontal deformation measurements, two

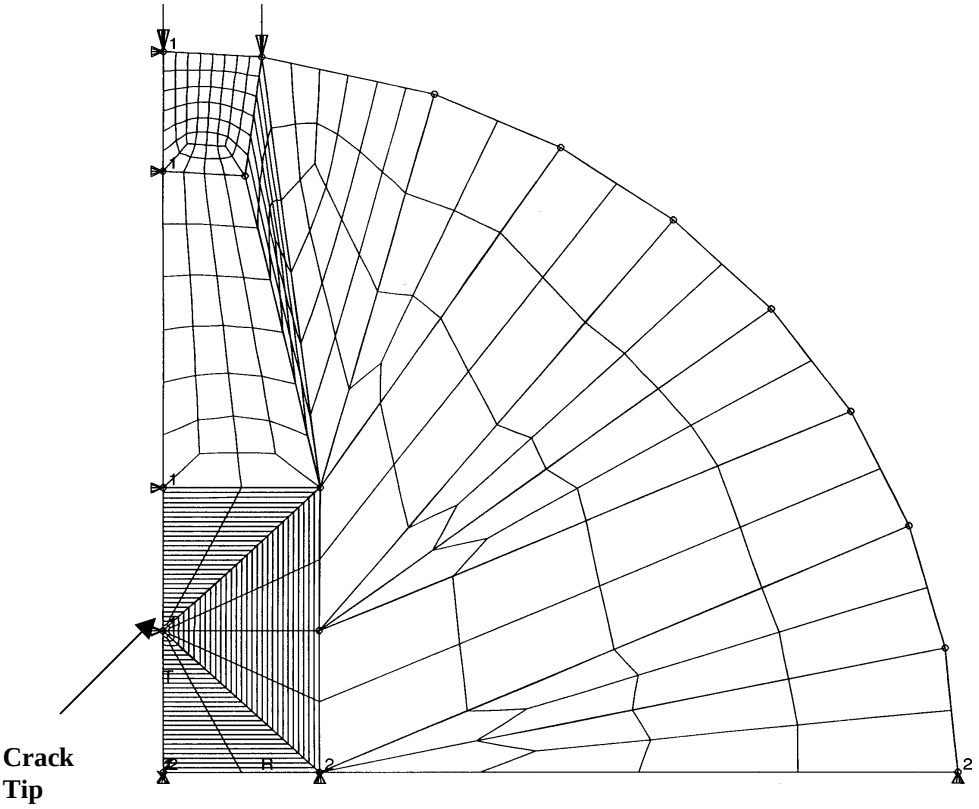

Figure 4.10 Finite Element Mesh of SuperPave™ IDT Without Hole but With Vertical Crack

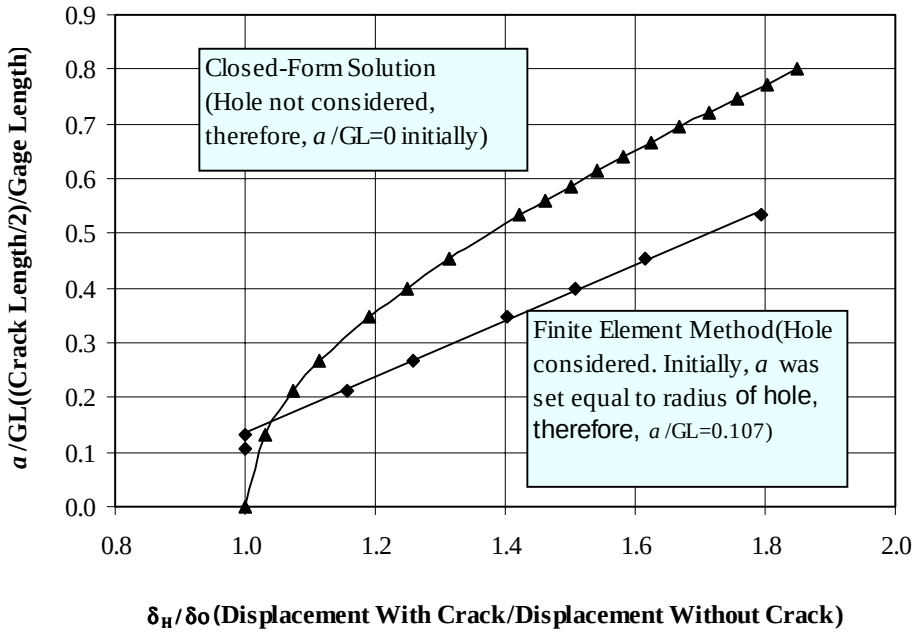

Figure 4.11 Theoretical Relations Between Normalized Crack Length and Normalized Horizontal Displacements from SuperPave™ IDT

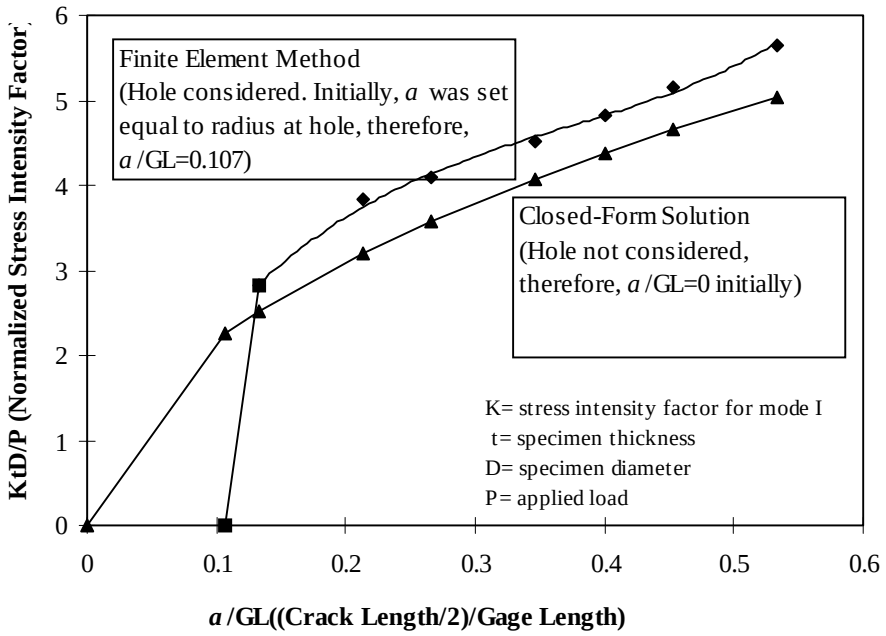

Figure 4.12 Relations Between Normalized Stress Intensity Factor and Normalized Crack Length

vertical deformation measurements, applied load and the corresponding time were recorded at a rate of 150 points per seconds (pps) for 5 seconds every 60 seconds until the specimen failed.

4.5 DATA INTERPRETATION METHODS

The procedure for determining fracture parameters from repeated load tests using the SuperPave™ IDT involves the following steps:

1. Obtain and plot resilient horizontal deformations as a function of loading repetitions (Figure 4.13).
2. Determine the initial resilient horizontal deformation (δ_o) that corresponds to the response of the specimen in the undamaged state. This value is used to normalize all subsequent deformations to determine change in crack length according to the relationships described in Figures 4.5 and 4.11 (approximate and rigorous solution, respectively). Additional discussion relating to the determination of this value is presented below.
3. Determine and plot of crack length as a function of load repetitions using the data obtained in steps 1 and 2 and the relationships presented in Figure 4.5 or Figure 4.11. The resulting plot corresponding to the test results presented in Figure 4.13, is presented in Figure 4.14, which shows both the rigorous (finite element) and the approximate (closed-form) solutions.
4. Determine the rate of crack growth (da/dN) at several points (number of load repetitions) during the test by determining the slope of the relationship between crack length (a) and number of load repetitions (N), as illustrated in Figure 4.14. This was accomplished in practice by fitting a third order polynomial to the a vs N relationship and taking its derivative at the desired number of load repetitions.

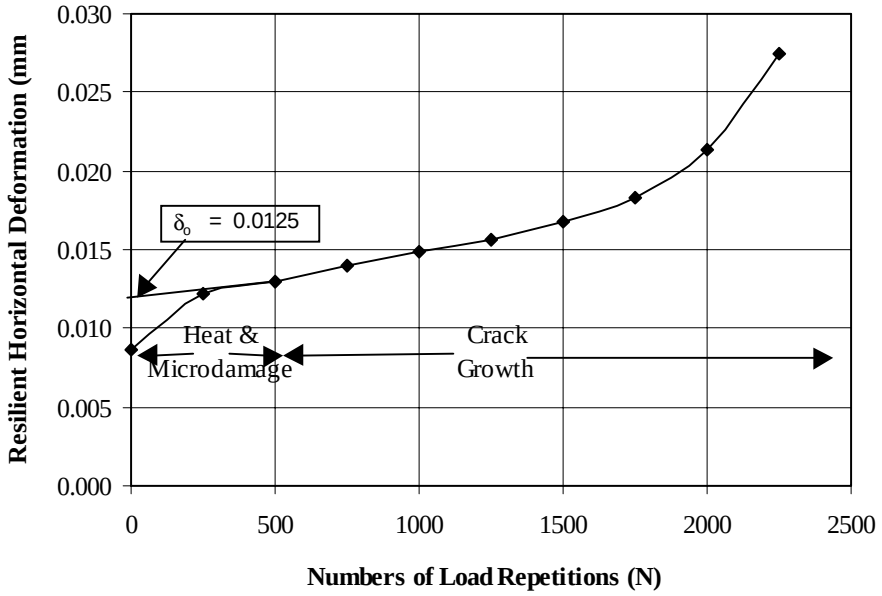

Figure 4.13 Resilient Horizontal Determination During Repeated Load Fracture Test

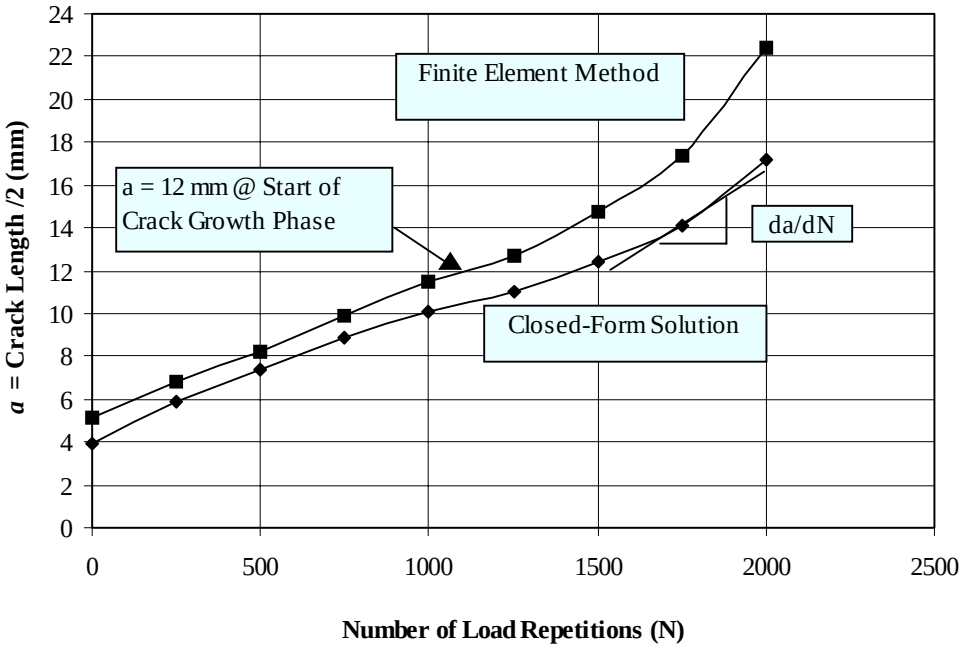

Figure 4.14 Effective Crack Length During Repeated Load Fracture Test

5. The stress intensity factor (K) was then obtained for the corresponding number of load repetitions by using the relationships presented in Figure 4.12.
6. Steps 4 and 5 result in a series of crack growth rates (da/dN) and corresponding stress intensity factors (K) that can be used to obtain the relationship between da/dN and K. Figure 4.15 shows this relationship corresponding to the example test data presented in Figures 4.13 and 4.14. The figure is generally plotted in log-log scale, which reflects the power law nature of Paris law (i.e., $da/dN = A(\Delta K)^n$).
7. The fracture parameters, A and n, for Paris law are obtained by regression analysis to determine the intercept and slope of the log-log relationship between da/dN and K. Their determination is illustrated in Figure 4.16, which show that only the linear portion of the relationship is used in their determination.

Additional details relating to the data reduction procedures established in this investigation and the significance and physical interpretation of some of the trends observed in the data are presented in the following sections.

Determination of Resilient Deformation

As indicated in the previous section, horizontal deformation measurements were recorded for 5 seconds every 60 seconds. Resilient horizontal deformations for use in the interpretation of fracture data were obtained by averaging the resilient horizontal deformations of three consecutive load cycles.

Determination of Initial Deformation

The trend between resilient deformation (δ) and number of load repetitions (N) is shown in Figure 4.13. Initially, there was a relatively rapid increase in resilient deformation, but the rate of increase reduced within the first few hundred load repetitions. This behavior makes no

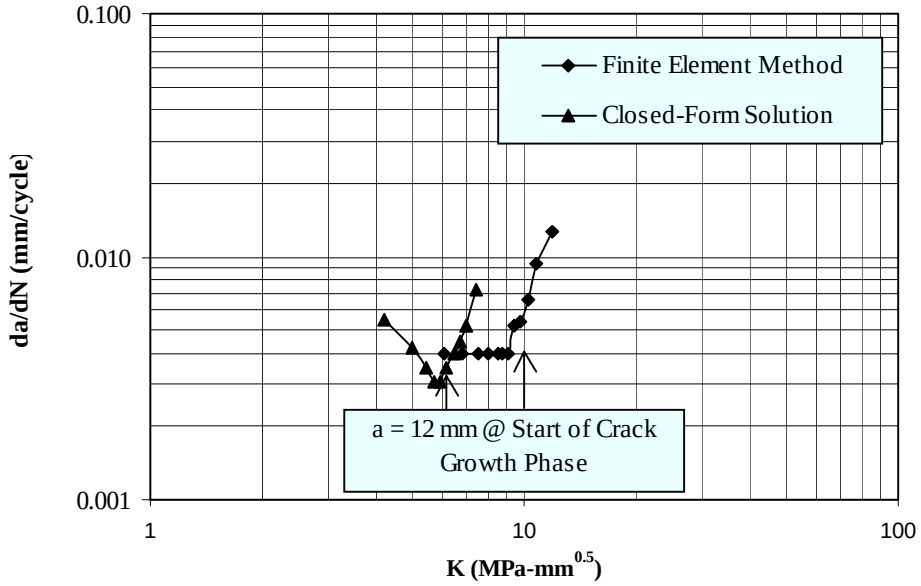

Figure 4.15 Relation Between Crack Growth Rate and Stress Intensity Factor

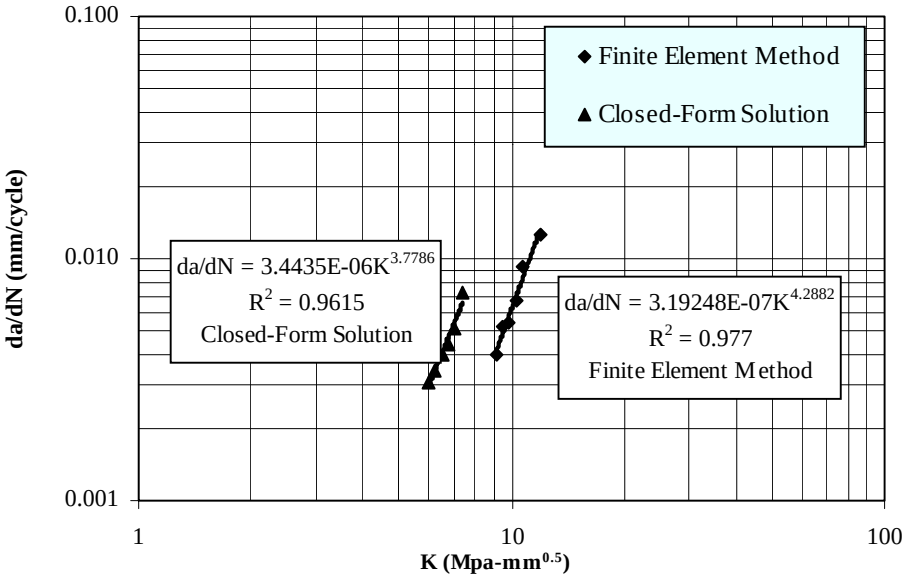

Figure 4.16 Determination of Fracture Parameters A and n, Where $da/dN = A(K)^n$

physical sense from the standpoint of crack growth or damage because the rate of damage should not decrease under the constant stress conditions if the crack or the damage zone is getting larger (corresponding to larger resilient deformation). Therefore, it was concluded that there was another reason for this initial rapid increase in resilient horizontal deformation.

Work by Di Bennedetto (1996) showed that significant increases in temperature could occur during the early part of repeated load tests on asphalt mixtures. The temperature increase reduces the stiffness of the asphalt mixture, which would explain the increase in resilient deformation. This is consistent with the observation in this study and provides a rational physical explanation for the data obtained. Therefore, as shown in Figure 4.13, increases in resilient deformation during the early part of the fracture test may be attributed to heat and damage. It may be further deducted that the temperature in the specimen has stabilized once the rate of increase of resilient deformation stabilizes.

This phenomenon has an effect on the interpretation and determination of the initial deformation (δ_o). In theory, δ_o represents the resilient horizontal deformation corresponding to the undamaged specimen, and this value is used to normalize deformations obtained during the course of the fracture test such that the effect of stiffness is eliminated from the determination of crack length. Therefore, δ_o should be obtained at conditions corresponding to the conditions after the specimen has reached temperature stability.

Given the reason presented above, the proper way to obtain δ_o is shown in Figure 4.13, which shows that an extrapolation of the δ_o vs N relation from the point where the rate of increase in resilient horizontal deformation stabilizes. The initial deformation (δ_o) is determined as the intercept of the straight-line extrapolation at N=0. Therefore, the extrapolation is performed by visually determining the location when the rate of deformation has stabilized.

Further Discussion on Determination of Fracture Parameters

Figures 4.14 through 4.16 show that the approximate (closed-form) solution resulted in significantly different predicted crack lengths and fracture parameters than the more rigorous solution that accounted more precisely for the presence of the hole in the test specimen. The approximate solution significantly overestimated the rate of crack growth for a given level of stress intensity (i.e., it significantly underestimated the fracture resistance of the mixture). These results clearly emphasize the importance of precisely controlling and/or accounting for notch geometry in the interpretation of fracture tests.

The trends in the data presented in Figures 4.13 through 4.16 support the validity of the more rigorous solution. The shape of the da/dN relationship for the approximate solution shown in Figure 4.15 is typical of fracture test results presented in the literature (Jacobs, Hopmann and Molenaar, 1996). During the initial part of the test, da/dN is shown to decrease as stress intensity factor (K) increases. This behavior has no physical meaning. The fact is that if a crack grows, then the stress intensity factor increases and da/dN must increase for a constant stress test.

This phenomenon could be explained by the more rigorous solution shown in Figure 4.15. Crack growth rate (da/dN) does not decrease, but instead remained constant, during the early part of the test. Since a notch is essentially a hole and a hole is not a crack, it takes time (or load repetitions) for the hole to develop into a true crack. Micro-damage is occurring during this time, which results in higher resilient horizontal deformations, but da/dN should not increase until a crack actually forms (i.e., the rate of damage should not increase until the geometry of the specimen changes).

The magnitudes of the crack lengths determined offer further evidence of the validity of the system developed in this investigation. Results presented in Figure 4.14 indicate that speci-

men failure (da/dN began to increase very rapidly) when the predicted crack length was about 45 mm (2*a*). This is a very reasonable result, since a 45 mm crack length within a 150-mm diameter specimen would cause substantial weakening such that overall specimen failure should be imminent. The crack length associated with the point when da/dN began to increase (i.e., the start of crack growth) was also reasonable. As shown in Figure 4.15, crack growth was determined to start at a crack length of 24 mm, such that half the crack length (*a*) was 12 mm. Given that the radius of the hole was 4 mm, this implies that the length of the crack in front of the hole immediately after crack initiation was about 8 mm. It is interesting to note that for all tests performed in this investigation, *a* was consistently determined to be between 11 and 13 mm at the beginning of crack propagation.

4.6 TEST RESULTS AND PRELIMINARY EVALUATION

In this part of investigation, a total of seven fracture tests were conducted. Five fracture tests were performed on the SuperPave™ coarse-graded mixture: two at a relatively high stress level; two at an intermediate stress level; and one at a low stress level. Two tests were conducted on the SuperPave™ fine-graded mixture: one at a high stress level, the other at an intermediate stress level. As indicated earlier, all tests were performed at 10C. The results of these tests are summarized in Figure 4.17.

Figure 4.17 shows that all five test results for the SuperPave™ coarse-graded mixtures appear to group rather nicely. This is consistent with the notion that fracture parameters are fundamental material properties that should be independent of the stress level or other experimental variables. The two results for the SuperPave™ fine-graded mixtures also appeared to line up well with each other.

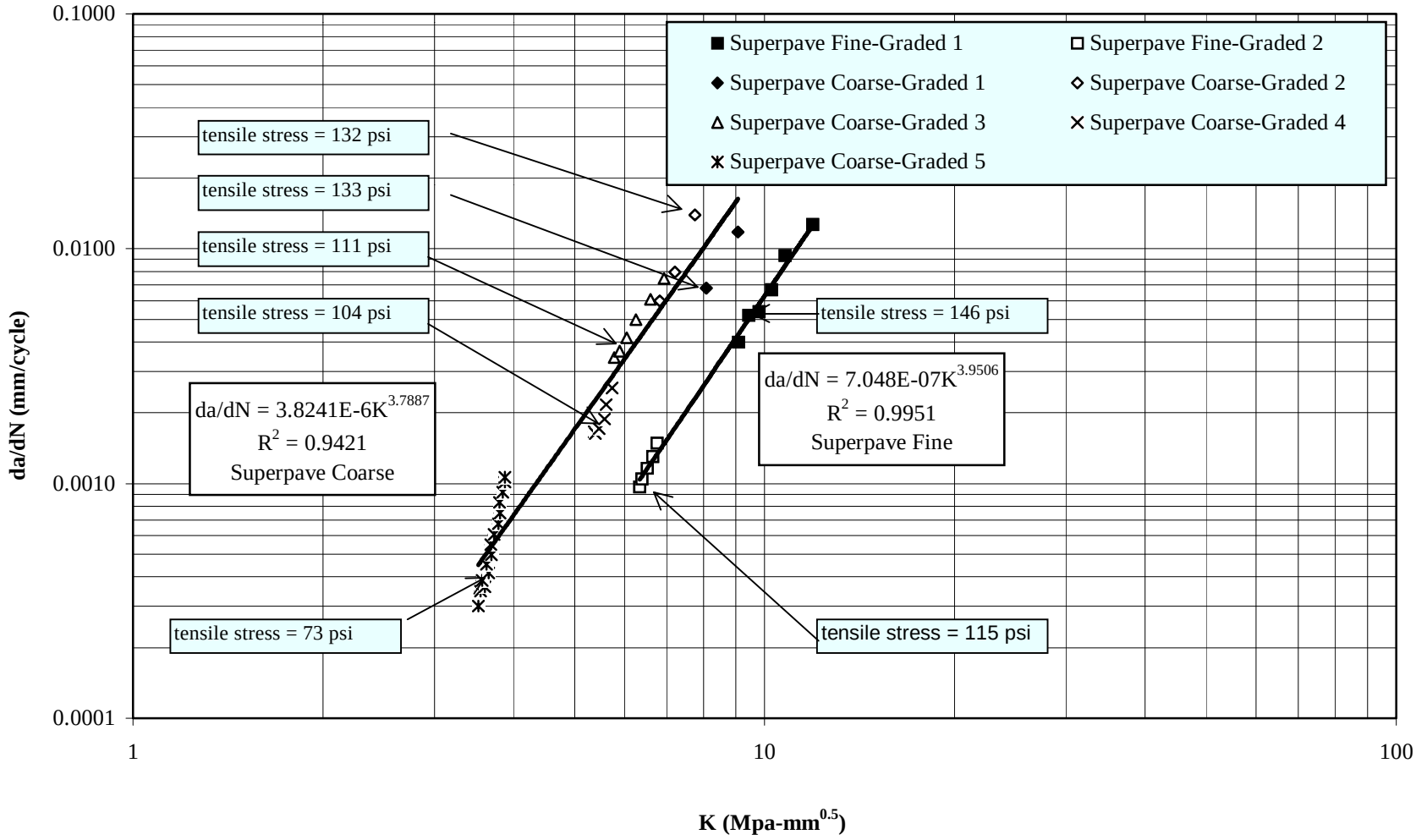

Figure 4.17 Fracture Test Results for SuperPave™ Coarse- and Fine-Graded Mixtures

On the other hand, the values of A and n for individual specimens presented in Tables 4.1 and 4.2, exhibited a significant amount of variability. This appears to imply, that as with most tests performed on asphalt mixtures, some replicate testing would be required to determine A and n reliably. Perhaps A and n determined using the composite results of all tests performed (Tables 4.1 and 4.2) may provide the best estimate of the true A and n for these mixtures. It should be noted that the n based on the composite results was less than the n for any individual tests. It appears that this effect is caused by the results obtained at lower stress levels, which appeared to result in da/dN values that were high relative to those obtained at higher stress levels. The reason for this may be related to the fact that micro-damage may play more of a role in the lower stress tests than in the higher stress tests. Additional work will be required to investigate the effects of stress levels on the determination of fracture parameters. Furthermore, the different fracture parameters, A and n, obtained for a given material at the different stress levels may indicate that A and n are stress-dependent parameters. It is obvious that this finding does not agree with the definition of A and n defined in Paris law, which indicates that A and n are material constants that are determined experimentally. However, this observation does agree with Jacob's work (1995), where he stated that A and n are parameters, depending on the material and on the experimental conditions (waveform, temperature, frequency). Therefore, the other possibility is that Paris law is not fundamental, and some other crack growth law is needed to properly model the crack behavior observed at different stress levels.

Other researchers have reported a broad range in A and n determined from fracture tests. Results obtained in the Netherlands (Jacobs, Hopmann and Molenaar, 1996) indicated that for dense-graded mixtures tested at 15C, the range in n was from 3.5 to 6.8, where most values were between 3.5 to 4.5. For the same mixtures, A ranged from 4×10^{-11} to 5×10^{-7}, where most

Table 4.1 Fracture Test Results for SuperPave™ Coarse-Graded Mixture @ 10C

Specimen No.	Stress Condition	Number of Cycles to Failure	A	n
1	High	1750	1.586×10^{-8}	6.6736
2	High	2750	3.687×10^{-7}	4.7088
3	Intermediate	5500	1.762×10^{-6}	4.3261
4	Intermediate	7750	1.670×10^{-8}	6.8151
5	Low	25000	4.886×10^{-11}	12.41
Composite of All Tests	-	-	3.824×10^{-6}	3.7887

Table 4.2 Fracture Test Results for SuperPave™ Fine-Graded Mixture @ 10C

Specimen No.	Stress Condition	Number of Cycles to Failure	A	n
1	High	2750	3.192×10^{-7}	4.2882
2	Intermediate	12250	6.075×10^{-9}	6.4897
Composite of All Tests	-	-	7.048×10^{-7}	3.9506

values were between 1×10^{-7} and 7×10^{-8}. The fracture parameters for A and n for the SuperPave™ coarse and SuperPave™ fine mixtures (Figure 4.17) are within this range, except that A for the fine-graded mixtures is slightly above the average.

Finally, the data presented in Figure 4.17 clearly show that the fine-graded SuperPave™ mixture has better fracture resistance than the coarse-graded SuperPave™ mixture, even though

the mixtures were produced with the same aggregates and asphalt cement, and were compacted to the same air void content. This appears to imply that aggregate structure may have an important effect on mixture fracture resistance. Although the void content of these mixtures was the same, the void structure was probably not the same. Some coarse-graded SuperPave™ mixtures have been found to have relatively high permeability, indicating the presence of fairly large and interconnected voids. These larger voids create larger stress concentrations that reduce the mixture's resistance to fracture. It appears that the finer-graded mixture had smaller voids that were more dispersed throughout the mixture.

4.7 PRELIMINARY SUMMARY AND CONCLUSIONS

A complete testing, data acquisition, reduction, and analysis system was developed in this study to determine fracture parameters using the SuperPave™ IDT (indirect tension test). The theoretical relationships and data reduction procedures developed preclude the need to measure crack growth rate directly during testing, or the need to obtain or estimate asphalt mixture stiffness or any other property to analyze the fracture test data. These two features not only make fracture testing easier to perform, but it may also be argued that better consistency can be achieved, since the variability introduced by using properties determined from independent tests, as well as the inherent inaccuracies involved in measuring crack growth rate directly, are eliminated. It also eliminates the need to produce and test another set of specimens.

Based on tests performed on two SuperPave™ mixtures, the system developed appeared to provide rational and consistent fracture test results that compared favorably with fracture parameters published in the literature for similar mixtures. Therefore, the system appears to provide a reliable approach for determining fracture resistance of asphalt mixtures produced with the SuperPave™ Gyratory compactor or of field cores obtained from pavements in the field.

Fracture tests performed on SuperPave™ mixtures indicated that the mixture graded on the coarse side of the restricted zone had significantly lower fracture resistance than the mixture graded on the fine side of the restricted zone. Both mixtures were produced with the same aggregate and asphalt cement and compacted to the same air void content. Therefore, it appears that the resulting void structure of these two mixtures may be significantly different, where the coarser-graded mixtures had larger voids that increased stress concentrations and reduced the mixture's resistance to crack propagation.

As a final note it must emphasize that great care must be taken in analyzing and reducing fracture data to obtain good results. In addition, it appears that as with most properties determined for asphalt mixtures, multiple tests are required to determine A and n reliably.

CHAPTER 5

FINDINGS AND ANALYSIS

5.1 INTRODUCTION

Crack growth parameters of eight field sections and four SuperPave™ mixtures (Three aged and three unaged specimens were tested in each mixture) were determined using the method developed in Chapter 4.

The fracture test results of eight field cores show the discrepancies between the laboratory tests and the field performance. Therefore, a considerable amount of effort had been expended to investigate the source of this discrepancy as it was felt that it would lead to the understanding necessary to relate laboratory to the field results, this includes: (1) evaluation of the fracture test results (Section 5.3); (2) verification of the threshold concept (Section 5.4); (3) evaluation of dissipated creep strain energy as a threshold (Section 5.5); (4) evaluation of yield strength as a threshold (Section 5.6); (5) re-evaluation of dissipated creep strain energy as a threshold (Section 5.7).

Given the analyses presented above, a fairly complete knowledge of cracking performance in the field was achieved by verifying and identifying threshold. Therefore, this knowledge could be the foundation to set up a cracking model for asphalt concrete pavement.

5.2 FRACTURE TEST RESULTS

The fracture test results of eight field sections and four SuperPave™ mixtures (including aged and unaged specimens in each mixture) are presented in this section.

5.2.1 Fracture Test Results on the Eight Field Sections

Forty-eight fracture test results performed on the field cores from each of eight test sections are summarized in Appendix A. The plots of crack growth rate (da/dN) versus the number of load replications (N), using the method presented in Chapter 4, for each section are shown in Figures A.1 to A.8 in Appendix A. The cracking performance of these eight field sections and other mixture properties are summarized in Sedwick's work (1998). At least four fracture tests were performed for each of the test sections. However, a different number of tests are presented for each test section because not all tests were considered to be valid. The test results were considered to be valid when the horizontal failure was clearly observed to occur on both sides of the specimen simultaneously before failure was observed on two vertical deformation measurements. A detailed examination of the deformation measurements is presented in Section 5.3 as a part of the evaluation of the fracture test results. The test results presented in Figures A.1 to A.8 in Appendix A are only the results of valid tests.

Since for a given material, temperature and load function, there is only one value of fracture parameters. It was decided that the fracture parameters would be obtained by averaging individual fracture tests from each test section. An example is illustrated in Figure 5.1, which had three individual valid tests in this case. Linear regression relationship between da/dN vs. K was obtained using the method developed in Chapter 4. The procedure for obtaining the average A and n involves the following steps:

Step 1: for each fracture test result

1. Identify the range of K. K is correspondent to half of the crack length (a) from 12mm (i.e., K equals to $K_{b,}$ beginning point) to 24mm (i.e., K equals to $K_{e,}$ ending point).
2. Divide the range of K into three equal increments, which is equal to $(\log K_e - \log K_b)/3$.

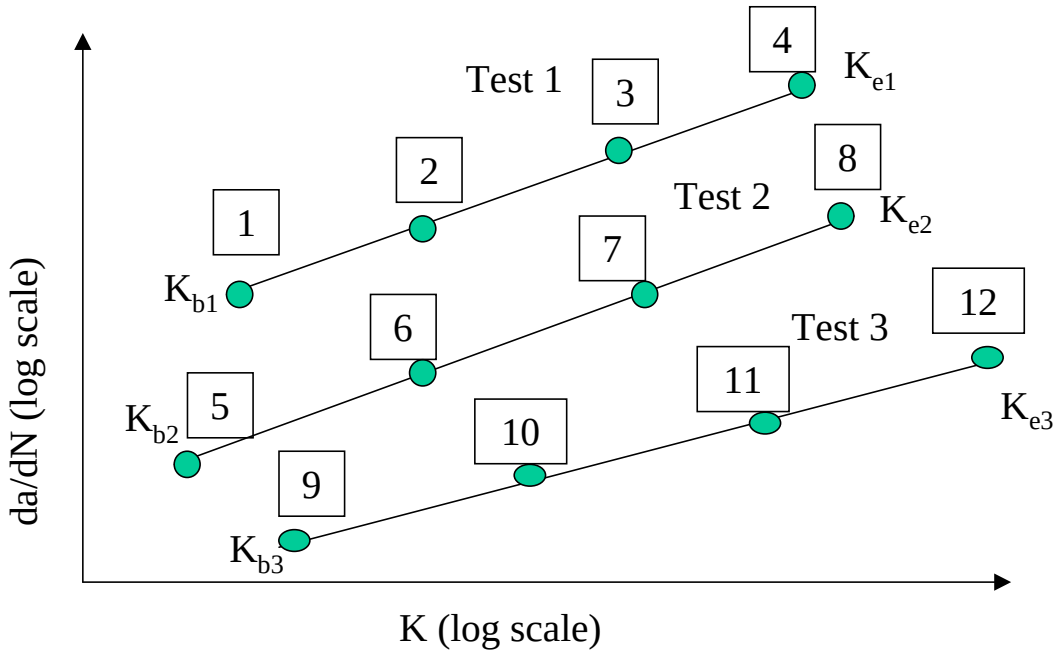

Figure 5.1 Determination of Average da/dN vs K

3. On linear regression, obtain da/dNs corresponding to the K values which divide regression line, from K_b to K_e, into three equal space.

   i.e., at point 1, da/dN at log K_b

   at point 2, da/dN at (log K_b + (log K_e - log K_b)/3)

   at point 3, da/dN at (log K_b + 2*(log K_e - log K_b)/3)

   at point 4, da/dN at log K_e

Step 2: repeat Step 1, obtain K and corresponding da/dN values for all valid tests. For example, in the case where there are three valid tests, a total of twelve points (i.e., twelve da/dNs and Ks) are obtained.

Step 3: Use the data (da/dNs and Ks) obtained in Step 2, run linear regression analysis to obtain average fracture parameters, A and n, for all valid tests.

Figure 5.2 shows the average fracture results for all field test sections along with the results for a SuperPave™ fine-graded mixture and a SuperPave™ coarse-graded mixture. For comparison purposes, the values of crack growth rate were obtained at a stress intensity factor of K=8 Mpa-mm$^{0.5}$ for the all test sections. Because K was around 8 Mpa-mm$^{0.5}$ when cracks propagate for most of the sections, according to our data analyses results.

From Figure 5.2, it was found that (1) the I-10 Madison County West section (I-10MW) exhibited the best fracture resistance (the lowest rate of crack propagation da/dN) while the I-10 Duval County East section (I10DE) exhibited the worst fracture resistance (the highest rate of crack propagation da/dN); (2) both US301 sections and the I-95 Saint Johns section (I-95SJ) exhibited similar values of crack growth rate, while the I-10 Madison County East section (I-10 ME), the I-10 Duval County West section (I-10DW) and the I-95 Duval West section (I-95 Duval W) also exhibited similar values of crack growth rate; (3) the I-10 Madison County East

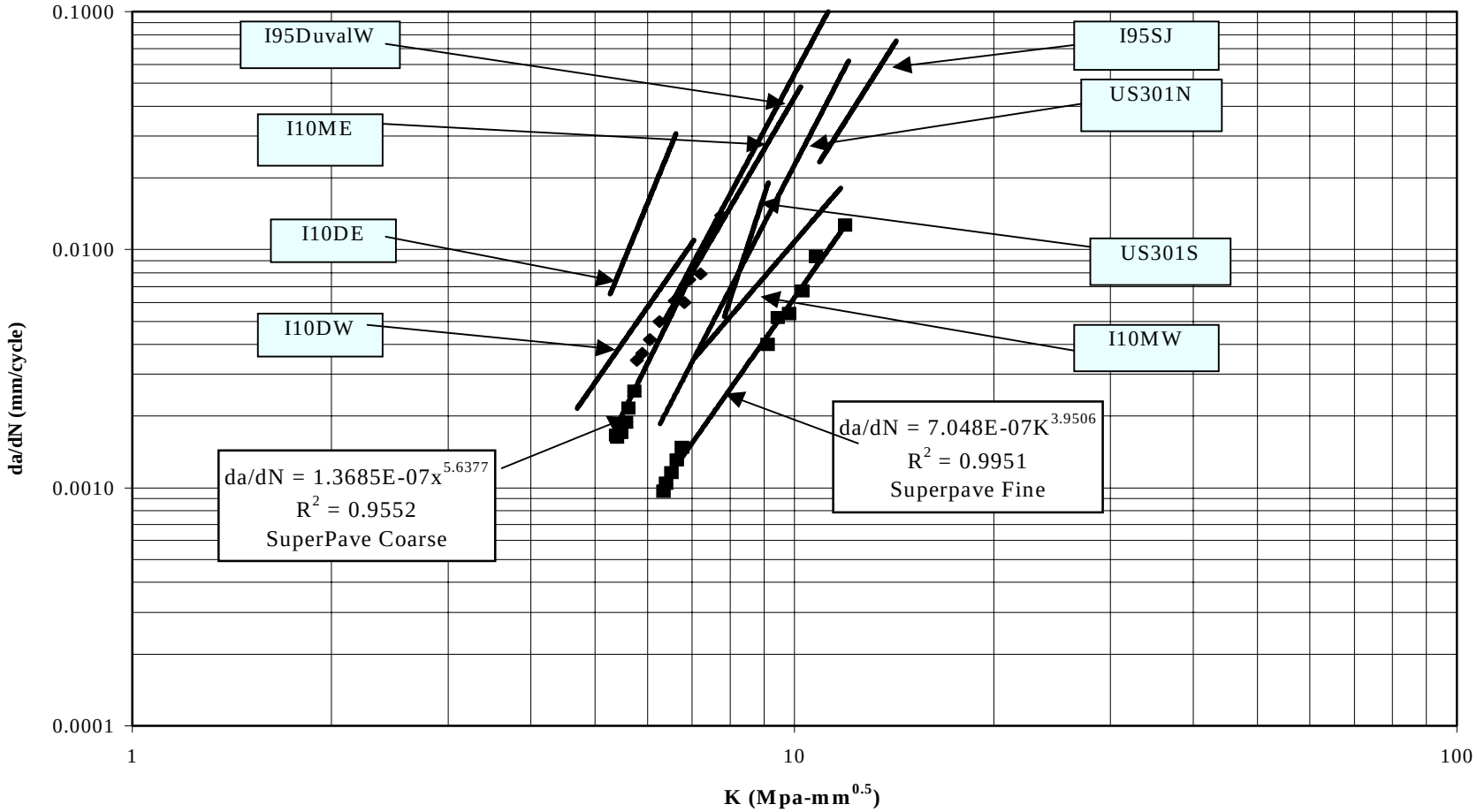

Figure 5.2 Fracture Test Results for the Mixtures from Eight Field Sections

section (I-10 ME), the I-10 Duval County West section (I-10 DW) and the I-95 Duval West section (I-95 Duval W) exhibited higher laboratory crack growth rates than both of the US301 sections and the I-95 Saint Johns (I-95 SJ) section.

5.2.2 Fracture Test Results on the SuperPave™ Coarse and SuperPave™ Fine Mixtures

Two SuperPave™ coarse mixtures and two SuperPave™ fine mixtures (aged and unaged) were used to perform the fracture tests using the SuperPave™ IDT (Honeycutt, 2000). Based on Honeycutt's research, she found that, in general, m-value, creep strain energy, fracture energy and crack growth rate of a mixture reduced with aging.

5.3 EVALUATION OF THE FRACTURE TEST RESULTS

Evaluation of the fracture test results presented in this section includes: (1) examination of the fracture test results (Section 5.3.1); (2) evaluation of permanent deformation (Section 5.3.2); (3) evaluation of Paris law (Section 5.3.3); (4) evaluation of alternative crack growth laws (Section 5.3.4.); and (5) introduction of the threshold concept (Section 5.3.5).

5.3.1 Examination of the Fracture Test Results

As presented in the above section, I-10 MW exhibited the best fracture resistance (lowest rate of crack propagation da/dN) while I-10 DE exhibited the worst fracture resistance. The I-10 MW section was the best performer in the field, while I-10 DE was one of the worst. However, it was noted that not all the fracture test results agreed with field performance. Most notably, I-95 Duval W exhibited higher laboratory crack growth rate than both the US301 sections and the I-95 SJ section. The I-95 Duval W section was considered to be an excellent performer in the field, while the US301 sections were among the worst.

A contradiction was also observed in the fracture test results of the SuperPave™ mixtures. Honeycutt's (2000) concluded that the laboratory measured crack growth rates alone cannot adequately describe cracking resistance of asphalt mixtures.

The fact that laboratory crack growth rates did not correlate with the observed field cracking performance and did not agree with the expected trends for the SuperPave™ mixtures indicated that (1) crack growth rates obtained from the SuperPave™ IDT may be invalid; (2) Paris law of crack propagation (i.e., $da/dN = A(K)^n$) may not be generally valid or at least that it may not be directly applied (in the current form) to predict cracking performance of pavements in the field. Therefore, investigations were undertaken to evaluate the validity of the data (in this section) and the validity of the Paris law of crack propagation (Section 5.3.2 and Section 5.3.3).

Careful re-examination of the fracture test results indicated that the test results were valid. It is strongly believed that the measured crack growth rates are representative of the true crack growth rates of the asphalt mixtures tested. In addition, results of multiple tests in each section indicate that da/dN is consistent between specimens of the mixture.

In further attempts to verify the validity of the test results, regression analyses were conducted, using SAS (Statistical Analysis System), to evaluate relationships between mixture properties and crack growth rate. Empirical and theoretical relationships presented in the literature (Jacobs, 1995) have indicated that laboratory measured crack growth rates are related to mixture tensile strength, modulus, m-value and fracture energy density. Therefore, measured values of these parameters were used to check whether these relationships resulted in reasonable correlation for the mixtures tested. The predicted crack growth rate da/dN versus the measured crack growth rate da/dN, the relationships between predicted crack growth rate (da/dN) and mixture properties, corresponding to K=7 Mpa-mm$^{0.5}$ and K=9 Mpa-mm$^{0.5}$, respectively, are

presented in Appendices B through E. The reason for selecting these two K values is that the average value of K applied in the laboratory was about 8 Mpa-mm$^{0.5}$.

The relationship presented in Figure 5.3 shows that these parameters are reasonably correlated with the crack growth rate for the ten mixtures tested (eight field sections and two SuperPave™ mixtures). Since the measured crack growth rate da/dN for I10DE appeared to be unusually high compared to all other measured da/dNs, a second relationship was developed without including this result. The resulting relationship is shown in Figure 5.4, which shows that the correlation improved slightly, but the general form of the relationship remained the same. The fact that reasonable correlations were obtained using these relationships from the literature, is further evidence that the results obtained are consistent with other laboratory test results presented in the literature. Once again, this provides support that the measured crack growth rates are valid.

5.3.2 Evaluation of Horizontal Permanent Deformation

This section (Section 5.3.2) concentrates on evaluating the validity of different fracture laws. One possibility was that Paris law parameters determined in the laboratory were not applicable to the field because of differences in restraint conditions between the laboratory specimen and the asphalt mixture in the real asphalt pavement. The specimen is essentially unrestrained in tension in the indirect tensile test such that the crack is allowed to open in an unrestrained manner. Therefore, one possibility is that the crack growth process is primarily governed by permanent deformations that occur in the laboratory specimen but may not allowed to occur in the field. Therefore, mixtures with high m-values or high creep rates would exhibit high da/dN in the laboratory but may perform well in the field because permanent deformation is not allowed to develop to the same degree as in the laboratory.

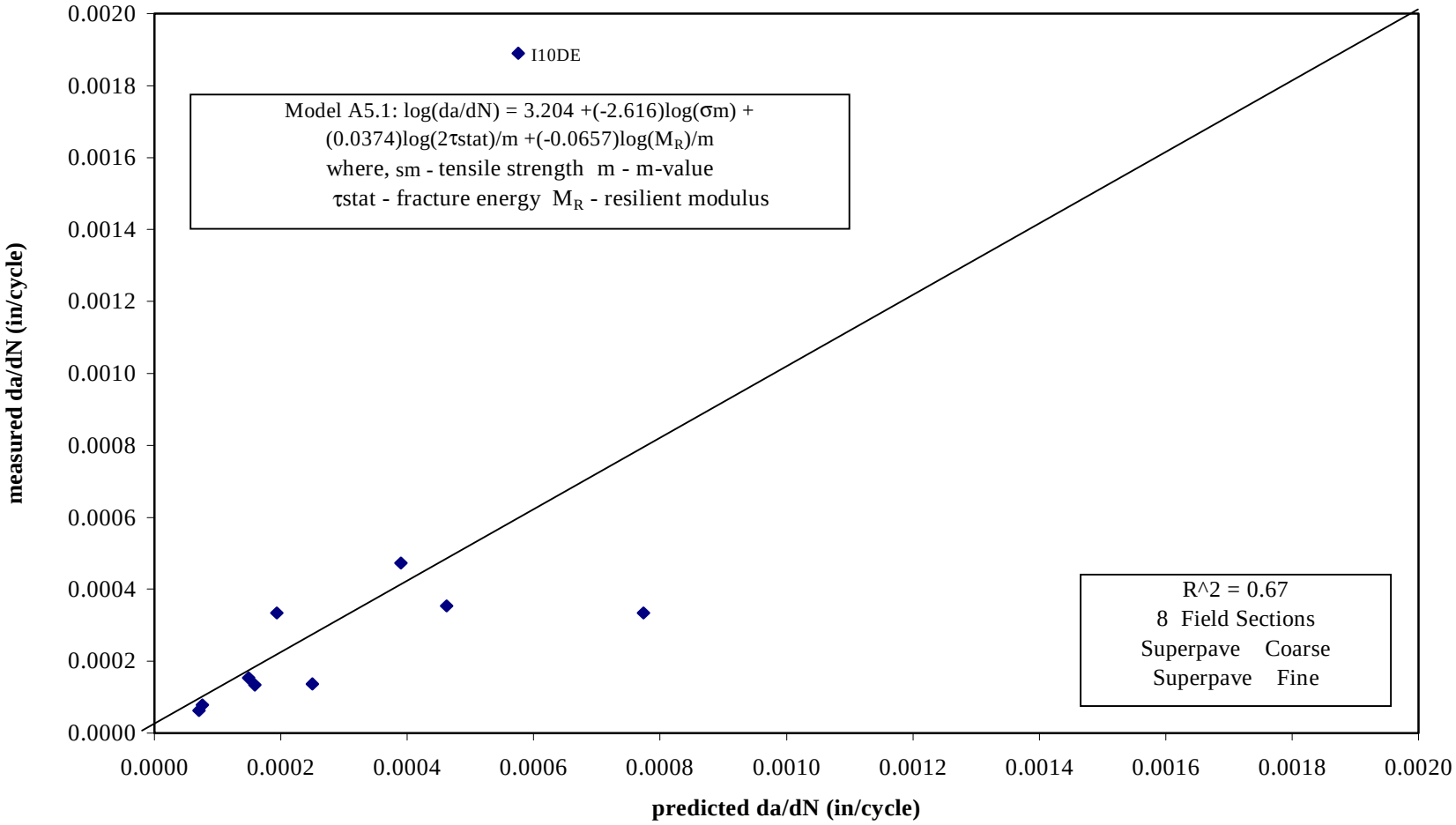

Figure 5.3 Relation Between Measured da/dN and Predicted da/dN from Model A5.1

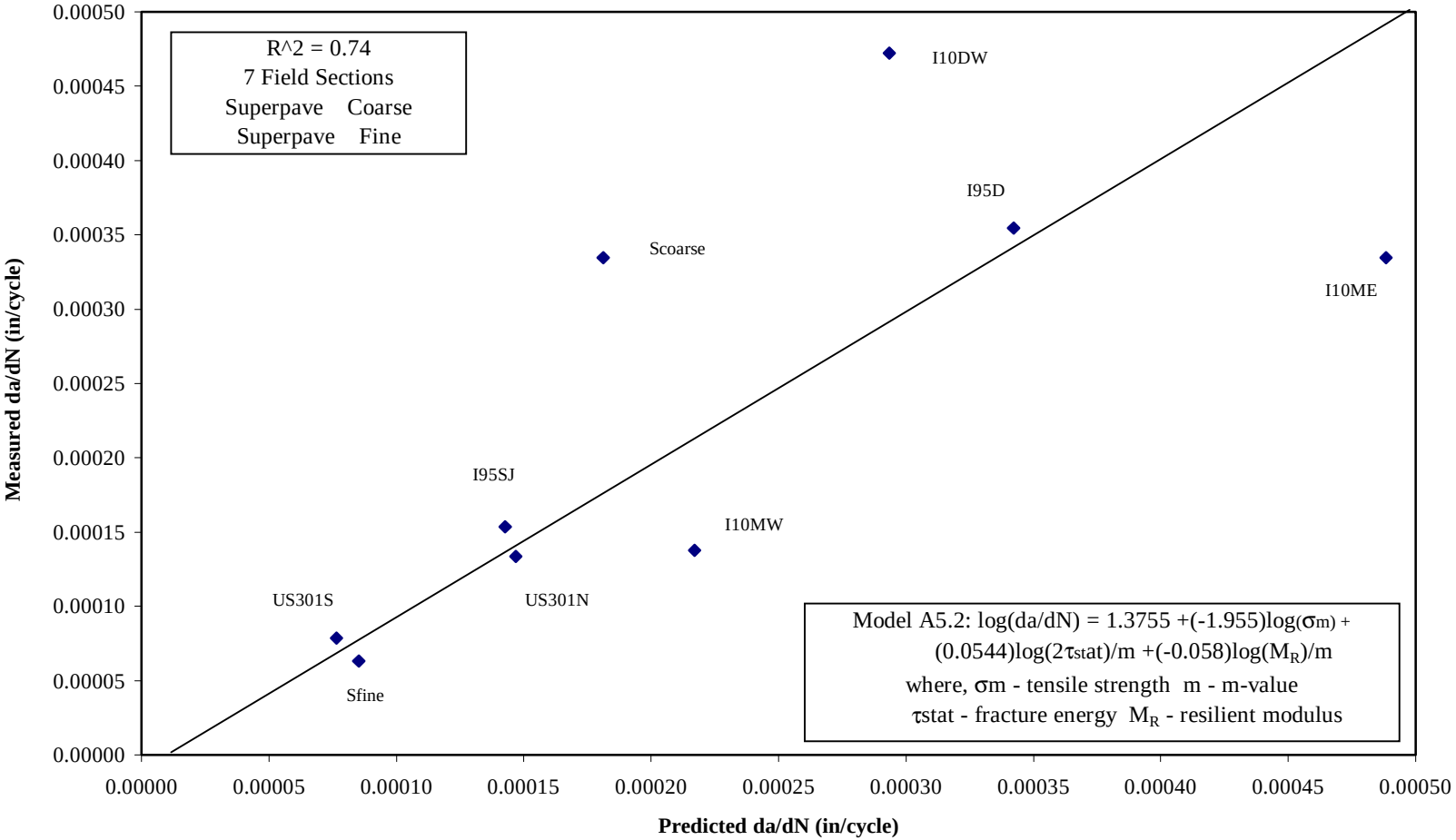

Figure 5.4 Relation Between Measured da/dN from Model A5.2

Given the explanation presented above, a careful examination of horizontal permanent deformation was conducted. The typical results are shown in Appendix F. Figures 5.5 and 5.6 exhibit the permanent deformation versus recorded points of two typical fracture tests (the m-value and tensile strength are presented in Table 5.1). One test was performed on a material with higher m-value and lower tensile strength ("ductile" material), while the other test was performed on a material with lower m-value and higher tensile strength ("brittle" material). Figure 5.5 shows that the rate of permanent deformation of a "ductile" material (e.g., I-10 Duval W) kept increasing until the specimen failed, while the rate of permanent deformation of a "brittle" material (e.g., US301N) remained constant for about two-thirds of the total testing time, and then increased rapidly until the specimen failed. Figure 5.6, which shows permanent deformation versus recorded points for 5 cycles, verifies the above observation by showing that a "ductile" material accumulated more permanent deformation per cycle than a "brittle" material. Therefore, it appears that under cyclic loading condition (laboratory test condition), if the applied load is very low, a "brittle" material may never fail while accumulation of permanent deformation in a "ductile" material might always result in failure. The further implication of this finding may reveal that if a certain strain or energy criterion is not exceeded, cracking may never occur.

The rate of permanent deformation was used to further investigate the process of permanent deformation. The creep compliance curves for the eight sections varied significantly (Figure 5.7). It should be noted that the slope of the creep compliance curve at longer loading time (e.g., 1000 seconds) is essentially a measure of the rate of permanent deformation: the higher the slope, the higher the rate of permanent deformation. Furthermore, it appears that these differences may in some cases explain the apparent discrepancies between laboratory crack growth rate and field performance. For example, the US301 sections and the I95SJ sections exhibited

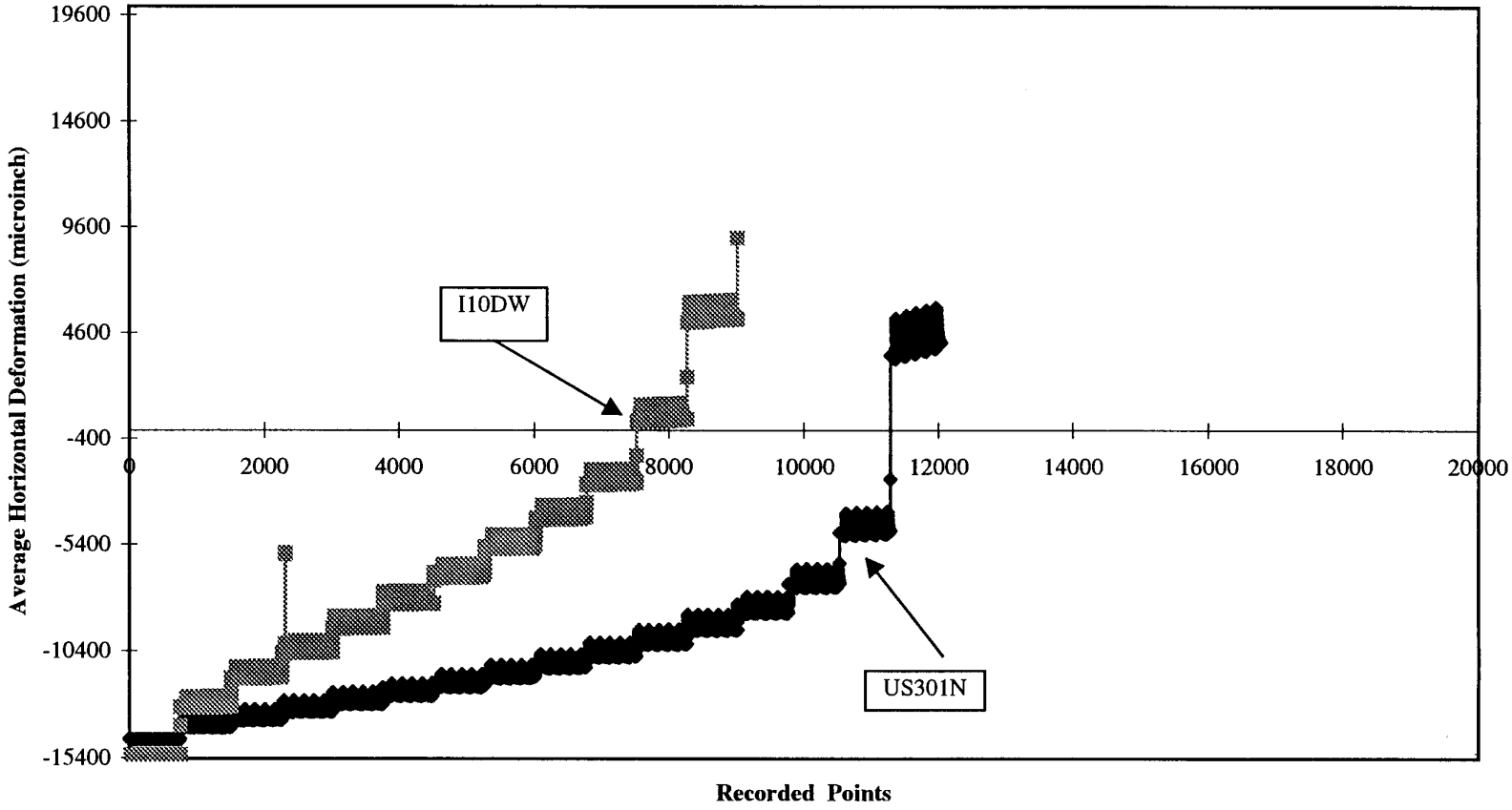

Figure 5.5 Average Deformation vs. Recorded Points

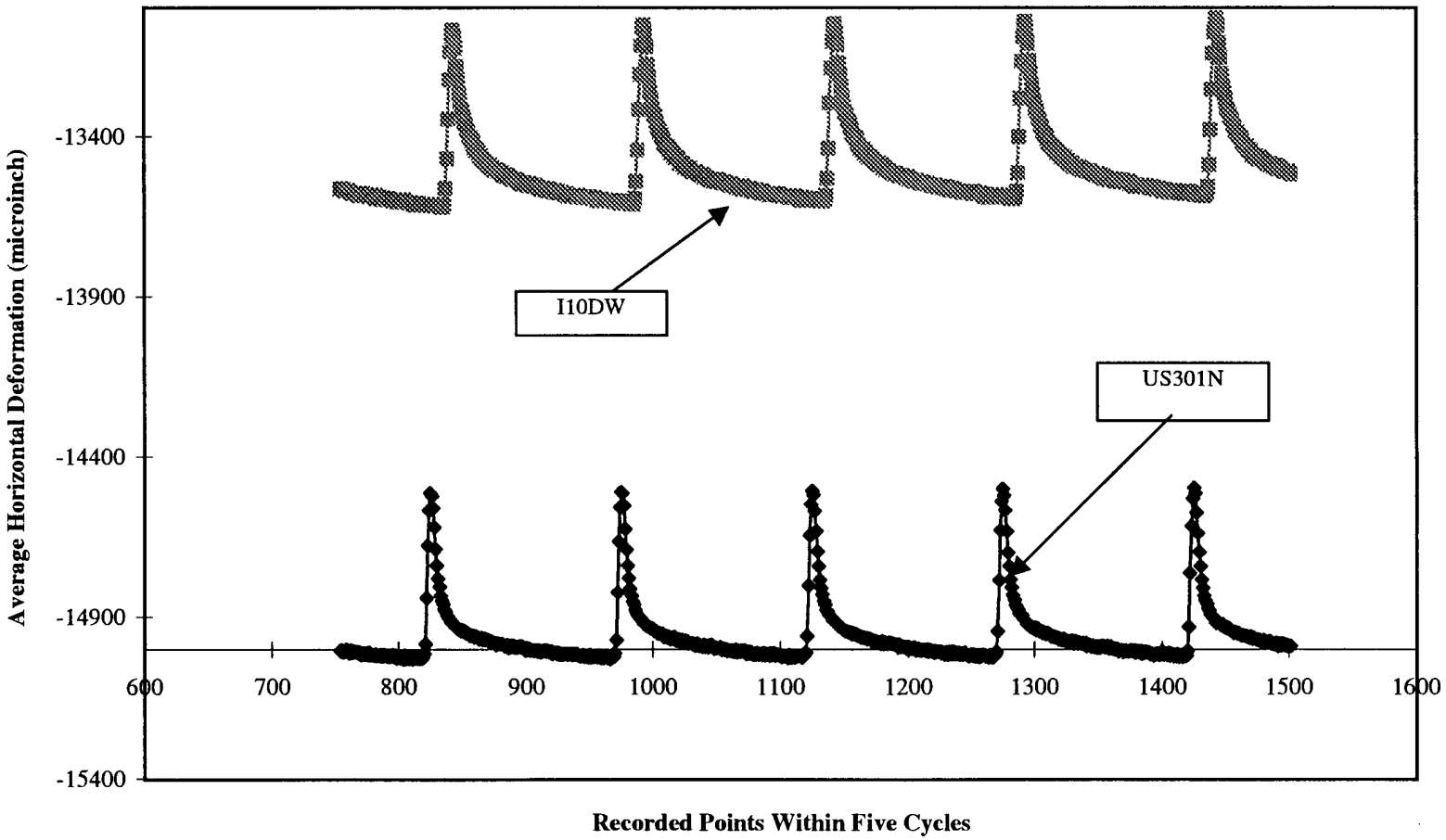

Figure 5.6 Average Deformation vs. Recorded Points Within Five Cycles

Table 5.1 Summary of m-Value, Tensile Strength, Yield Strength and Average Stress

SECTION	m-Value	Tensile Strength (psi)	Yield Strength (psi)	Average Stress (psi)
SuperPave™ Coarse 1	0.80	238	374	274
SuperPave™ Coarse 2	0.77	247	283	222
SuperPave™ Fine 1	0.66	302	392	282
SuperPave™ Fine 2	0.56	271	410	302
SuperPave™ Coarse 1 (A)	0.55	306	615	406
SuperPave™ Coarse 2 (A)	0.58	299	575	385
SuperPave™ Fine 1 (A)	0.57	299	337	251
SuperPave™ Fine 2 (A)	0.50	371	605	410
I-10 MW	0.60	264	795	541
I-95 D	0.49	189	492	342
I-95 SJ	0.47	281	578	421
I-10 DE	0.55	181	238	185
I-10 DW	0.46	193	282	210
I-10 ME	0.61	171	No Data Available	
US301 BN	0.26	164	240	206
US301 BS	0.18	135	No Data Available	

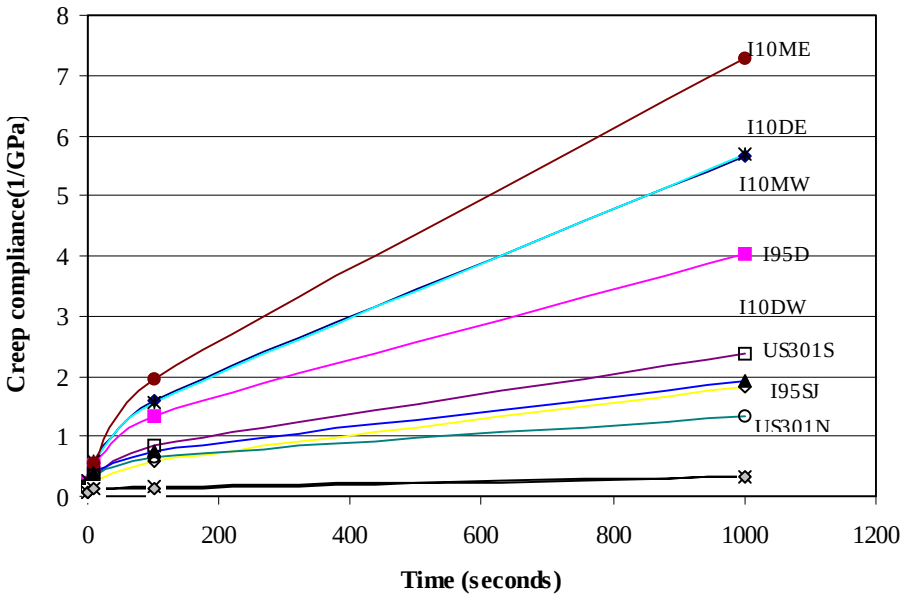

Figure 5.7 Creep Compliance vs. Time

the lowest rate of permanent deformation, while the I-95 Duval (I-95 D) section exhibited a significantly higher rate of permanent deformation. As indicated earlier, the I-95 D section exhibited higher crack growth rate in the laboratory than the US301 sections or the I-95 SJ section, but better field performance than all three. On the other hand, the I-10 MW section had one of the highest rates of permanent deformation, yet it exhibited the best performance of all sections. Obviously, permanent deformation may not be the whole story, or at least it may not explain the apparent discrepancies in performance for all mixtures. I-10 MW had extremely high tensile strength, high stiffness (resilient modulus), and high fracture energy density, and these factors apparently overcame the effects of high permanent deformation in the laboratory. In addition, I-10 MW is a very fine-graded mixture compared to the I-95 sections or the US301 sections. Therefore, perhaps the influence of permanent deformation on crack growth rate is mixture-dependent. In other words, permanent deformation, tensile strength, resilient modulus and fracture energy density could have a combined effect on the crack growth rates obtained from the laboratory tests.

5.3.3 Evaluation of Paris Law

As indicated earlier, based on the fracture test results, it was decided that further investigations were necessary to evaluate the validity of the data and the validity of Paris law. Evaluation of the validity of fracture test results described in Section 5.3.2 verified the results are valid, therefore, this section concentrates on evaluating the validity of Paris law.

Several correlations between mixture properties and crack growth rates were evaluated to not only further verify the validity of the data but also help to further understand the mechanism of cracking performance in laboratory and field. As mentioned earlier, theoretical and empirical work (Jacobs, 1995) has indicated that crack growth rate is a function of tensile strength, m-

value (slope of the linear portion of the log compliance-log time curve), fracture energy density and resilient modulus.

Regression analyses were conducted to determine relationship between the mixture properties (tensile strength, m-value, fracture energy density and resilient modulus) and measured crack growth rates (Figures 5.3 and 5.4). In these analyses, the values of K=7 Mpa-mm$^{0.5}$ and K=9 Mpa-mm$^{0.5}$ were selected. In addition, since the measured crack growth rate (da/dN) for I-10 DE appeared to be unusually high compared to other values, a second relationship of the same general form, was also developed. Additional details of the relationships are presented in Appendices B to E.

As mentioned in Section 5.3.1 , the form of the relationships were similar to the relationships presented by researchers in the literature (Jacobs, 1995), and Figures 5.3 and 5.4 show that crack growth rates predicted from the resulting relationship agree with measured crack growth rates. It was observed that the relatively low R^2 (0.67 and 0.77 for 10 and 9 mixtures, respectively) was expected because of the variability of mixture testing and relatively small number of test sections. However, the fact that the predicted and measured values are correlated is evident, even though the correlation is not suitable for prediction purposes.

Sensitivity analyses were also conducted with the relationship to evaluate the influence of mixture properties on crack growth rate. As an example, the relationship between crack growth rate and tensile strength using the relationship presented in Figure 5.3 was obtained by varying tensile strength while holding the other parameters (i.e., m-value, resilient modulus and fracture energy density) constant at a value corresponding to the average value of the ten mixtures tested. The range in tensile strengths used corresponded to the range in values measured for the ten mixtures tested. Results of these analyses are shown in Figures 5.8 through 5.11 for the relationship

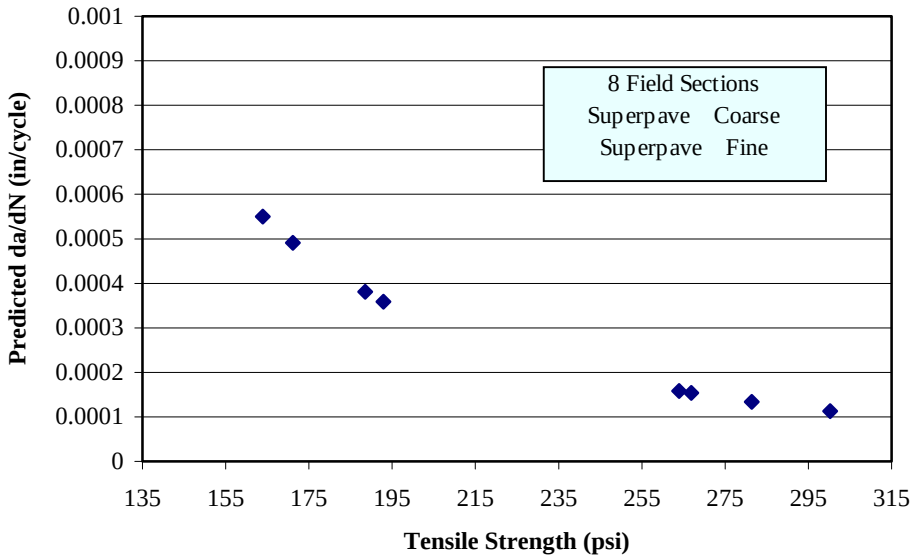

Figure 5.8 Relation Between Predicted da/dN vs. Tensile Strength Using Model A5.1

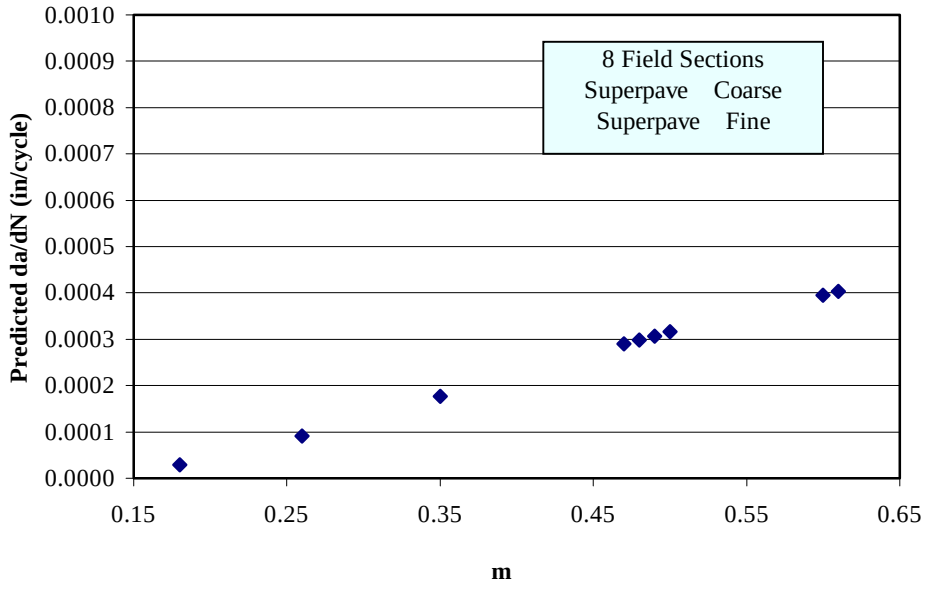

Figure 5.9 Relation Between Predicted da/dN vs. m-Value Using Model A5.1

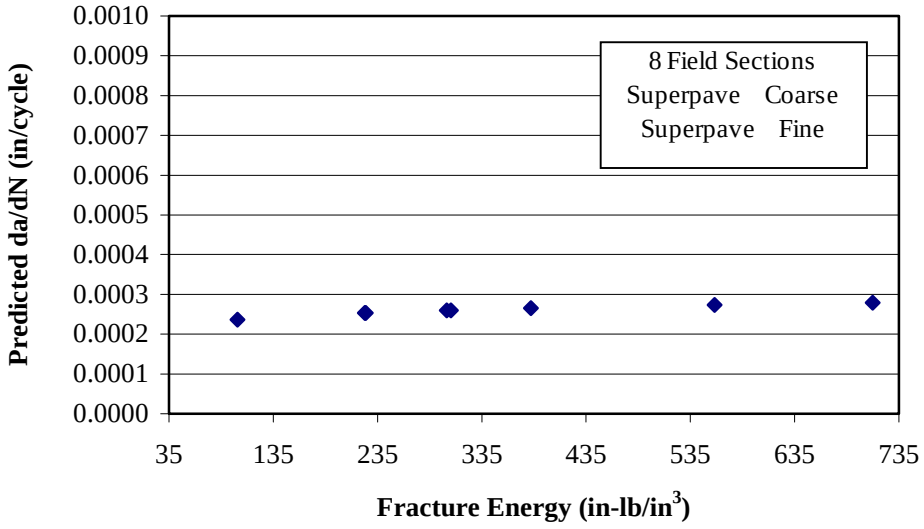

Figure 5.10 Relation Between Predicted da/dN vs. Fracture Energy Density Using Model A5.1

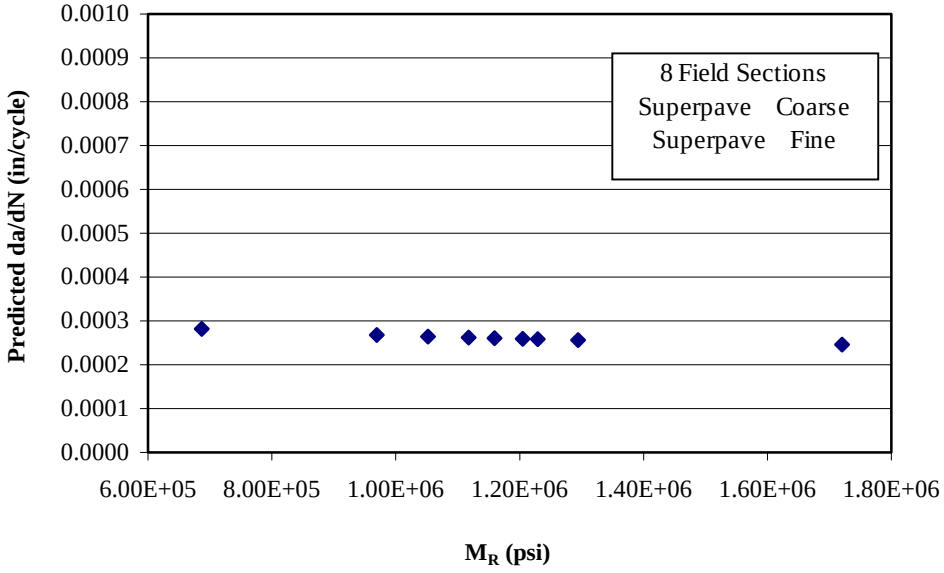

Figure 5.11 Relation Between Predicted da/dN vs. Resilient Modulus Using Model A5.1

presented in Figure 5.3. As shown in these figures, it appears that crack growth rate da/dN was primarily related to the tensile strength and m-value of the mixture, while fracture energy density had only a minor effect and resilient modulus had little or no effect on crack growth rate da/dN.

Therefore, another different form of relationship was attempted which did not include resilient modulus as a variable. The results is shown in Figure 5.12, which shows that the correlation coefficient R^2 was the same as when resilient modulus was included, verifying that resilient modulus had no effect on crack growth rate da/dN. Results of sensitivity analyses performed on this new relationship presented in Figures 5.13 through 5.15 indicated that da/dN was almost entirely controlled by tensile strength and m-value, while fracture energy density had no effect on crack growth rate da/dN.

Finally, the last relationship was developed using only tensile strength and m-value (Figure 5.16). Figure 5.16 shows the same correlation coefficient R^2 as when fracture energy density was included. Figures 5.17 and 5.18 indicate that crack growth rate (da/dN) is controlled by tensile strength and m-value. In fact, it was noted that the same correlation coefficients R^2 were obtained for these three models, which further confirmed that crack growth rate da/dN was dominated by tensile strength and m-value.

Results of sensitivity analyses for these three relationships indicate that crack growth rate da/dN decreases as tensile strength increases and m-value decreases. This is a reasonable outcome, it is expected that mixtures with higher strength have better crack propagation resistance than mixtures with lower strength. The relationship between m-value and crack growth rate (i.e., higher m-value, higher crack growth rate) may be explained by the fact that m-value is essentially a measure of the rate of creep or permanent deformation of the mixture. Therefore, mixtures that exhibit higher rates of permanent deformation also exhibit higher crack growth rates.

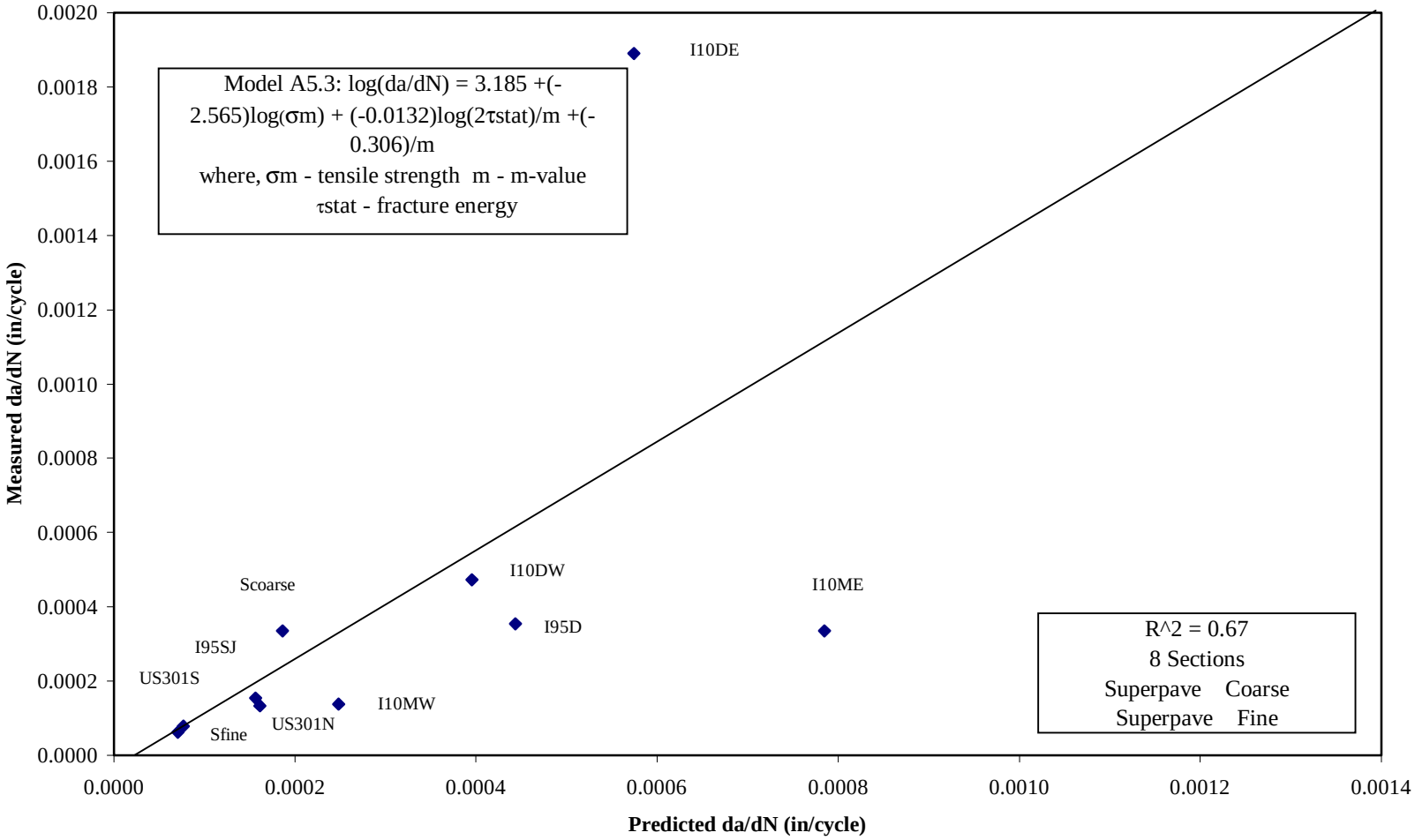

Figure 5.12 Relation Between Measured da/dN and Predicted da/dN from Model A5.3

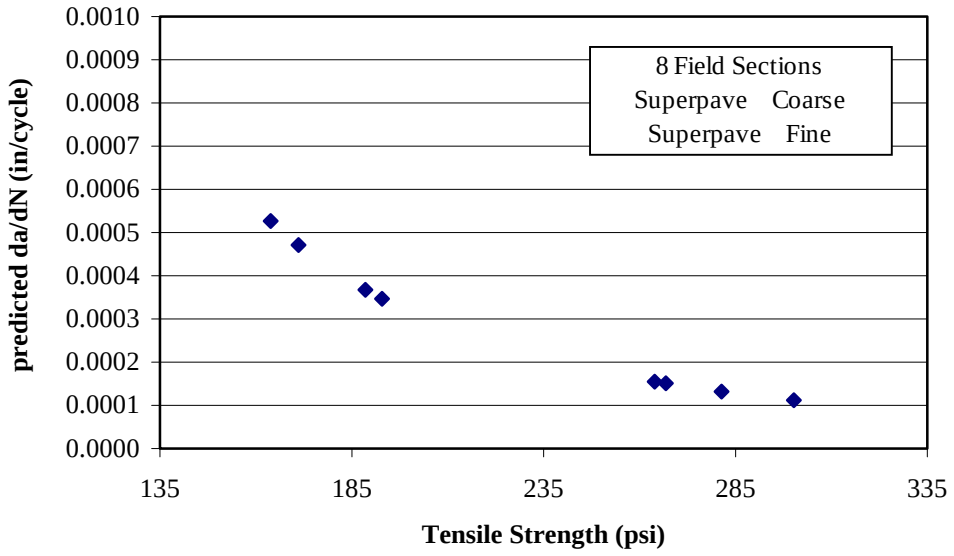

Figure 5.13 Relation Between Predicted da/dN vs. Tensile Strength Using Model A5.3

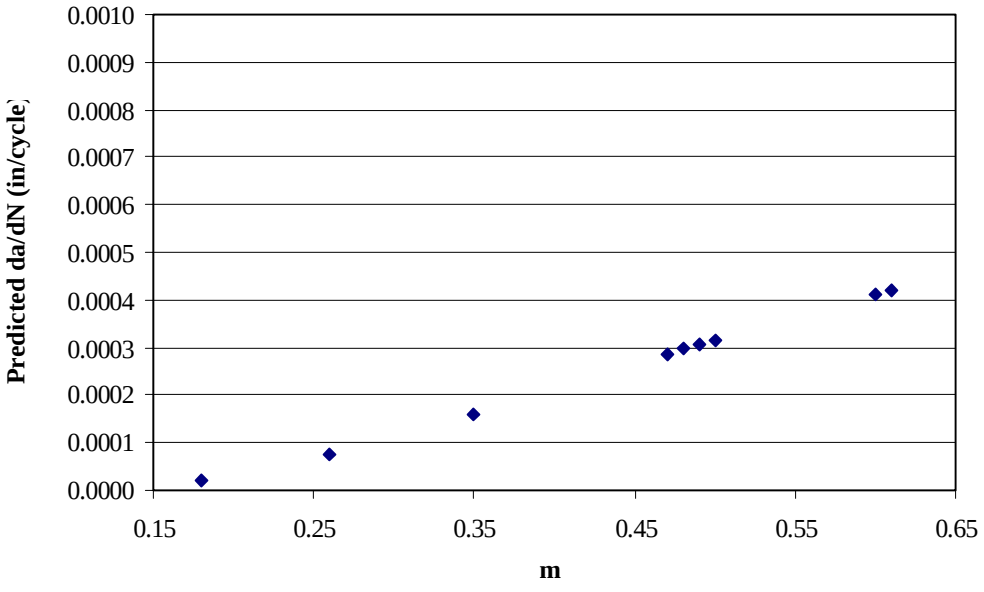

Figure 5.14 Relation Between Predicted da/dN vs. m-Value Using Model A5.3

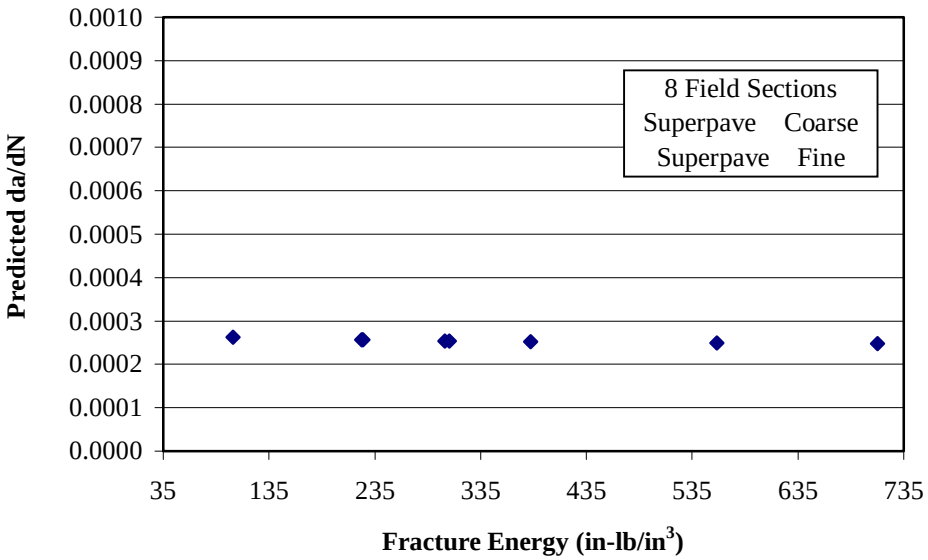

Figure 5.15 Relation Between Predicted da/dN vs. Fracture Energy Density Using Model A5.3

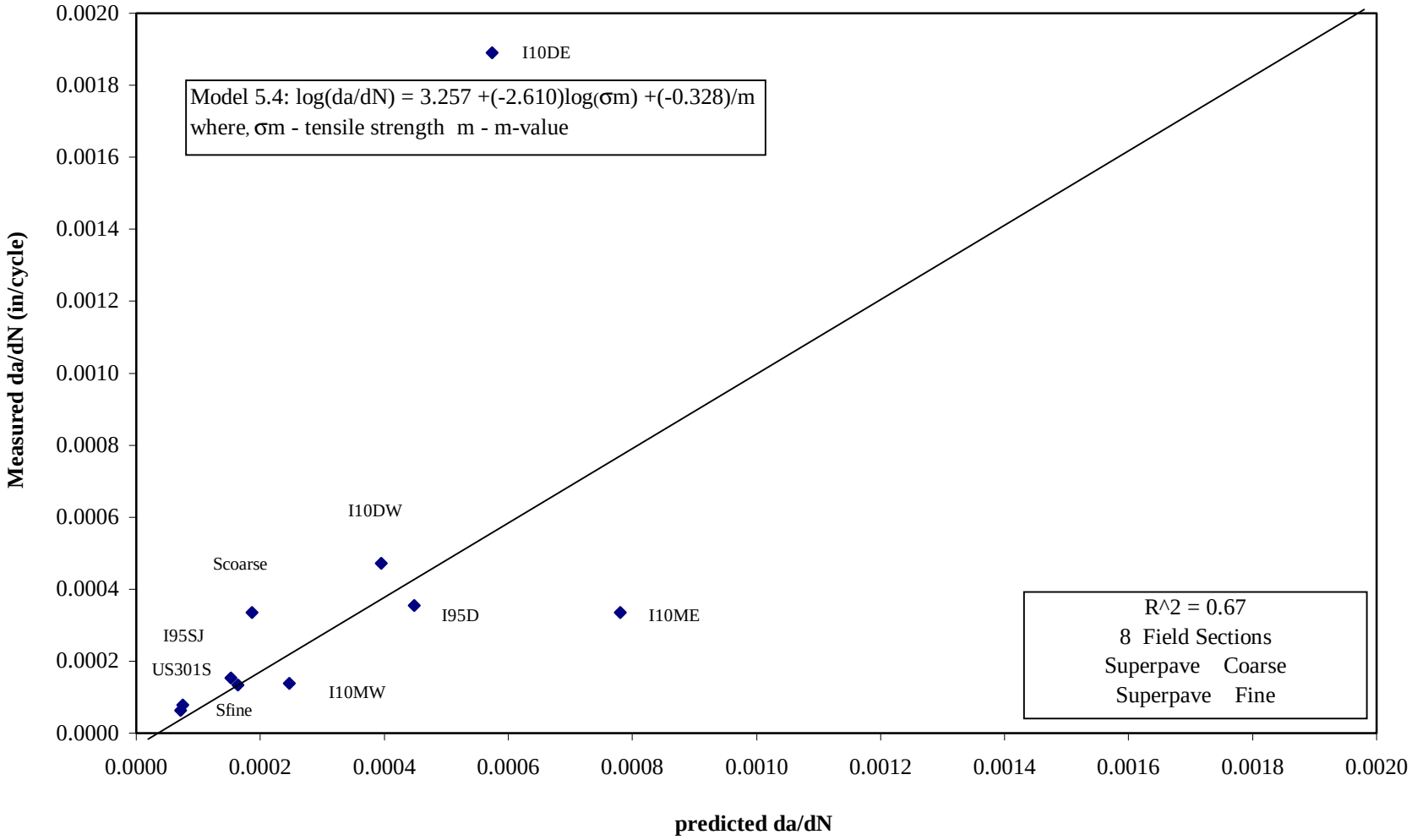

Figure 5.16 Relation Between Measured da/dN and Predicted da/dN from Model A5.4

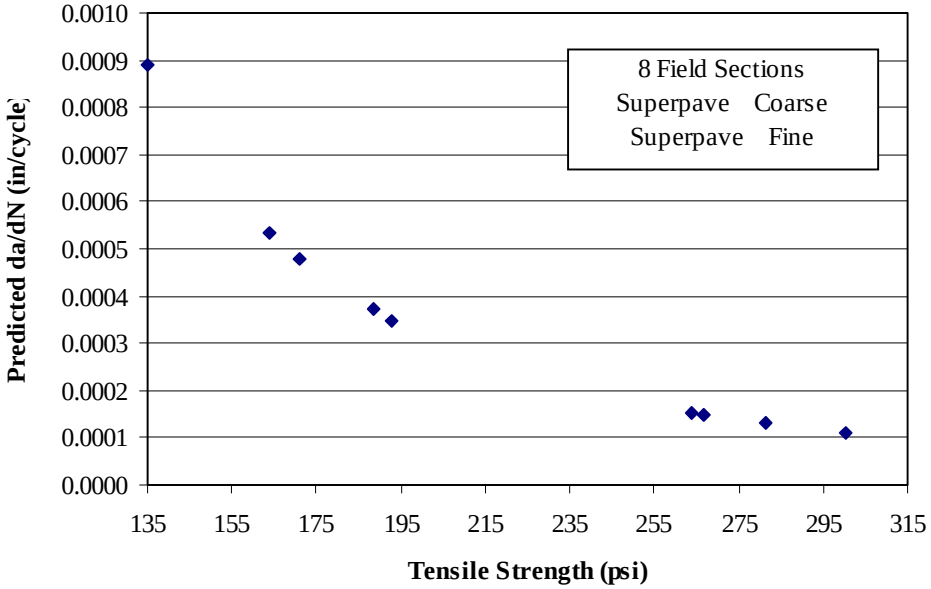

Figure 5.17 Relation Between Predicted da/dN vs. Tensile Strength Using Model A5.4

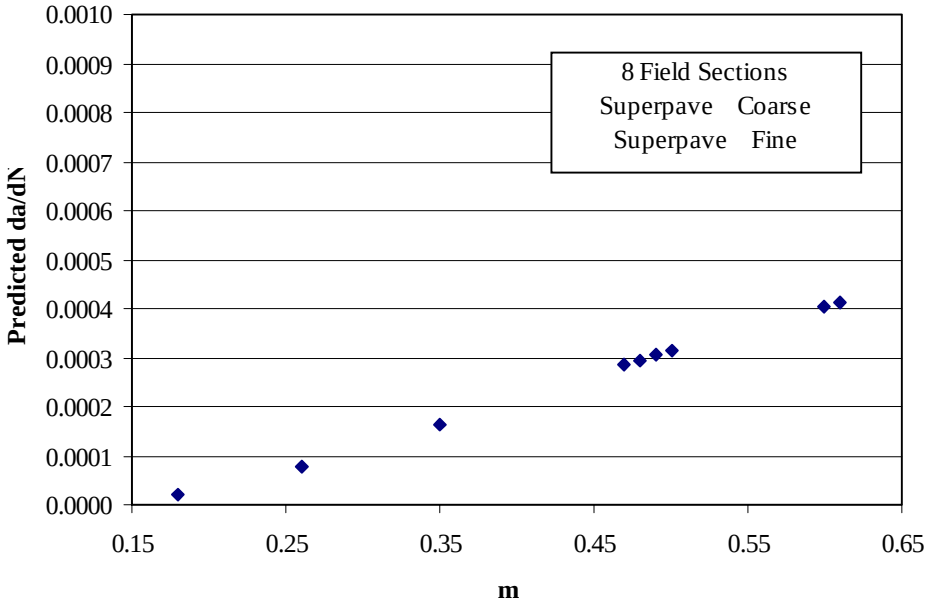

Figure 5.18 Relation Between Predicted da/dN vs. m-Value Using Model A5.4

5.3.4 Evaluation of Alternative Crack Growth Laws

As indicated earlier, it was noted that Paris law may not be directly applied to predict cracking performance of pavements in the field, therefore, alternative crack growth laws were needed to reconcile the potential differences between laboratory and field. The feature of these laws includes: (1) using a more fundamental crack growth law that uses mixture failure limits such as tensile strength, failure strain, and/or fracture energy density to determine the rate of crack growth because these parameters are much easier to obtain in the laboratory; (2) using permanent deformation as a parameter (or at least one of the parameters) controlling crack growth rate. In other words, the crack growth law obtained could be applied to the laboratory and the field by predicting permanent deformation for the boundary condition associated with each of the two cases (i.e., the laboratory test and the pavement in the field). Given the reason presented above, crack growth laws based on fundamental properties were identified and evaluated to determine whether these could be used to reconcile the apparent differences observed between laboratory tests and field performance.

Two crack growth laws were identified: one based on a permanent strain criterion; the other based on a tensile strength criterion. A fracture mechanics model was used to predict local stresses and strains in the vicinity of the crack tip and a computer model was written in EXCEL to keep track of stresses, strains (elastic and permanent), and crack growth. As a first approximation, a 0.05 second square load was assumed in the analysis to approximate the 0.1 second harversine load, which would be much more difficult to model. The slope of the linear portion of the creep compliance curves shown in Figure 5.7 was used to determine the rate of permanent deformation for each mixture. Resilient modulus, tensile strength, and failure strains were also used in the analysis.

The first crack growth law, based on permanent strain criterion, was developed to predict permanent deformation using failure strain as a criterion. It involves the following steps:

Step 1: Determination of viscosity from the creep test:

(1) elastic strain is defined:

$$\varepsilon(t)_{creep} = D(t)\left(\sigma_{x-creep} - \sigma_{y-creep}\right) \tag{5.1}$$

where,

$\sigma_{x\text{-}creep}$ and $\sigma_{y\text{-}creep}$ - far away stresses obtained from the creep test

$D(t) = D(0.05) = 1/M_R$

$$\sigma_{x-creep} = \frac{2P}{\pi t D} C_x$$
$$\sigma_{y-creep} = \frac{-6P}{\pi t D} C_y \tag{5.2}$$

where,

P - creep load

t - specimen thickness

D - specimen diameter

C_x, C_y - stress correction factor

(2) strain rate is obtained from equation (5.1):

$$\dot{\varepsilon}(t)_{creep} = \frac{dD(t)}{dt}\left(\sigma_{x-creep} - \nu\sigma_{y-creep}\right) \tag{5.3}$$

(3) viscosity is determined:

$$\eta = \frac{1}{\dot{\varepsilon}(t)_{creep}}\left(\sigma_{x-creep} - \nu\sigma_{y-creep}\right) \tag{5.4}$$

Step 2: Determination of failure strain from the fracture test:

failure strain is defined:

$$\varepsilon_f = \dot{\varepsilon}(t)_{fracture}(\Delta t)N = \frac{dD(t)}{dt}\left(\sigma_{x-fracture} - \nu\sigma_{y-fracture}\right)(\Delta t)N \quad (5.5)$$

where,

)t - assumed to be 0.05-second in this case

N - number of load replications to fail the specimen

$\sigma_{x\text{-}fracture}$ and $\sigma_{y\text{-}fracture}$ - far away stresses, obtained from the fracture test

From equation (5.4),

$$\frac{dD(t)}{dt} = \frac{1}{\eta}$$

Step 3: At a given initial crack length (e.g., a=12mm), determine crack length within the number of load replications obtained from the fracture tests:

(1) the model was assumed to be a Single Edge Notched Tension (SENT) model, therefore, stress intensity factor for mode I (K_I) was determined:

$$K_I = \frac{P}{t\sqrt{D}}\left\{\frac{\sqrt{2\tan\frac{\pi\alpha}{2D}}}{\cos\frac{\pi\alpha}{2D}}\left[0.752 + 2.02\left(\frac{\alpha}{D}\right) + 0.37\left(1 - \sin\frac{\pi\alpha}{2D}\right)^3\right]\right\} \quad (5.6)$$

where,

a - crack length

(2) from Equation (5.4), strain rate is determined:

$$\dot{\varepsilon}(t)_{fracture} = \frac{1}{\eta}\left(\sigma_{x-fracture} - \nu\sigma_{y-fracture}\right) \quad (5.7)$$

where η is obtained from Equation (5.4).

According to definition of stress intensity factor, far away stresses are determined:

$$\sigma_x = \frac{K_I}{\sqrt{2\pi r}}$$

$$\sigma_y = \frac{K_I}{\sqrt{2\pi r}} + \left(- \frac{2P}{\pi t D} C_y \right) \quad (5.8)$$

where,

r - distance from crack tip (e.g., r = 0.01mm)

(3) elastic strain is described:

$$\varepsilon(t)_{elastic} = D(t)(\sigma_x - \sigma_y) \quad (5.9)$$

where,

σ_x and σ_y - stresses obtained from distribution curve in front of crack tip (Equation (5.9))

$D(t) = D(0.05) = 1/M_R$

(4) permanent stain is defined:

$$\varepsilon(t)_{permanent} = \dot{\varepsilon}(t)_{fracture} (\Delta t) N \quad (5.10)$$

where,

$\varepsilon(t)_{fracture}$ rate is determined from Equation (5.7)

)t - assumed to be 0.05-second in this case

N - number of load replications, to be determined

(5) total strain in the fracture test, including elastic strain and permanent strain, is obtained:

$$\varepsilon(t)_{Total} = \varepsilon(t)_{elastic} + \varepsilon(t)_{permanent} \quad (5.11)$$

(6) set total strain, Equation (5.11), equal to failure strain (Equation (5.5)), and solve for the number of load replications N

(7) repeat the procedures from (2) to (6) by increasing r value (e.g., r = 0.02mm). In order to simplify the calculation, the constant increment of r was selected (e.g.,)r = 0.01mm)

(8) repeat the procedures from (2) to (7) until the number of load replications N, determined in this procedure, is equal to the number of load replications, corresponding to N from the initial crack length (e.g., a=12 mm) to failure state, obtained from the fracture tests. Therefore, the total crack length is determined to be a+r.

In summary, the results and implications of this crack growth law may be summarized as follows:

- Crack growth predictions based on predicted permanent deformation and using failure strain as a criterion resulted in number of cycles to failure that were reasonably close to those observed on tests performed on indirect tensile specimens. However, a closer investigation of the prediction indicated that the mechanism of failure resulting from the predictions did not appear to be reasonable. It appears that even though stress and rate of permanent deformation were higher near the crack tip, they were not high enough to advance the crack tip fast enough, such that the permanent deformation at all locations away from the crack tip exceeded the failure strain of the mixture after the crack had advanced only a couple of millimeters. In other words, this model predicted almost no crack growth after many hundred cycles, then complete failure in just a few cycles. Even though the cycles predicted were reasonable, the mechanism does not agree with laboratory observations.

The second crack growth law, based on tensile strength criterion, was used to predict crack growth rate. The procedure of this law is the same as the previous one. In this case, the

predicted crack progression was more reasonable than that predicted using the permanent deformation model, but the predicted number of cycles to failure were far less than those measured in the laboratory. It is anticipated that part of the problem with these models is the results are highly dependent on the stress states predicted in the vicinity of the crack tip. Therefore, minor discrepancies between predicted and actual stresses in this area may have a significant influence on predicted crack growth rate.

Based on these preliminary analysis and results, it was decided these models could not be used, at least in their present form, to explain the observed differences between laboratory and field results. Therefore, a decision was made to not pursue this particular alternative crack growth laws any further.

5.3.5 Introduction of the Threshold Concept

The results and analyses presented above indicate that the crack growth rates measured in the laboratory are accurate and reasonable, and these crack growth rates are controlled primarily by mixture tensile strength and m-value. Furthermore, the results also lead to two contradictions regarding these measured crack growth rates:

- Crack growth rates measured in the laboratory did not correlate directly with the field performance of these mixtures.
- The fracture energy density was found to correlate very strongly with the field performance of the same asphalt mixtures (i.e., it was a good indicator for resistance to cracking: high fracture energy density, high resistance to cracking in the field). However, it did not correlate well with measured crack growth rates in the laboratory.

It appears that these two contradictions are related and may lead to the identification of an appropriate and fundamental crack growth law that applies equally well to the laboratory and field performance of these mixtures.

Therefore, further investigations were undertaken to identify the potential cracking mechanism between laboratory tests and field performance. It was noted that one apparent difference between laboratory tests and field performance is the loading conditions which may result in potential differences between the cracking mechanism of the asphalt mixture in the field and the cracking mechanism induced in laboratory tests. Laboratory tests are conducted such that failure is forced to occur under repeated loading after a relatively short period of time. However, the loading conditions in the field are significantly different than this in several important ways. First, the mixture in the field is exposed to a wide range of stresses, depending upon wheel load magnitude and positions relative to the location of interest. Therefore, the mixture in the field may be exposed to very few stresses of the magnitude used to force failure (crack propagation) in the laboratory. Secondly, temperature changes and times between loading in the field may result in a significant amount of healing, that is not allowed to occur in laboratory. In other words, healing will significantly increase resistance to crack propagation of asphalt mixtures. Damage of asphalt mixtures may take the form of either micro-cracks or macro-cracks. Micro-cracks may fully or partially heal if given a relatively long time or as the temperature increases, or may develop into macro-cracks if repeated loading is continued. Therefore, if loading is discontinued and/or temperature increases such that healing is allowed to occur before a macro-crack develops, then the rate of crack development will be significantly lower than if loading is continued and no time is allowed for healing. The explanation presented above would

clearly explain how for the same material, crack growth rate is different between laboratory tests and field performance.

Based on the above investigation, a threshold concept was introduced in this study. According to the current understanding, a threshold is defined as a material's state between micro-damage and macro-crack development. It may be a value of fracture energy density, stress or strain. If the threshold is not reached, microdamage in the specimen is healable and crack will not propagate. However, once the threshold is exceeded, then crack will grow. It appears that the threshold is not related to the rate of crack propagation, where mixtures with low thresholds may exhibit relatively low crack growth rates and mixtures with high thresholds may exhibit high crack growth rates.

This threshold is not a factor in laboratory tests because the continuous loading conditions without the opportunity for healing essentially guarantee that the threshold is exceeded during the course of the test and a macro-crack is always forced to develop. Conversely, the threshold plays a critical role in the performance of pavements in the field. Therefore, mixtures with high threshold may exhibit excellent field performance, even though they exhibit relatively high da/dN in laboratory tests.

Illustration of the threshold is presented in Figures 5.19 and 5.20. As an example, dissipated creep strain energy (DE_{cs}) threshold is selected as a criterion under repeated loading condition while fracture energy density (FE) threshold is selected as a criterion under critical loading condition. The crack will propagate when either of these thresholds is exceeded (Figure 5.19). However, propagation will not occur under single load events that do not exceed the fracture energy density threshold even when this event results in energy greater than the dissipated creep strain energy threshold. While under field condition (Figure 5.20), because of healing

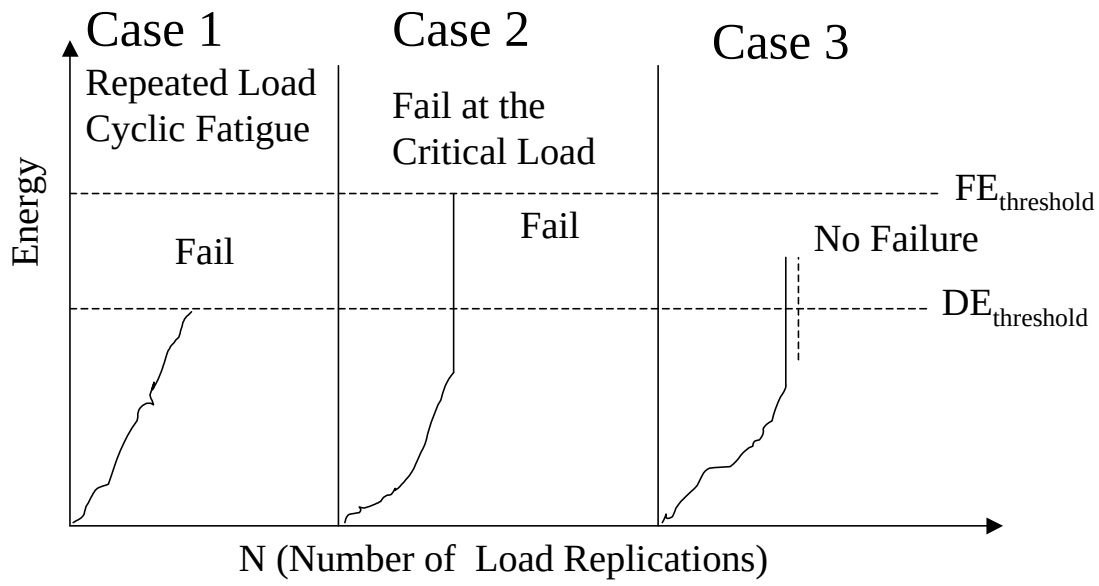

Figure 5.19 Illustration of Potential Loading Condition (Continuous Loading)

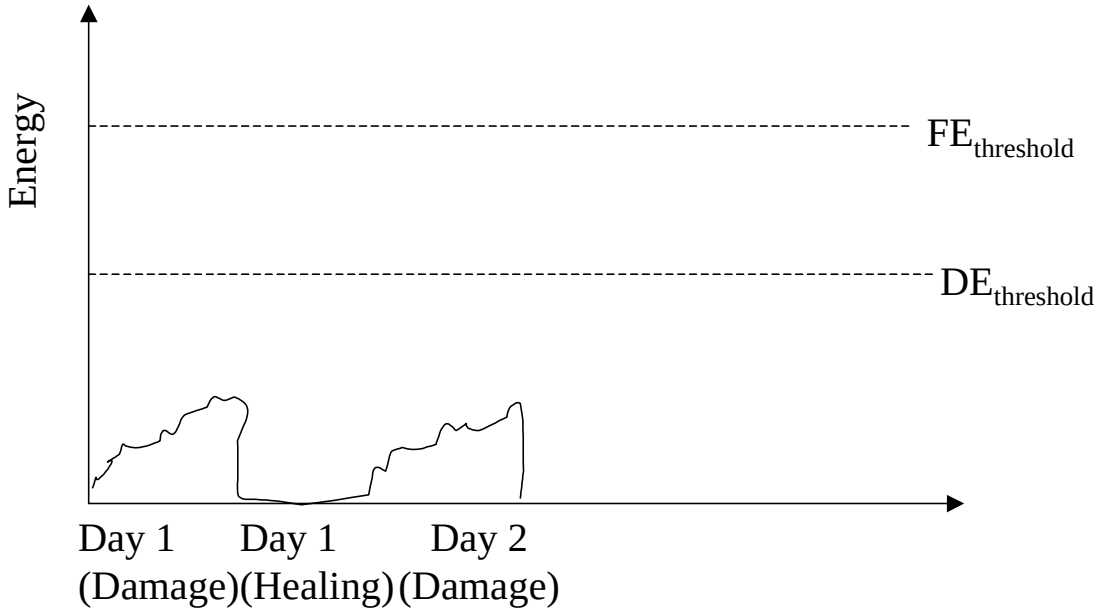

Figure 5.20 Illustration of Potential Loading Condition in Field

effect, the accumulated energy in the specimen may never reach the criteria, therefore, cracks in asphalt concrete pavements may not propagate.

This concept may provide a reasonable explanation to the contradiction between the laboratory test results and field performance. For example, even though the US301 sections exhibit lower da/dN in the laboratory tests than the I-95 Duval section, the threshold of the US301 sections is lower than that of I-95 Duval section. The lower threshold of the US301 sections may result in lower resistance to crack development and poorer performance in the field than the I-95 Duval section.

Based on the analyses presented above, it appears that the definition of this threshold concept is a key element in defining the fracture resistance of asphalt mixtures for specification and design. In summary, the key points associated with the threshold include:

- The threshold is defined as the material's state between micro-crack and macro-crack.
- The threshold may be a value of fracture energy density, stress or strain.
- If the threshold is not reached, microdamage in the specimen is healable and cracks will not propagate.
- Cracks will advance only if the threshold is exceeded.
- The level of the threshold is not necessarily related to the rate of crack growth.
- Different mixtures may have different thresholds.
- Mixtures with low crack growth rate (da/dN) may exhibit high rates of cracking in the field if they have low thresholds.
- In laboratory tests, the threshold was always exceeded, however, the threshold may or may not be exceeded in the field when realistic loading conditions are applied.

It was strongly believed that further exploration of the threshold concept would result in the development of a foundation for a new cracking model which could predict cracking performance in the field under realistic loading conditions. Therefore, a considerable amount of effort was expanded to achieve this goal, which included verifying if there was a threshold and identifying a suitable parameter to define the threshold. The details of this research are presented in the following sections.

5.4 VERIFICATION OF THE THRESHOLD CONCEPT

As indicated in the previous section, it seems that the threshold concept is the key element in defining fracture resistance of asphalt mixtures. Based on the discussion presented, it was believed that the most important feature of the threshold concept is that if the threshold is not exceeded, micro-damage is healable during rest periods and/or when temperature increases; but once the threshold is exceeded, a non-healable macro-crack will propagate. It was noted that as a concept, threshold appeared to be rational, however, it was clearly necessary to verify the validity of the threshold concept for the purpose of analyzing and/or modeling asphalt concrete pavements. Therefore, as a starting point, the concept of healing of microdamage for loading that did not exceed the threshold was evaluated in the laboratory. The healing tests performed in the laboratory include: (1) materials and testing procedures (Section 5.4.1); (2) testing results (Section 5.4.2).

Through this preliminary investigation, a basic knowledge of the threshold concept was achieved and more confidence was obtained to continue further investigation.

5.4.1 Materials and Testing Procedures

SuperPave™ coarse mixtures and I-95 Saint Johns sections (I-95 SJ) were selected for this preliminary investigation. Based on previous fracture test results, it was found that the rates

of crack propagation of these two mixtures were relatively low. In other words, perhaps these two mixtures are the more "ductile" materials and were expected to obtain more healing as temperature and rest period increase, resulting in more changes in resilient deformations before and after healing, which could be easier to observe in the test.

The SuperPave™ coarse mixtures was designed on the coarse side of the restricted zone. Specimens were compacted using a SuperPave™ Gyratory compactor to produce 4500g, 150 mm diameter specimens, to an air void content of 7 percent (±0.5 percent). Gyratory compacted specimens were sliced to obtain test specimens that were approximately 25-mm thick. Up to three 25-mm thick specimens can be obtained from each Gyratory-compacted specimen. Additional details about SuperPave™ mixtures are presented in Honeycutt's work (2000). As a reference, four specimens from the I-95 Saint Johns section (I95SJ) were also used in this investigation. Detailed information about the field cores is included in Sedwick's work (1998).

A masonry bit was used to drill an 8 mm diameter hole at the center of each specimen in order to develop crack initiation. Additional details regarding specimen preparation are presented in Chapter 3.

All tests for checking healing effect were performed at 10C. Specimens were placed in an environmental chamber and allowed to reach temperature stability overnight. Three different types of tests were conducted to examine healing effects:

<u>Test A (three SuperPave™ coarse specimens were used to perform this test):</u>

- Apply repeated load, consisting of a 0.1-second harversine load followed by a 0.9-second rest period, for 600 load applications at 10C.
- Place the specimen in oven at 30C for 12 hours.
- Cool the specimen to 10C and apply the same load as in step 1 (same magnitude and frequency) for 600 load application.

Test B (three SuperPave™ coarse specimens were used to perform this test):

- Apply repeated load, consisting of a 0.1 second harversine load followed by a 0.9 second rest period, for 100 load applications.
- Place the specimen in oven at 30C for 12 hours.
- Cool the specimen to 10C and apply the same load as in step 1 (same magnitude and frequency) until the specimen failed.

Test C (six SuperPave™ coarse specimens and four field cores from I-95 SJ were used to perform this test):

- Apply repeated load, consisting of a 0.1 second harversine load followed by a 0.9 second rest period, until the slope in the relationship of deformation vs. number of load applications changed (this phenomenon was visually observed during each test).
- Place the specimen in oven at 30C for 12 hours.
- Cool the specimen to 10C and apply the same load as in step 1 (same magnitude and frequency) until the specimen failed.

5.4.2 Test Results and Evaluation

The test results for examining healing effects on asphalt mixtures are presented in Figures 5.21 through 5.24, and Appendix G. It was noted that six SuperPave™ coarse specimens and four field cores from I-95 SJ were used to conduct type C test. However, only two test results from SuperPave™ coarse specimens and three test results from field cores were considered to be valid. The reason is that for Test C, damage on the steel loading platens was observed after the first loading period. Consequently, loading on side of the specimen, during the second loading period, caused the test to be invalid.

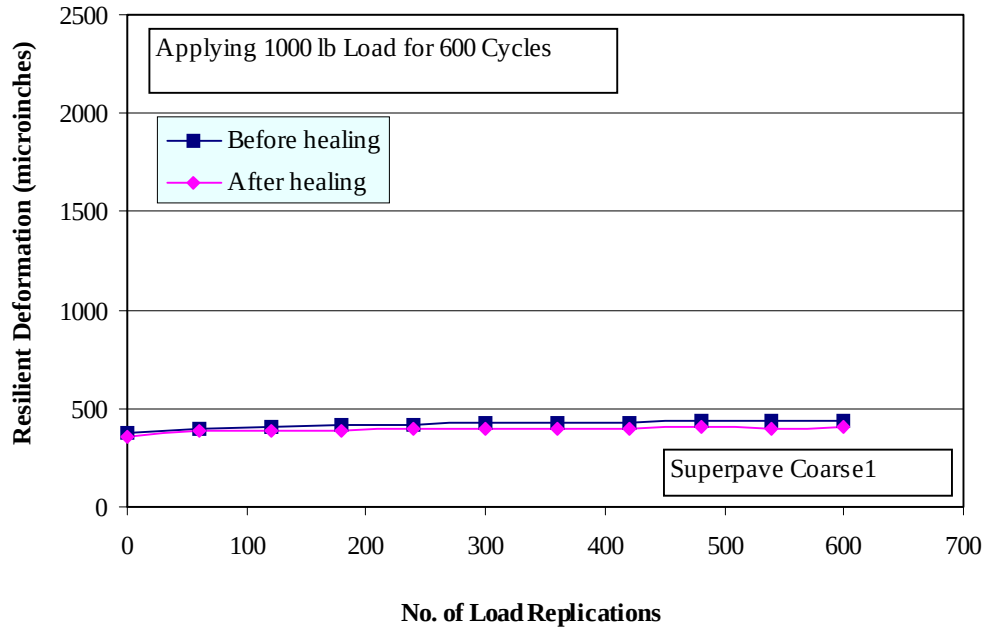

Figure 5.21 Resilient Deformation Before and After Healing

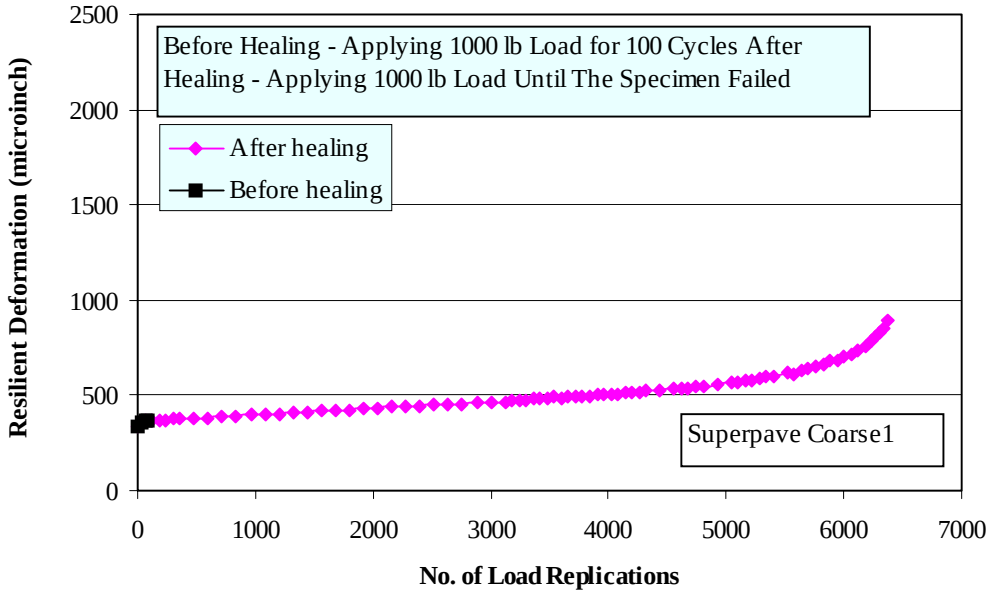

Figure 5.22 Resilient Deformation Before and After Healing

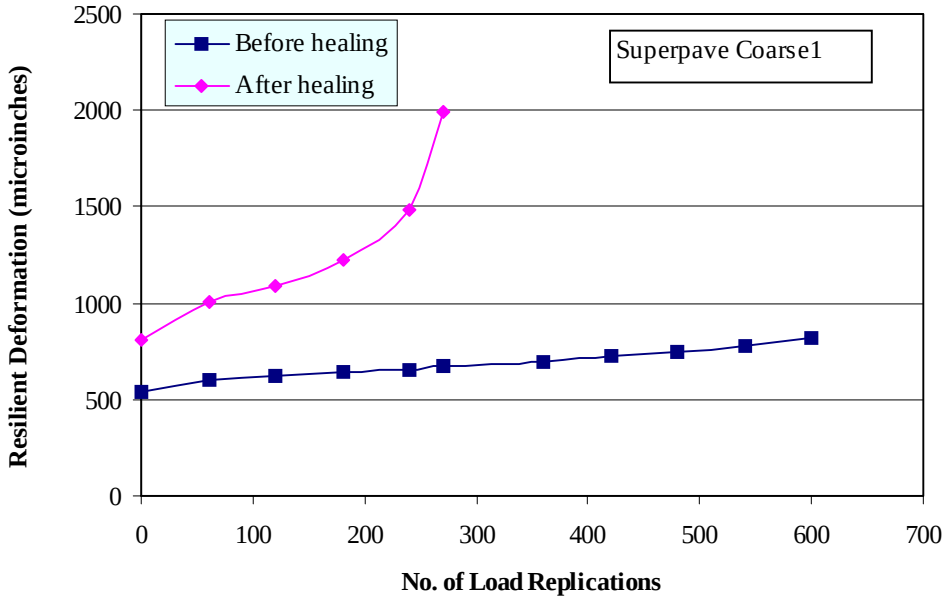

Figure 5.23 Resilient Deformation Before and After Healing

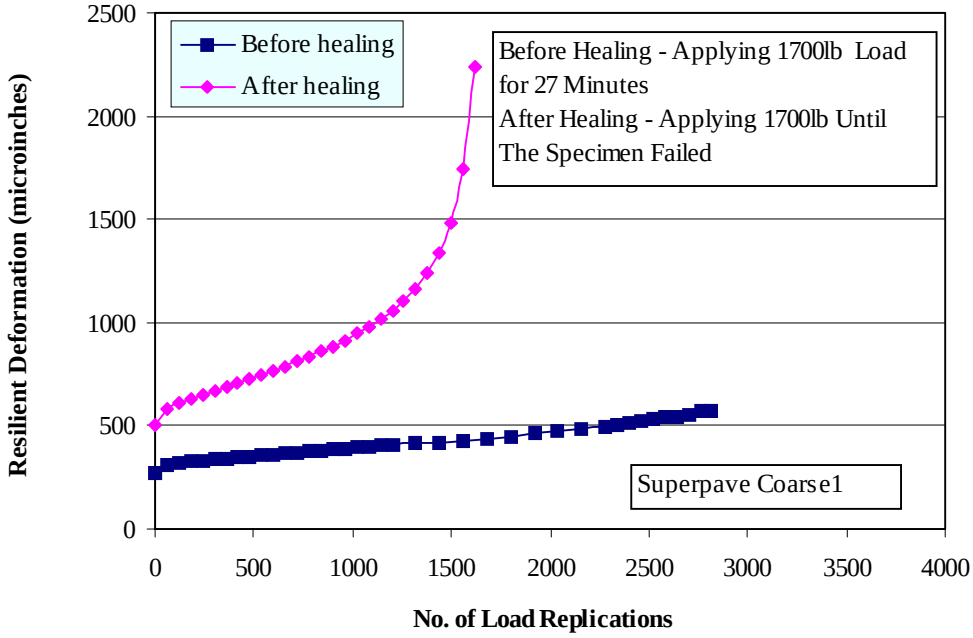

Figure 5.24 Resilient Deformation Before and After Healing

As shown in Figure 5.21 (Test A), the slopes in the relationship, resilient deformation vs. number of load replications, are essentially the same before and after healing. The constant slope indicates that only micro-damage occurred under 600 repeated loading condition because the change in slope represents the change from micro-damage state to macro-damage state.

Furthermore, it was observed that resilient deformations decreased about 5 percent after healing. Obviously, the healing of the asphalt mixtures, caused by placing the specimen in the oven at 30C for 12 hours, is the explanation for the reduction in resilient deformation. It was believed that if micro-damage was not fully healable, resilient deformation would increase when the load was reapplied. Therefore, the decreased resilient deformation indicates that micro-damage is at least partially, if not fully healable.

Also, it must be noted that one possible reason attributing to decline in resilient deformation may age-hardening, which drives asphalt mixtures to become more brittle. Therefore, further investigations were conducted to examine the aging effect.

Figure 5.22 shows that resilient deformations are essentially the same before and after healing, which indicates that short-term aging (30C, 12 hours) had little or no effect on the asphalt mixture. Therefore, it was confirmed that healing was the primary factor resulting in decreased resilient deformation presented in Figure 5.21. In other words, it is clear that micro-damage can be partially or fully healed.

As shown in Figures 5.23 and 5.24, it was observed that the slope of the relationship between resilient deformation and number of load applications increases, which indicates macro-damage occurred during the first loading period. Then, once reloaded, the resilient deformation continued to increase, following the magnitude of the deformation at end of the first loading period. Therefore, it was concluded that macro-damage (crack propagation) is not healable.

As indicated earlier, this was a preliminary investigation for the purpose of verifying the existence of a threshold. The obvious limitation involved in this study is the limited number of mixtures and specimens tested. However, the observations from the tests provide the evidence to support the goal of this investigation.

In summary, this preliminary investigation on healing effects verifies the presence of a threshold, indicating the fact that micro-damage is healable if the threshold is not exceeded; macro-crack is not healable once the threshold is exceeded. As indicated previously, since the existence of the threshold was verified, further investigation were conducted to identify the parameter that controls the threshold. This work is presented in the following sections.

5.5 EVALUATION OF DISSIPATED CREEP STRAIN ENERGY AS A THRESHOLD

According to the threshold concept introduced herein, the threshold is the state separating the micro-crack state and macro-crack state of a material. Therefore, the threshold should be a constant value at a given temperature, and also, it should not be related to the mode of load. Based on Sedwick's work (1998), it was found that fracture energy was a good indicator of cracking resistance in asphalt concrete pavements. Therefore, it was felt that the fracture energy should be related to the threshold of asphalt mixtures.

Given the reason presented above, evaluation of dissipated creep strain energy as a threshold was conducted by comparing the dissipated creep strain energy from cyclic loading tests to the dissipated creep strain energy determined from strength tests. This work included: (1) calculation of dissipated creep strain energy parameters from cyclic loading tests (Section 5.5.1); (2) calculation of dissipated creep strain energy from strength tests (Section 5.5.2); (3) evaluation of dissipated creep strain energy as a threshold (Section 5.5.3).

5.5.1 Calculation of Dissipated Creep Strain Energy Parameters from Cyclic Loading Tests

Calculation Procedure:

Determination of dissipated creep strain energy parameters from cyclic loading tests using the SuperPave™ IDT involves the following steps (Figure 5.25):

1. Determine the point when the threshold was reached from the plot of resilient deformation (δ_H) vs. number of load repetitions (N). Point A corresponds to crack length *a* = 12mm (i.e., based on the previous analyses, the energy corresponding to this point is the threshold, separating micro-damage state and macro-damage state)
2. Determine the initial resilient horizontal deformation (δo) that corresponds to the response of the specimen in the undamaged state. There are two methods of determining δo, one is an extrapolation method excluding temperature effect, the other is directly using the laboratory data at N=0. It was believed that Method 1 is more reasonable. However, as a reference, Method 2 was also used in this investigation. A detailed description of these two methods is presented below:
   - Method 1: as shown in Figure 5.25, an extrapolation of the δ_H vs. N relation from the points A and B is plotted. Point A corresponds to the number of cycles when the crack begins to propagate (i.e., in general, a=12 mm, determined by the method presented in Chapter 4), and B is any point within the region where the rate of increase in resilient horizontal deformation stabilizes. The initial deformation (δ_o) is determined as the intercept of the straight-line extrapolation at N=0 (more detailed information is included in Chapter 4).
   - Method 2: use the value at point C, corresponding to N=0.

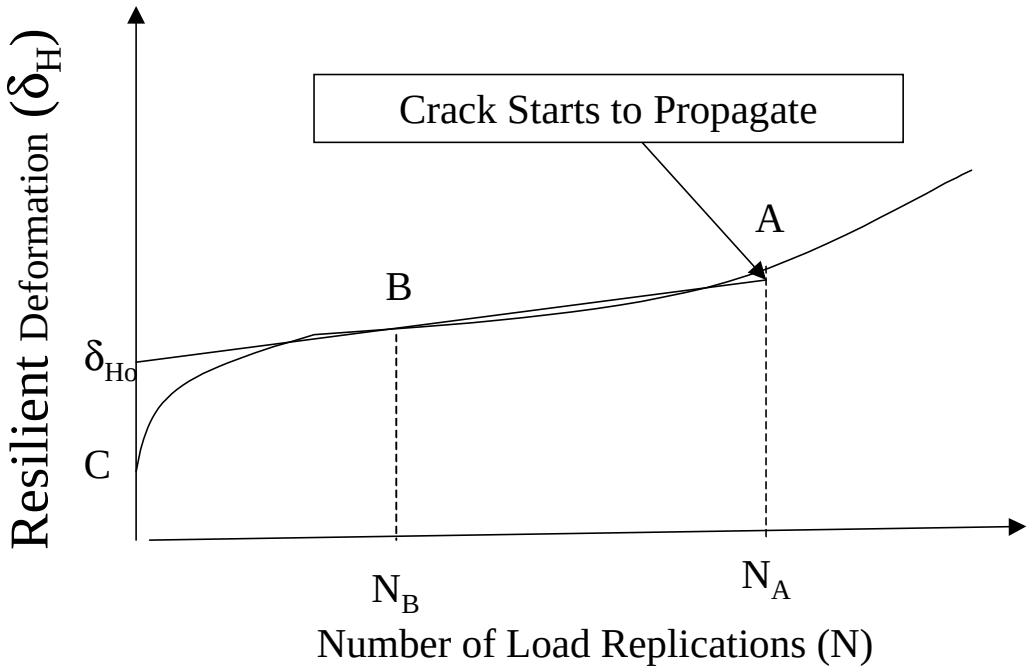

Figure 5.25 Resilient Deformation vs. Number of Load Replications

3. Determine the permanent deformation corresponding to point A, point B, and point C. Plot the permanent horizontal deformation vs. recorded points. As shown in Figure 5.26, the horizontal deformation at point A was determined by visually selecting the mid-point of the fifth cycle (the largest value of permanent deformation in five loading cycles), while the horizontal deformation at point B (or point C) was determined by visually selecting the mid-point of the first cycle (the smallest value of permanent deformation in five loading cycles) (Figures 5.27 and 5.28).
4. Determination of dissipated creep strain energy. Assuming total dissipated creep strain energy per cycle is constant:

$$\text{Dissipated Creep Strain Energy} = \frac{1}{2}\sigma\varepsilon * N_A$$

$$\text{Dissipated Creep Strain Energy} = \frac{1}{2}\left(\frac{2P}{\pi t D}\right) * \left(\frac{\delta_A - \delta_B}{GL * (N_A - N_B)}\right) * N_A \qquad (5.12)$$

Obviously, the limitation in the method presented above is that it does not account for the effect of the hole at the center of the specimen. In addition, average stress ($2P/\pi tD$) is assumed to develop cracks. Therefore, the dissipated creep strain energy calculated here is actually a dissipated creep strain energy parameter, which is related to the dissipated energy to create cracks.

Results and Evaluation:

The dissipated creep strain energy parameters were calculated for two SuperPave™ coarse mixtures (aged and unaged), two SuperPave™ fine mixtures (aged and unaged), and eight field sections. The results obtained from Method 1, determining the initial resilient horizontal deformation (δo) using the extrapolation method, are shown in Figures 5.29 and 5.30. The results obtained from Method 2, determining the initial resilient horizontal deformation (δo) using the raw laboratory data at N=0, are shown in Appendix H. Since the result patterns from

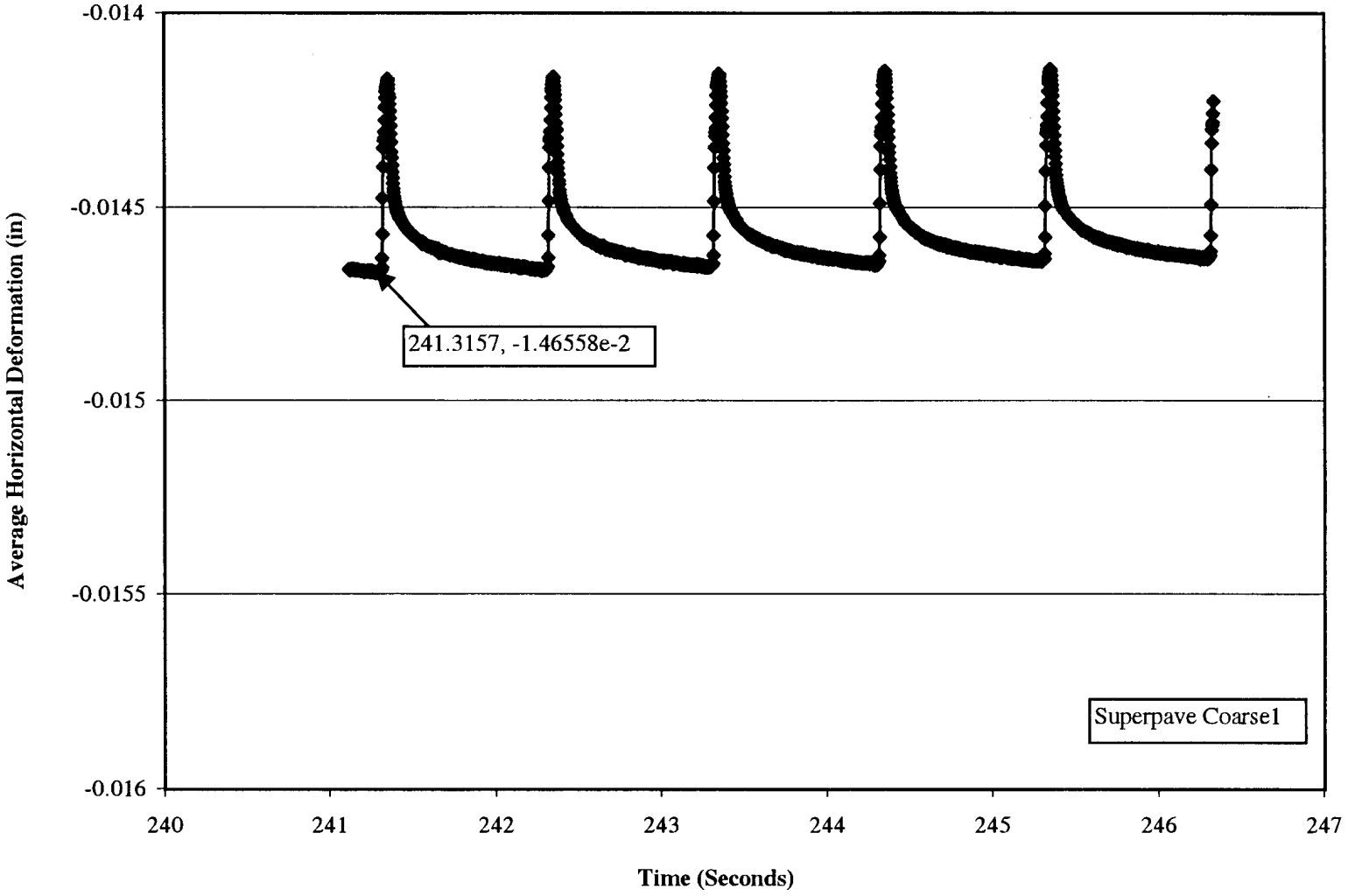

Figure 5.26 Average Horizontal Deformation vs. Time @ 240 Seconds

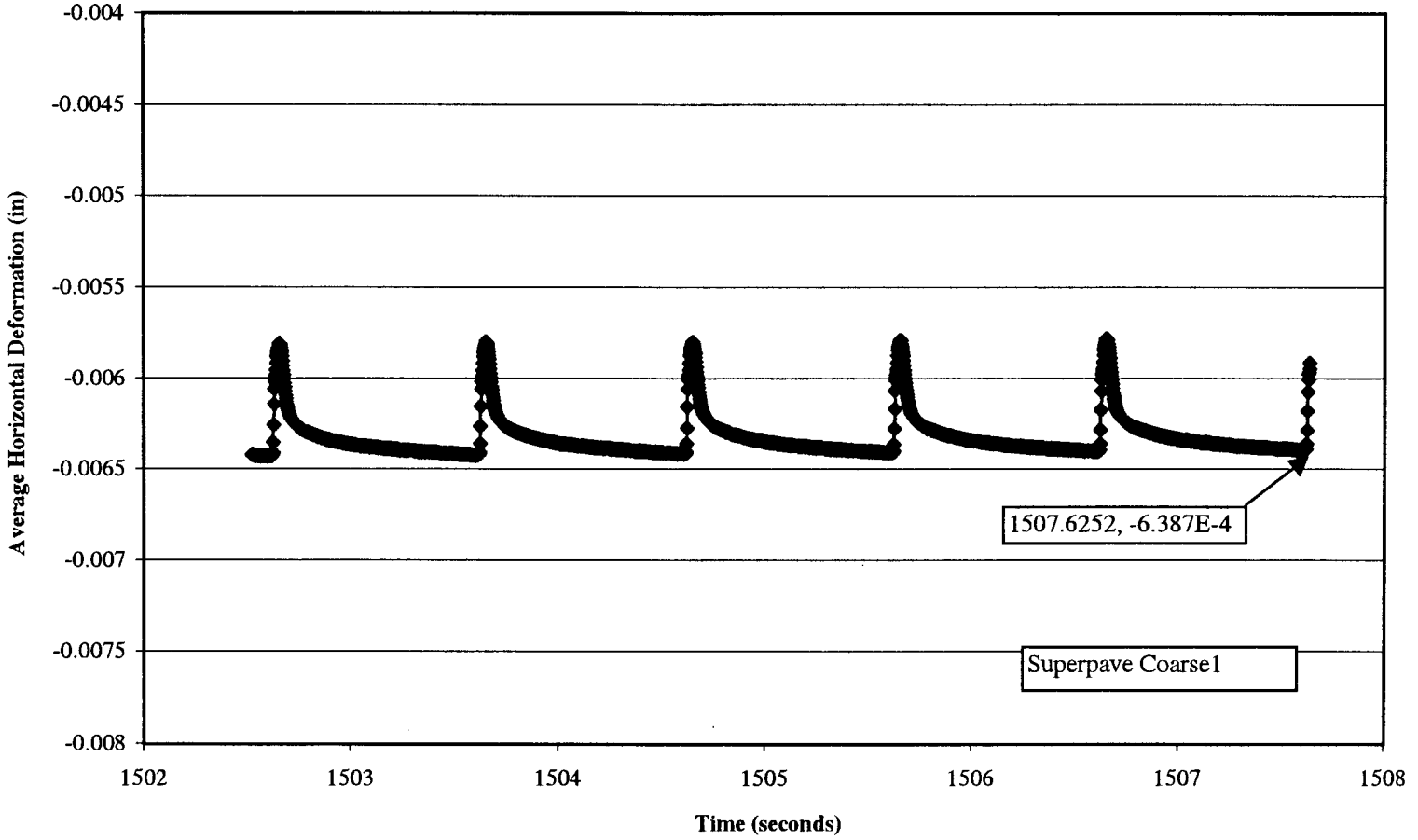

Figure 5.27 Average Horizontal Deformation vs Time @ About a = 12 mm (cracks start to propagate)

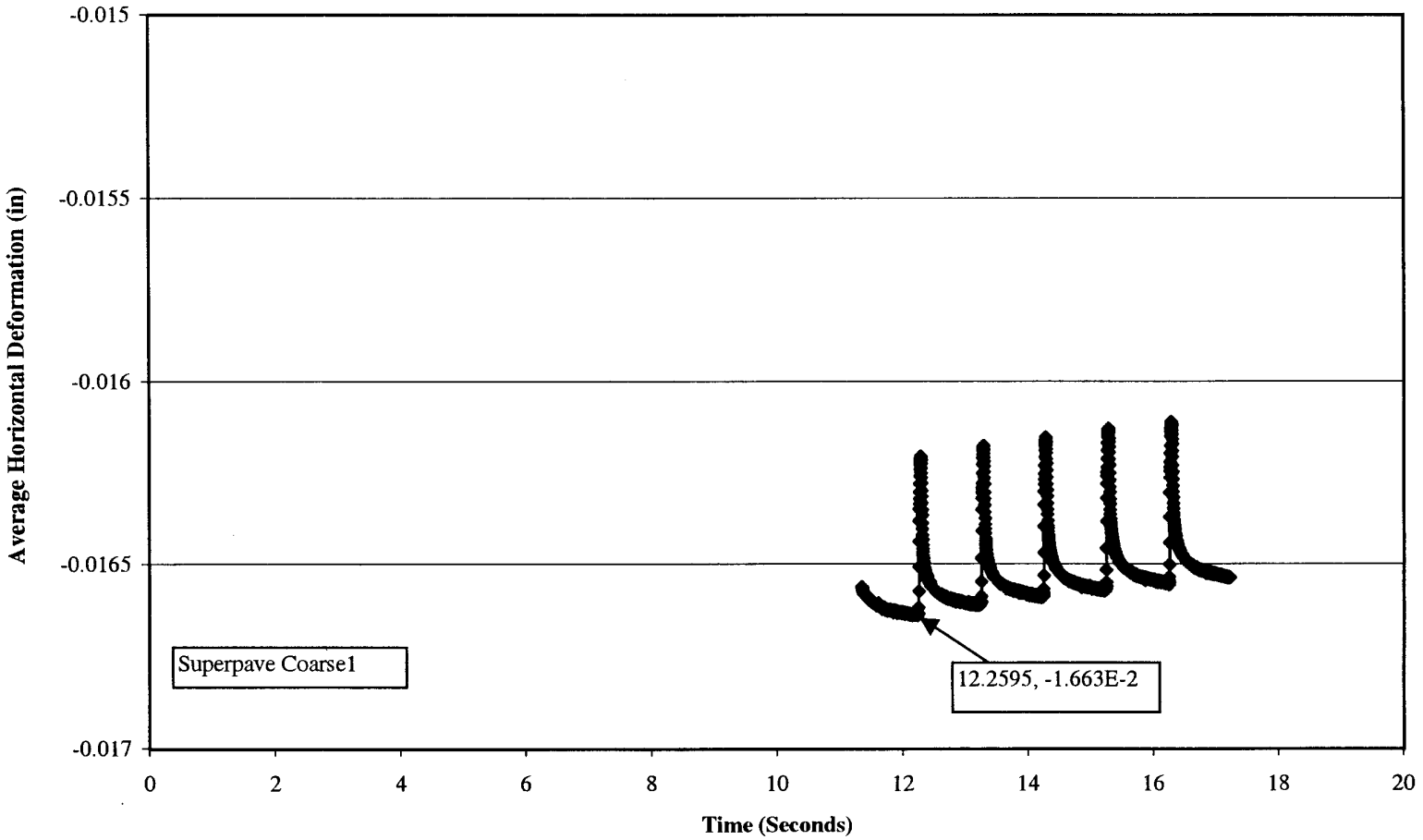

Figure 5.28 Average Horizontal Deformation vs. Time @ the Beginning of the Test

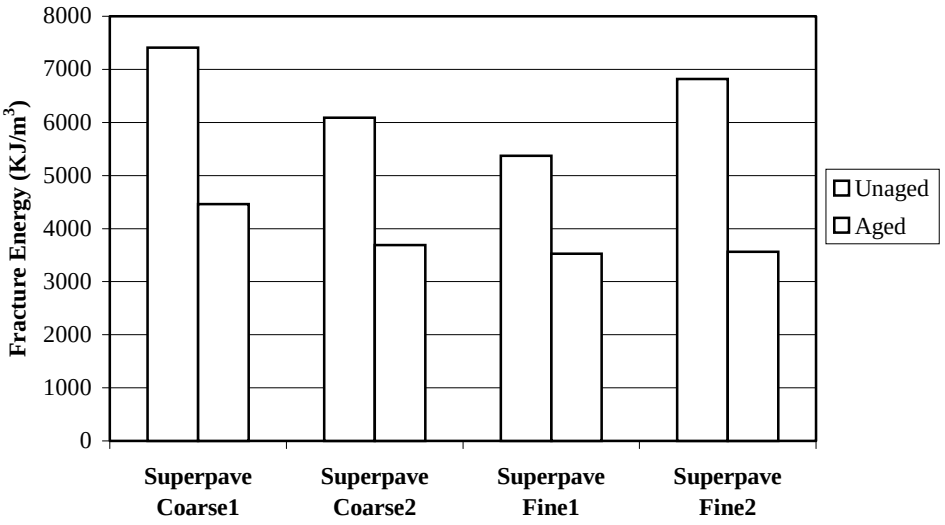

Figure 5.29 Fracture Energy Density of SuperPave™ Mixtures @ 10C

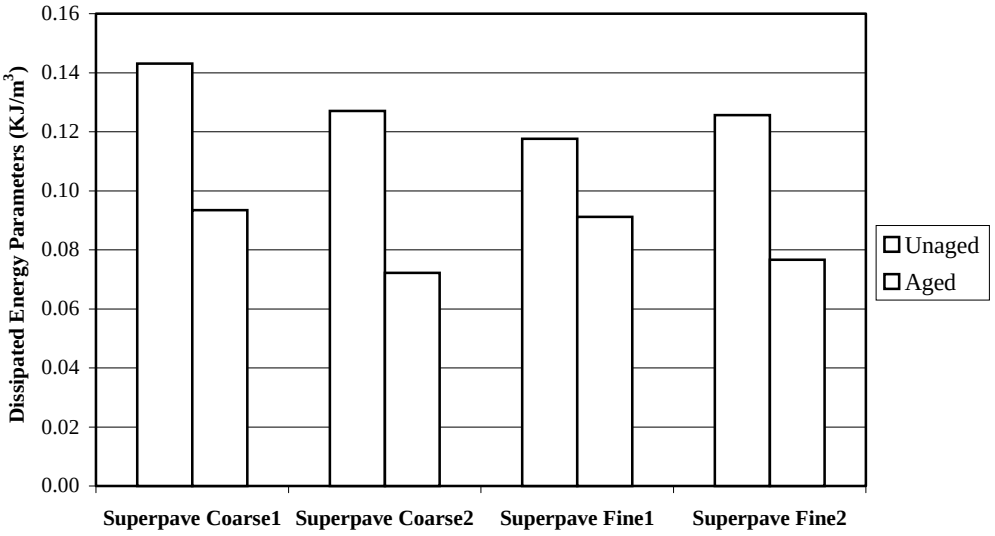

Figure 5.30 Dissipated Creep Strain Energy Parameters of SuperPave™ Mixtures @ 10C

Method 1 and Method 2 are essentially the same, the results from Method 1 are selected for evaluation purpose.

Figure 5.30 shows that the rank of the dissipated creep strain energy parameters for the SuperPave™ mixtures is similar to that of the fracture energy. Not surprisingly, Figure 5.30 shows that the dissipated creep strain energy parameters correlate well with the fracture energy for the SuperPave™ mixtures. It is known that fracture energy is a good indicator related to cracking resistance, therefore, it seems that the dissipated creep strain energy parameter is also a good parameter. Furthermore, it may be a suitable threshold, representing cracking performance of SuperPave™ mixtures. However, as shown in Figures 5.31 and 5.32, the results for the eight field sections do not agree with the above conclusion. In other words, it appears that the rank of dissipated creep strain energy parameters does not agree with the fracture energy, especially for the I-95 SJ section, which had the highest value of the dissipated creep strain energy parameters, and was 46 percent higher than that of the I-10 MW section (I-10 MW is the best performer) (Figure 5.33). The reason for this was unclear, but may be related to the fact that more variables affect field performance than the laboratory performance.

It was noted that the fracture energy obtained from the strength tests included elastic energy, which deformed the specimen; and dissipated creep strain energy, which cracked the specimen. Therefore, further investigation led to the comparison of dissipated creep strain energy parameters from cyclic loading tests to the dissipated creep strain energy from strength tests, which did not include the elastic energy component.

5.5.2 Calculation of Dissipated Creep Strain Energy from Strength Tests

Calculation of dissipated creep strain energy from strength tests involves the following steps:

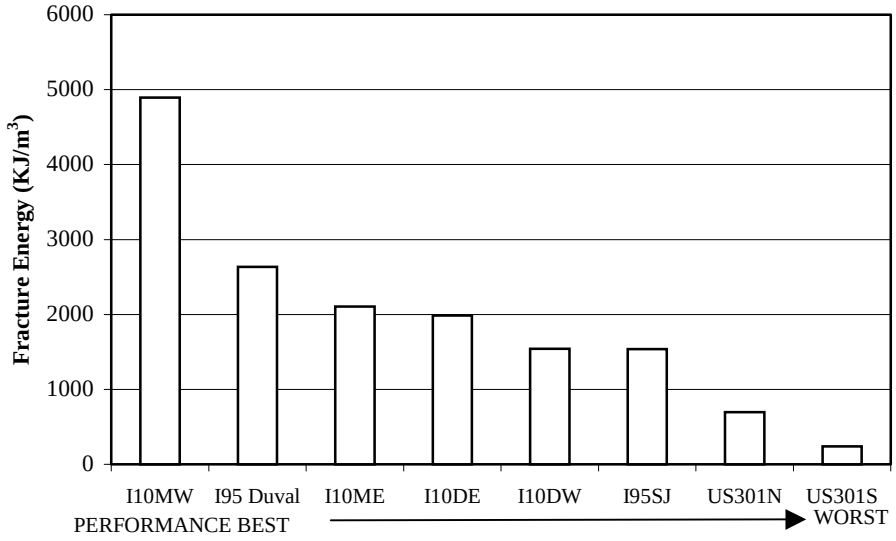

Figure 5.31 Fracture Energy Density of Eight Field Sections @ 10C

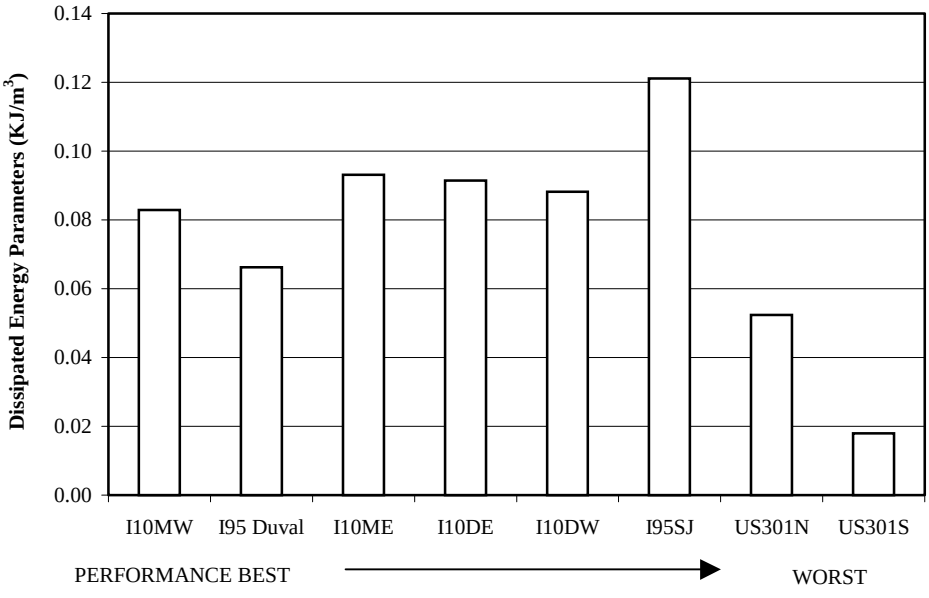

Figure 5.32 Dissipated Creep Strain Energy Parameters of Eight Field Sections @ 10C

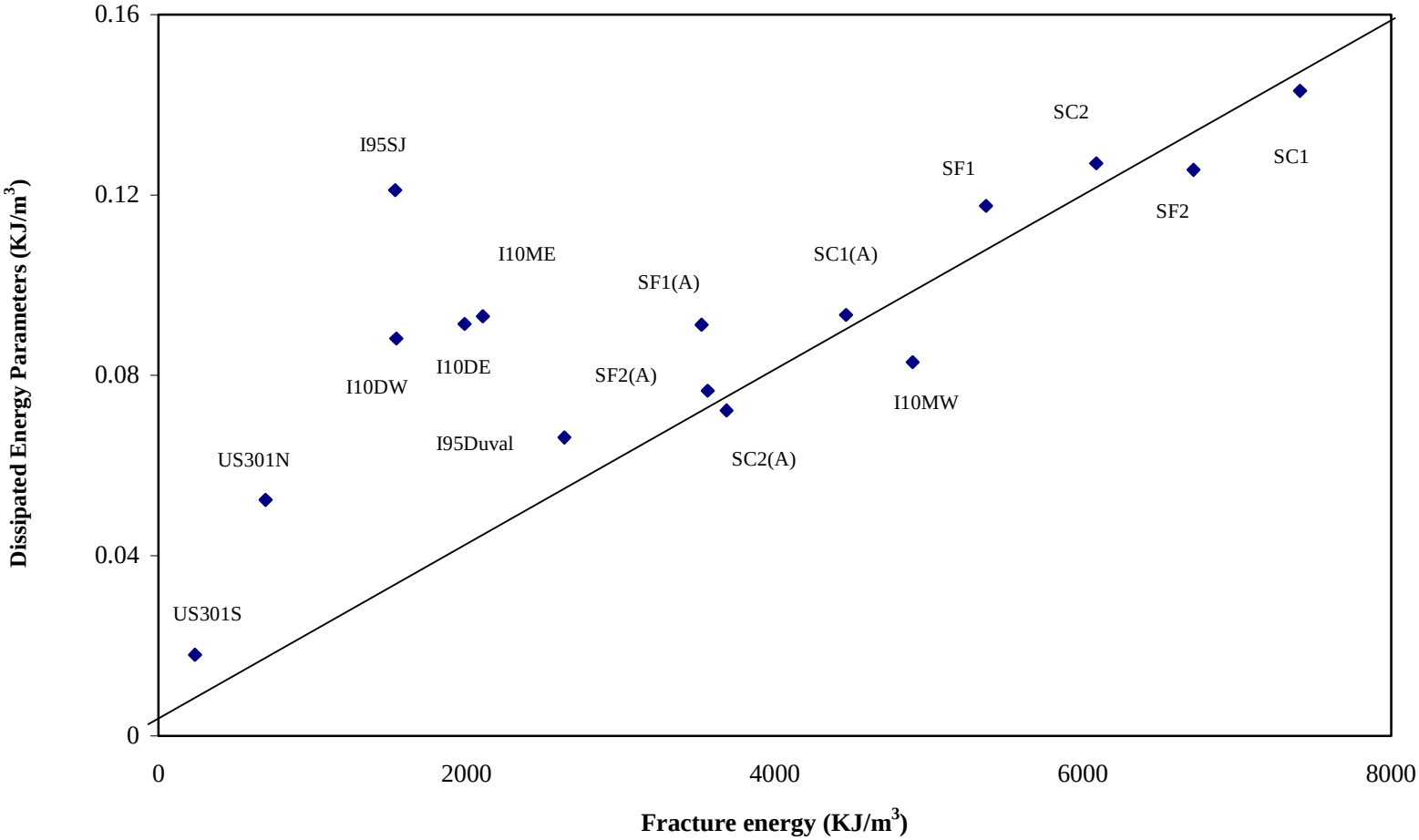

Figure 5.33 Relation Between Fracture Energy Density and Dissipated Creep Strain Energy Parameters @ 10C

1. Determine the strain at point C (ε_o). As shown in Figure 5.34, the resilient modulus was used as a slope of the straight-line separating dissipated creep strain energy and elastic energy. According to definition of elastic energy, it is the energy resulting in elastic deformation. Therefore, it was believed that selecting M_R as a slope and defining the area of ABC as elastic energy was more reasonable than defining the area of ABO as elastic energy, which is a more general method in defining elastic energy for a material. The area defined by triangle ABC, ε_o may be determined as follows:

$$M_R = \frac{S_t}{\varepsilon_f - \varepsilon_o} \tag{5.13}$$

therefore,

$$\varepsilon_o = \frac{M_R \varepsilon_f - S_t}{M_R} \tag{5.14}$$

2. Determine elastic energy. Elastic energy is the area of triangle ABC:

$$\text{Elastic Energy} = \frac{1}{2} S_t \left(\varepsilon_f - \varepsilon_o\right) \tag{5.15}$$

3. Determine dissipated creep strain energy. As indicated earlier, dissipated creep strain energy from the strength test is equivalent to the difference between the total fracture energy and elastic energy:

   Dissipated Creep Strain Energy = FractureEnergy – ElasticEnergy

   where fracture energy is obtained from strength test.

5.5.3 Evaluation of Dissipated Creep Strain Energy as a Threshold

Dissipated creep strain energy parameters from cyclic loading tests, and dissipated creep strain energy from strength tests for the SuperPave™ mixtures and the field sections are presented in Figures 5.35 through 5.37.

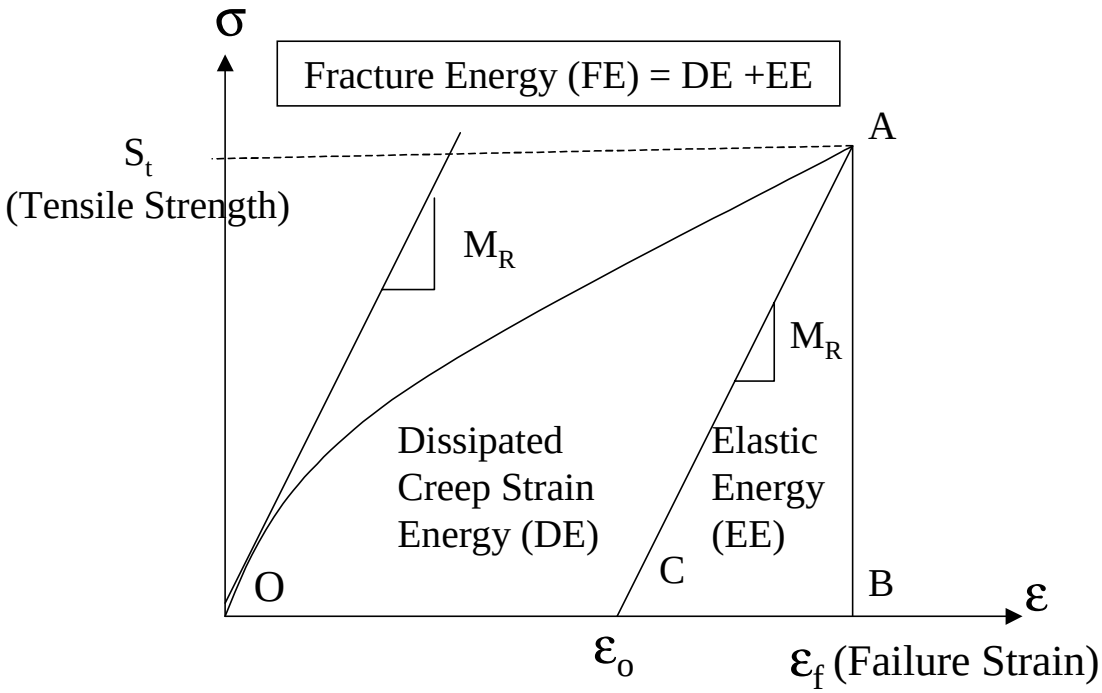

Figure 5.34 Determination of Dissipated Creep Strain Energy

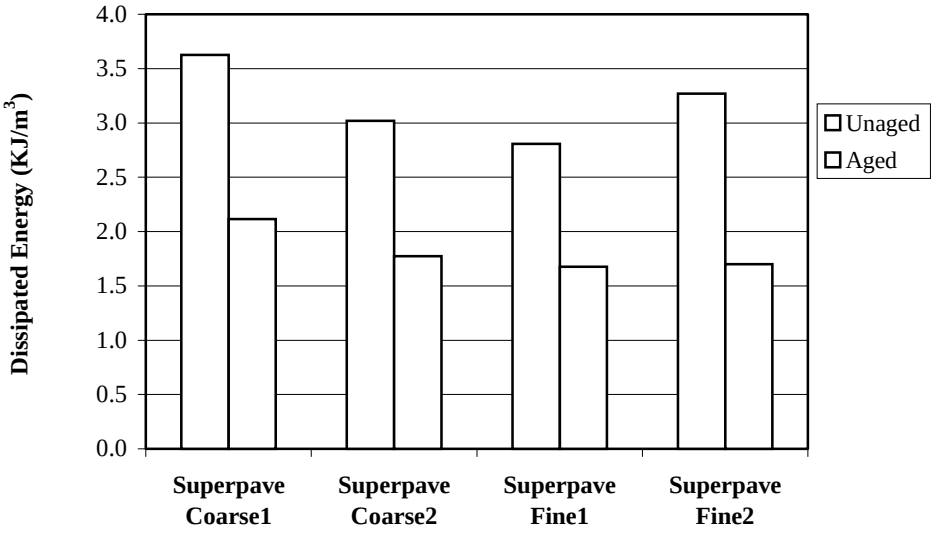

Figure 5.35 Dissipated Creep Strain Energy of SuperPave™ Mixtures from Strength Tests @ 10C

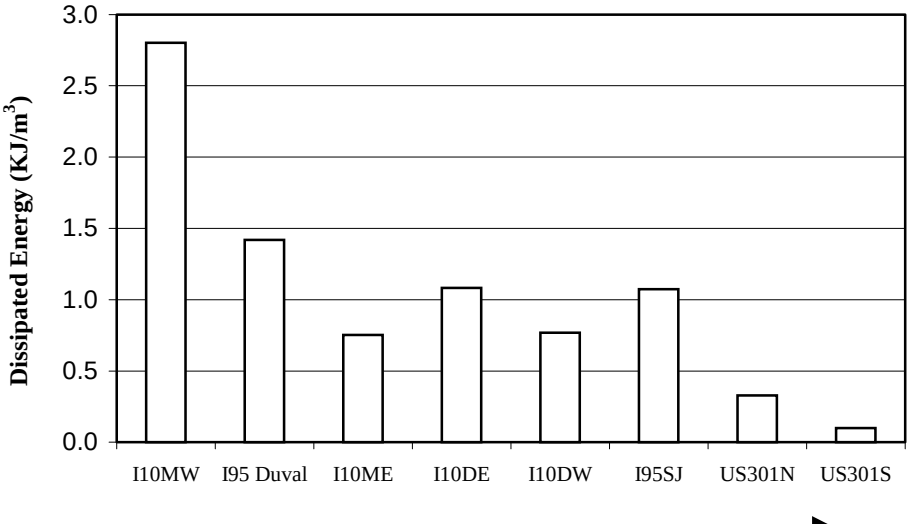

Figure 5.36 Dissipated Creep Strain Energy of Eight Field Sections from Strength Tests @ 10C

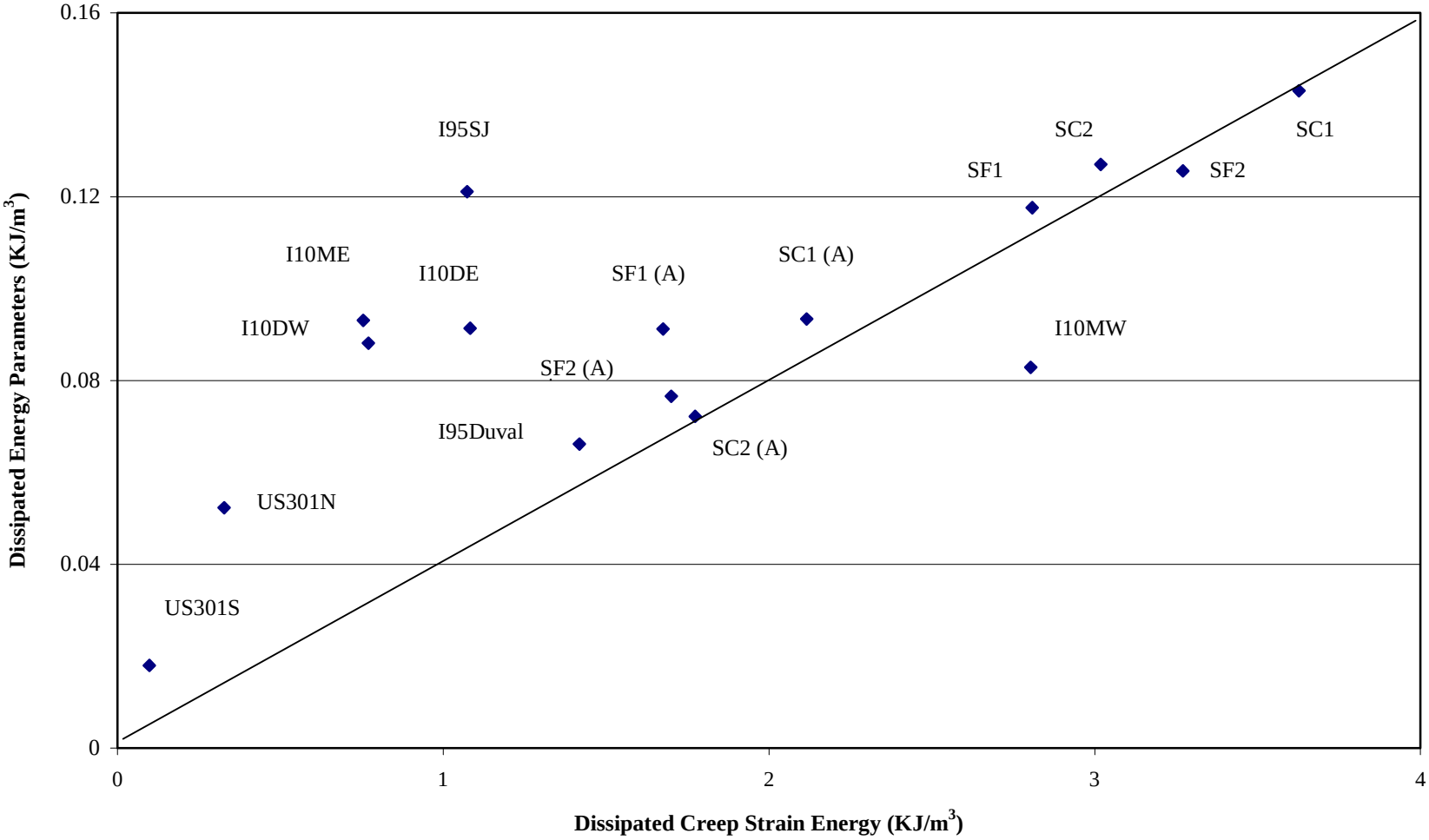

Figure 5.37 Relation Between Dissipated Creep Strain Energy and Dissipated Creep Strain Energy Parameters @ 10C

Figure 5.35 shows that the rank of dissipated creep strain energy for the SuperPave™ mixtures has a similar pattern as in the rank of measured dissipated creep strain energy parameters (Figure 5.30). Figure 5.37 shows the good correlation between the dissipated creep strain energy parameters and dissipated creep strain energy for the SuperPave™ mixtures. Clearly, the calculation of dissipated creep strain energy parameters is approximate.

Figure 5.36 presents the dissipated creep strain energy parameters for eight field sections. It appears that the rank of dissipated creep strain energy parameters slightly disagrees with in fracture energy. However, accounting for the variables in the materials and tests, it was still believed that the results are reliable. Figure 5.37 shows no correlation and no close values between the dissipated creep strain energy parameters and the dissipated creep strain energy.

Given the results presented above, it is obvious that dissipated creep strain energy parameters obtained in this approach can not be used as a threshold, because it does not agree with dissipated creep strain energy obtained from strength test. As indicted earlier, the apparent limitation in this approach is that it does not consider the effect of the hole and assumes average stress distribution near the crack tip. Therefore, this could introduce significant inaccuracy in this approach. In addition, it is noted that some factors (e.g., applied load was a harversine load) were considered in an approximate manner in this approach, which could also result in some inaccuracy.

Given the analyses presented above, it appears that this method of evaluating dissipated creep strain energy as a threshold did not work. One reason is that the result is highly dependent on the stress state predicted in the vicinity of the crack tip. It was recognized that the stress near crack tip is so important in the resulting development and propagation of crack that further

investigation towards the determination of a threshold were focused on more detailed evaluation of the stress distribution near the crack tip.

5.6 EVALUATION OF YIELD STRENGTH AS A THRESHOLD

Since stress distribution near crack tip is highly dependent on the vicinity of crack tip, a material may fail locally at some critical combination of stress and strain. According to fracture mechanics (Dowling, 1993), yield strength for a given material is defined as the value of stress where a small increase in stress usually causes a relatively large increase in deformation, begins to be important. In other words, yield strength, for a given material, is defined as the stress at which a material fails locally when the maximum stress in the material exceeds this value. Therefore, it was felt that yield strength may an important factor in crack development and propagation (i.e., local failure) in asphalt mixtures and asphalt pavements. If this hypothesis holds true, yield strength could be a value of threshold, contributing to crack performance in asphalt mixtures and asphalt pavements. Evaluation of this hypothesis included: (1) calculation of yield strength (Section 5.6.1); (2) evaluation of yield strength as a threshold (Section 5.6.2).

5.6.1 Calculation of Yield Strength

Calculation Procedure:

The basic concept used to determine yield strength is that dissipated creep strain energy required to initiate or propagate cracks (indicated in Section 5.5) in cyclic load tests must be equal to the dissipated creep strain energy to failure from strength tests. The procedure of calculation of yield strength involves the following steps:

1. Determine the size of plastic zone. According to fracture mechanics (Dowling, 1993), the radius of plastic zone ($r_{o\sigma}$) for plane stress (the LEFM theory) is defined as (Figure 5.38):

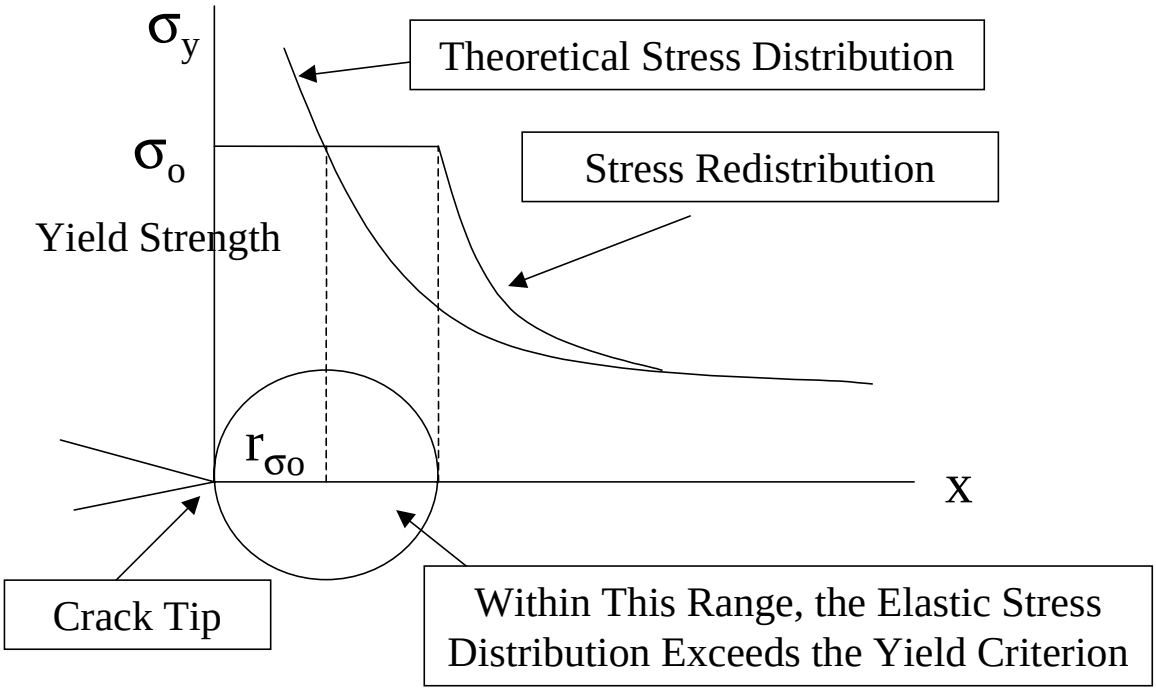

Figure 5.38 Estimation of Plastic Zone Size for Plane Stress

$$
\begin{aligned}
2r_{o\sigma} &= \frac{1}{\pi}\left[\frac{K_I}{\sigma_O}\right]^2 \\
2r_{o\sigma} &= \frac{1}{\pi}\left[\frac{\sigma_{FA}\sqrt{\pi\alpha}}{\sigma_o}\right]^2 \\
2r_{o\sigma} &= \left(\frac{\sigma_{FA}}{\sigma_o}\right)^2 \alpha
\end{aligned}
\tag{5.16}
$$

where σ_{FA} is the far away stress, σ_o is the yield strength, and *a* is the crack length. Based on the results presented in Chapter 4, the crack length immediately after crack initiation was equal to 12 mm.

2. Determine the size of a process zone. As shown in Figure 5.39, it was assumed that the difference of external energy applied to the body of a specimen (i.e., external load applied at the steel loading platens times the deformation between the top and bottom steel loading platens) contributes to the creation and propagation of cracks. Therefore, the following factors remain the same before and after crack propagation: (1) damage in the vicinity of the steel loading platens; (2) the stress state beyond the process zone (i.e., the area of ABCDEFGH). The total force in the process zone should be the same before and after crack propagation. In other words, the total force in the area of EFGH is equal to that in the area of ABCDE:

$$
\begin{aligned}
\sigma_{FA}(\alpha + 2r + x) &= \sigma_o(2r) + (\sigma_o + \sigma_{FA})\frac{x}{2} \\
x &= \frac{\sigma_{FA}\sigma_o - \left(\sigma_o^2 + \sigma_{FA}^2\right)}{(\sigma_{FA} - \sigma_o)\sigma_o^2}\, 2\alpha\sigma_{FA}
\end{aligned}
\tag{5.17}
$$

3. Determine the dissipated creep strain energy per cycle from cyclic loading test. As indicated in Chapter 3, the applied load is the repeated load consisting of 0.1 second

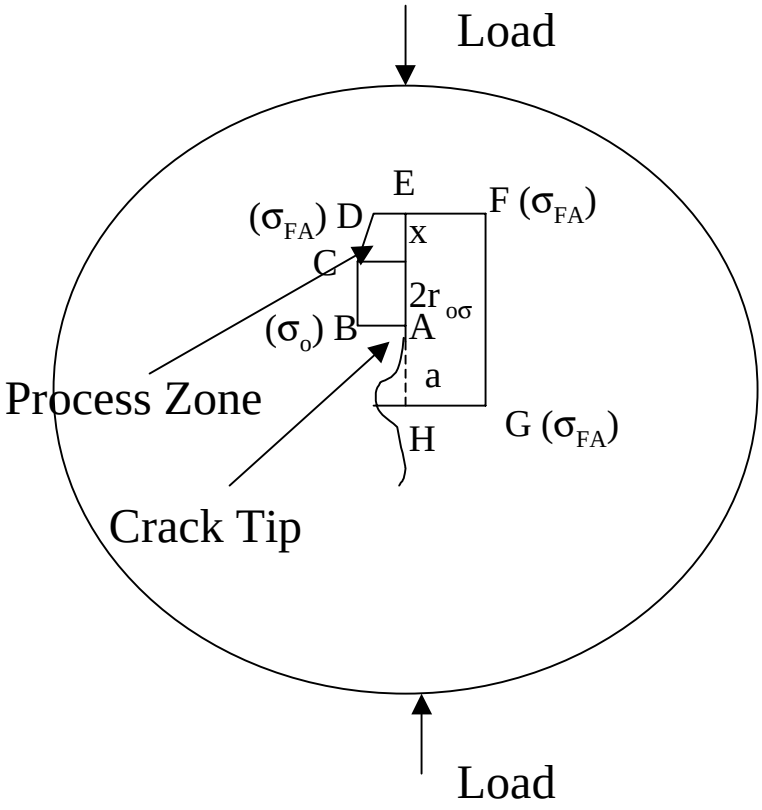

Figure 5.39 Size of the Process Zone

harversine load followed by 0.9 second rest period. Therefore, the dissipated creep strain energy per cycle ($DE_{creepstrain}$ /cycle) was defined as:

$$DE_{creepstrain}/cycle = \int_o^{0.1} \sigma_{AVE} \sin(10\pi t)\, dt \tag{5.18}$$

where σ_{AVE} is the average stress in the area of ABCDE, and ε_{Pmax} rate is the maximum strain rate determined from 100-second creep test. Based on the relationship between strain and creep compliance:

$$\begin{aligned} \varepsilon(t) &= \sigma_{AVE} D(t) \\ D(t) &= D_o + D_1 t^m \end{aligned} \tag{5.19}$$

therefore,

$$\dot{\varepsilon}_p = \sigma_{AVE} \frac{dD(t)}{dt} = \sigma_{AVE} D_1 m t^{m-1} \tag{5.20}$$

then, the maximum strain rate is determined:

$$\dot{\varepsilon}_{Pmax} = \sigma_{AVE} \frac{dD(t)}{dt} = \sigma_{AVE} D_1 m (100)^{m-1} \tag{5.21}$$

where D_1 and m are obtained from creep tests.

Substituting Equation (5.21) into Equation (5.18), dissipated creep strain energy per cycle is obtained:

$$\begin{aligned} DE_{creepstrain}/cycle &= \int_0^{0.1} \sigma_{AVE} \sin(10\pi t)\, \dot{\varepsilon}_{Pmax} \sin(10\pi t)\, dt \\ DE_{creepstrain}/cycle &= \sigma_{AVE}\, \dot{\varepsilon}_{Pmax} \frac{1}{10\pi} \left[\frac{10\pi t}{2} - \frac{\sin(20\pi t)}{4} \right]_0^{0.1} \\ \therefore DE_{creepstrain}/cycle &= \frac{1}{20} \sigma_{AVE}\, \dot{\varepsilon}_{Pmax} \\ DE_{creepstrain}/cycle &= \frac{1}{20} \sigma_{AVE} (\sigma_{AVE} D_1 m (100))^{m-1} \end{aligned} \tag{5.22}$$

The number of cycles, N, corresponding to crack initiation can be obtained from cyclic load tests, and the dissipated creep strain energy per cycle is:

$$\sigma_{AVE} = \left[\frac{20 DE_{creepstrain} / Cycle}{D_1 m (100)^{m-1}} \right]^{1/2} \tag{5.23}$$

$$DE_{creepstrain/cycle} = DE_{creepstrain} / N$$

$$DE_{creepstrain} = \text{Fracture Energy} - \text{Elastic Energy} \tag{5.24}$$

4. Determine the average stress σ_{AVE} under the area of ABCDE (Figure 5.39):

$$\sigma_{AVE}(2r + x) = \sigma_o(2r) + (\sigma_o + \sigma_{AVE})\frac{x}{2}$$

$$\therefore \sigma_{AVE} = \frac{\sigma_o(2r) + (\sigma_o + \sigma_{AVE})\frac{x}{2}}{(2r + x)} \tag{5.25}$$

Substituting the values of r (equation 5.16) and x (equation 5.17) into equation (5.23), σ_{AVE} is obtained:

$$\sigma_{AVE} = \frac{(\sigma_{FA} - \sigma_o)\sigma_{FA}\sigma_o + (\sigma_{FA} + \sigma_o)(\sigma_{FA}\sigma - \sigma_o^2 - \sigma_{FA}^2)}{(\sigma_{FA} - \sigma_o)\sigma_{FA} + 2(\sigma_{FA}\sigma - \sigma_o^2 - \sigma_{FA}^2)} \tag{5.26}$$

5. The yield strength (σ_o) is determined by solving equations (5.23) and (5.26).

This approach for determining yield strength appears to be rational and to provide the following advantages: (1) the actual stress distribution near crack tip was considered (i.e., stress redistribution caused by the material having a maximum strength, σ_o, was considered); (2) dissipated creep strain energy per cycle was determined by integrating the stress and strain functions associated with the actual loading condition (i.e., the harversine load); (3) strain rate was used in determination of dissipated creep strain energy, which accounts for the effects of viscoelasticity during repeated loading test. It was noted that half of the total crack length (*a*) was

needed in order to determine the size of plastic zone $r_{o\sigma}$. Therefore, based on the results presented in Chapter 4, *a* value of 12 mm, corresponding to half the crack length immediately after crack initiation, was used. In addition, the number of cycles N corresponding to *a*=12 mm in this approach was also determined by using the data interpretation method presented in Chapter 4 for each specimen.

5.6.2 Evaluation of Yield Strength as a Threshold

Calculation Results:

The results of yield strength for four SuperPave™ mixtures (aged and unaged) and eight field sections are summarized in Table 5.1. As a reference, the average stress is also included in Table 5.1. It was noted that the yield strengths for the I10ME section and the US301N section were negative values. In physical meaning, the negative value could be treated as a compressive stress which is used to close cracks. However, in fact that yield strength calculated in this approach is the maximum tensile stress that a material can withstand without cracking. Therefore, the yield strengths for the I10ME section and the US301N section were thought to be invalid. The reason for obtaining negative values was unknown, however, this may be related to the fact that these mixtures had high m-value and low tensile strength or very low m-value and tensile strength, which may have led to significant inaccuracies in the calculations.

Table 5.1 clearly shows that the yield strengths are greater than the tensile strengths for all other mixtures. Furthermore, in general, for a material with higher tensile strength, a higher yield strength was obtained. This finding is consistent with the expectation that for a given material, resistance to local failure is higher than resistance to global failure.

From the data presented in Table 5.1, it appears that the aged SuperPave™ mixtures have higher yield strength than the unaged SuperPave™ mixtures, except for the aged SuperPave™

Fine 1. This agrees with the fact that a material becomes more brittle after aging, resulting in higher tensile strength and yield strength. In other words, since a material becomes more brittle, the tensile strength increases globally and locally. As mentioned earlier, SuperPave™ Fine 1 is an exception, however, it was noted that the tensile strength remained the same after aging. Perhaps the effect of other factors (e.g., void structure and/or aggregate structure) may have played a part in these results.

Finally, the data presented in Table 5.1 indicates that the I-10 MW section (best performer) exhibited the highest yield strength while the US301 N section (one of the worst performers) exhibited the lowest yield strength.

The reasonable yield strengths obtained from this calculation method provides further evidence to support this approach. Therefore, according to the evaluation results from the analysis method and the laboratory data, it was concluded that this approach in determination of yield strength is rational and reliable.

Evaluation:

The yield strengths calculated appeared to be valid. However, in order to evaluate whether yield strength could be used as a threshold, further attempts to confirm the calculated results were conducted by evaluating relationships between yield strength and other mixture properties. The results are summarized in Figures 5.40 through 5.42, and Appendix I. It was anticipated that yield strength increases as dissipated creep strain energy increases. The reason for this is that if a material needs more energy to develop and propagate cracks, this material could have high yield strength to prevent crack formation. However, Figure 5.40 shows poor correlation between yield strength and dissipated creep strain energy. Furthermore, it was expected that yield strength may decrease as m-value increases since the specimen will become

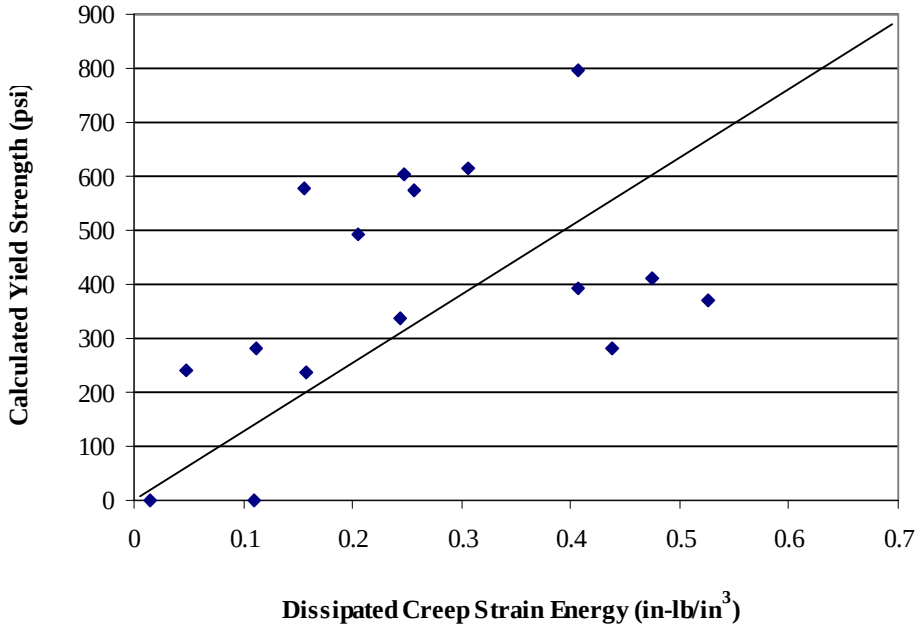

Figure 5.40 Relation Between Calculated Yield Strength and Dissipated Creep Strain Energy from Strength Tests

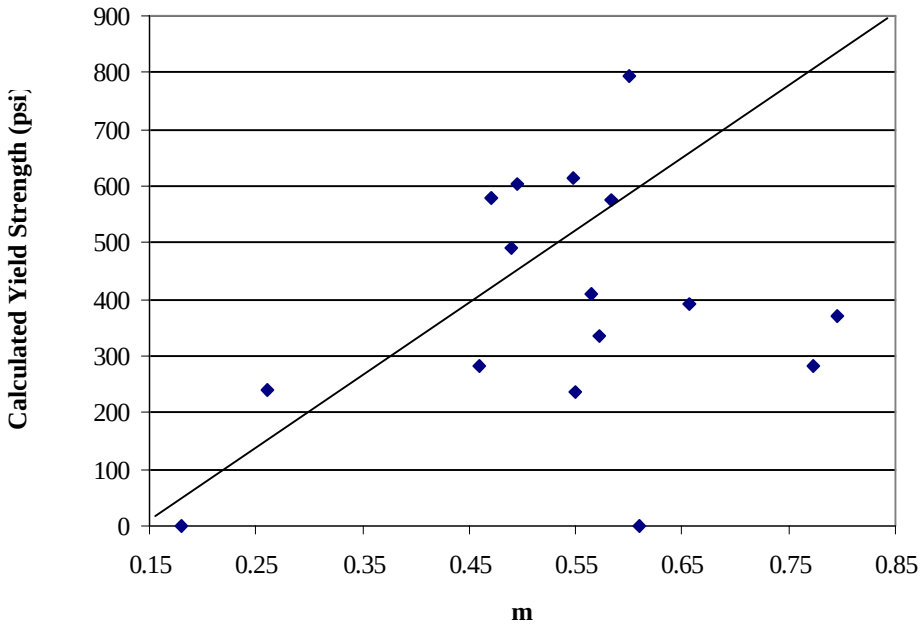

Figure 5.41 Relation Between Calculated Yield Strength and m-Value

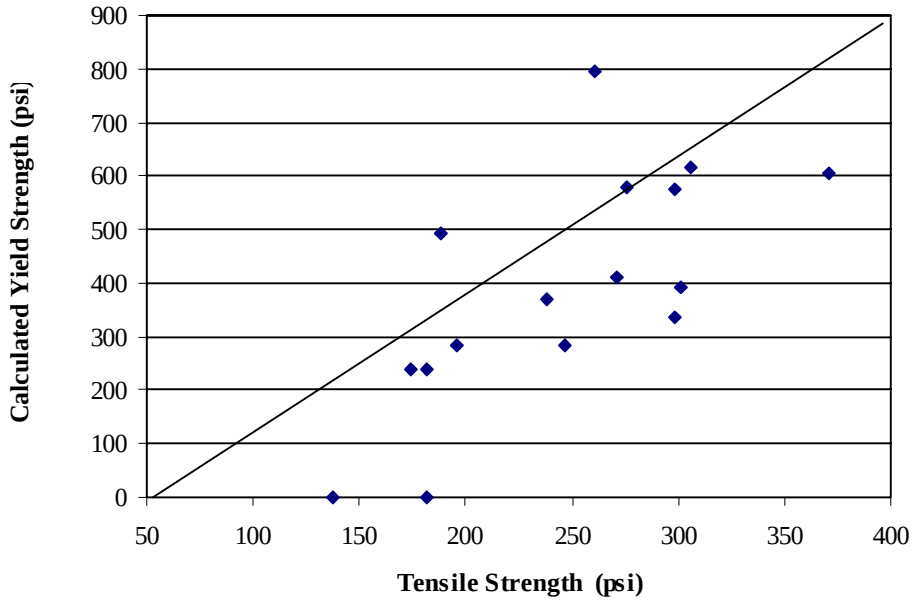

Figure 5.42 Relation Between Calculated Yield Strength and Tensile Strength

more compliant. However, very little or no trend of this relationship was observed in Figure 5.41. Finally, Figure 5.42 does show a reasonable correlation between yield strength and tensile strength: as indicated earlier, high tensile strength, high yield strength. However, this correlation was not strong.

Based on the results presented above, it was concluded that there was poor correlation between yield strength and mixture properties. However, it was recognized that the correlations were based on linear relationship. Therefore, further efforts concentrated on evaluating the reasonableness of relationships between yield strength and mixture properties.

Regression analyses (SAS was used) were conducted to evaluate relationships between mixture properties (i.e., tensile strength, dissipated creep strain energy and m-value) and yield

strength. The relationships were evaluated to not only evaluate the use of yield strength as a threshold but also to help further understand the mechanism of cracking performance in asphalt mixtures and asphalt pavements. Figures 5.43 through 5.46 show that yield strengths predicted from the relationships, which are presented in figures, do not correlate well with calculated yield strength because of the very low correlation coefficient (i.e., R^2 was less than 0.50).

Although low R^2 values were obtained for these relationships, it was felt that there could be a good correlation between yield strength and mixture properties, as it seemed that yield strength was related to crack behavior. It was believed that further investigations in determining a reasonable relationship could lead to achieve a better understanding of crack mechanism in asphalt mixtures and pavements. However, after a great deal of time and care that was already taken to determine the relationships presented above, it was decided to re-examine the relationships between calculated yield strength and mixture properties, including the single parameter (e.g., m-value) and its interaction (i.e., m-value*tensile strength), before developing other relationships. The results are shown in Figures 5.47 through 5.52.

The data presented in Figures 5.47 through 5.52 exhibited low correlation coefficient R^2 for all these relationships. As the final attempt, the three relationships presented in Figures 5.53 to 5.55 were developed. Once again, low correlation coefficients (i.e., R^2 was less than 0.50) were obtained for these relationships.

Based on these preliminary results and observations, the decision was made to not to pursue these relationships any further. However, one possible implication may be achieved from these relationships: although yield strength is related to crack performance, the influence of yield strength to crack behavior may not be significant since yield strength is not sensitive to mixture properties. Therefore, yield strength can not be used as a threshold.

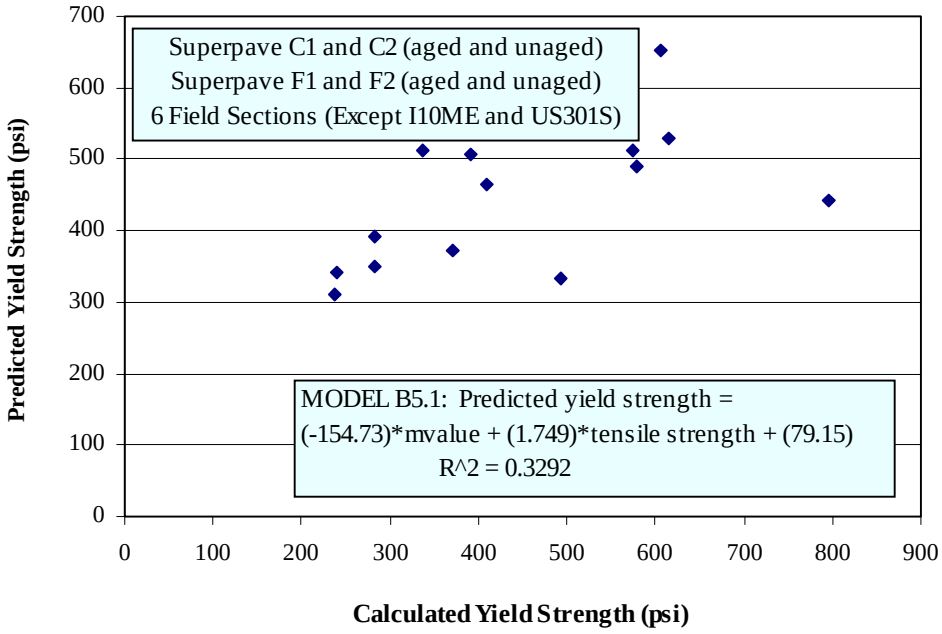

Figure 5.43 Relation Between Predicted Yield Strength and Calculated Yield Strength Using Model B5.1

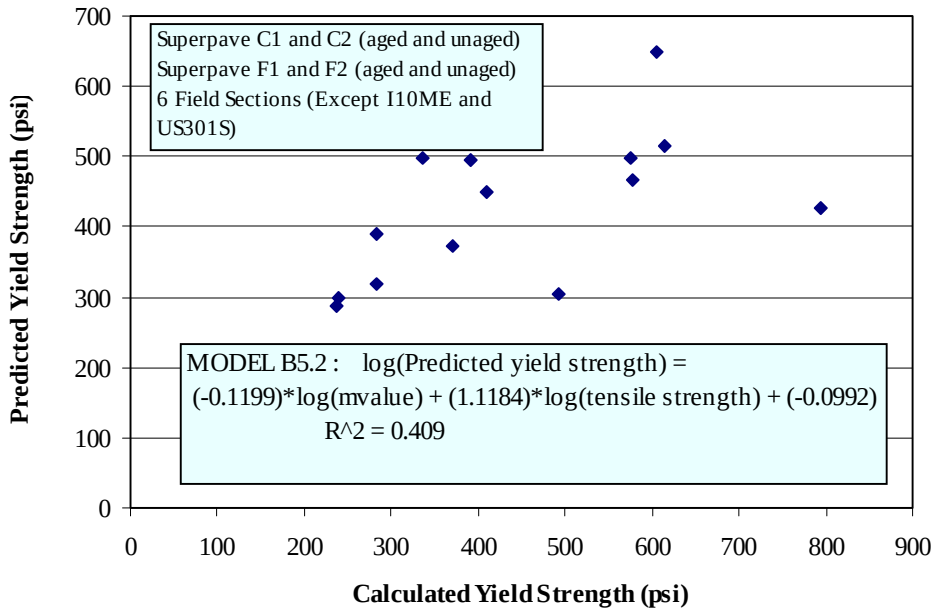

Figure 5.44 Relation Between Predicted Yield Strength and Calculated Yield Strength Using Model B5.2

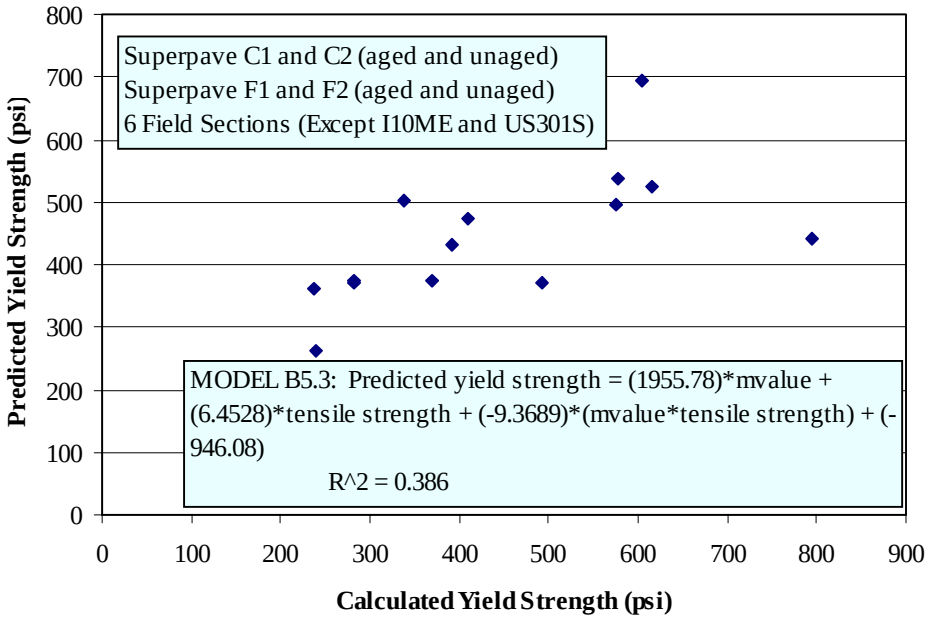

Figure 5.45 Relation Between Predicted Yield Strength and Calculated Yield Strength Using Model B5.3

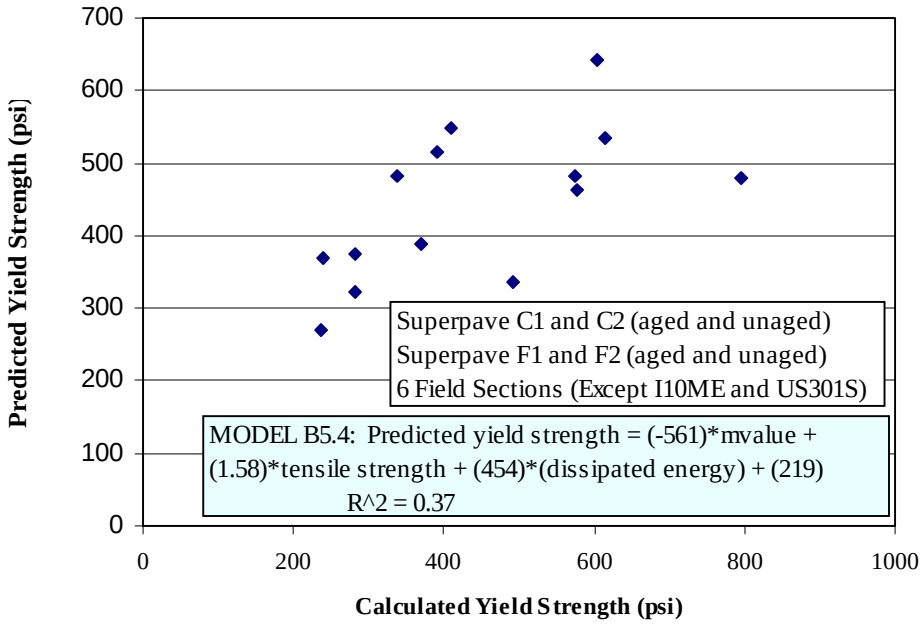

Figure 5.46 Relation Between Predicted Yield Strength and Calculated Yield Strength Using Model B5.4

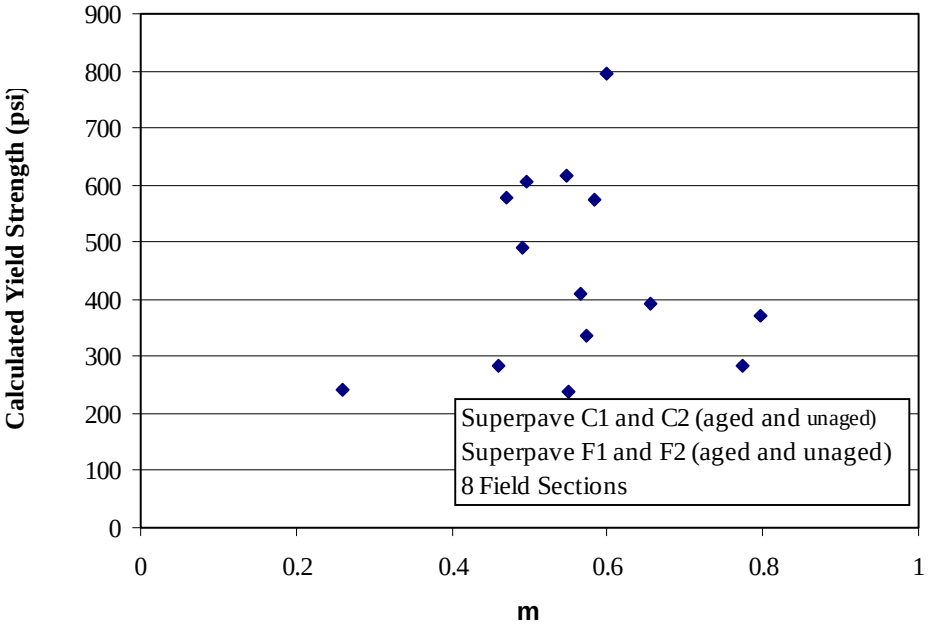

Figure 5.47 Relation Between Calculated Yield Strength and m-Value Using Model B5.4

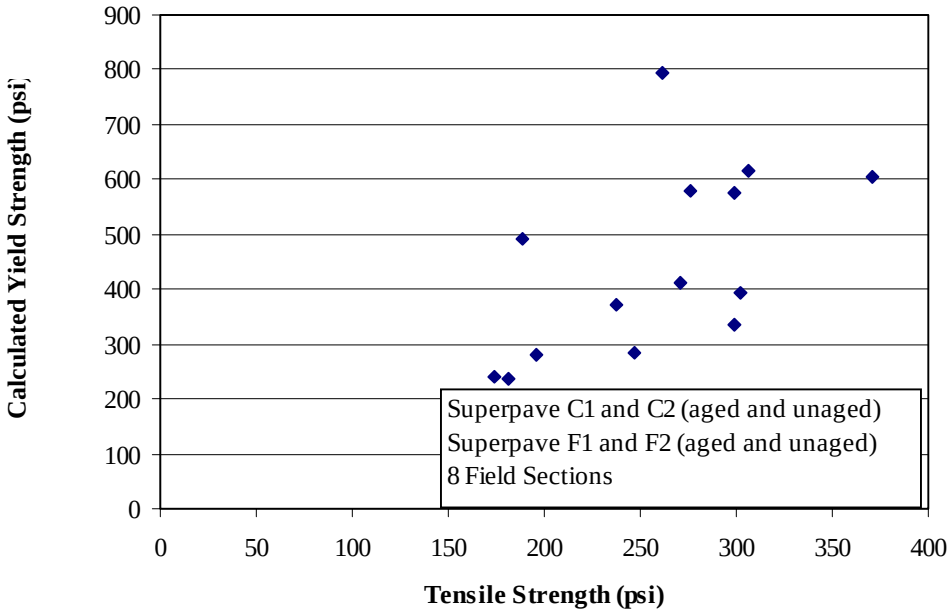

Figure 5.48 Relation Between Calculated Yield Strength and Tensile Strength Using Model B5.4

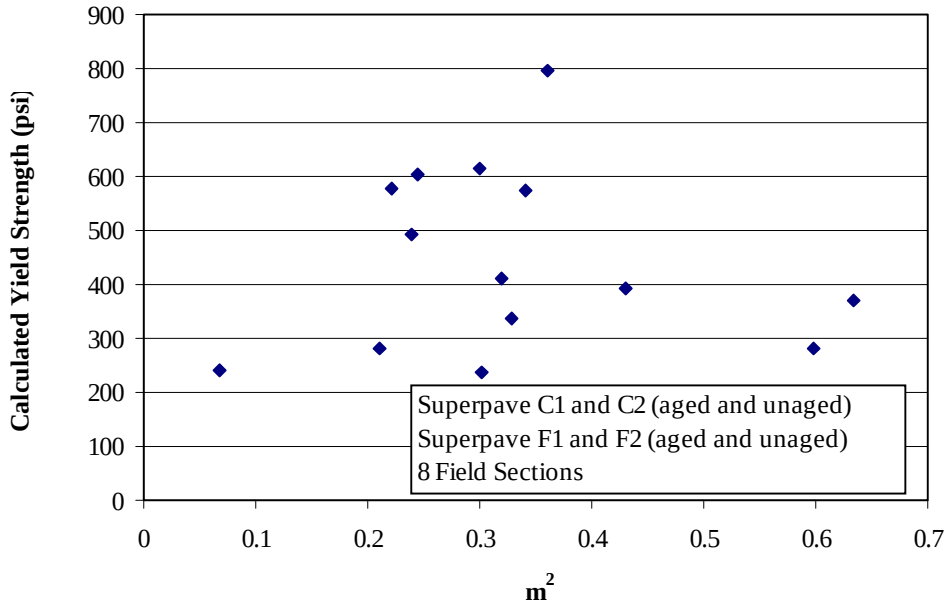

Figure 5.49 Relation Between Calculated Yield Strength and (m-Value)^2 Using Model B5.4

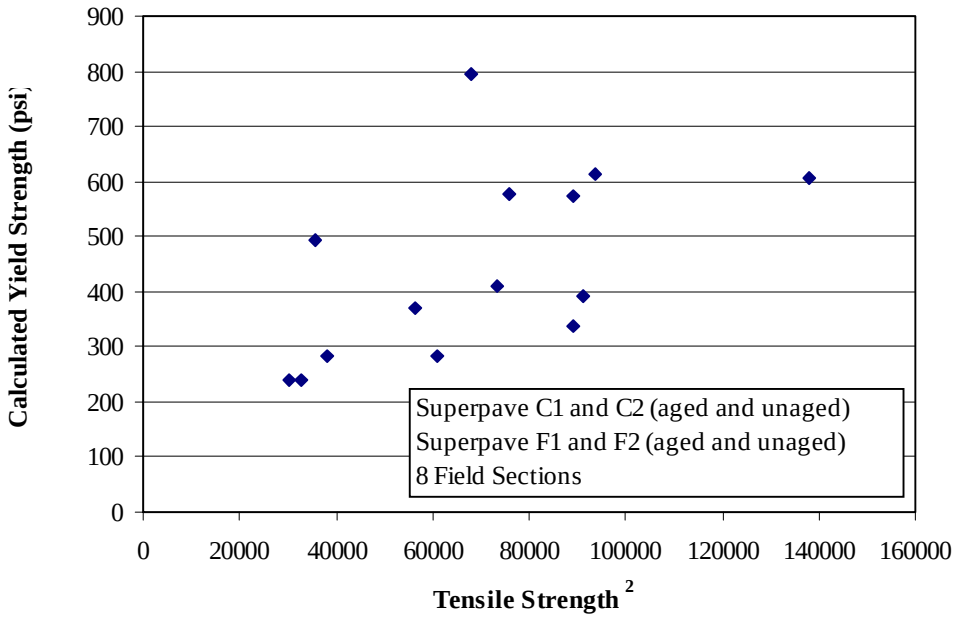

Figure 5.50 Relation Between Calculated Yield Strength and (Tensile Strength)^2 Using Model B5.4

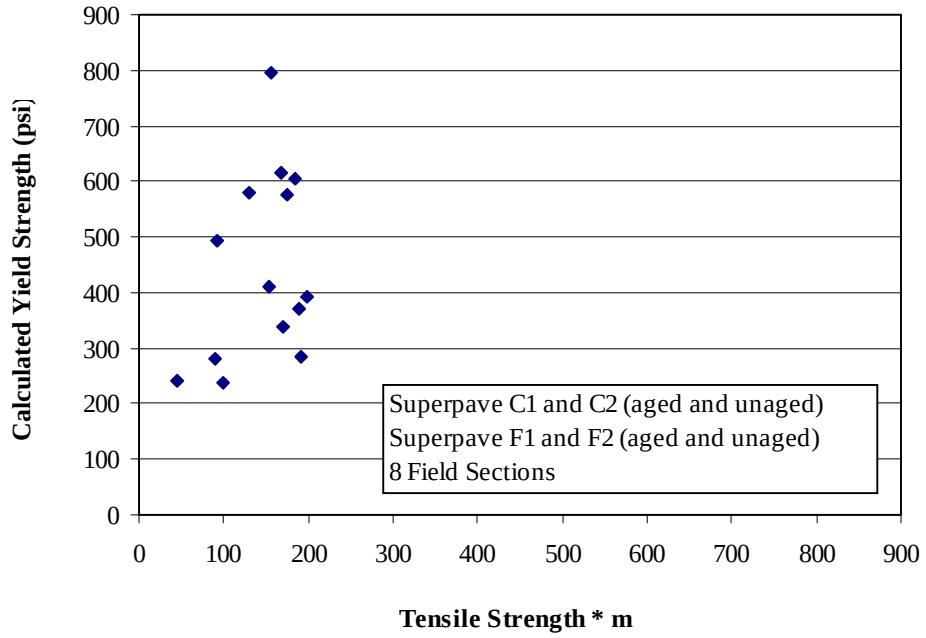

Figure 5.51 Relation Between Calculated Yield Strength and (Tensile Strength)*m-Value Using Model B5.4

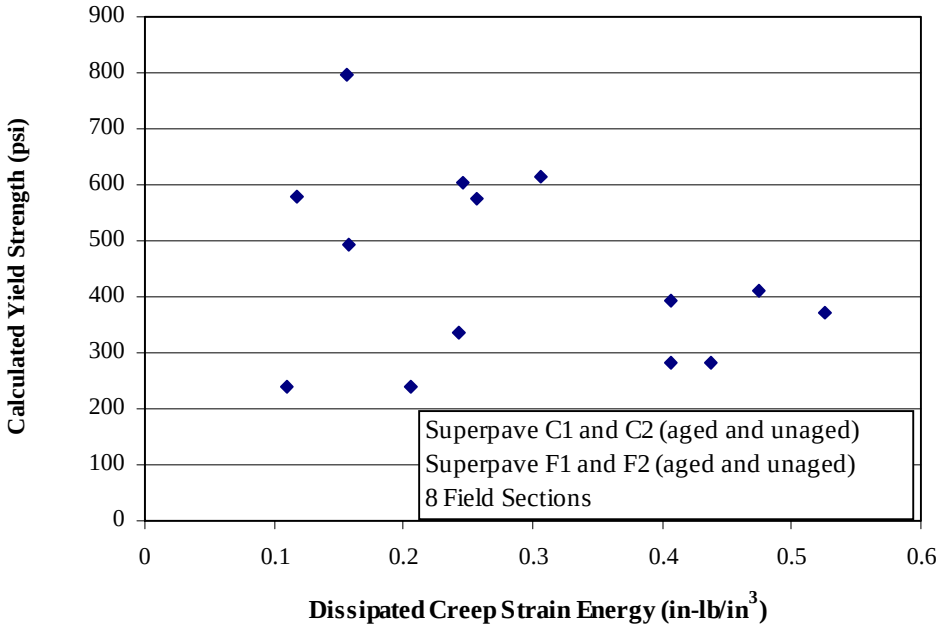

Figure 5.52 Relation Between Calculated Yield Strength and Dissipated Creep Strain Energy Using Model B5.4

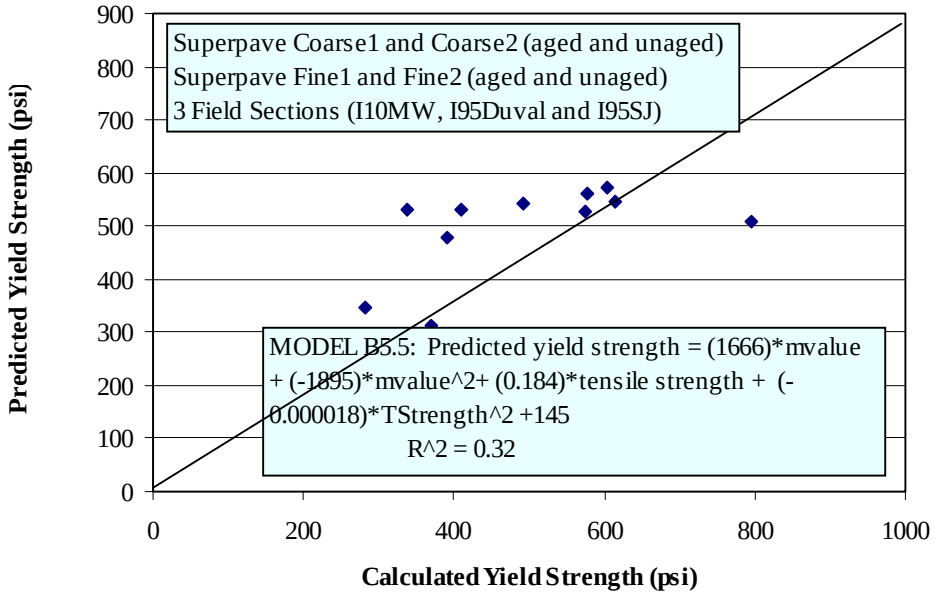

Figure 5.53 Relation Between Predicted Yield Strength and Calculated Yield Strength Using Model B5.5

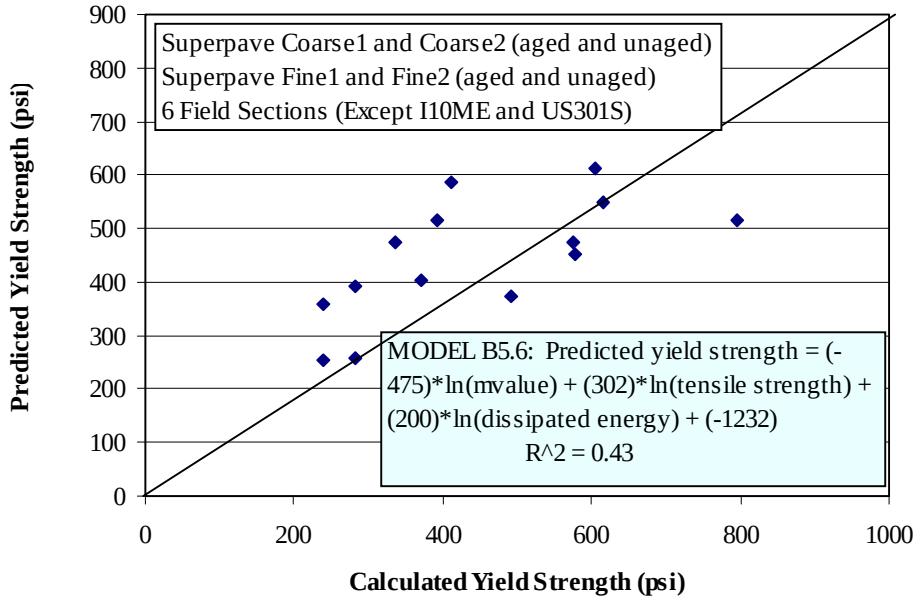

Figure 5.54 Relation Between Predicted Yield Strength and Calculated Yield Strength Using Model B5.6

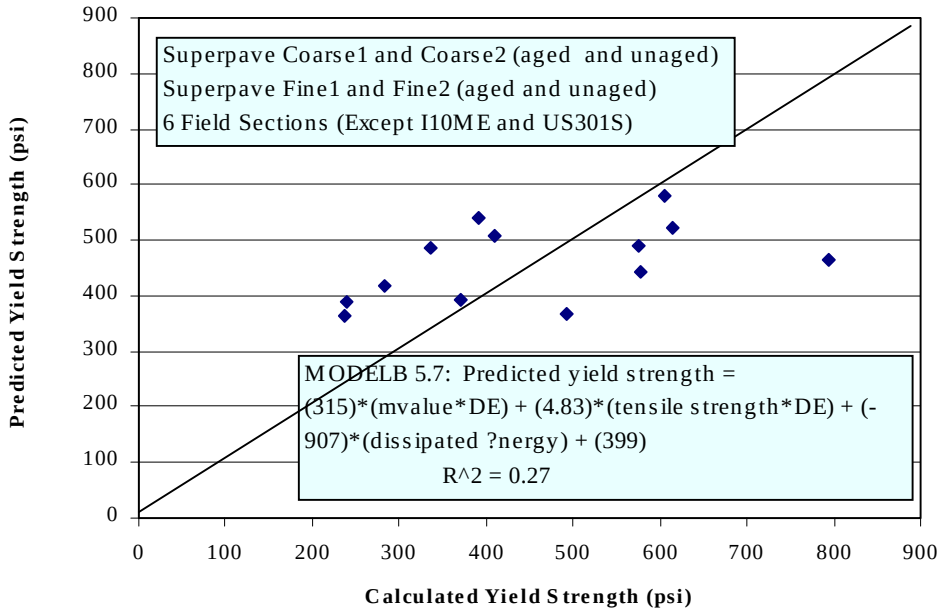

Figure 5.55 Relation Between Predicted Yield Strength and Calculated Yield Strength Using Model B5.7

5.7 RE-EVALUATION OF DISSIPATED CREEP STRAIN ENERGY AS A THRESHOLD

As indicated in Section 5.5, it was strongly believed that the threshold should be related to the energy to failure. However, the dissipated creep strain energy calculated in the section 5.5 was highly dependent on the stress state in the vicinity near the crack tip, therefore, the dissipated creep strain energy obtained could not be used as a threshold. Section 5.6 provided a rational approach to determine yield strength based on energy concept. However, it was found that the yield strength may not significantly affect crack performance in asphalt mixtures and pavements. Based on these two conclusions, it was felt that the threshold could be determined using dissipated creep strain energy determined using the energy approach presented in Section 5.6. Therefore, re-evaluation of dissipated creep strain energy as a threshold was conducted on

this basis, including (1) calculation procedure (Section 5.7.1); and (2) results and evaluation (Section 5.7.2).

5.7.1 Calculation Procedure

Calculation of total dissipated creep strain energy from repeated loading test involves the following steps:

1. Determine dissipated creep strain energy per cycle. From Equation (5.22) in Section 5.5, the dissipated creep strain energy per cycles is obtained:

$$DE_{creepstrain} / cycle = \frac{1}{20}\sigma_{AVE}(\sigma_{AVE} D_1 m(100))^{m-1} \quad (5.27)$$

   where σ_{AVE} is obtained from equation (5.26) in which σ_o is the predicted yield strength determined from each relationship between yield strength and mixtures properties, and D_1 and m are determined from creep tests.

2. Determine the total dissipated creep strain energy. The total dissipated creep strain energy is determined as follows:

$$\text{Total } DE_{creepstrain} = DE_{creepstrain} / \text{cycle} * \text{Number of Cycles}$$

$$\therefore \text{Total } DE_{creepstrain} = \frac{1}{20}\ \sigma_{AVE}(\sigma_{AVE} D_1 m(100))^{m-1} * \text{Number of Cycles} \quad (5.28)$$

5.7.2 Results and Evaluation

As an example, the relationship between yield strength and mixture properties presented in Figure 5.46 was selected in this study because this relationship was simple (i.e., linear relationship between predicted yield strength and mixture properties) and all mixture properties (i.e., m-value, tensile strength and dissipated creep strain energy) were included. Figure 5.56 shows the relationship between the total dissipated creep strain energy from cyclic load test and the total dissipated creep strain energy from strength test. Since the predicted yield strengths were

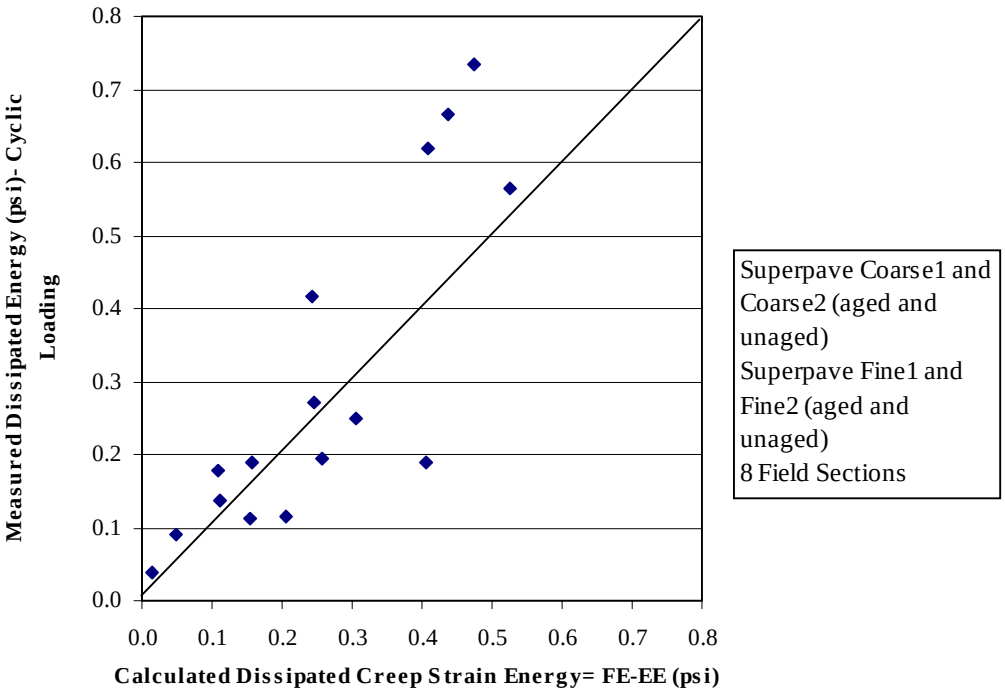

Figure 5.56 Relation Between Measured Dissipated Creep Strain Energy and Calculated Dissipated Creep Strain Energy Using Model B5.4

not available for the I-10 ME section and the US301S section, tensile strengths in these sections were used instead of predicted yield strengths.

From the data presented in Figure 5.56, it was noted that: (1) the measured dissipated creep strain energy from cyclic loading test and the measured dissipated creep strain energy test are well correlated; (2) the magnitudes of these two dissipated energies are one to one correspondence. In addition, for the purpose of verifying the above statement, the dissipated creep strain energy from cyclic loading test was calculated by using the different relationship (e.g., the relationship presented in Figure 5.55). Figure 5.57 also shows the same observation stated above.

Given the results presented above, it appears that predicted yield strength from any relationship had low correlation with calculated yield strength, however, the dissipated creep

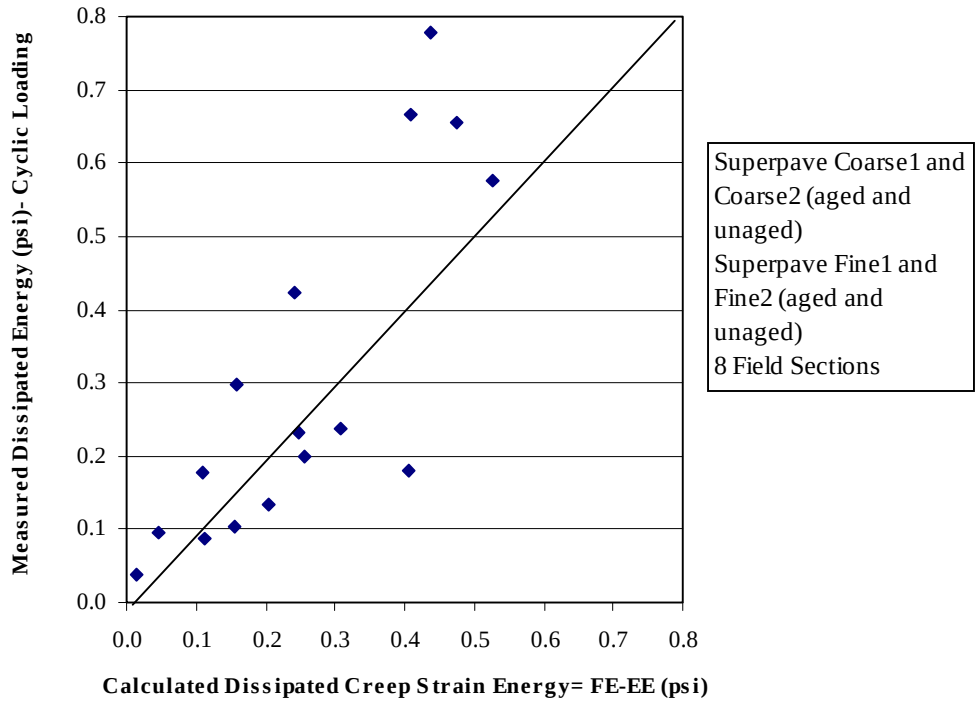

Figure 5.57 Relation Between Measured Dissipated Creep Strain Energy and Calculated Dissipated Creep Strain Energy Using Model B5.7

strain energy, using Equation (5.28), from cyclic loading (i.e., predicted yield strength was used) correlated well with the dissipated creep strain energy from strength tests. This finding provides further confidence to conclude that (1) yield strength does not appear to have a significant influence on crack performance; (2) dissipated creep strain energy to failure for cyclic loading test can be obtained from strength tests, which has the obvious benefit of simplifying the test process; (3) since dissipated creep strain energy determined by Equation (5.28) was almost the same for the different relationships, this indicates that dissipated creep strain energy is a good criterion, a fundamental property related to a material. Therefore, dissipated creep strain energy can be used as a threshold.

5.8 SUMMARY OF FINDINGS AND ANALYSES

The results of this chapter has led to the identification of a fundamental crack growth law that can be the foundation for developing a crack prediction model for asphalt pavements. Discrepancies between laboratory tests and field performance were observed. Evaluation of results verified the validity of the test results. Through examination of permanent deformation and investigation on alternative crack growth laws, it was concluded that threshold is the key feature in explaining the discrepancies between laboratory data and field performance. The outcome from examination of healing effect indicated that micro-damage is healable. However, once the threshold is exceeded, macro-cracks develop, and can not be healed.

Since the threshold is a material state between micro-damage state and macro-crack state, a value of threshold should not be related to the mode of loading (i.e., cyclic loading test or strength test). A rational and reliable approach was developed in this study to determine yield strength based on energy approach. The results indicated that yield strength is not a significant factor affecting crack resistance. Therefore, yield strength can not be used as a threshold. Finally, based on the work performed in this study (evaluation of dissipated creep strain energy or yield strength as a threshold), it was determined that dissipated creep strain energy to failure is not related to the mode of loading, and is constant at a given temperature. Therefore, dissipated creep strain energy can be used as a threshold. Furthermore, it was found that the value of dissipated creep strain energy to failure can be determined from strength test instead of cyclic loading test.

CHAPTER 6

HMA FRACTURE MECHANICS MODEL

As indicated in Chapter 5, dissipated creep strain energy to failure appears to be a reasonable threshold to control crack performance in asphalt pavements. Based on the research performed, it was strongly believed that the introduction of a threshold could be the foundation to set up a fundamental model to predict cracks in asphalt pavements. In other words, this model could simulate crack behavior on asphalt pavements (i.e., crack initiation and propagation and/or healing resulting from realistic loading and healing effects) using dissipated creep strain energy as a criterion.

In this chapter, the basic concept of HMA (Hot-Mix-Asphalt) Fracture Mechanics Model is presented in Section 6.1; development of HMA Fracture Mechanics Model is described in Section 6.2; and recommendation on evaluation of HMA Fracture Mechanics Model is presented in Section 6.3.

6.1 BASIC CONCEPT OF HMA FRACTURE MECHANICS MODEL

It is known that cracks always occur on asphalt pavements, and cracks will propagate under realistic repeated loading condition. However, as mentioned in Chapter 5, it was found that crack growth rate da/dN measured in the laboratory does not correlate well with field performance. The reason for this is that crack growth rate measured in the laboratory is not a fundamental property related to cracking performance in the field because it does not consider realistic loading history and healing effect on real pavements.

Based on the analyses and discussion presented in Chapter 5, it was believed that the threshold concept, associated with the idea that micro-damage is healable if the threshold is not

exceeded, while macro-damage is not healable once threshold is exceeded, would help to explain the effect of loading history and healing on asphalt pavement cracking.

Preliminary laboratory tests verified the presence of a threshold. Further investigation on identification of threshold led to the key findings that the dissipated creep strain energy obtained from cyclic loading test corresponding to the number of cycles at which cracks start to propagate correlated well with the dissipated creep strain energy to failure from strength tests. It appears that this finding may imply that dissipated creep strain energy, resulting in crack initiation and propagation, is a fundamental material property, which is a constant value at a given temperature and is not related to the mode of loading (i.e., static or dynamic load, stress controlled or strain controlled test). Therefore, it was concluded that under repeated loading condition, dissipated creep strain energy can be used as a threshold, and the value of threshold can be simply obtained from strength test. It was also recognized that under critical loading conditions, fracture energy can be used as a threshold since it is the energy required to fail the asphalt mixtures instantly.

In addition, it was found that yield strength did not have a significant effect on cracking behavior of asphalt mixtures, since the research results showed that yield strength was not sensitive to material properties (i.e., m-value, tensile strength, and dissipated energy) measured in the laboratory. Therefore, one may conclude that for modeling purposes, the tensile strength (global failure) could be used instead of yield strength (local failure).

Furthermore, based on the threshold concept, it was assumed that in real pavements, all micro-damage will be healed within a day while macro-damage will not be healed. This is a rational assumption consistent with the literature (Jacobs, Hopman, Molenaar, 1996), which mentioned that discontinuity in crack propagation of asphalt mixtures was observed in the laboratory. Therefore, it appears that cracks do not grow continuously, but rather discontinuously

(i.e., in a step-wise manner), represented by a repeating process of crack initiation and crack propagation stage.

Finally, the key points associated with HMA (Hot-Mix-Asphalt) Fracture Mechanics Model are summarized as the follows:

- The threshold concept is introduced in this model which is associated with the key feature that if threshold is not exceeded, micro-damage is healable, once threshold is exceeded, macro-damage is not healable.
- Under repeated loading condition, dissipated creep strain energy can be used as a threshold, and it can be easily obtained from strength tests using the Superpave Indirect Tensile Test system (IDT).
- Under critical loading condition, fracture energy obtained from strength test can be used as a threshold.
- Since asphalt is a viscoelastic material, crack initiation and crack propagation stages can not be distinguished, cracks grow discontinuously (i.e., crack grows in a step-wise manner).
- This model can handle realistic repeated loading condition and healing effect on asphalt pavements using dissipated creep strain energy and/or fracture energy as a criterion.
- All parameters needed to describe crack growth are obtained from relatively simple Indirect Tensile Test (IDT) (i.e., resilient modulus, creep response – m-value, fracture energy to failure and tensile strength).

6.2 DEVELOPMENT OF HMA FRACTURE MECHANICS MODEL

As a first step, the development of HMA Fracture Mechanics Model is presented in this section. The purpose of this model was to determine the relationship between crack parameters

(i.e., crack length *a*, crack growth rate da/dN, and stress intensity factor) and the number of cycles N. It was realized that more standardized procedures are needed to be developed for the application of this model to real pavements. As a beginning, a preliminary model was created in order to achieve the above purposes. The procedure of this model involves the following steps (Figure 6.1):

1. Determine the stress distribution near the crack tip. It was noted that the actual stress distribution near the crack tip was unknown at this time, however, it can be obtained from modeling (i.e., FEM outcome will provide stress distribution near crack tip). However, as a starting point, the stress distribution was assumed in this model. According to the definition of stress intensity factor K_I, the stress distribution within the range of 0.1*a* (*a* is half of the crack length) was assumed to be $\sigma_{FA}(1/2r)^{1/2}$. Beyond a distance r, which is the length of the process zone in front of the crack tip, (r was assumed equal to 5 mm based on laboratory data corresponding to the half of initial crack length of 10 mm), stress was assumed equal to the far away stress. Within the range from 0.1*a* to r, stress distribution was assumed to be a linear distribution between these two points.
2. Determine the size of process zone. The size of the process zone is determined based on the stress distribution. This is an energy-based approach, dissipated creep strain energy accumulates in each zone until failure occurs within the zone. The size of each zone is constant and can be determined initially for different crack length. For example:
   At half the initial crack length a_i, the stress distribution within 0.1*a* is:

$$\sigma = \frac{\sigma_{FA}\sqrt{a_i}}{\sqrt{2r}} \tag{6.1}$$

   Zone 1:

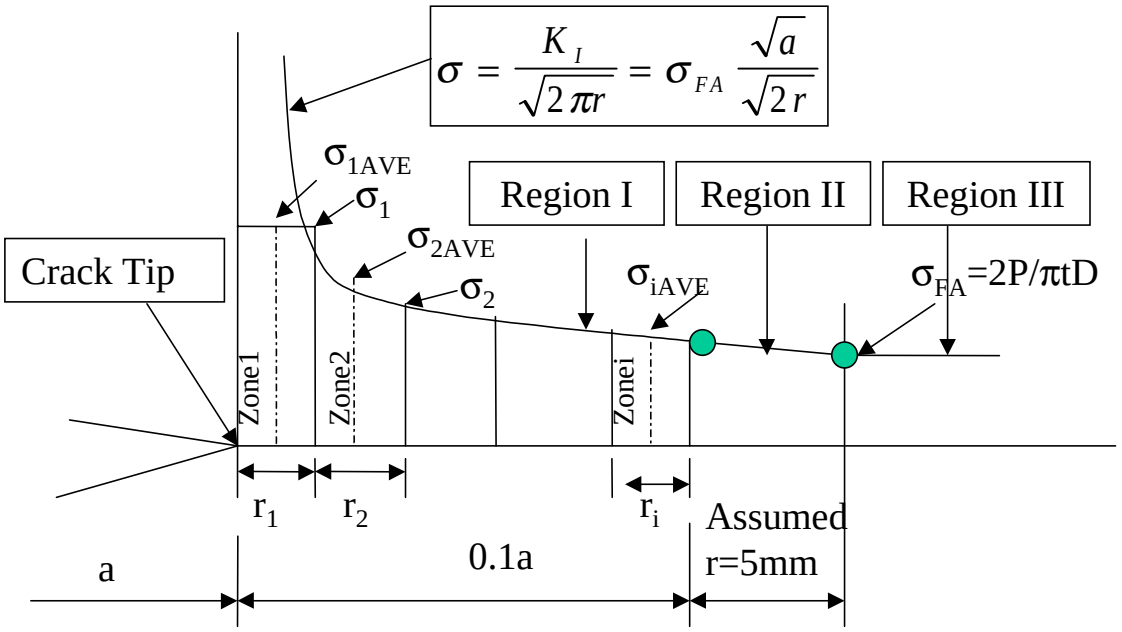

Figure 6.1 Stress Distribution Near the Crack Tip

The size of zone 1 is determined corresponding to the half of crack length a_i. Maximum stress (i.e., yield strength) was assumed to be equal to tensile strength S_t, and far away stress σ_{FA} equaled $2P/\pi tD$ for indirect tensile test (IDT) specimen. Therefore,

$$r_1 = \frac{1}{2}\left(\frac{\sigma_{FA}}{S_t}\right)^2 a_i \qquad (6.2)$$

Zone 2:

The size of zone 2 is determined corresponding to the half of crack length $a_i + r_1$

$$r_2 = \frac{1}{2}\left(\frac{\sigma_{FA}}{S_t}\right)^2 (a_i + r_1) \qquad (6.3)$$

Zone n:

Similarly, the size of zone n corresponding to the half of maximum crack length $a_i + r_1 + r_2 + r_i + \ldots\ldots + r_n$ (the assumed maximum crack length to fail the specimen is 56 (28 x 2) mm based on the laboratory data. Detailed information is presented in Chapter 4)

$$r_n = \frac{1}{2}\left(\frac{\sigma_{FA}}{S_t}\right)^2 (a_i + r_1 + r_2 + ...r_i + r_n) \tag{6.4}$$

3. Determine the dissipated creep strain energy accumulated in each zone with the number of cycles N_1, which is the number of cycles to fail Zone 1. The basic concept in this step is that if the total energy accumulated in each zone equals to the threshold, then the crack will propagate through this zone:

Zone 1:

Tensile strength (i.e., maximum stress) equals to the average stress, therefore,

$$\begin{aligned} DE_{creepstrain}/cycle &= \int_0^{0.1} (S_t)(\dot{\varepsilon}_{P\,max})dt \\ \therefore DE_{creepstrain}/cycle &= \frac{1}{20}(S_t)^2 D_1 m t^{m-1} \end{aligned} \tag{6.5}$$

the number of cycles to fail this zone is:

$$N_1 = \frac{\text{Total Dissipated Creep Strain Energy from Strength Test}}{DE_{creepstrain}/cycle} \tag{6.6}$$

Zone 2:

Step 1: determine the stress σ_2 corresponds to $r_1 + r_2$ on the stress distribution curve. The average stress in zone 2 is:

$$\sigma_{2AVE} = \frac{1}{2}(\sigma_1 + \sigma_2) \tag{6.7}$$

Step 2: determine the dissipated creep strain energy accumulated under N_1:

where $DE21_{creepstrain}$/cycle is the dissipated creep strain energy per cycle in zone 2 caused by N_1, and Total$DE21_{creepstrain}$ is the total dissipated creep strain energy in zone 2 caused by N_1

$$DE21_{creepstrain}/cycle = \frac{1}{20}(\sigma_{AVE})^2(D_1 m t^{m-1})$$
$$\therefore Total\ \ DE21_{creepstrain} = (DE21_{creepstrain}/cycle) * N_1 \quad (6.8)$$

Zone n:

Repeat this process and determine Total $DE31_{creepstrain}$ through Total $DEn1_{creepstrain}$, where Total $DEn1_{creepstrain}$ is the total dissipated creep strain energy in zone n (i.e., half of the crack length =28 mm) caused by N_1

4. Determine the number of cycles N_2 to fail zone 2. Since zone 1 already failed, the half of crack length increases to a_i+r_1, the dissipated creep strain energy per cycle to fail zone 2 is the same as presented in Equation (6.5)

   In addition to N_1, ΔN_2 is needed to fail zone 2. ΔN_2 is determined:

$$\Delta N_2 = \frac{TotalDissipatedCreepStrainEnergyfromStrengthTest - TotalDE21_{creepstrain}}{DE_{creepstrain}/cycle} \quad (6.9)$$

   therefore, the total number of cycles to fail zone 2 is determined:

$$N_2 = N_1 + \Delta N_2 \quad (6.10)$$

   Repeat Step 3, and determine the total dissipated creep strain energy from zone 3 through zone n caused by ΔN_2.

5. Repeat Steps 3 and 4, and determine the total number of cycles N to fail the specimen (i.e., determine the number of cycles N to fail zone n, corresponding to the half of crack length = 28 mm)

As indicated earlier, this is a preliminary approach to set up a cracking model. The obvious advantage of this approach is that it provided the possible methodology to apply the threshold as a criterion to predict crack length *a* in a model. It was noted that the relationships between crack length *a* and the number of load applications N, and crack growth rate da/dN and stress intensity factor K can be obtained from this model. However, it was realized that several points needed to be modified before applying this approach in a real pavement model, for example:(1) determination of stress distribution near crack tip under realistic loading conditions and healing effect; (2) defining and determination of far away stress σ_{FA} for real pavements; (3) determination of the size of each interested zone. Since the size of each zone is related to far away stress σ_{FA}, it is not constant under different loading conditions as crack length increases.

6.3 RECOMMENDATION ON EVALUATION OF HMA FRACTURE MECHANICS MODEL

Recommendation on evaluation of the HMA (Hot-Mix-Asphalt) Fracture Mechanics Model includes the following aspects:

1. Compare the relationships between crack length and the number of load applications from this model and the laboratory data. Preliminary work was performed on SuperPave™ coarse. Figures 6.2 and 6.3 show that the relationship between crack length and the number of load replications obtained from this model is very similar to that obtained from the laboratory test. This result indicates that this model is rational and reliable to predict cracking behavior of asphalt mixtures. Furthermore, it provides the further verification that threshold can be a criterion controlling crack performance.
2. Compare the relationships between crack growth rate da/dN and stress intensity factor K from this model and the laboratory results. The purpose of this evaluation is to examine

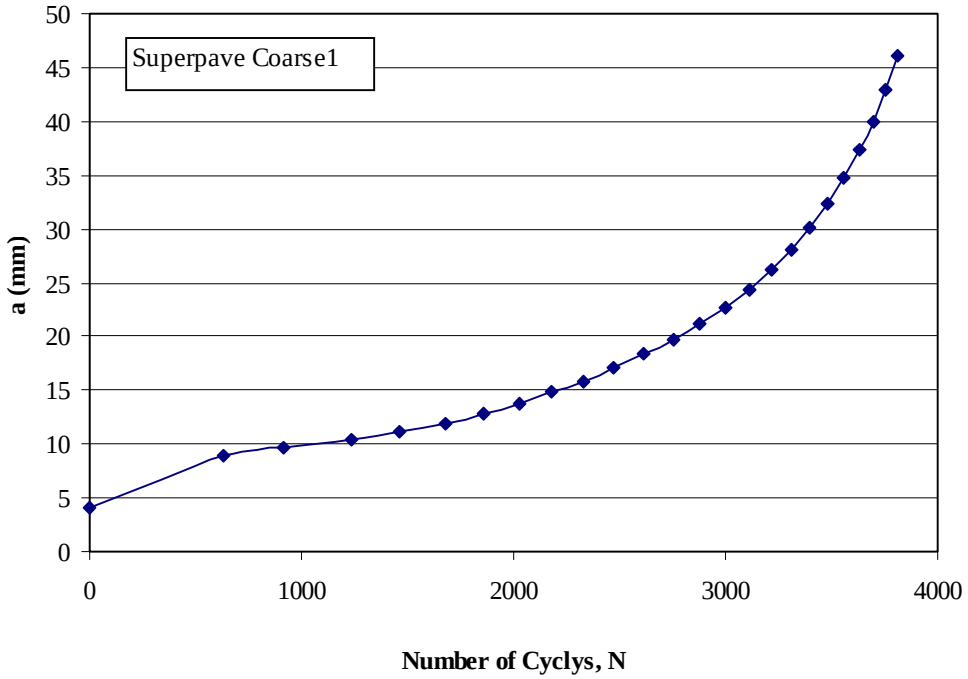

Figure 6.2 Crack Length vs. Load Replications Using HMA Fracture Mechanics Model

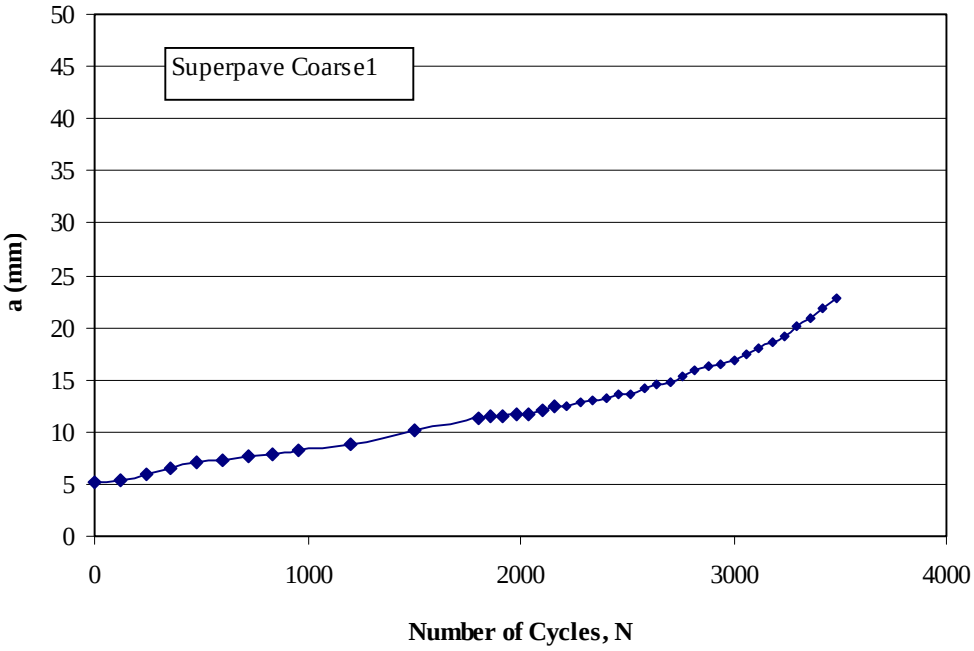

Figure 6.3 Crack Length vs. Load Replications from Fracture Test

the influence of stress level. As shown in Figure 4.17, it was noted that the slope of da/dN versus K at lower stress level is higher than that at higher stress level. If this pattern would be obtained from this model, it implies that fracture parameters, A and n, are not fundamental properties because they are related to stress level.

3. Compare the shapes of relationship between crack growth rate da/dN and stress intensity factor K from this model and the laboratory data. The purpose of this work is to provide further evidence that this model would accurately predict crack performance for asphalt mixtures.

4. In addition to the above aspects, this model could provide a rational explanation on the discrepancies between the laboratory data and field performance. For example, it was known that the US301N section had lower crack growth rate da/dN than in the I-95 DN section in the laboratory measurements, while the US301N was one of the worst performer, however, the I-95 DN section was one of the best performer in the field. From this model, it may show that under repeated loading condition, the crack growth rate in the US301 section is lower than that in the I-95 DN section, however, under realistic loading condition and healing effect, the US301N section may have longer crack length than that in I-95 DN section. This result may be explained by the fact that the US301N section had a lower threshold and less micro-damage, while the I-95 Duval N section had higher threshold and more micro-damage in the field. Therefore, the US301N section probably experienced more non-healable damage, which resulted in worst performance, while the I-95 Duval N section experienced more healable damage, which resulted in good performance in the filed. However, in the laboratory test, healing was not allowed to occur, so micro-damage was forced to form macro-damage under repeated loading

condition. Therefore, this could result in higher crack growth rate da/dN in the I-95 Duval N section than in the US301 section in the laboratory test results

CHAPTER 7

FINDINGS, CONCLUSIONS, AND RECOMMENDATIONS

7.1 SUMMARY OF FINDINGS

Prior work recommended further development and use of the SuperPave™ IDT to achieve a better understanding of the cracking mechanisms in asphalt mixtures and the primary mixture properties that control them. This work focused on developing laboratory testing systems to measure and characterize crack growth behavior of asphalt mixtures using the SuperPave™ IDT. Crack growth tests were then performed on asphalt pavement cores obtained from field sections of known cracking performance. Discrepancies were found between laboratory crack growth rates and observed field performance, which indicated that the mechanisms of cracking in the field are significantly different than the mechanisms used to induce cracking in traditional laboratory fatigue and fracture tests. Specifically, loading conditions are different between the laboratory and the field. In the laboratory, specimens are forced to fail under repeated loading conditions, whereas asphalt mixtures may heal under realistic loading conditions and/or temperature increases.

Based on these findings and observations, a threshold concept was introduced, which appears to be a key element in defining the cracking mechanisms of asphalt mixtures. It was further determined that two material properties that are easily obtained from the SuperPave™ IDT, total fracture energy (FE_f) and the dissipated creep strain energy to failure ($DCSE_f$), appear to accurately define the threshold for asphalt mixtures. These properties were also determined to be fundamental which means that they can be used to evaluate and control fracture for any type of loading condition (e.g., stress-cotnrolled, strain-controlled, repeated cycling, critical

conditions, etc.). It also means that they can be determined from very simple laboratory testing procedures, which is exceedingly advantageous from the standpoint of practical application.

It was determined that only five mixture properties, which are easily obtained from the SuperPave™ IDT, are needed to control the cracking performance of asphalt mixtures subjected to any loading condition:

1. The m-value, which was determined to be directly related to the rate of micro-crack development in asphalt mixtures.
2. The dissipated creep strain energy to fracture ($DCSE_f$), which was determined to be the threshold energy above which macro-cracks develop under repeated loading conditions.
3. The total energy to fracture (FE_f), which was determined to be the threshold energy above which macro-cracks will develop under a single critical load.
4. The resilient modulus (M_R), which affects the stress level for a given load and pavement structure, and is needed to determine $DCSE_f$.
5. The creep compliance (D(t)), which affects the thermal stress level for a given cooling condition.

Testing and data reduction procedures and software were developed to determine these properties simply and reliably from the following tests using the SuperPave™ IDT:

1. A 100 second creep test (m-value and creep compliance).
2. A 10 second tensile strength test ($DCSE_f$ and FE_f).
3. A 5 second resilient modulus test (M_R).

In addition, a fundamental crack initiation and growth law that can predict the cracking performance of asphalt mixtures subjected to any generalized loading condition was developed and evaluated. The test procedures and crack growth law developed in

this study provide FDOT, as well as the pavement community in general, with the tools needed to design and specify asphalt mixtures and pavements that resist cracking.

7.2 RECOMMENDATIONS

The primary recommendations from this work are as follows:

- The FDOT should immediately begin the process of developing a mixture specification based on the crack growth law and associated mixture properties identified in this study. The following steps should be taken to begin this process:
  1. Systematically begin to measure these properties for a broad range of mixtures and pavements in-service.
  2. Establish a comprehensive database, including these properties, as well as all available performance information.
  3. Conduct a preliminary analysis and evaluation of all available data and performance information to develop a rational mixture specification framework.
  4. Perform a comprehensive analysis of the database to begin identifying reasonable specification limits for key mixture properties (i.e., m-value, $DCSE_f$, FE_f, and creep compliance).
- The FDOT should immediately begin to establish procedures to integrate the crack growth law and specifications with the pavement design process. The following steps should be taken to begin this process:
  1. Perform sensitivity analyses to evaluate the effects of different material properties and pavement structural characteristics on pavement cracking performance.
  2. Based on these analyses and other available data and performance information, identify loading and environmental conditions that must be considered in the

structural pavement design process. Note that identification of these conditions is also critical for development of a rational mixture specification.

- The FDOT should immediately begin using the SuperPave™ IDT systems and crack growth law developed in this study to investigate the effects of different mixture characteristics on cracking performance. Effects of gradation, asphalt content, film thickness, aggregate type, and binder type should be investigated to develop guidelines for optimizing mixtures to mitigate cracking.

Implementation of these recommendations should clearly result in improved cracking performance of pavements in Florida and elsewhere.

REFERENCES

Anderson, T.L. 1991. Fracture Mechanics - Fundamentals and Applications, Boca Raton, FL: CRC Press, 361 pp.

Bazin, P., & J.B. Saunier. 1967. "Deformability, Fatigue and Healing Properties of Asphalt Mixes." Proc., Second International Conference on the Structural Design of Asphalt Pavements, Ann Arbor, MI, pp. 553-569.

Button, J.W., D.N. Little, Y. Kim, & J. Ahmed. 1987. "Mechanistic Evaluation of Selected Asphalt Additives." Proceedings of the Association of Asphalt Paving Technologists, Vol. 56, pp. 62-90.

Chomton, G., & P.J. Valayer. 1972. "Applied Rheology of Asphalt Mixes, Practical Applications." Proceedings of the Third International Conference on the Structural Designing of Asphalt Pavements, London, Vol. I, pp. 214-232.

Di Bennedetto, H., A.A. Soltani, & P. Chaverot. 1996. "Fatigue Damage for Bituminous Mixtures: A Pertinent Approach." Journal of the Association of Asphalt Paving Technologists, Vol. 65, pp. 142-158.

Dowling N.E. 1993. Mechanical Behavior of Materials, Englewood Cliffs, NJ: Prentice Hall, 773 pp.

Dowling, N.E., & J.A. Begley. 1976. "Fatigue Crack Growth During Cross Plasticity and the J Integral." ASTM STP 590, American Society for Testing and Materials, Philadelphia, pp. 82-103.

Elber, W. 1970. "Fatigue Crack Closure Under Cyclic Tension." Engineering Fracture Mechanics, Vol. 2, pp. 37-45.

Foreman, R.G., V.E. Keary, & R.M. Engle. 1967. "Numeral Analysis of Crack Propagation in Cyclic-Loaded Structures." Journal of Basic Engineering, Vol. 9, pp. 459-464.

Harvey, J., & B.W. Tsai. 1996. "Effect of Asphalt Content and Air Void Content on Mix Fatigue and Stiffness." Transportation Research Board, Record 1543, pp. 38-45.

Irwin, L.H. 1977. "Use of Fracture Energy as A Fatigue Failure Criterion." Journal of the Association of Asphalt Paving Technologists, Vol. 46, pp. 41-59.

Jacobs, M.M.J., P.C. Hopman, & A.A.A. Molenaar. 1996. "Application of Fracture Mechanics Principles to Analyze Cracking in Asphalt Concrete." Journal of the Association of Asphalt Paving Technologists, Vol. 65, pp.1-39.

Jacobs, M.M.J. 1995. “Crack Growth in Asphaltic Mixes.” Ph.D. Dissertation, Delft University of Technology, Road and Railroad Research Laboratory.

Kim, Y.R., D.L. Little, & F. Benson. “Chemical and Mechanical Evaluation on Healing Mechanism of Asphalt Concrete.” Journal of the Association of Asphalt Paving Technologists, Vol.59, pp.240-276, 1990.

Kim, Y.R., H-J. Lee, & D.N. Little. 1997. “Fatigue Characterization of Asphalt Concrete Using Viscoelasticity and Continuum Damage Theory.” Journal of the Association of Asphalt Paving Technologists, Vol. 66, pp. 520-569.

Kim, Y.R., H-J. Lee, & D.N. Little. 1997. “Mechanistic Evaluation of Fatigue Damage Growth and Healing of Asphalt Concrete: Laboratory and Field Experiments.” Eighth International Conference on Asphalt Pavements, Seattle, WA, pp. 1089-1107.

Klesnil, M., & P. Lukas, 1972. “Influence of Strength and Stress History on Growth and Stabilization of Fatigue Cracks.” Engineering Fracture Mechanics, Vol. 4, pp. 77-92.

Little, D.N., R.L. Lytton, D. Williams, & Y.R. Kim. 1999. “An Analysis of the Mechanism of Microdamage Healing Based on the Application of Micromechanics First Principles of Fracture and Healing.” Journal of the Association of Asphalt paving Technologists, Vol. 68, pp. 501-542.

Lytton R.L., J. Uzan, E.G. Fernando, R. Roque, D. Hiltunen, & S.M. Stoffels. 1993. “Asphalt Concrete Pavement Distress Prediction: Laboratory Testing, Analysis, Calibration and Validation.” Report SHRP_A005 Project RF 7157-2. Washington, DC.

Majidzadeh K., E.M. Kaufmann, & D.V. Ramsamooj. 1971. “Application of Fracture Mechanics in the Analysis of Pavement Fatigue.” Journal of the Association of Asphalt Paving Technologists, Vol. 40, pp. 227-246.

McEvily, A.J. 1988. “On Closure in Fatigue Crack Growth.” ASTM STP 982, American Society for Testing and Materials, Philadelphia, pp. 35-43.

Monismith, C.L. 1981. “Fatigue Characteristics of Asphalt Paving Mixtures and Their Use in Pavement Design.” Proceedings of the Eighteenth Paving Conference, East Lansing, MI.

Monismith, C.L., J.A. Epps, & F.N. Finn. 1985. “Improved Asphalt Mix Design.” Proceedings, Association of Asphalt Paving Technologists, Vol. 55, pp. 347-406.

Paris, P.C. & F. Erdogan. 1963. “A Critical Analysis of Crack Propagation Laws.” Transactions of the ASME, Journal of Basic Engineering, Series D, 85, No. 3.

Pronk, A.C., & P.C. Hopman. 1990. “Energy Dissipation: the Leading Factor of Fatigue.” Conferences Proceedings, The United States Strategic Highway Research Program–Sharing the Benefits, London, pp. 225-237.

Ramsamooj, D.V. 1991. “Prediction of Fatigue Life of Asphalt Concrete Beams from Fracture Test.” Journal of Testing and Evaluation, JTEVA, Vol. 19, No. 3, pp. 231-239.

Read, J.M., & A.C. Collop. 1997. “Practical Fatigue Characterization of Bituminous Paving Mixtures.” Journal of the Association of Asphalt Paving Technologists, Vol. 66, pp. 74-108.

Roque, R., & W.G. Buttlar. 1992. “The Development of a Measurement and Analysis System to Accurately Determine Asphalt Concrete Properties Using the Indirect Tensile Mode.” Journal of the Association of Asphalt Paving Technologists, Vol. 61, pp. 304-332.

Roque, R. W.G. Buttlar, B.E. Ruth, M. Tia, S.W. Dickison, & B. Reid. 1997. “Evaluation of SHRP Indirect Tension Tester to Mitigate Cracking in Asphalt Pavements and Overlays.” Final Report to the Florida Department of Transportation, 364 pp.

Roque, R., Z. Zhang, & B. Sankar. 1999. “Determination of Crack Growth Tate Parameters of Asphalt Mixtures Using the Superpave.” Journal of the Association of Asphalt Paving Technologists, Vol. 68, pp. 404-433.

Salam Y.M., & C.L. Monismith. 1972. “Fracture Characteristics of Asphalt Concrete.” Journal of the Association of Asphalt Paving Technologists, Vol. 41, pp. 216-254.

Schapery R.A. 1973. “A Theory of Crack Growth in Visco-Elastic Media.” Report MM 2764-73-1, Mechanics and Materials Research Center, Texas A & M University, College Station, TX.

Schapery R.A. 1975. “A Theory of Crack Initiation and Growth in Visco-Elastic Media: I: Theoretical Development, II: Approximate Methods of Analysis, III: Analysis of Continuous Growth.” International Journal of Fracture, Vol. 11, No. 1, pp. 141-159, Vol., No. 3, pp. 369-388, and Vol. 11, No. 4, pp. 549-562.

Schapery R.A. 1984. “Corresponding Principles and a Generalized J Integral for Large Deformation and Fracture Analysis of Viscoelastic Media.” International Journal of Fracture, Vol. 25, pp. 195-223.

Sedwick, S.C. 1998. “Effect of Asphalt Mixture Properties and Characteristics on Surface-Initiated Longitudinal Wheel Path Cracking.” Master’s thesis, University of Florida, Gainesville.

Sousa, J.B., G. Way, & J. Harvey. 1996. “Performance-Based Mix Design and Field Quality Control for Asphalt-Aggregate Overlays.” Transportation Research Board, Record No. 1543, pp. 46-62.

Tayebali A., G. Rowe, & J. Sousa. 1992. “Fatigue Response of Asphalt-Aggregate Mixtures.” Paper Presented at the Annual Meeting of the Association of Asphalt Paving Technologists.

Tseng, K., & R.L. Lytton. 1990. “Fatigue Damage Properties of Asphaltic Concrete Pavements.” presented at The 69th Annual Meeting of the Transportation Research Board, pp. 43.

van Dijk, W. 1975. “Practical Fatigue Characterization of Bituminous Mixes.” Proceedings, Association of Asphalt Paving Technologists, Vol. 44, pp. 38-75.

van Dijk, W., & W. Visser. 1977. “The Energy Approach to Fatigue for Pavement Design.” Journal of the Association of Asphalt Paving Technologists, Vol. 46, pp. 1-38.

Weertman, J. 1966. “Rate of Growth of Fatigue Cracks Calculated from the Theory of Infinitesimal Dislocations Distributed on a Plane.” International Journal of Fracture Mechanics, Vol. 2, pp. 460-467.

APPENDIX A
FRACTURE TEST RESULS FOR EIGHT FIELD SECTIONS

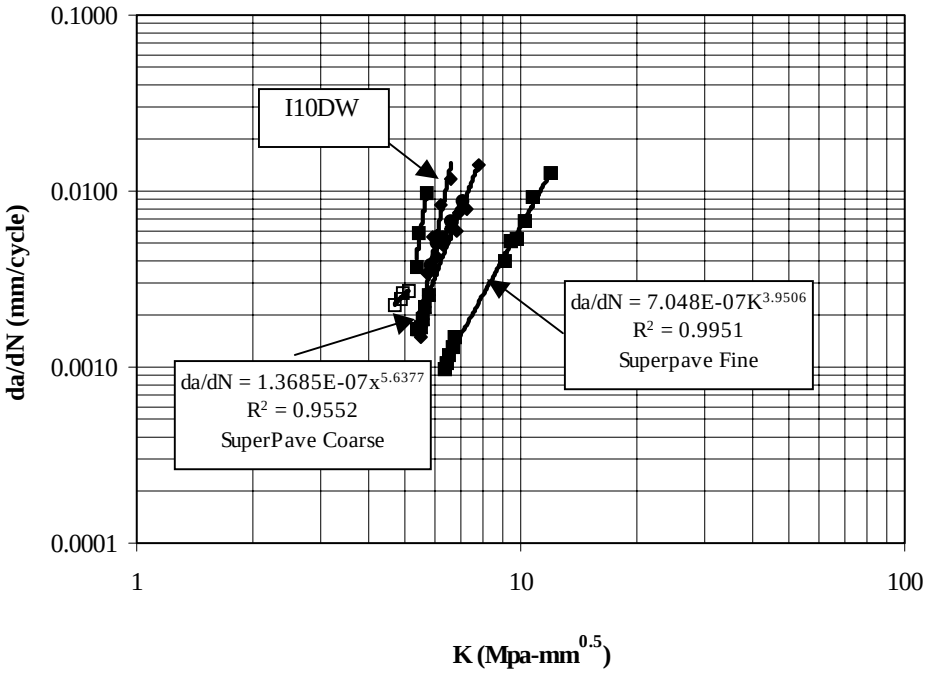

Figure A.1: Fracture Test Results from I10DW Section

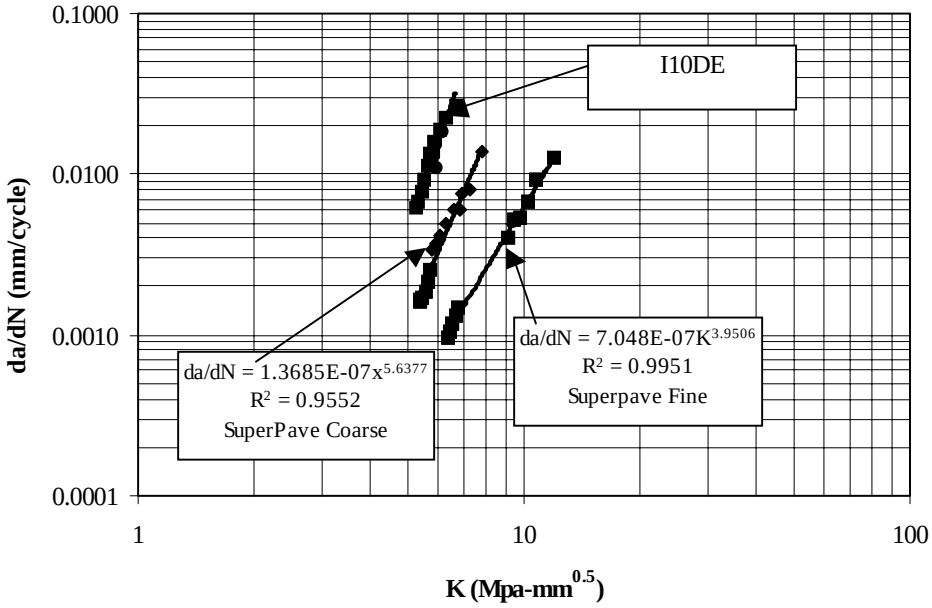

Figure A.2: Fracture Test Results from I10DE Section

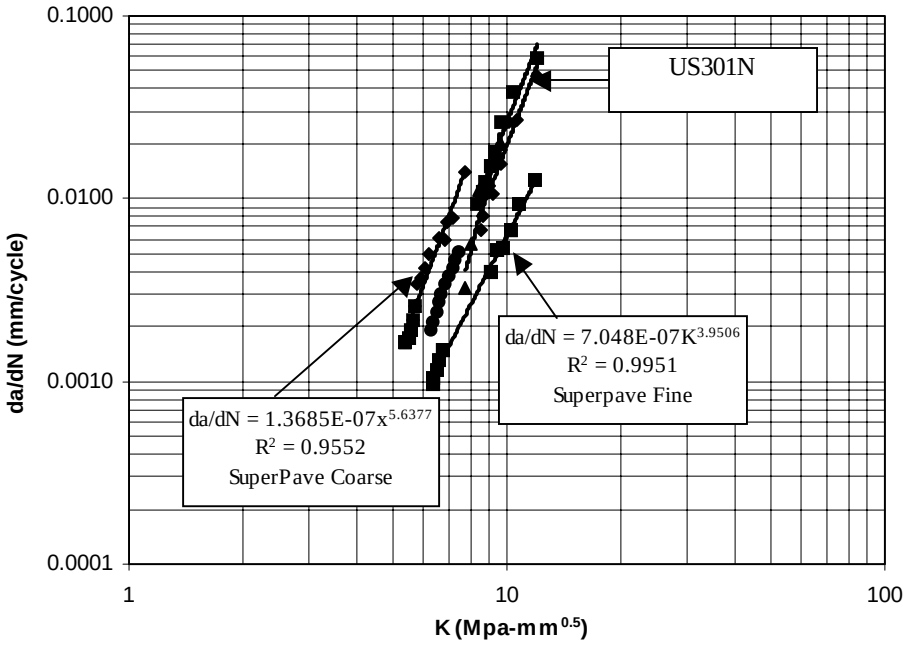

Figure A.3: Fracture Test Results from US301N Section

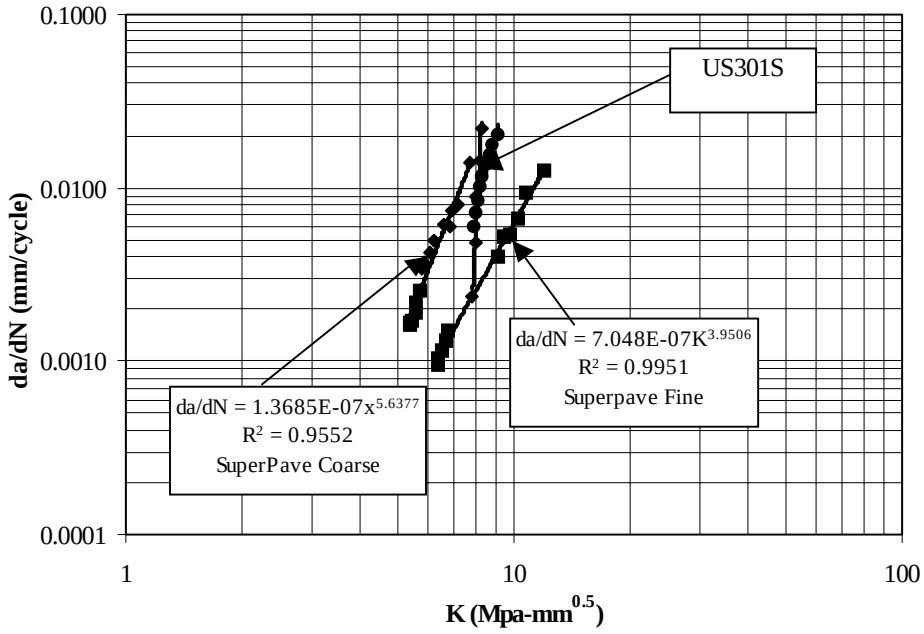

Figure A.4: Fracture Test Results from US301S Section

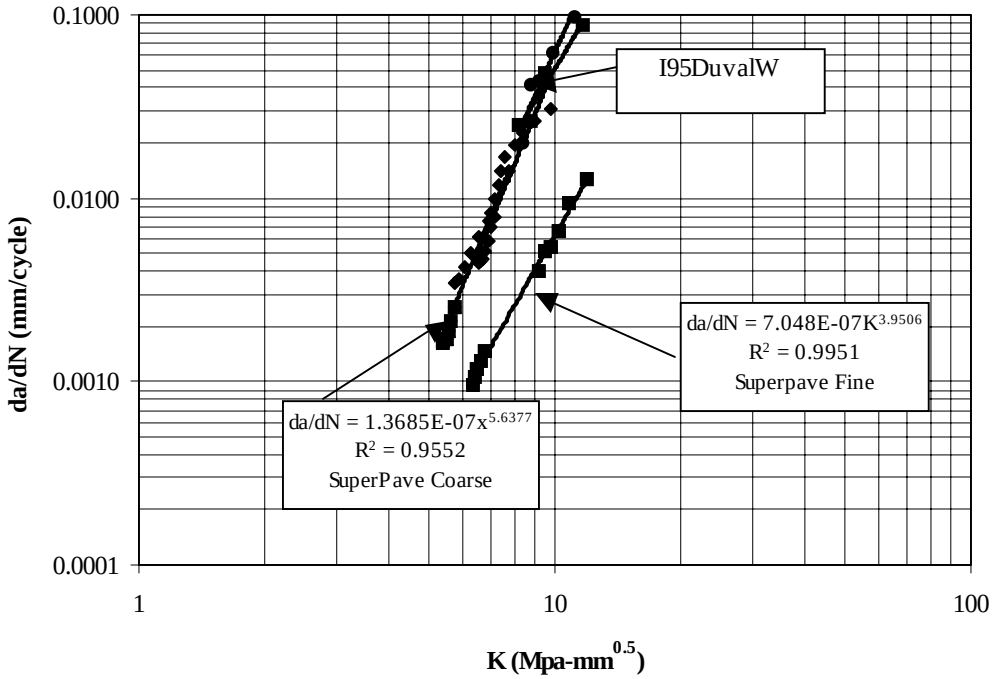

Figure A.5: Fracture Test Results from I95DuvalW Section

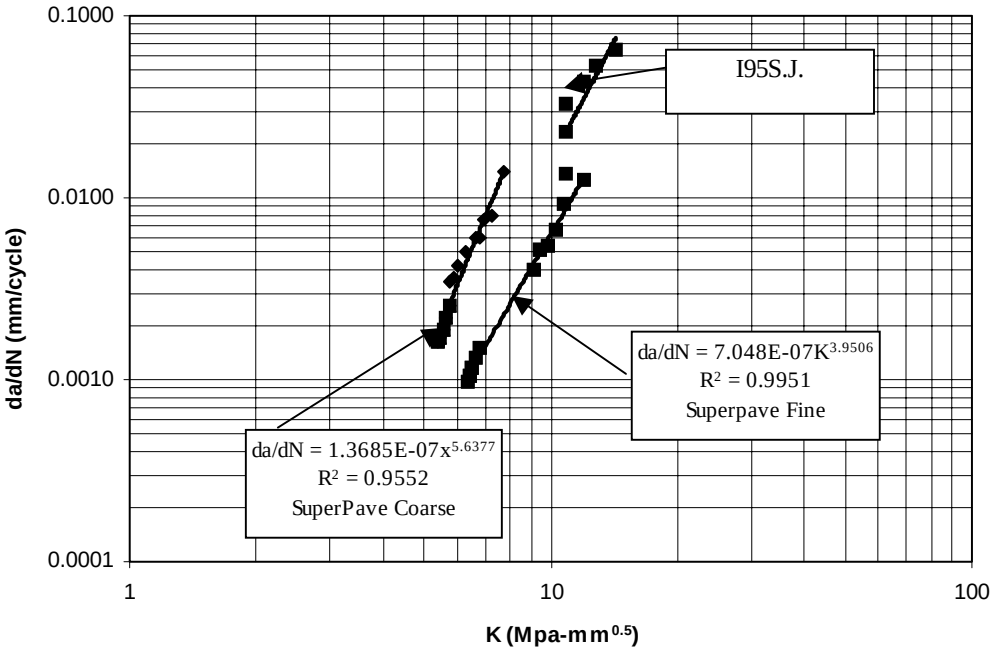

Figure A.6: Fracture Test Results from I95SJ Section

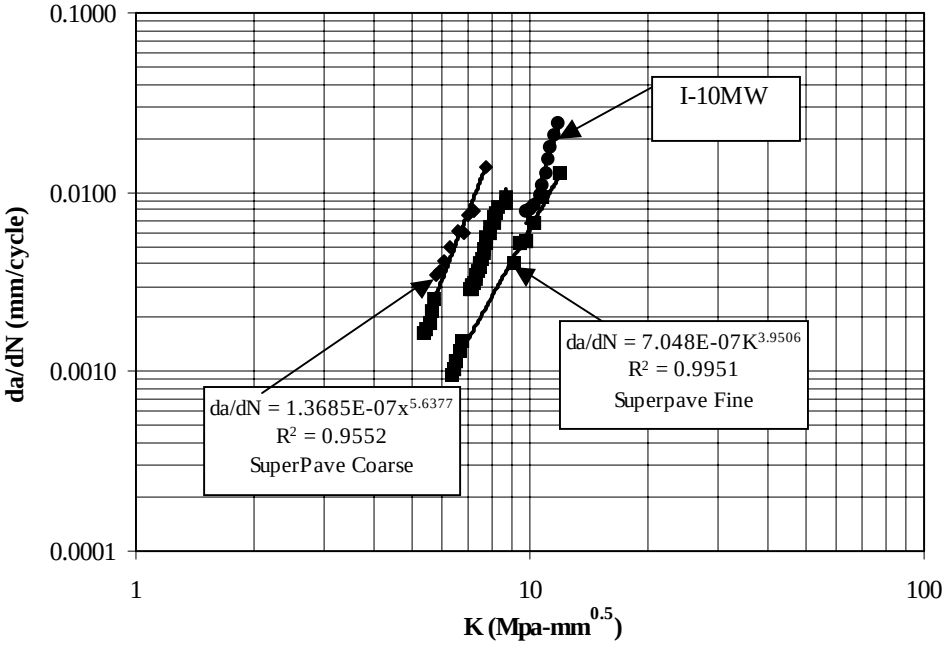

Figure A.7: Fracture Test Results from I10MW Section

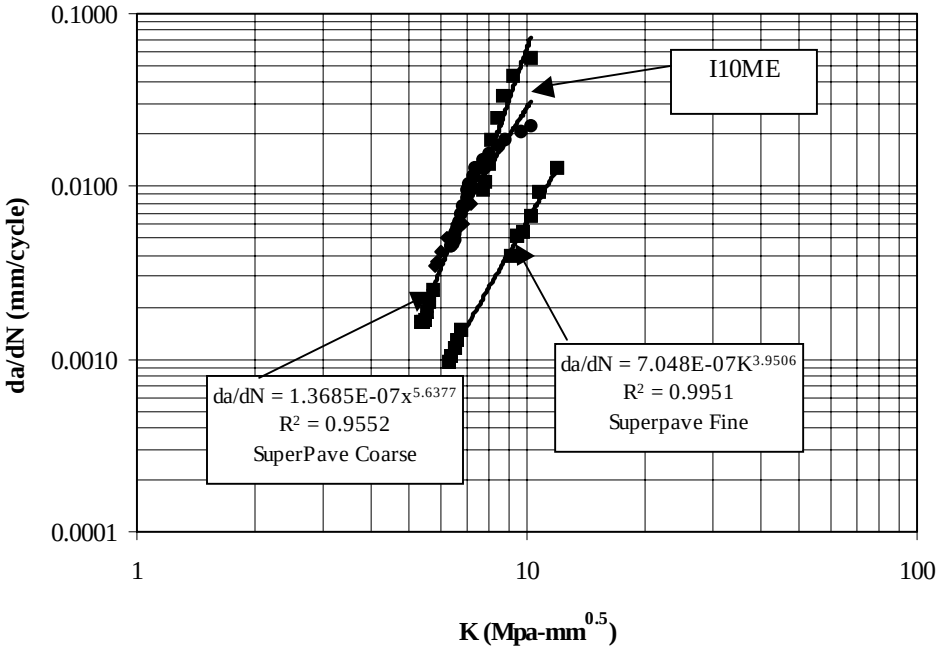

Figure A.8: Fracture Test Results from I10ME Section

Table A.1: Summary of Fracture Tests on the Field Cores (10C)

Section	No. of Specimen	Diameter (in)	Thickness (in)	Air Void	Applied Load (lb)	N – Cracks Start to Propagate	N – Specimen's Failure	Note
I10 MW	1	5.625	1	2.33	1215	4870	7390	-
	2	5.625	0.875	2.30	1723	730	1270	-
I95DN	3	5.625	0.875	5.09	1278	60	300	-
	4	5.750	1.000	4.16	1317	430	670	-
	5	5.750	1.000	4.16	1119	2100	3000	-
	6	5.940	2.000	4.89	2000	2000	3000	2in thickness
	7	5.80	2.000	4.51	2000	3000	5000	2in thickness
	8	5.750	2.000	4.45	2500	2500	3500	2in thickness
	9	5.750	2.125	4.72	2500	3500	5750	2in thickness
I95SJ	10	5.625	0.875	2.94	1671	910	1210	-
	11	5.625	1.000	3.6	1200	-	The bottom of the load cell twisted	
	12	5.625	1.000	3.12	1500	1416	Loading on one side	
	13	5.625	1.000	1.90	1488	-	Bending occurred on the specimen	
	14	5.625	0.875	1.54	1611	Loading on one side		
	15	5.800	2.000	3.83	2500	2000	3600	2in thickness
	16	5.800	2.000	4.39	2500	1750	4000	2in thickness
	17	5.750	2.125	2.58	3000	3500	5750	2in thickness
I10DE	18	5.625	1.000	0.95	1000	2910	3630	-
	19	5.625	0.875	3.6	950	740	1230	-
	20	5.625	1.125	1.23	1000	2950	5110	-
	21	5.625	1.000	1.180	1000	2130	2850	Not enough data
	22	5.750	0.875	2.74	-	-	Loading on one side	
	23	5.625	1.000	0.42	-	-	Loading on one side	

Table A.1: Summary of Fracture Tests on the Field Cores (10C) (Continued)

Section	No. of Specimen	Diameter (in)	Thickness (in)	Air Void	Applied Load (lb)	N – Cracks Start to Propagate	N – Specimen's Failure	Note
I10DW	24	5.750	1.250	1.59	1300	2740	3520	-
	25	5.625	1.125	1.62	1300	1660	2380	-
	26	5.625	1.250	3.17	1500	490	670	-
	27	5.750	1.000	1.31	1250	2000	2750	-
	28	5.750	1.000	2.5	1250	1750	3000	-
	29	5.750	1.000	0.91	1250	2000	3250	-
	30	5.750	1.000	1.46	1250	2000	2250	-
	31	5.750	1.000	0.08	1500	-	The bottom of the load cell twisted	
	32	5.940	1.000	2.06	700	3750	7250	Load was too low
	33	5.940	1.000	1.95	950	5000	10500	Load was too low
	34	5.800	2.000	2.46	2500	1000	2400	2in thickness
I10ME	35	5.625	0.875	2.36	1180	1570	1990	-
	36	5.625	1.000	0.21	1080	4030	5170	-
	37	5.626	0.875	2.30	1500	1290	Severe damage on the loading head	
	38	5.750	1.900	0.80	2000	12000		Load was too low
US301 N	39	5.625	1.000	3.19	1400	2250	3500	-
	40	5.625	1.000	2.93	1600	3500	5750	-
	41	5.625	0.875	2.81	1400	1500	1800	-
	42	5.626	0.875	2.92	1400	1500	1800	-
	43	5.625	1.125	1.79	1500	2250	5000	Loading on one side
	44	5.626	1.000	1.97	1500	-	-	Test was repeated

Table A.1: Summary of Fracture Tests on the Field Cores (10C) (Continued)

Section	No. of Specimen	Diameter (in)	Thickness (in)	Air Void	Applied Load (lb)	N for Beginning a Crack	N for Ending a Crack	Note
US301S	45	5.625	0.875	3.14	1180	3850	4270	-
	46	5.625	1.000	5.53	1400	1450	2110	-
	47	5.750	0.750	2.36	1000	2000	3100	Loading on one side
	48	5.625	1.000	1.97	1500	-	-	Test was repeated

APPENDIX B

THE MODELS FOR PREDICTING CRACK GROWTH RATE (da/dN) - STRESS INTENSITY FACTOR K= 7 Mpa-mm $^{0.5}$: 8 FIELD SECTIONS, A SUPERPAVE COARSE MIXTURE AND A SUPERPAVE FINE MIXTURE WERE USED AS INPUT DATA IN THE MODELS

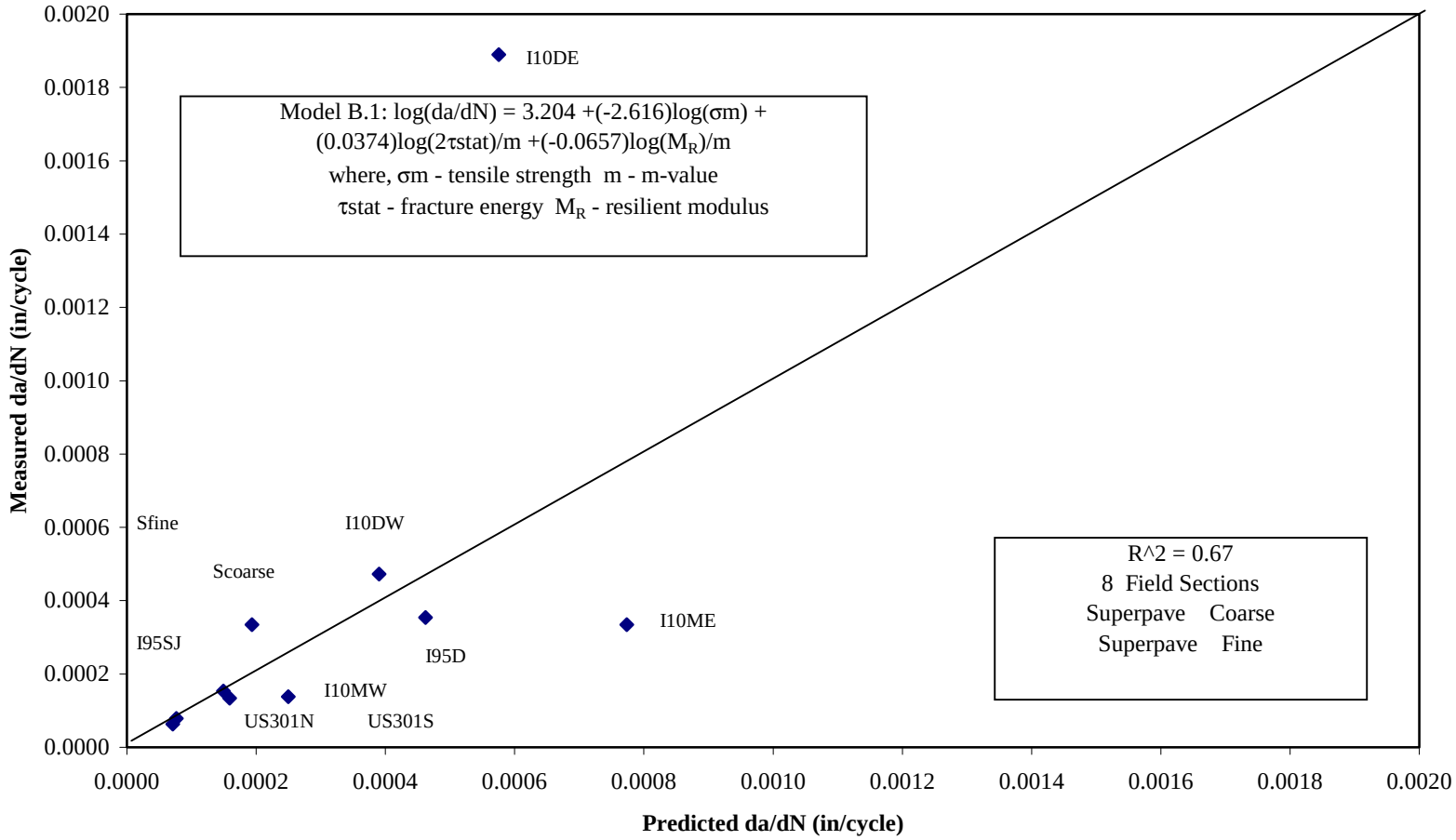

Figure B.1: Relation Between Measured da/dN and Predicted da/dN from Model B.1

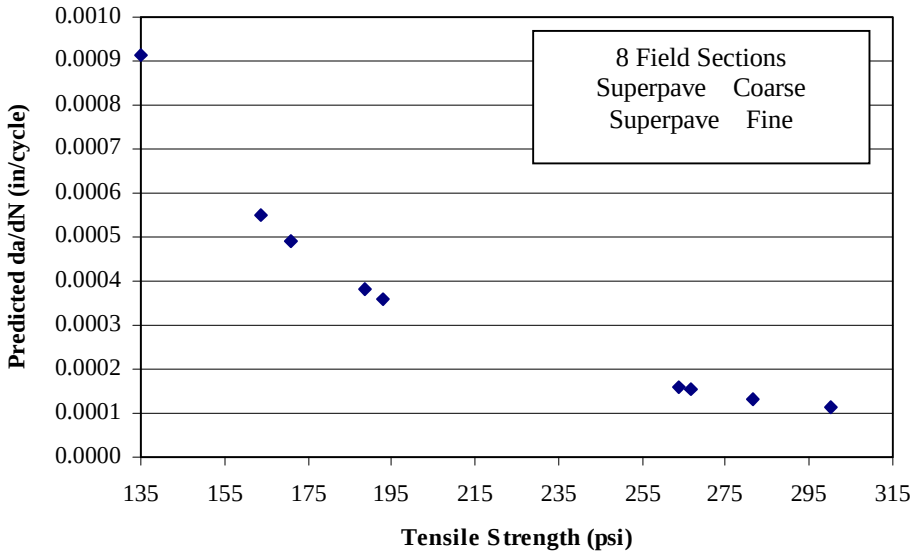

Figure B.2: Relation Between Predicted da/dN vs.Tensile Strength Using Model B.1

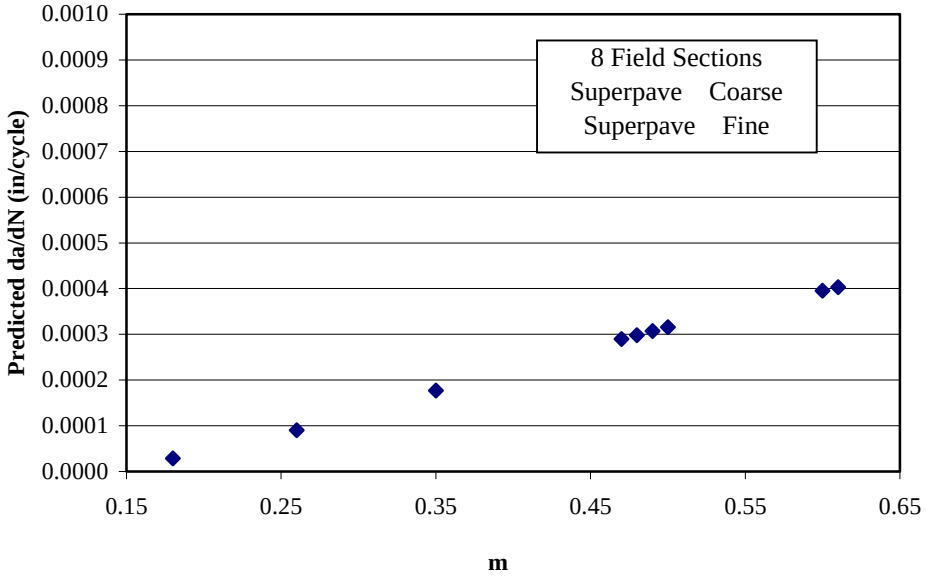

Figure B.3: Relation Between Predicted da/dN vs. m-Value Using Model B.1

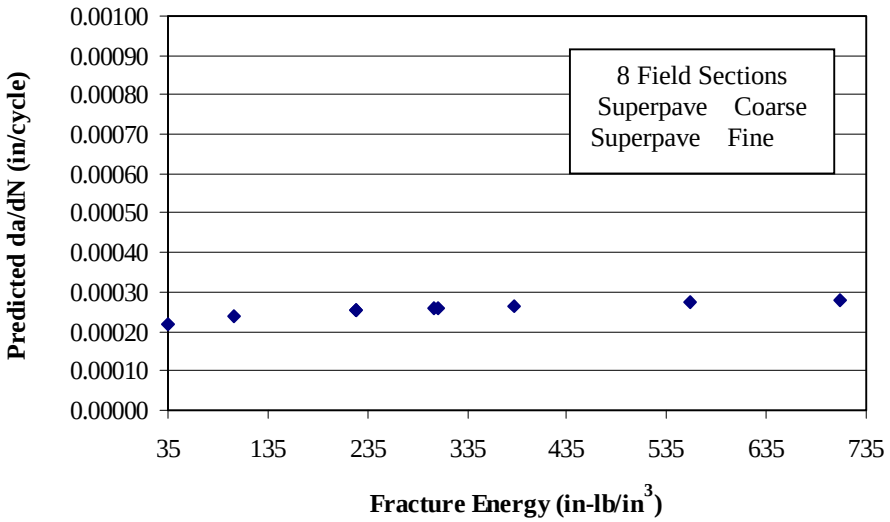

Figure B.4: Relation Between Predicted da/dN vs. Fracture Energy Density Using Model B1.1

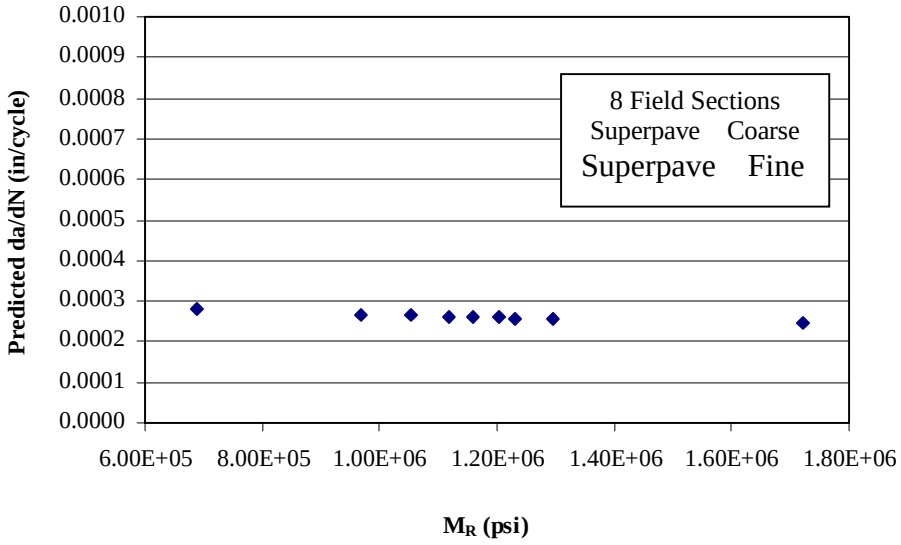

Figure B.5: Relation Between Predicted da/dN vs. Resilient Modulus Using Model B1.1

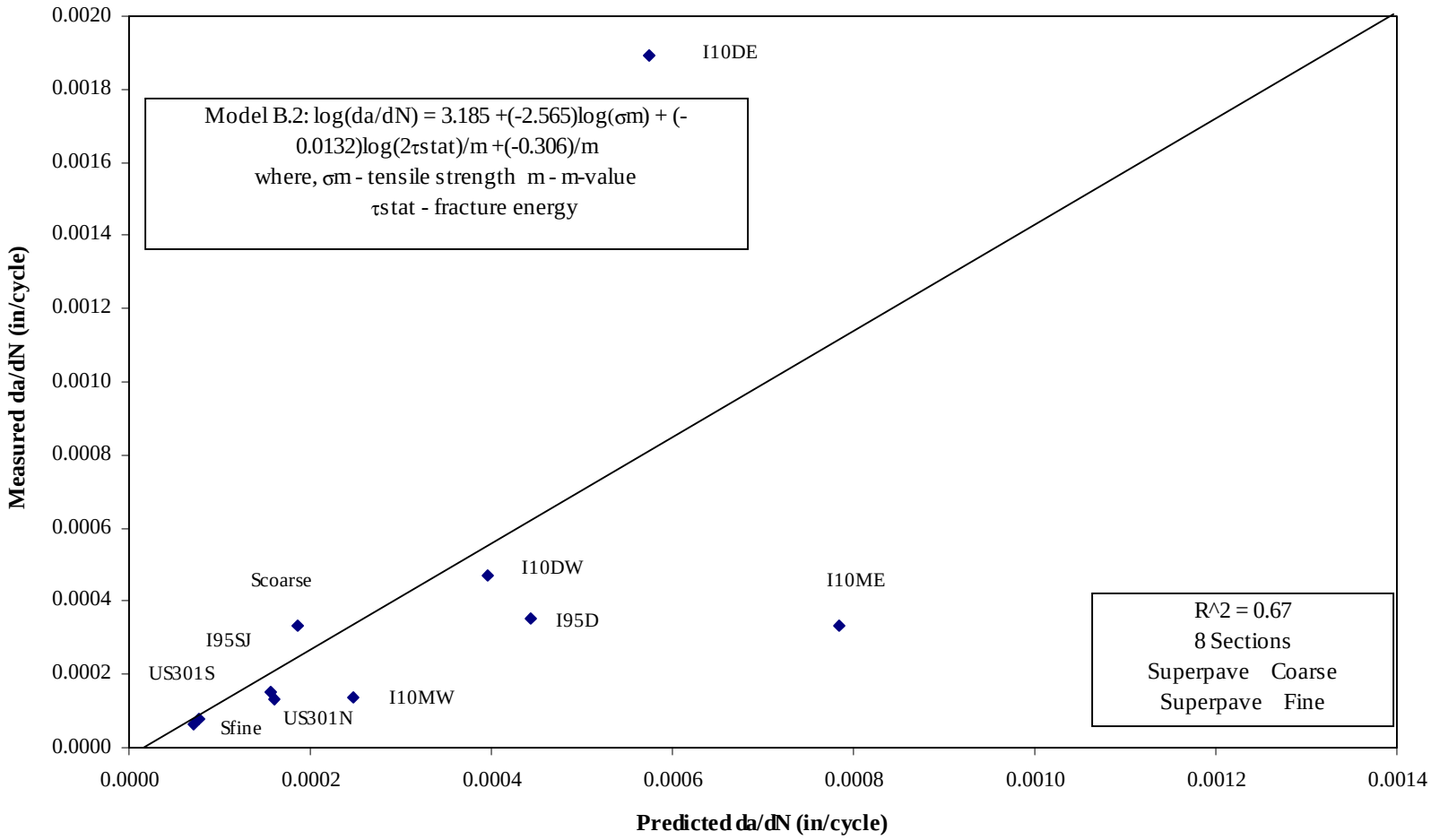

Figure B.6: Relation Between Measured da/dN and Predicted da/dN from Model B.2

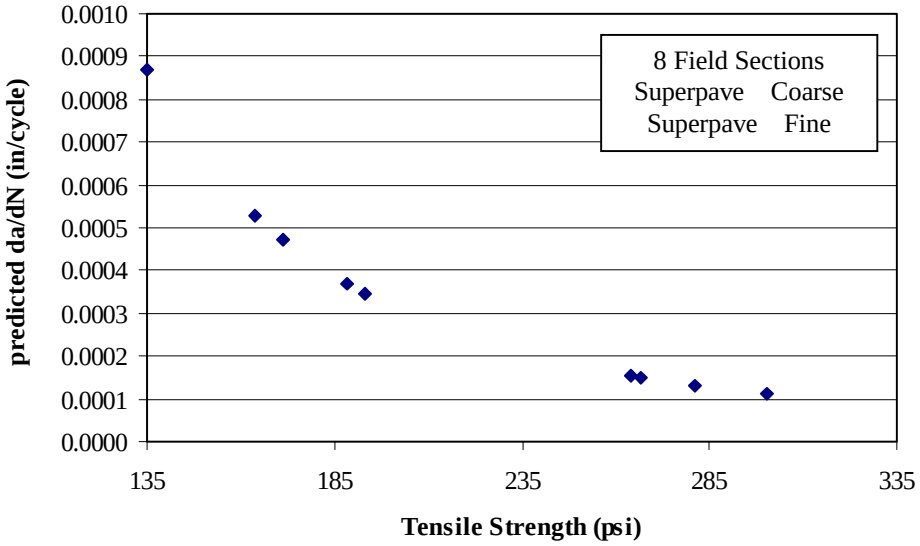

Figure B.7: Relation Between Predicted da/dN vs. Tensile Strength Using Model B.2

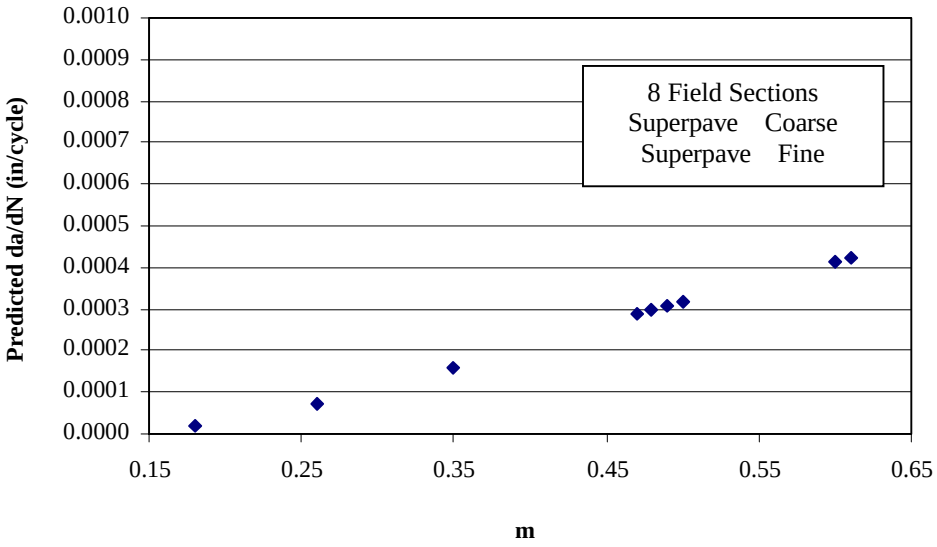

Figure B.8: Relation Between Predicted da/dN vs. m-Value Using Model B.2

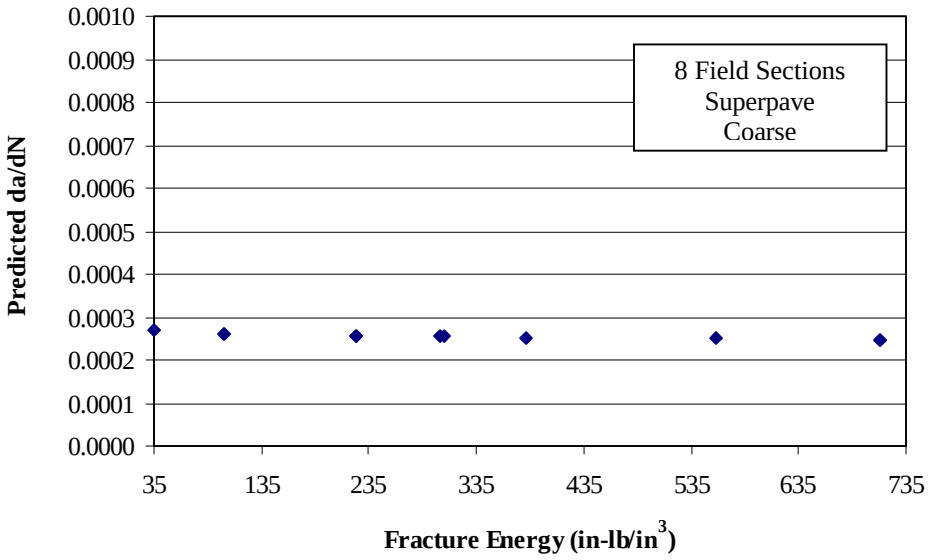

Figure B.9: Relation Between Predicted da/dN vs. Fracture Energy Density Using Model B.2

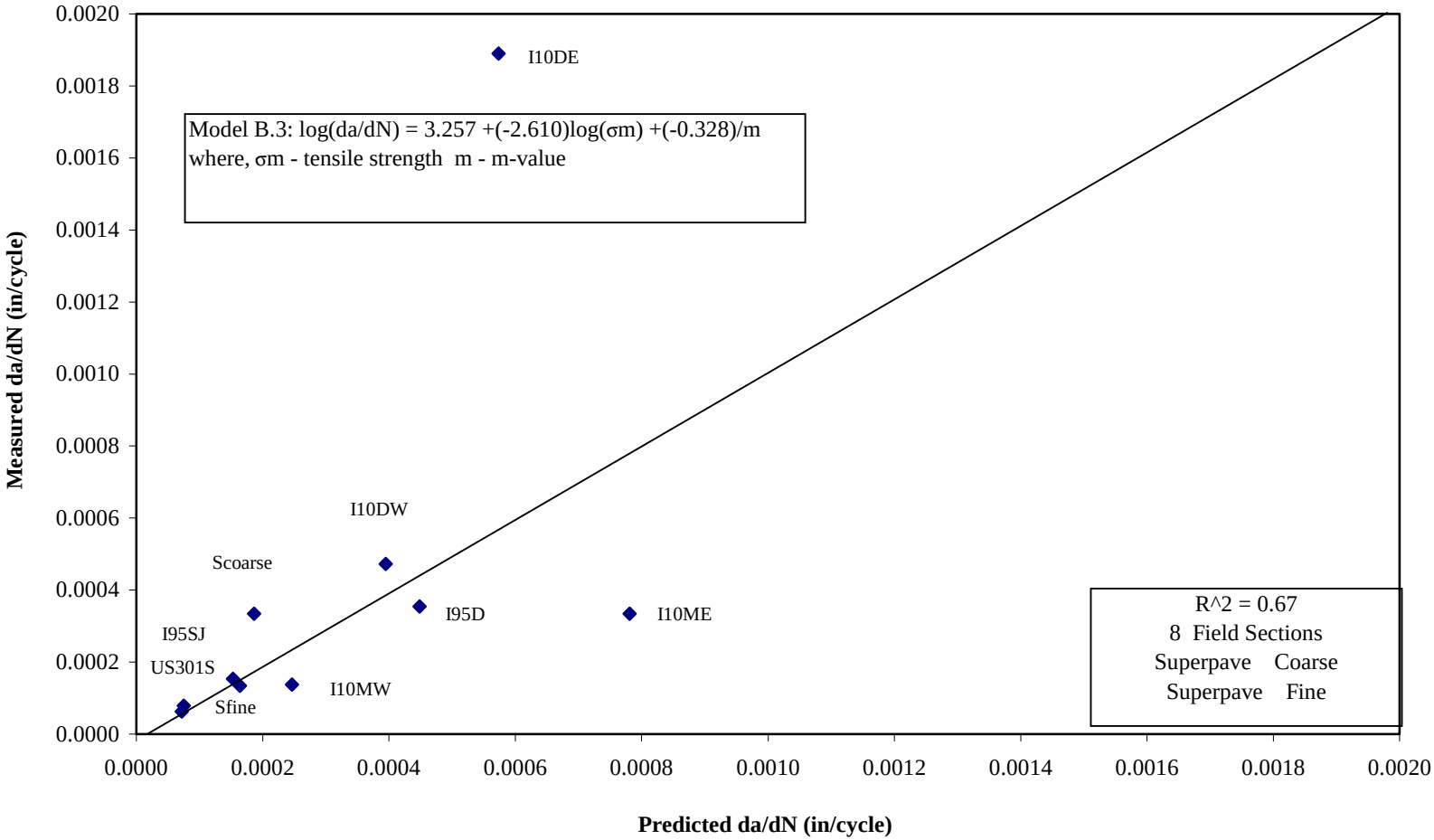

Figure B.10: Relation Between Measured da/dN and Predicted da/dN from Model B.3

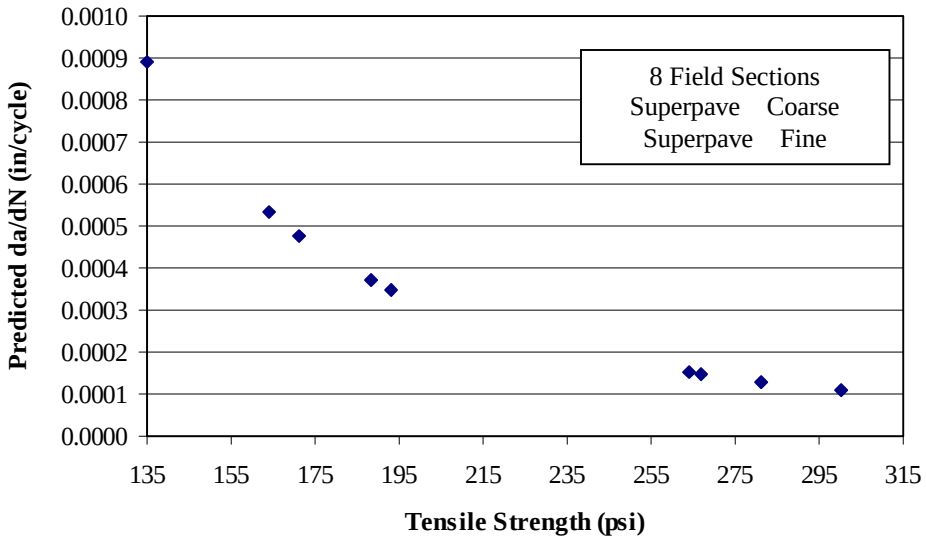

Figure B.11: Relation Between Predicted da/dN vs. Tensile Strength Using Model B.3

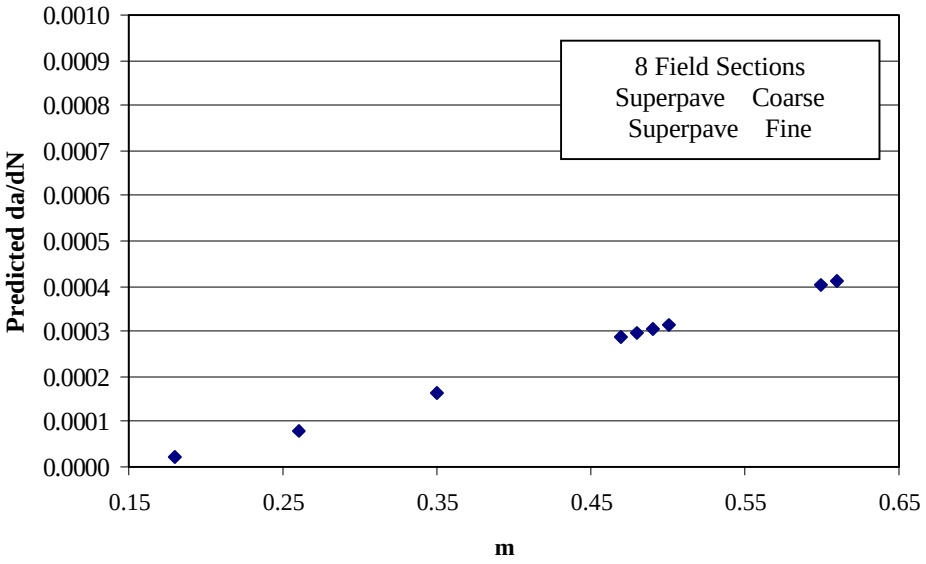

Figure B.12: Relation Between Predicted da/dN vs. m-Value Using Model B.3

```
/*      model B1.sas     K = 7
   1.   THE PURPOSE OF THIS PROGRAM IS TO FIND THE MODEL TO DETERMINE
        logda/dN(rate) = A*log(TensileStrength) +B*log(2*Fracture
                  Energy)/m-value + C*log(Mr)/m-value + D
   2.   IN THIS PROGRAM, DATA FROM 8 FIELD SECTIONS AND SUPERPAVE
COARSE AND FINE WERE USED
 */


data one;
input rate St FE Mr;
cards;

-3.861    2.421     5.254   10.19
-3.451    2.275     5.884   12.29
-3.814    2.449     5.518   12.63
-2.724    2.258     5.112   11.08
-3.326    2.285     5.640   12.87
-3.475    2.233     4.567   9.81
-3.873    2.215     8.863   23.42
-4.104    2.130     10.217  32.43
-3.475    2.426     6.096   12.16
-4.201    2.477     7.944   17.82


proc print;

proc glm;
model rate = St FE Mr/p clm;

output out = new predicted = yhat residual = Residual;

proc print data = new;

proc corr;
var rate yhat;

run;
```

```
/*      Model B2.sas     K = 7
   1.   THE PURPOSE OF THIS PROGRAM IS TO FIND THE MODEL TO DETERMINE
        logda/dN(rate) = A*log(TensileStrength) +B*log(2*Fracture
Energy)/m-value + C/m-value + D
   2.   IN THIS PROGRAM, DATA FROM 8 FIELD SECTIONS AND SUPERPAVE
COARSE AND FINE WERE USED
 */


data one;
input rate St FE Mr;
cards;

-3.861    2.421     5.254   1.67
-3.451    2.275     5.884   2.04
-3.814    2.449     5.518   2.08
-2.724    2.258     5.112   1.85
-3.326    2.285     5.640   2.13
-3.475    2.233     4.567   1.64
-3.873    2.215     8.863   3.85
-4.104    2.130     10.217  5.56
-3.475    2.426     6.096   2.00
-4.201    2.477     7.944   2.86


proc print;

proc glm;
model rate = St FE Mr/p clm;

output out = new predicted = yhat residual = Residual;

proc print data = new;

proc corr;
var rate yhat;

run;
```

```
/*      Model B3.sas     K = 7
   1.   THE PURPOSE OF THIS PROGRAM IS TO FIND THE MODEL TO DETERMINE
        logda/dN(rate) = A*log(TensileStrength) + C/m-value + D
   2.   IN THIS PROGRAM, DATA FROM 8 FIELD SECTIONS AND SUPERPAVE
COARSE AND FINE WERE USED
 */


data one;
input rate St m;
cards;

-3.861    2.421     1.67
-3.451    2.275     2.04
-3.814    2.449     2.08
-2.724    2.258     1.85
-3.326    2.285     2.13
-3.475    2.233     1.64
-3.873    2.215     3.85
-4.104    2.130     5.56
-3.475    2.426     2.00
-4.201    2.477     2.86


proc print;

proc glm;
model rate = St  m/p clm;

output out = new predicted = yhat residual = Residual;

proc print data = new;

proc corr;
var rate yhat;

run;
```

APPENDIX C

THE MODELS FOR PREDICTING CRACK GROWTH RATE (da/dN) - STRESS INTENSITY FACTOR K= 7 Mpa-mm $^{0.5}$: 7 FIELD SECTIONS, A SUPERPAVE COARSE MIXTURE AND A SUPERPAVE FINE MIXTURE WERE USED AS INPUT DATA IN THE MODELS

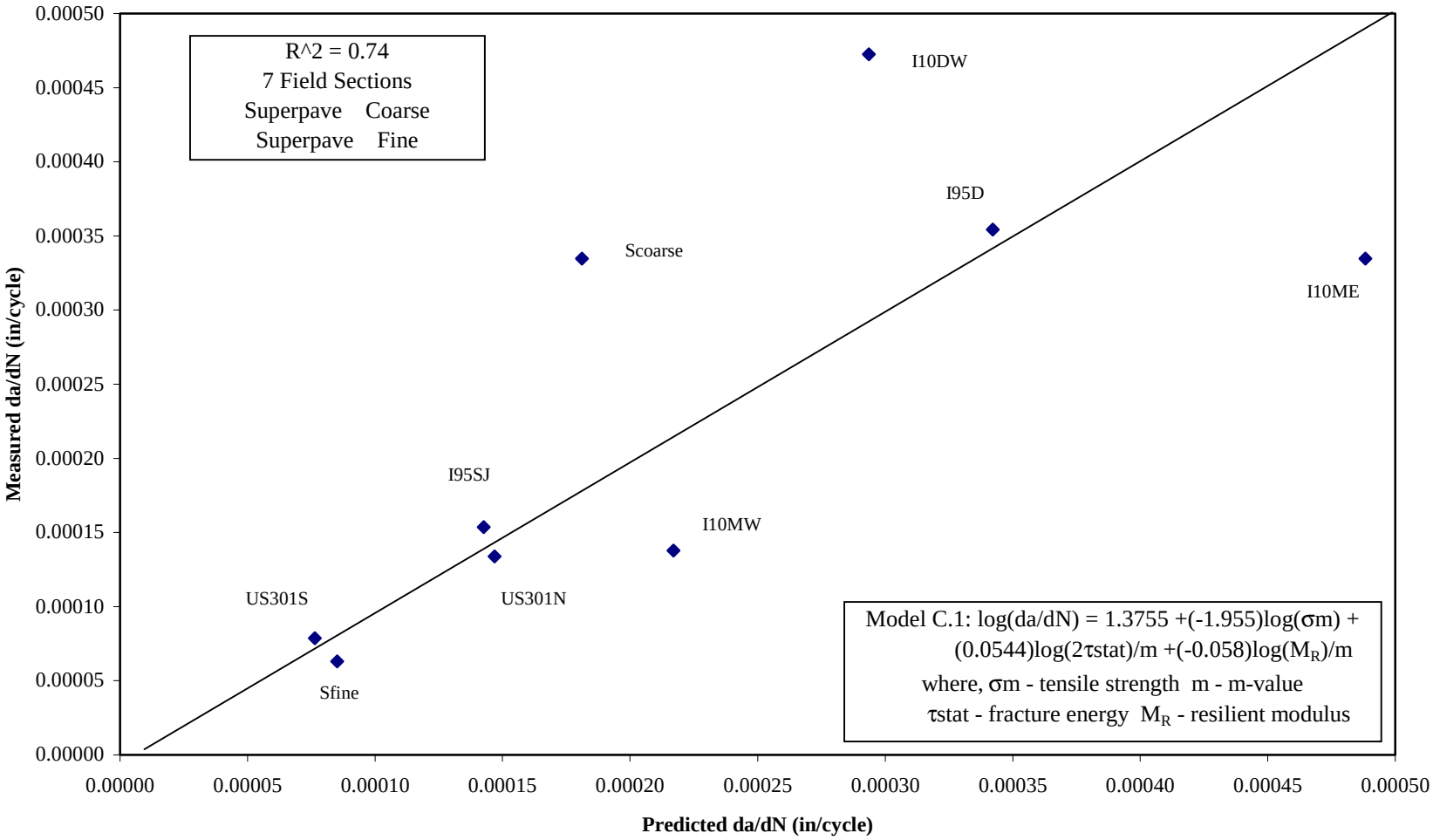

Figure C.1: Relation Between Measured da/dN and Predicted da/dN from Model C.1

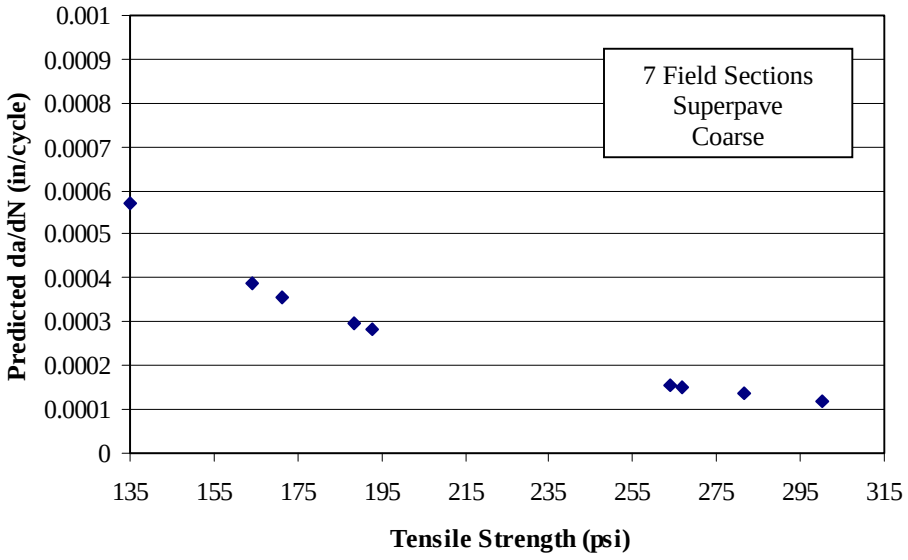

Figure C.2: Relation Between Predicted da/dN vs. Tensile Strength Using Model C.1

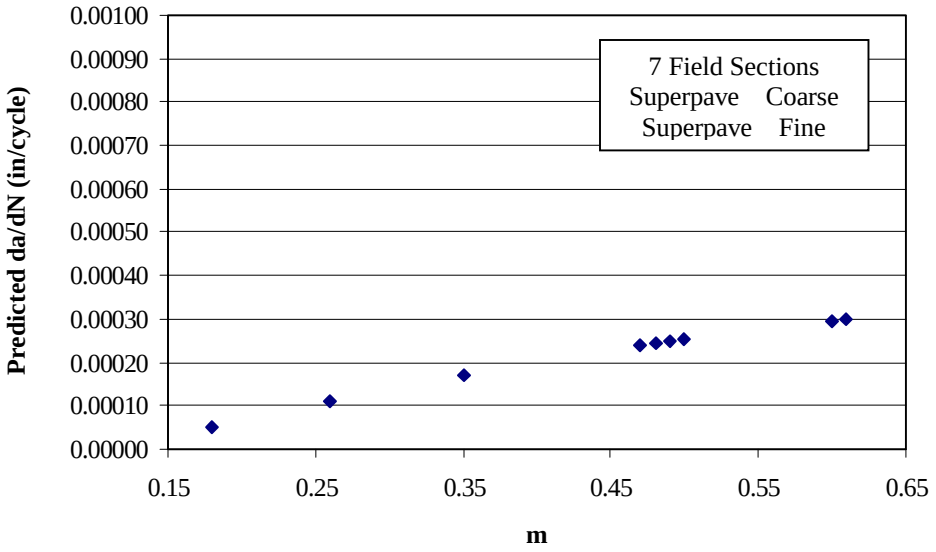

Figure C.3: Relation Between Predicted da/dN vs. m-Value Using Model C.1

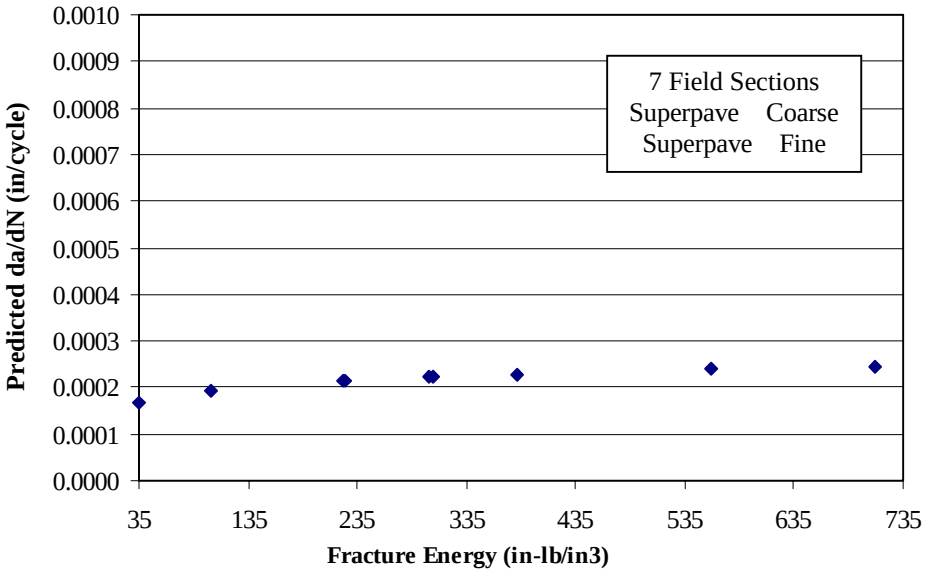

Figure C.4: Relation Between Predicted da/dN vs. Fracture Energy Density Using Model C.1

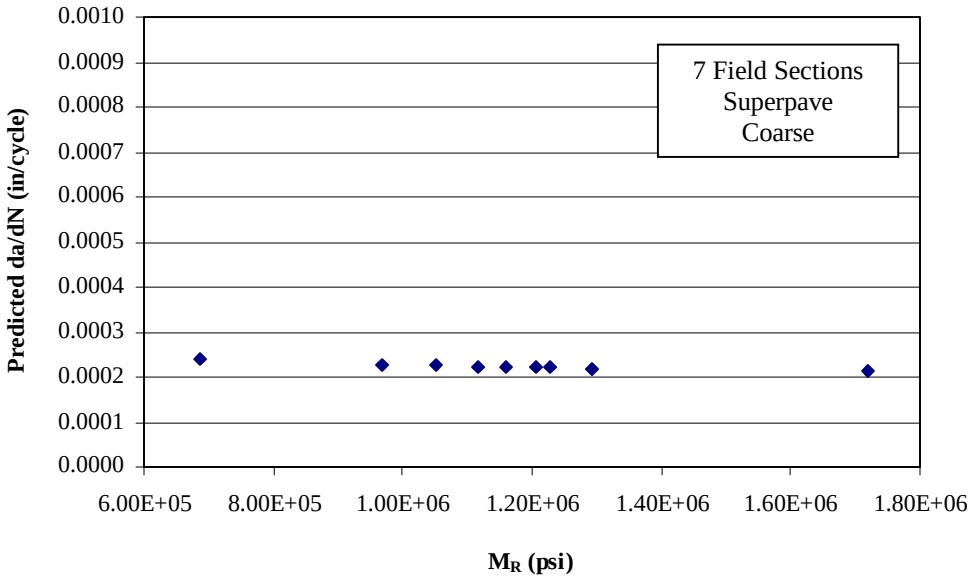

Figure C.5: Relation Between Predicted da/dN vs. Resilient Modulus Using Model C.1

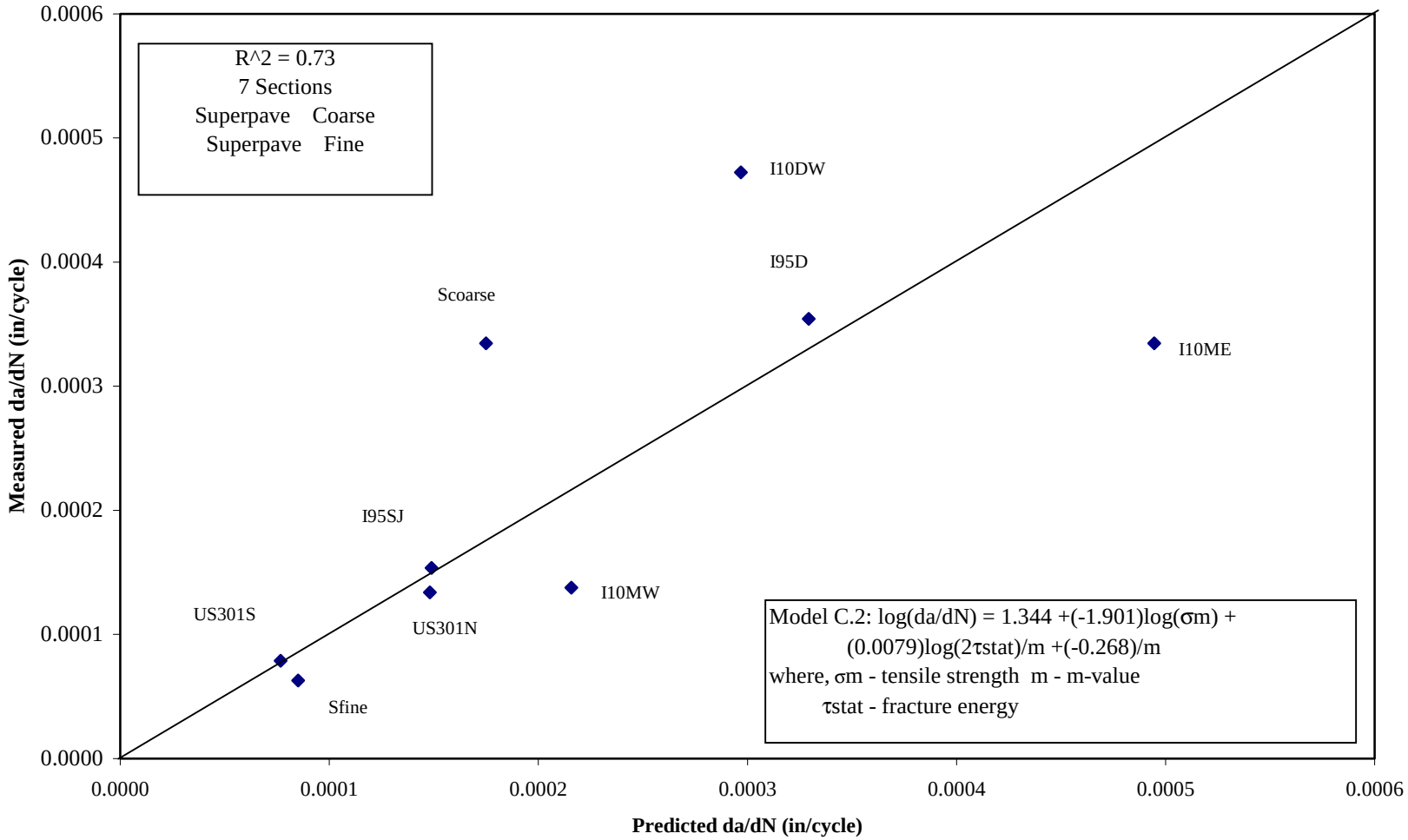

Figure C.6: Relation Between Measured da/dN and Predicted da/dN from Model C.2

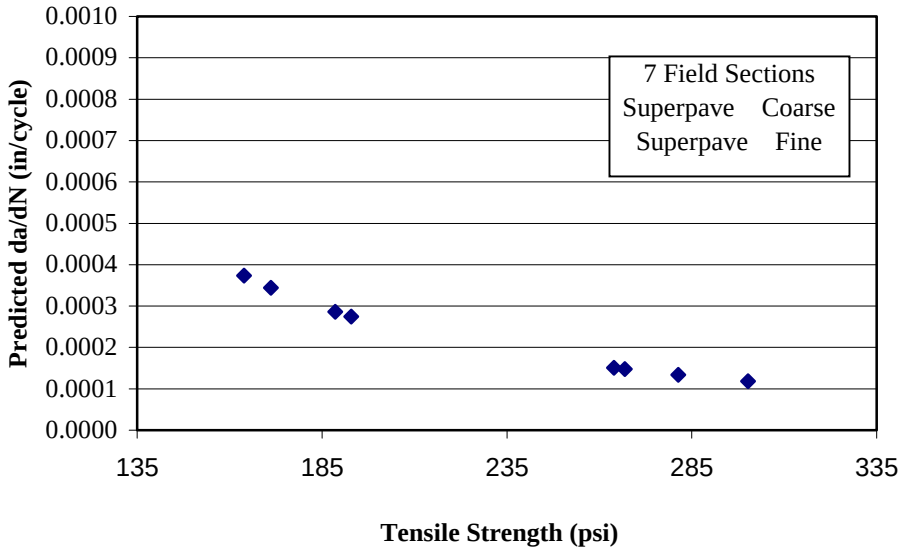

Figure C.7: Relation Between Predicted da/dN vs. Tensile Strength Using Model C.2

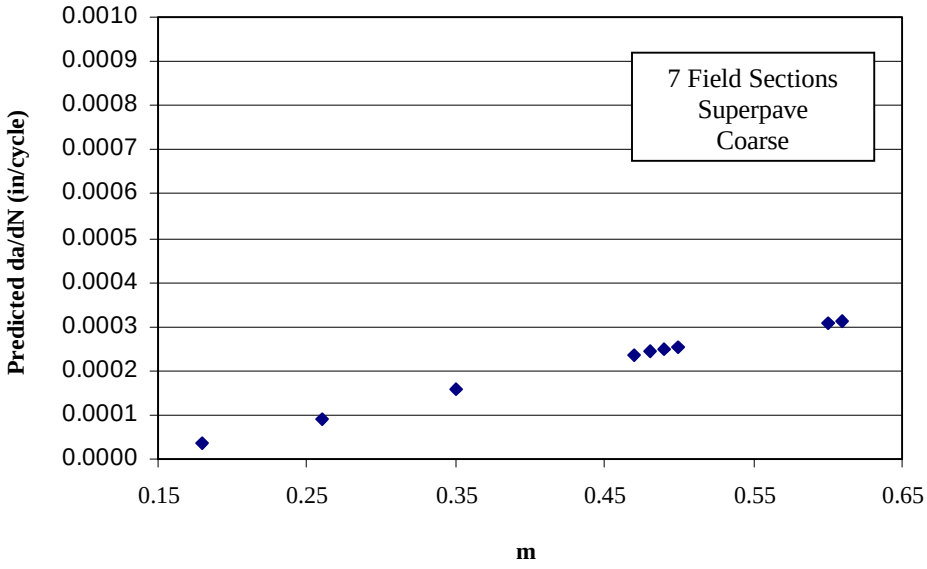

Figure C.8: Relation Between Predicted da/dN vs. m-Value Using Model C.2

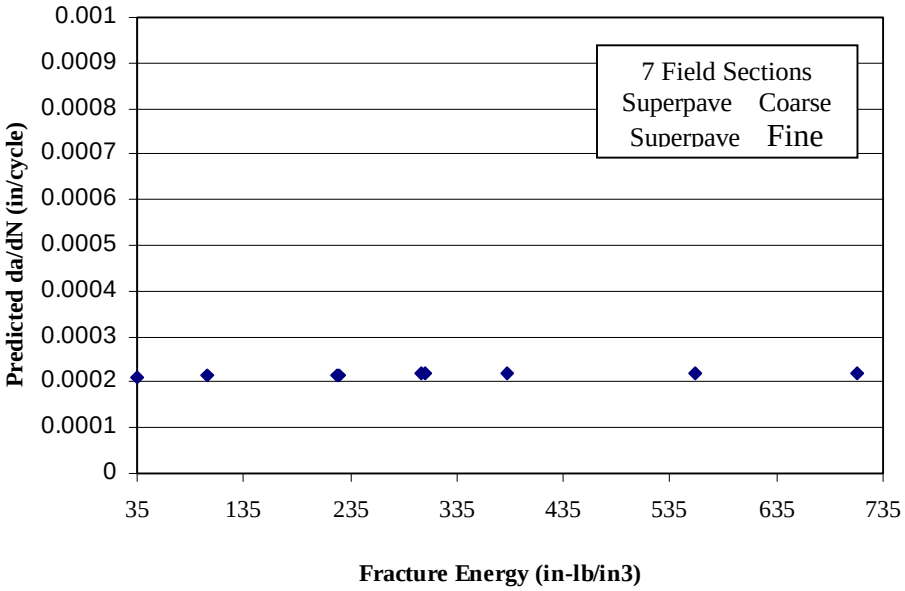

Figure C.9: Relation Between Predicted da/dN vs. Fracture Energy Density Using Model C.2

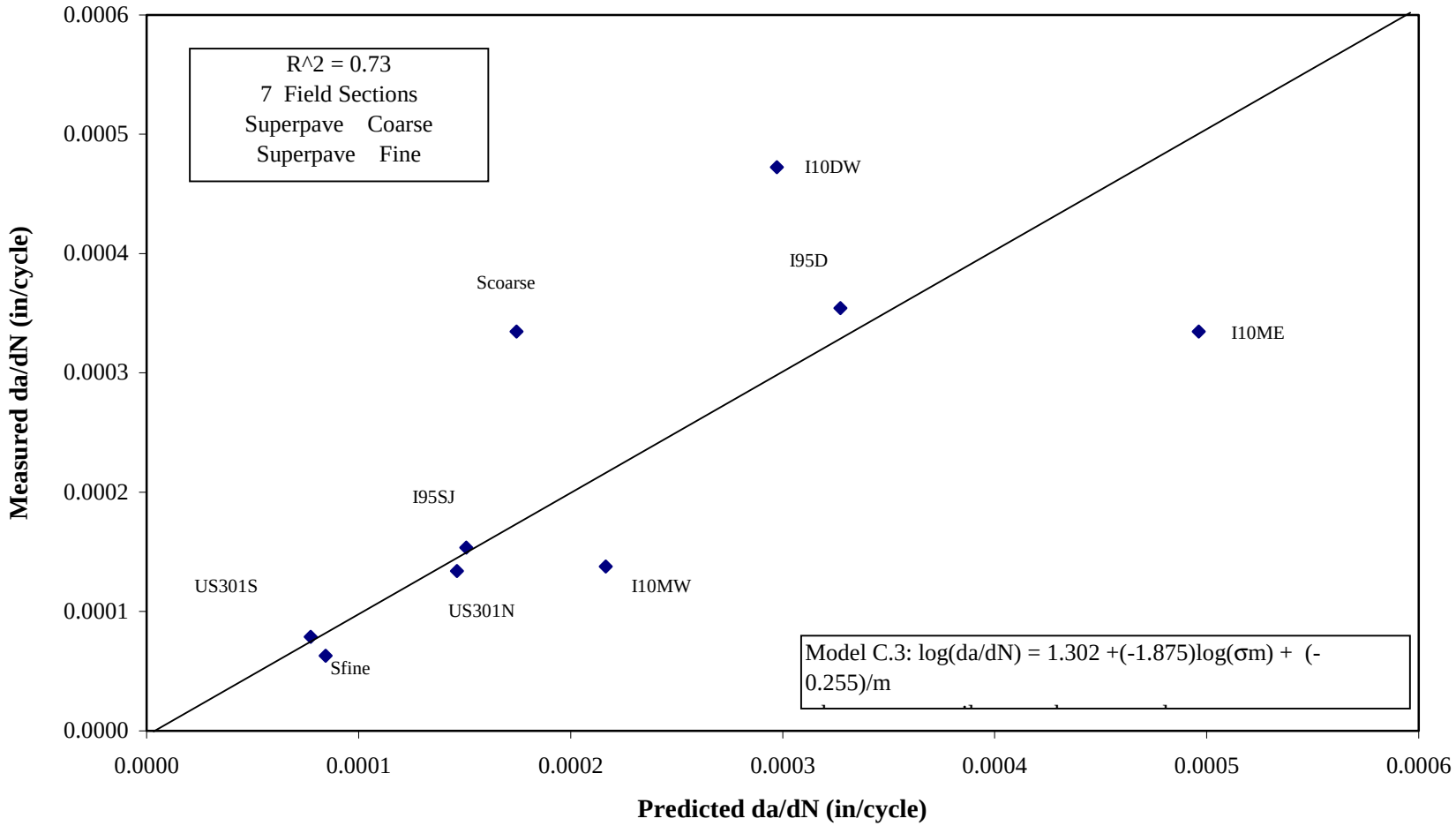

Figure C.10: Relation Between Measured da/dN and Predicted da/dN from Model C.3

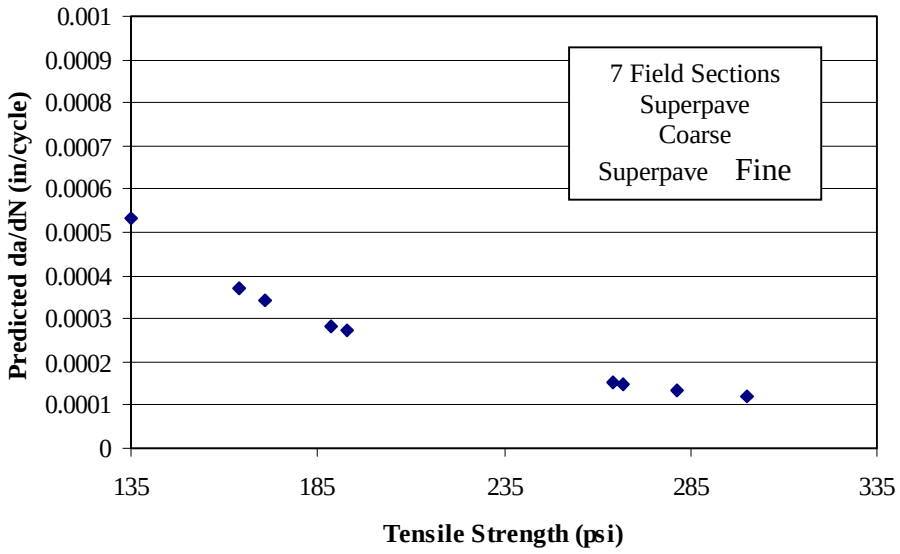

Figure C.11: Relation Between Predicted da/dN vs. Tensile Strength Using Model C.3

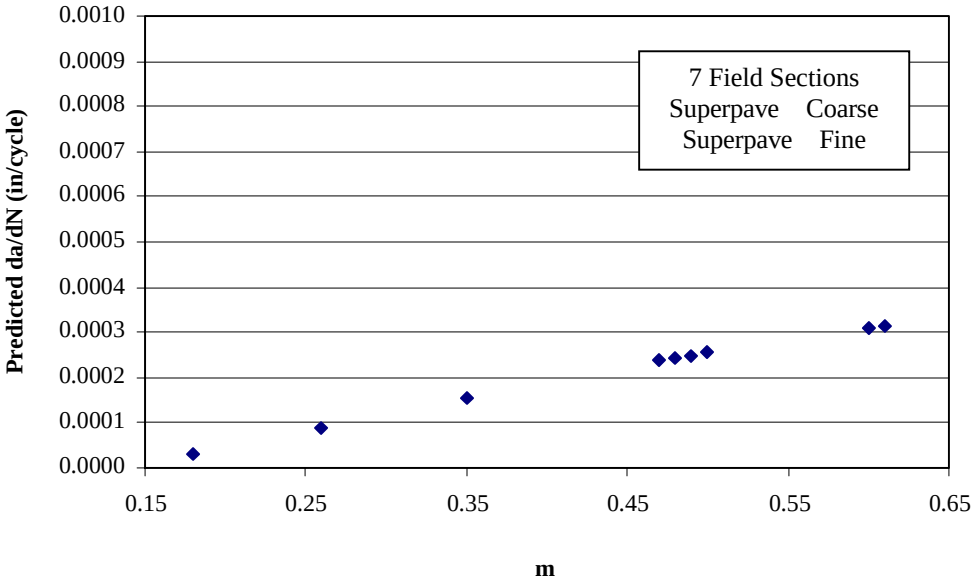

Figure C.12: Relation Between Predicted da/dN vs. m-Value Using Model C.3

```
/*      Model C1.sas     K = 7
   1.   THE PURPOSE OF THIS PROGRAM IS TO FIND THE MODEL TO DETERMINE
        logda/dN(rate) = A*log(TensileStrength) +B*log(2*Fracture
Energy)/m-value + C*log(Mr)/m-value + D
   2.   IN THIS PROGRAM, DATA FROM 7 FIELD SECTIONS AND SUPERPAVE
COARSE AND FINE WERE USED
   3.   I10DE WAS NOT INCLUDED
 */


data one;
input rate St FE Mr;
cards;

-3.861    2.421     5.254   10.19
-3.451    2.275     5.884   12.29
-3.814    2.449     5.518   12.63
-3.326    2.285     5.640   12.87
-3.475    2.233     4.567   9.81
-3.873    2.215     8.863   23.42
-4.104    2.130     10.217  32.43
-3.475    2.426     6.096   12.16
-4.201    2.477     7.944   17.82


proc print;

proc glm;
model rate = St FE Mr/p clm;

output out = new predicted = yhat residual = Residual;

proc print data = new;

proc corr;
var rate yhat;

run;
```

```
/*      Model C2.sas     K = 7
   1.   THE PURPOSE OF THIS PROGRAM IS TO FIND THE MODEL TO DETERMINE
        logda/dN(rate) = A*log(TensileStrength) +B*log(2*Fracture
Energy)/m-value + C/m-value + D
   2.   IN THIS PROGRAM, DATA FROM 7 FIELD SECTIONS AND SUPERPAVE
COARSE AND FINE WERE USED
   3.   I10DE WAS NOT INCLUDED
 */


data one;
input rate St FE m;
cards;

-3.861    2.421     5.254   1.67
-3.451    2.275     5.884   2.04
-3.814    2.449     5.518   2.08
-3.326    2.285     5.640   2.13
-3.475    2.233     4.567   1.64
-3.873    2.215     8.863   3.85
-4.104    2.130     10.217  5.56
-3.475    2.426     6.096   2.00
-4.201    2.477     7.944   2.86


proc print;

proc glm;
model rate = St FE m/p clm;

output out = new predicted = yhat residual = Residual;

proc print data = new;

proc corr;
var rate yhat;

run;
```

```
/*      Model C3.sas     K = 7
   1.   THE PURPOSE OF THIS PROGRAM IS TO FIND THE MODEL TO DETERMINE
        logda/dN(rate) = A*log(TensileStrength)+ + C/m-value + D
   2.   IN THIS PROGRAM, DATA FROM 7 FIELD SECTIONS AND SUPERPAVE
COARSE AND FINE WERE USED
   3.   I10DE WAS NOT INCLUDED
 */


data one;
input rate St m;
cards;

-3.861    2.421     1.67
-3.451    2.275     2.04
-3.814    2.449     2.08
-3.326    2.285     2.13
-3.475    2.233     1.64
-3.873    2.215     3.85
-4.104    2.130     5.56
-3.475    2.426     2.00
-4.201    2.477     2.86


proc print;

proc glm;
model rate = St  m/p clm;

output out = new predicted = yhat residual = Residual;

proc print data = new;

proc corr;
var rate yhat;

run;
```

APPENDIX D

THE SAS MODELS FOR PREDICTING CRACK GROWTH RATE (da/dN) - STRESS INTENSITY FACTOR K= 9 Mpa-mm $^{0.5}$: 8 FIELD SECTIONS, A SUPERPAVE COARSE MIXTURE AND A SUPERPAVE FINE MIXTURE WERE USED AS INPUT DATA IN THE MODELS

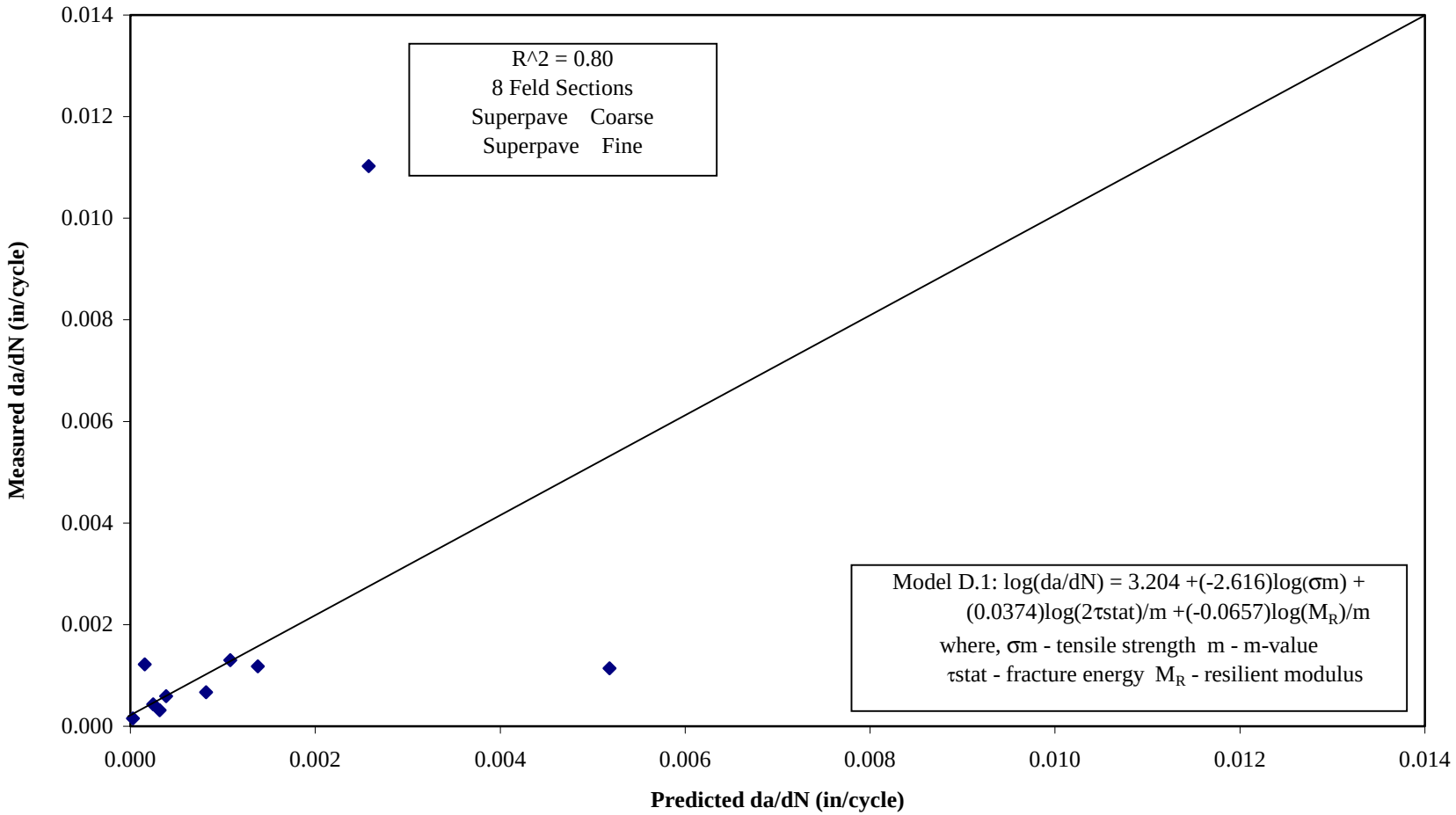

Figure D.1: Relation Between Measured da/dN and Predicted da/dN from Model D.1

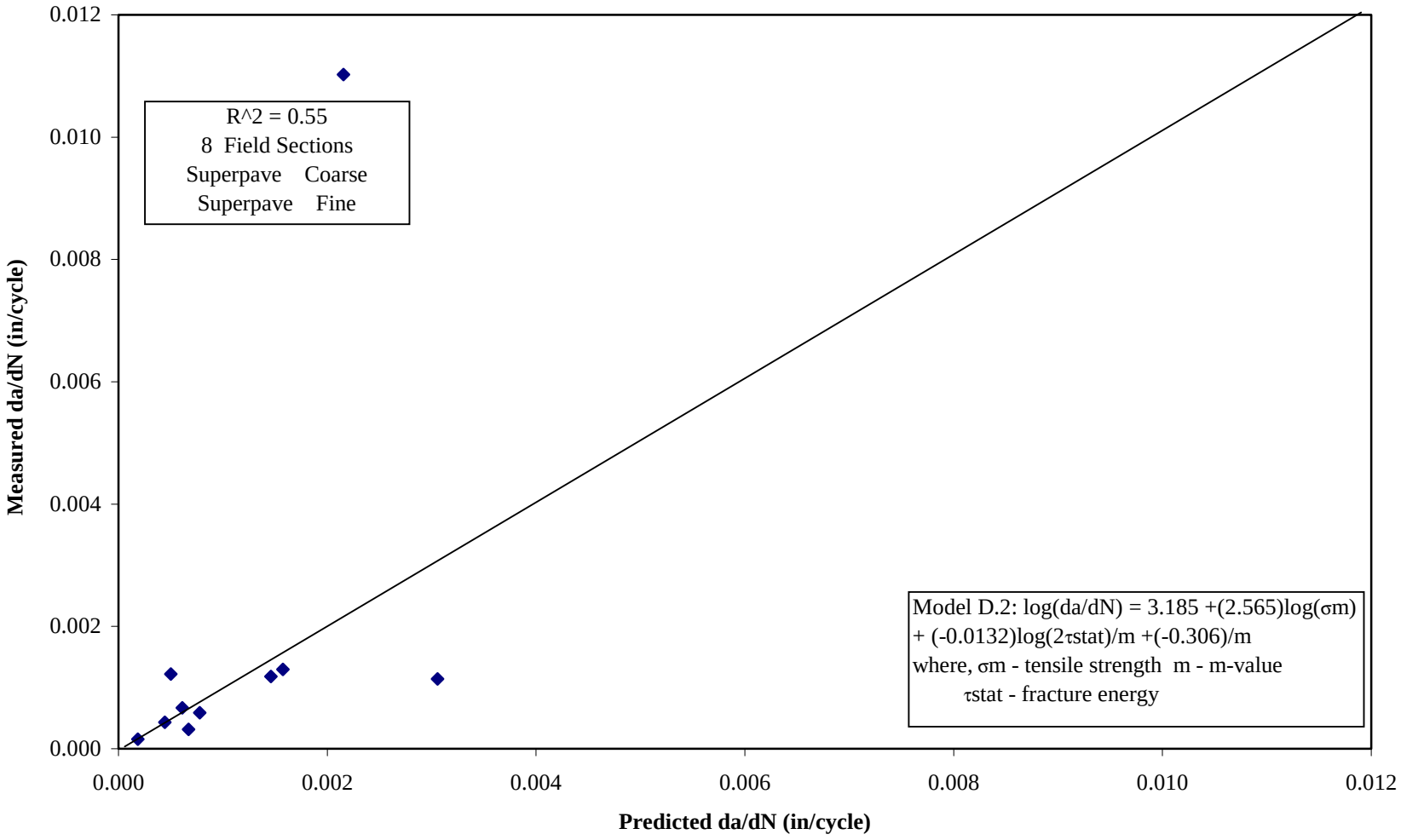

Figure D.2: Relation Between Measured da/dN and Predicted da/dN from Model D.2

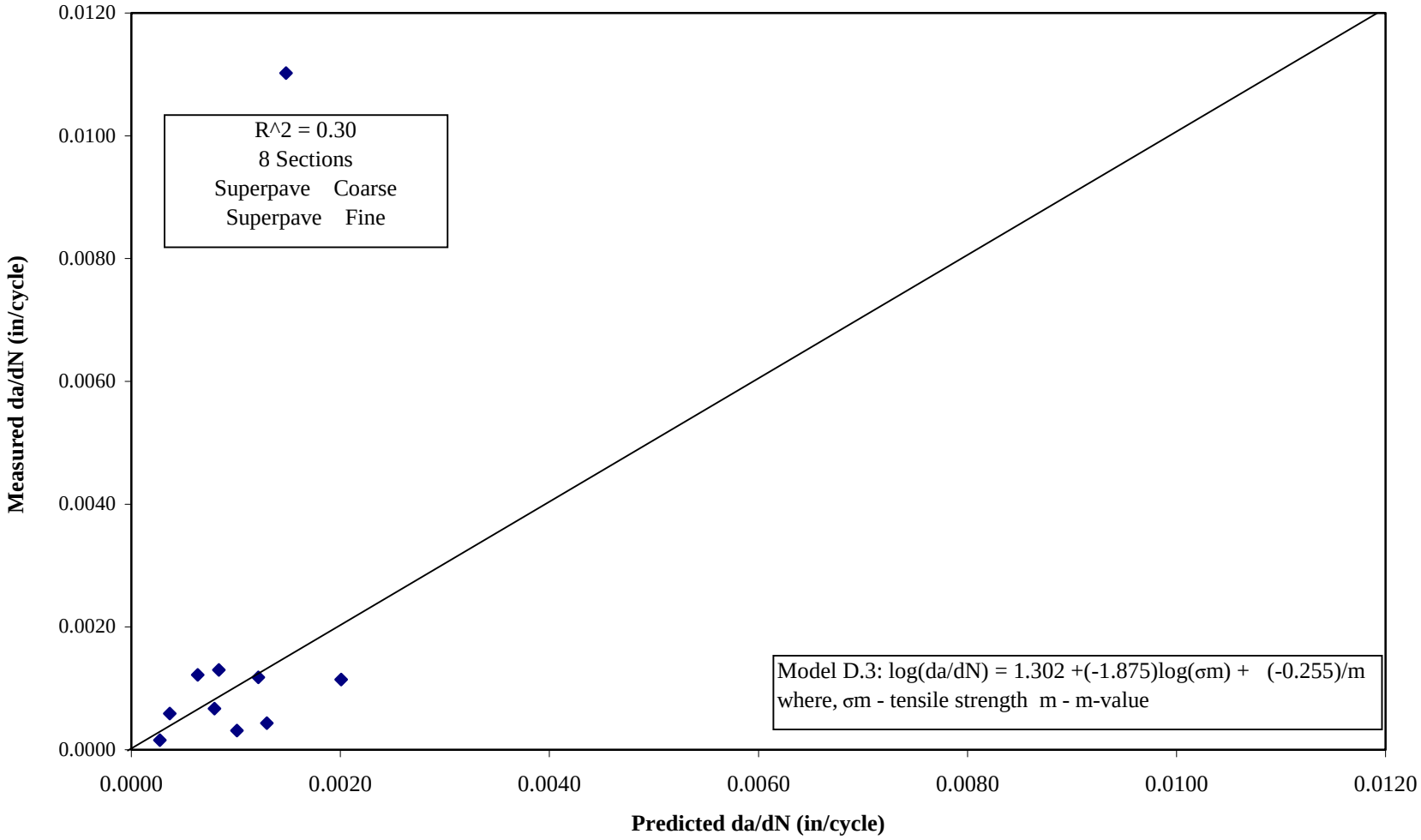

Figure D.3: Relation Between Measured da/dN and Predicted da/dN from Model D.3

```
/*      Model D1.sas     K = 9
   1.   THE PURPOSE OF THIS PROGRAM IS TO FIND THE MODEL TO DETERMINE
        logda/dN(rate) = A*log(TensileStrength) +B*log(2*Fracture
Energy)/m-value + C*log(Mr)/m-value + D
   2.   IN THIS PROGRAM, DATA FROM 8 FIELD SECTIONS AND SUPERPAVE
COARSE AND FINE WERE USED
 */


data one;
input rate St FE Mr;
cards;

-3.502    2.421     5.254   10.19
-2.886    2.275     5.884   12.29
-3.363    2.449     5.518   12.63
-1.958    2.258     5.112   11.08
-2.928    2.285     5.640   12.87
-2.942    2.233     4.567   9.81
-3.229    2.215     8.863   23.42
-3.174    2.130     10.217  32.43
-3.914    2.426     6.096   12.16
-4.803    2.477     7.944   17.82


proc print;

proc glm;
model rate = St FE Mr/p clm;

output out = new predicted = yhat residual = Residual;

proc print data = new;

proc corr;
var rate yhat;

run;
```

```
/*      Model D2.sas     K = 9
   1.   THE PURPOSE OF THIS PROGRAM IS TO FIND THE MODEL TO DETERMINE
        logda/dN(rate) = A*log(TensileStrength) +B*log(2*Fracture
Energy)/m-value + C/m-value + D
   2.   IN THIS PROGRAM, DATA FROM 8 FIELD SECTIONS AND SUPERPAVE
COARSE AND FINE WERE USED
 */


data one;
input rate St FE m;
cards;

-3.502    2.421     5.254   1.67
-2.886    2.275     5.884   2.04
-3.363    2.449     5.518   2.08
-1.958    2.258     5.112   1.85
-2.928    2.285     5.640   2.13
-2.942    2.233     4.567   1.64
-3.229    2.215     8.863   3.85
-3.174    2.130     10.217  5.56
-2.914    2.426     6.096   2.00
-3.803    2.477     7.944   2.86

proc print;

proc glm;
model rate = St FE m/p clm;

output out = new predicted = yhat residual = Residual;

proc print data = new;

proc corr;
var rate yhat;

run;
```

```
/*      Model D3.sas     K = 9
   1.   THE PURPOSE OF THIS PROGRAM IS TO FIND THE MODEL TO DETERMINE
        logda/dN(rate) = A*log(2*Fracture Energy)/m-value
                         + B/m-value + C
   2.   IN THIS PROGRAM, DATA FROM 8 FIELD SECTIONS AND SUPERPAVE
COARSE AND FINE WERE USED
 */


data one;
input rate  FE m;
cards;

-3.502    5.254   1.67
-2.886    5.884   2.04
-3.363    5.518   2.08
-1.958    5.112   1.85
-2.928    5.640   2.13
-2.942    4.567   1.64
-3.229    8.863   3.85
-3.174    10.217  5.56
-2.914    6.096   2.00
-3.803    7.944   2.86

proc print;

proc glm;
model rate = FE m/p clm;

output out = new predicted = yhat residual = Residual;

proc print data = new;

proc corr;
var rate yhat;

run;
```

APPENDIX E

THE SAS MODELS FOR PREDICTING CRACK GROWTH RATE (da/dN) - STRESS INTENSITY FACTOR K= 9 Mpa-mm $^{0.5}$: 7 FIELD SECTIONS, A SUPERPAVE COARSE MIXTURE AND A SUPERPAVE FINE MIXTURE WERE USED AS INPUT DATA IN THE MODELS

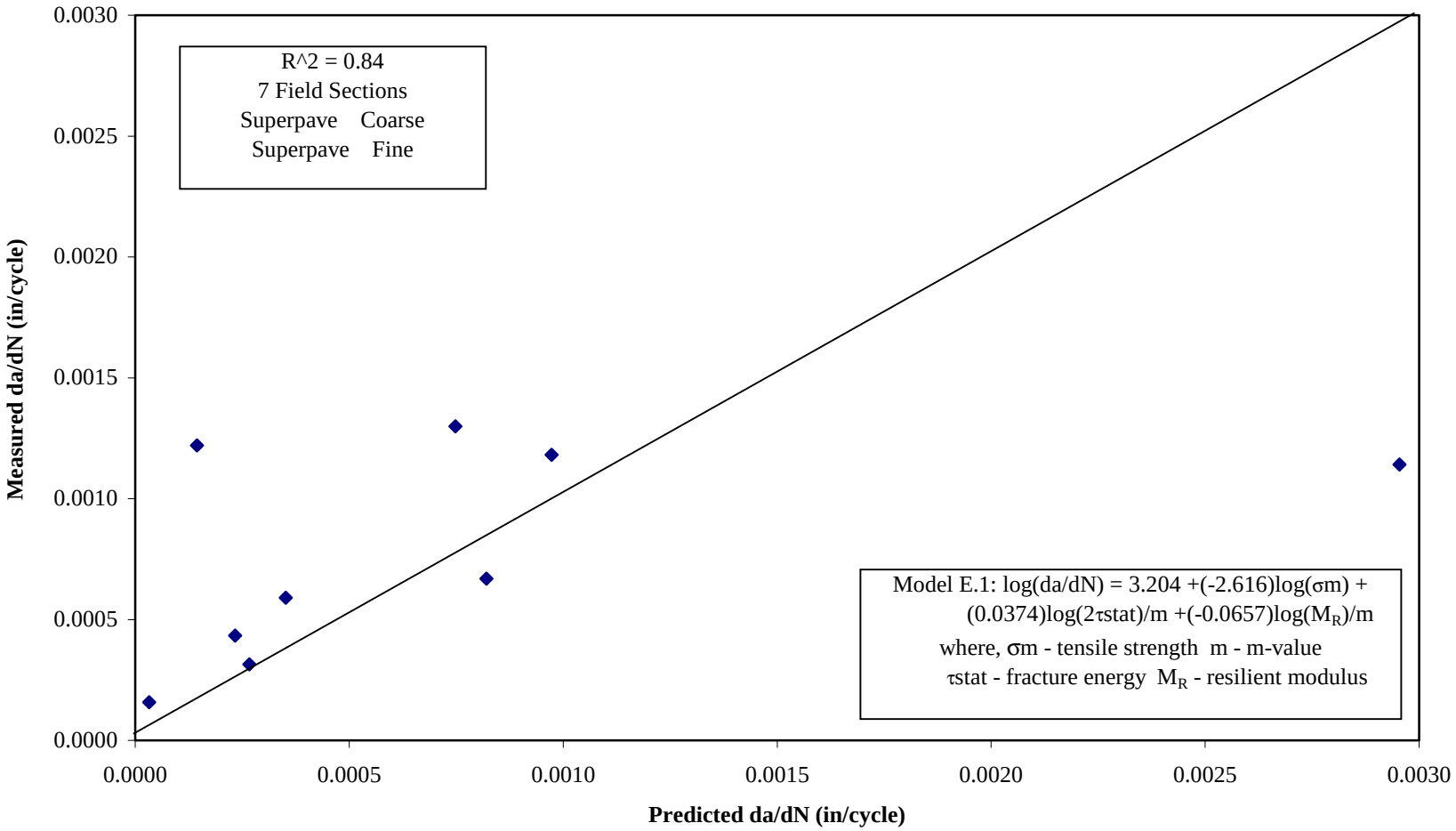

Figure E.1: Relation Between Measured da/dN and Predicted da/dN from Model E.1

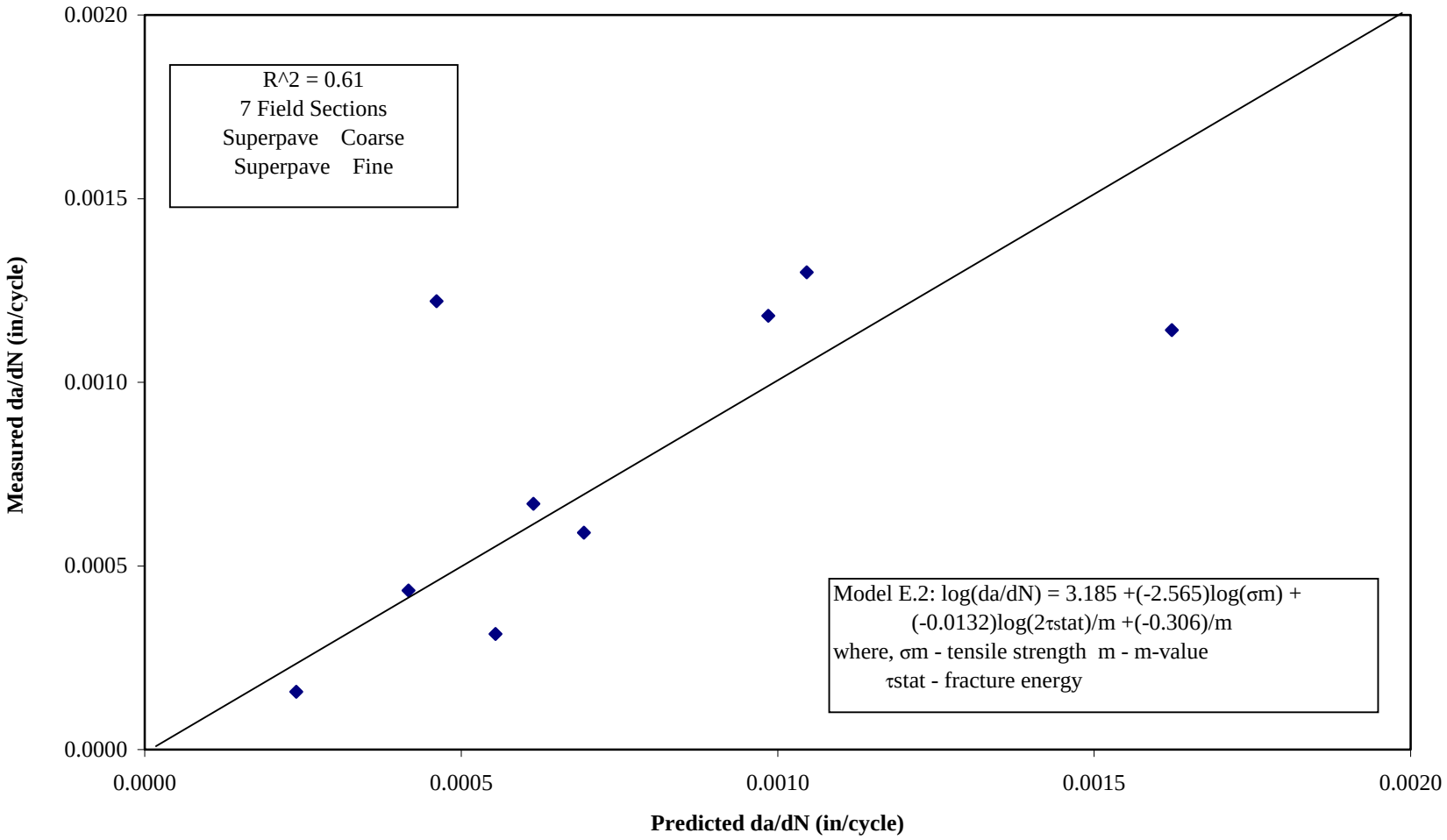

Figure E.2: Relation Between Measured da/dN and Predicted da/dN from Model E.2

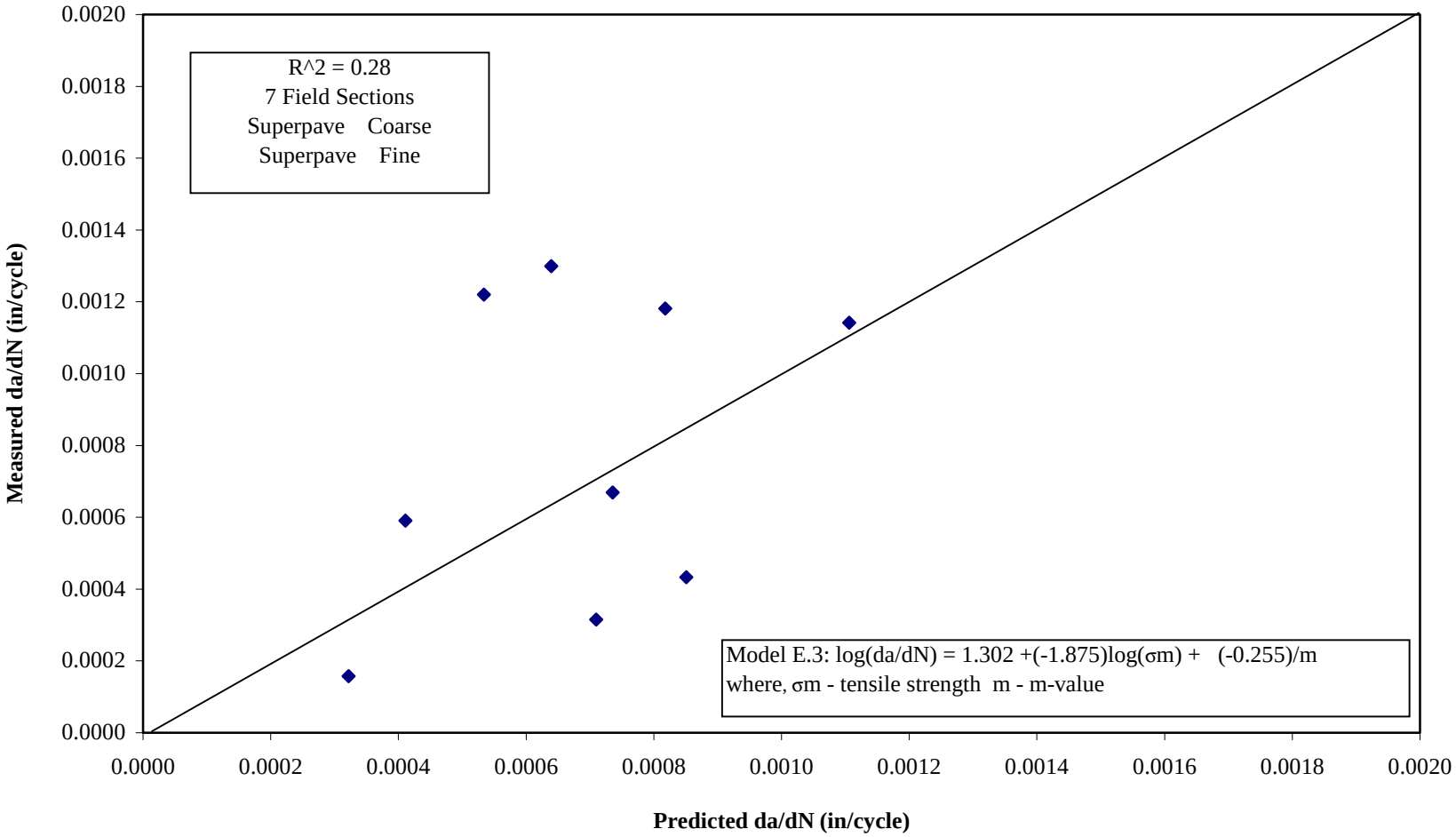

Figure E.3: Relation Between Measured da/dN and Predicted da/dN from Model E.3

```
/*      Model E1.sas     K = 9
   1.   THE PURPOSE OF THIS PROGRAM IS TO FIND THE MODEL TO DETERMINE
        logda/dN(rate) = A*log(TensileStrength) +B*log(2*Fracture
Energy)/m-value + C*log(Mr)/m-value + D
   2.   IN THIS PROGRAM, DATA FROM 7 FIELD SECTIONS AND SUPERPAVE
COARSE AND FINE WERE USED
   3.   I10DE WAS NOT INCLUDED
 */


data one;
input rate St FE Mr;
cards;

-3.502    2.421     5.254   10.19
-2.886    2.275     5.884   12.29
-3.363    2.449     5.518   12.63
-2.928    2.285     5.640   12.87
-2.942    2.233     4.567   9.81
-3.229    2.215     8.863   23.42
-3.174    2.130     10.217  32.43
-3.914    2.426     6.096   12.16
-4.803    2.477     7.944   17.82


proc print;

proc glm;
model rate = St FE Mr/p clm;

output out = new predicted = yhat residual = Residual;

proc print data = new;

proc corr;
var rate yhat;

run;
```

```
/*      Model E2.sas     K = 9
   1.   THE PURPOSE OF THIS PROGRAM IS TO FIND THE MODEL TO DETERMINE
        logda/dN(rate) = A*log(TensileStrength) +B*log(2*Fracture
Energy)/m-value + C/m-value + D
   2.   IN THIS PROGRAM, DATA FROM 7 FIELD SECTIONS AND SUPERPAVE
COARSE AND FINE WERE USED
   3.   I10DE WAS NOT INCLUDED
 */


data one;
input rate St FE m;
cards;

-3.502    2.421     5.254   1.67
-2.886    2.275     5.884   2.04
-3.363    2.449     5.518   2.08
-2.928    2.285     5.640   2.13
-2.942    2.233     4.567   1.64
-3.229    2.215     8.863   3.85
-3.174    2.130     10.217  5.56
-2.914    2.426     6.096   2.00
-3.803    2.477     7.944   2.86

proc print;

proc glm;
model rate = St FE m/p clm;

output out = new predicted = yhat residual = Residual;

proc print data = new;

proc corr;
var rate yhat;

run;
```

```
/*      Model E3.sas     K = 9
   1.   THE PURPOSE OF THIS PROGRAM IS TO FIND THE MODEL TO DETERMINE
        logda/dN(rate) = A*log(2*Fracture Energy)/m-value
                         + B/m-value + C
   2.   IN THIS PROGRAM, DATA FROM 7 FIELD SECTIONS AND SUPERPAVE
COARSE AND FINE WERE USED
   3.   I10DE WAS NOT INCLUDED
 */


data one;
input rate  FE m;
cards;

-3.502    5.254   1.67
-2.886    5.884   2.04
-3.363    5.518   2.08
-2.928    5.640   2.13
-2.942    4.567   1.64
-3.229    8.863   3.85
-3.174    10.217  5.56
-2.914    6.096   2.00
-3.803    7.944   2.86

proc print;

proc glm;
model rate = FE m/p clm;

output out = new predicted = yhat residual = Residual;

proc print data = new;

proc corr;
var rate yhat;

run;
```

APPENDIX F
HORIZONTAL DEFORMATION VS. RECORDED POINTS

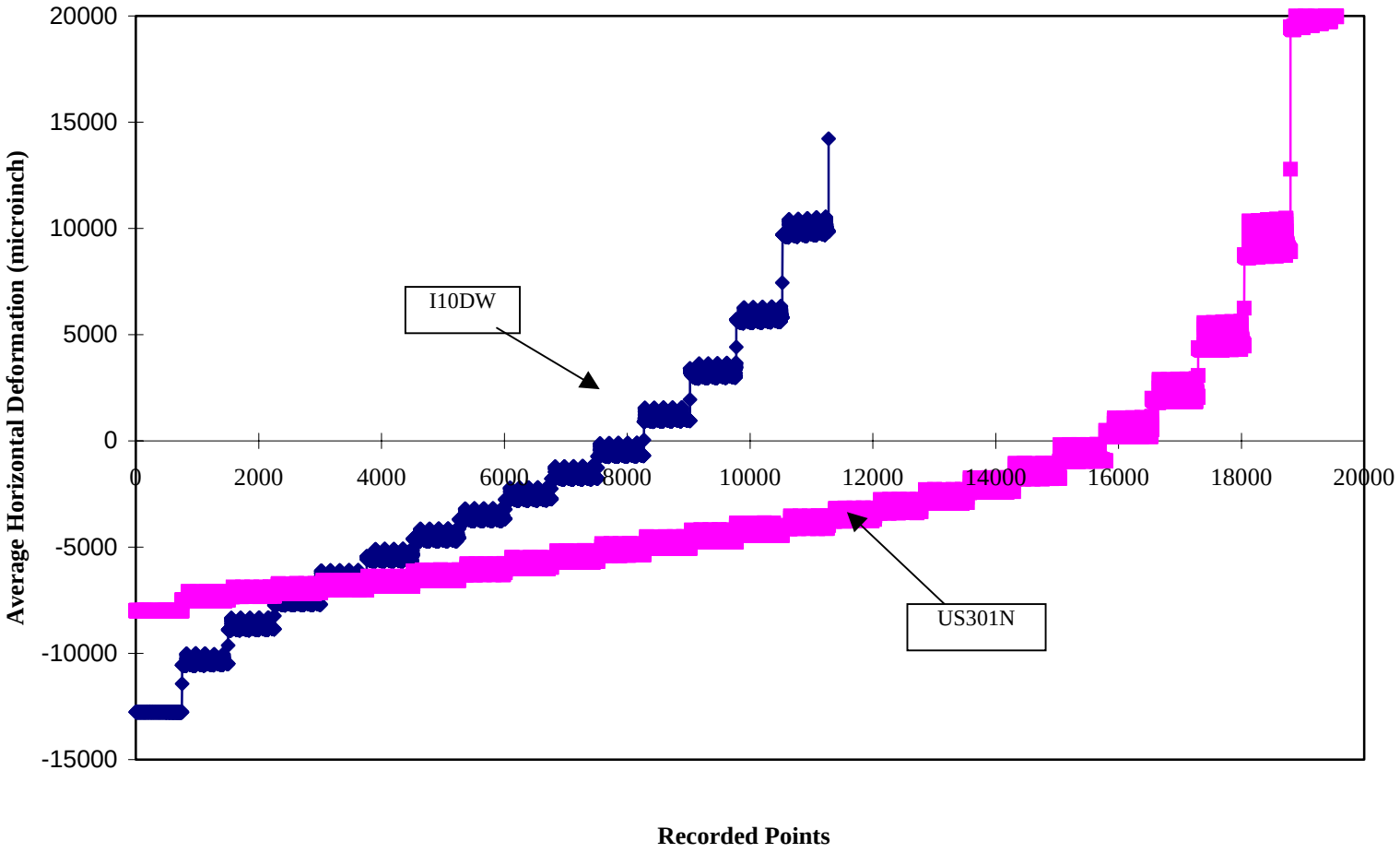

Figure F.1: Average Horizontal Deformation vs. Recorded Points

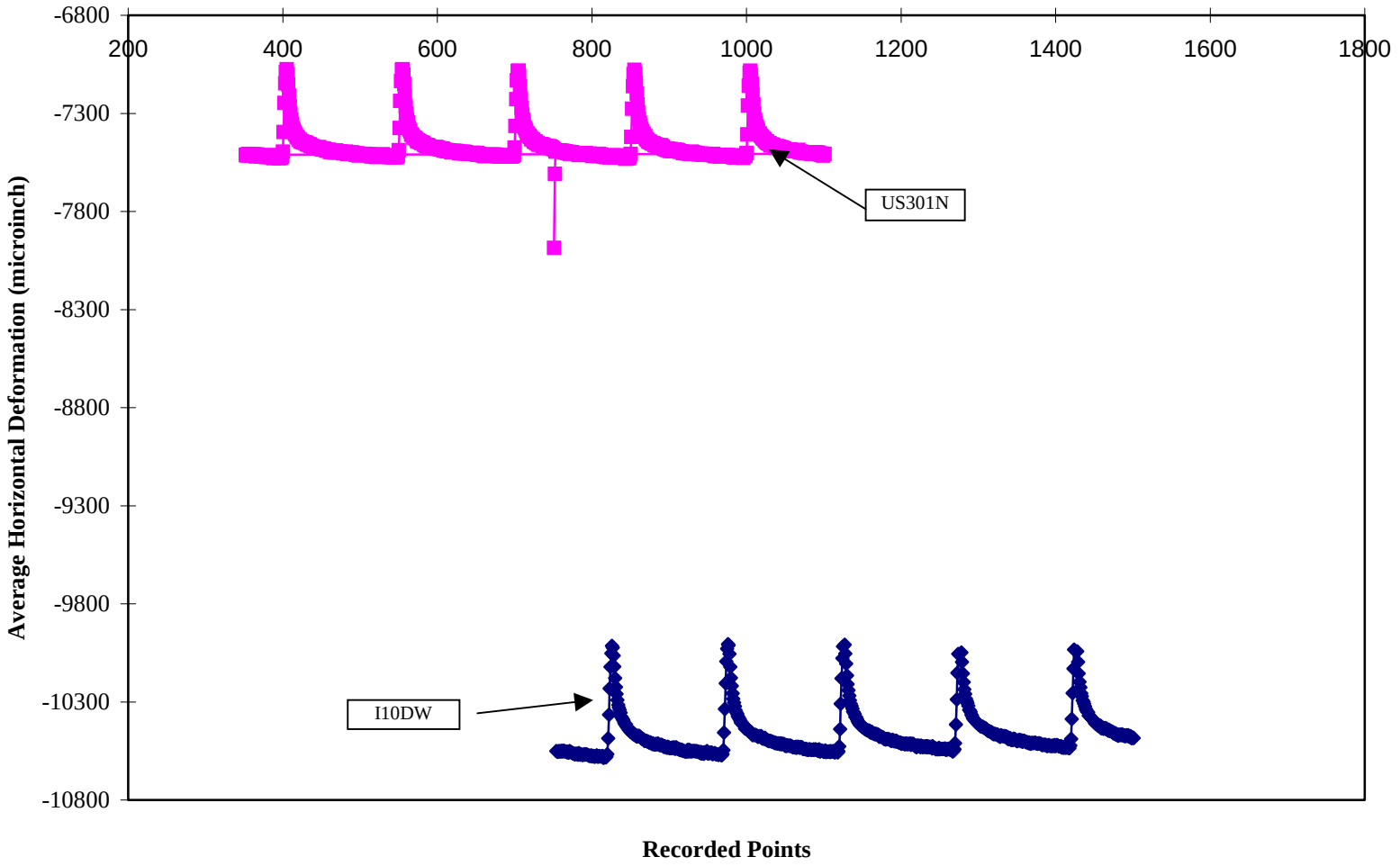

Figure F.2: Average Horizontal Deformation vs. Recorded Points Within Five Cycles

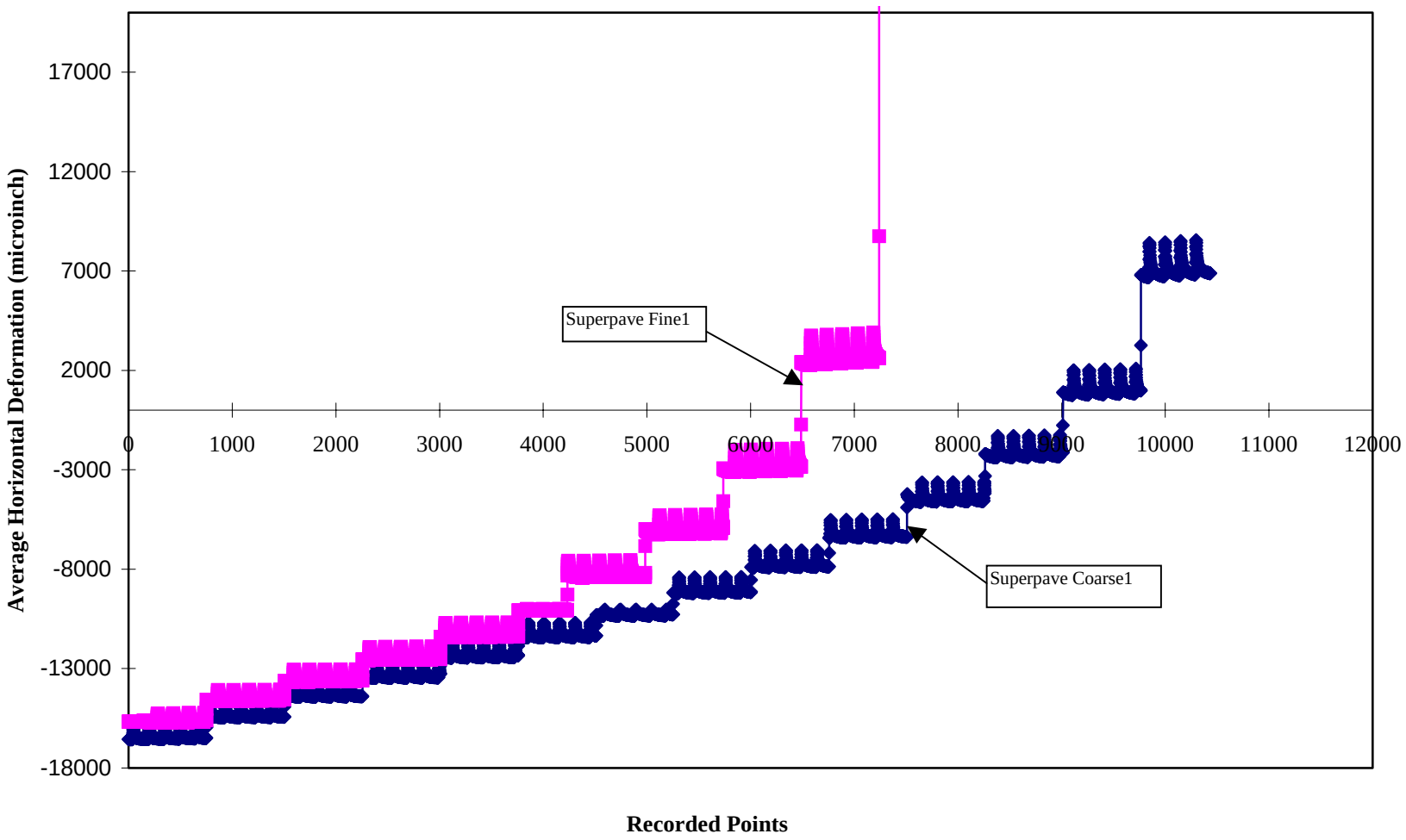

Figure F.3: Average Horizontal Deformation Vs. Recorded Points

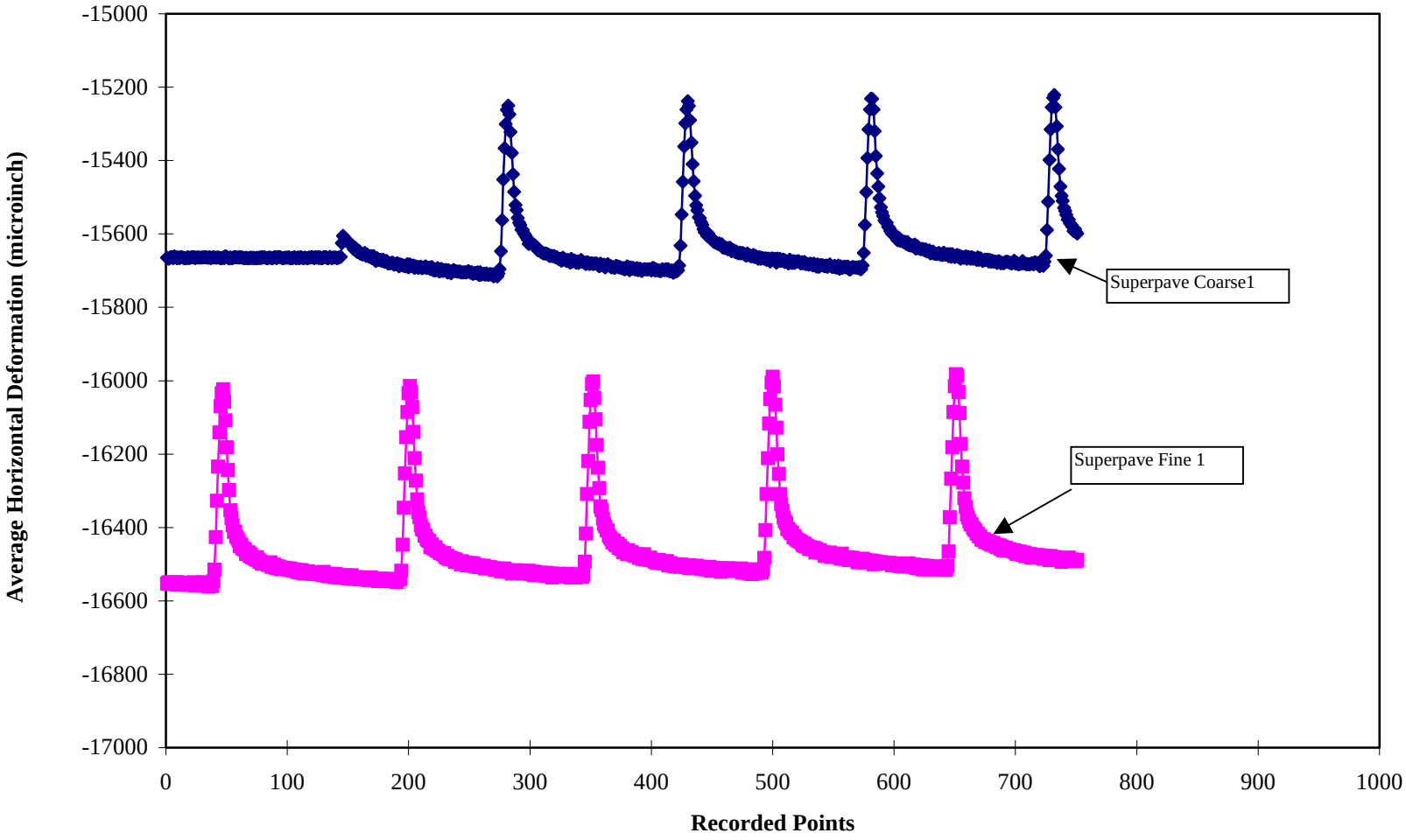

Figure F.4: Average Horizontal Deformation vs. Recorded Points Within Five Cycles

APPENDIX G
EXAMINATION OF HEALING EFFECT

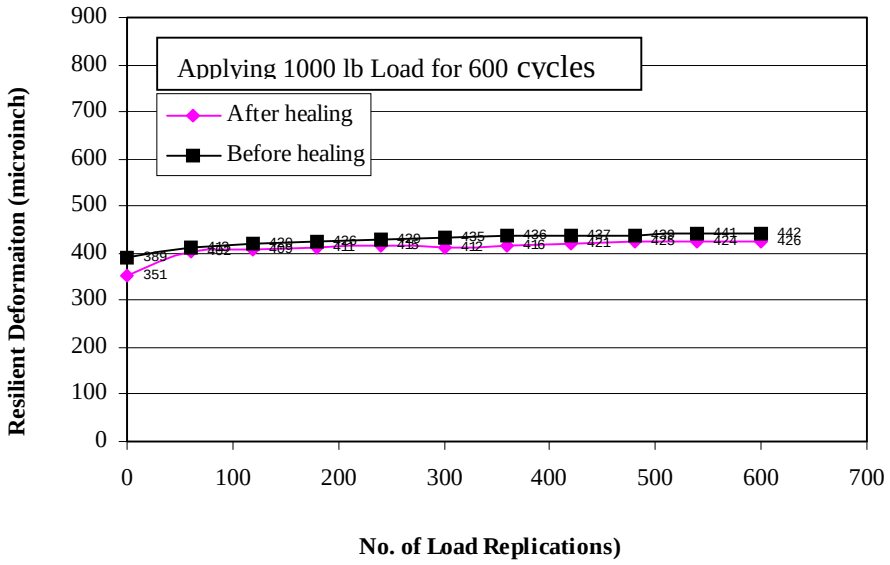

Figure G.1: Resilient Deformation Before and After Healing

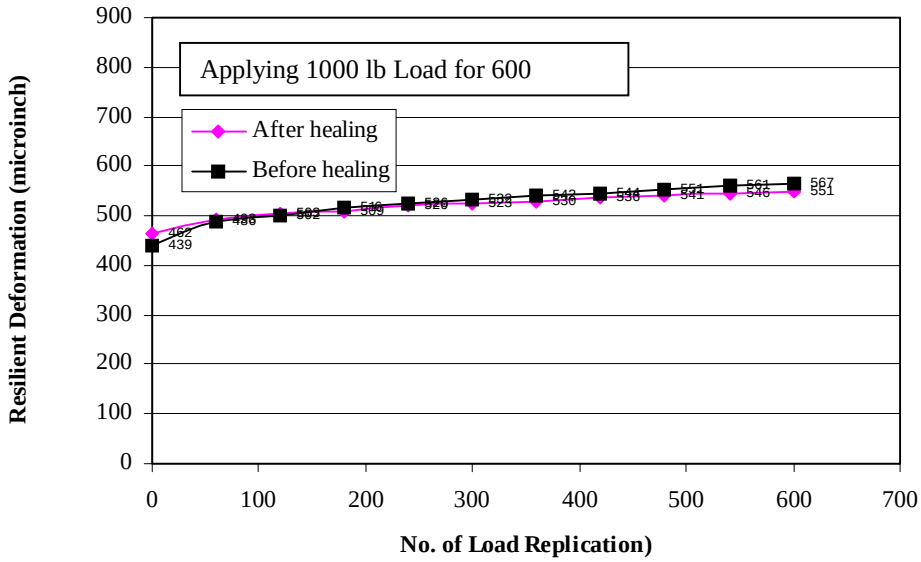

Figure G.2: Resilient Deformation Before and After Healing

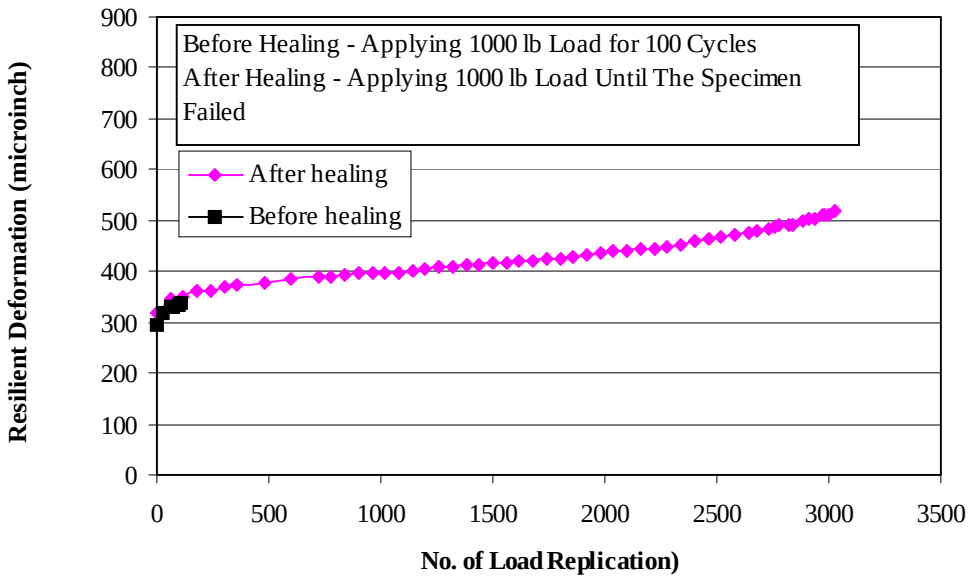

Figure G.3 Resilient Deformation Before and After Healing

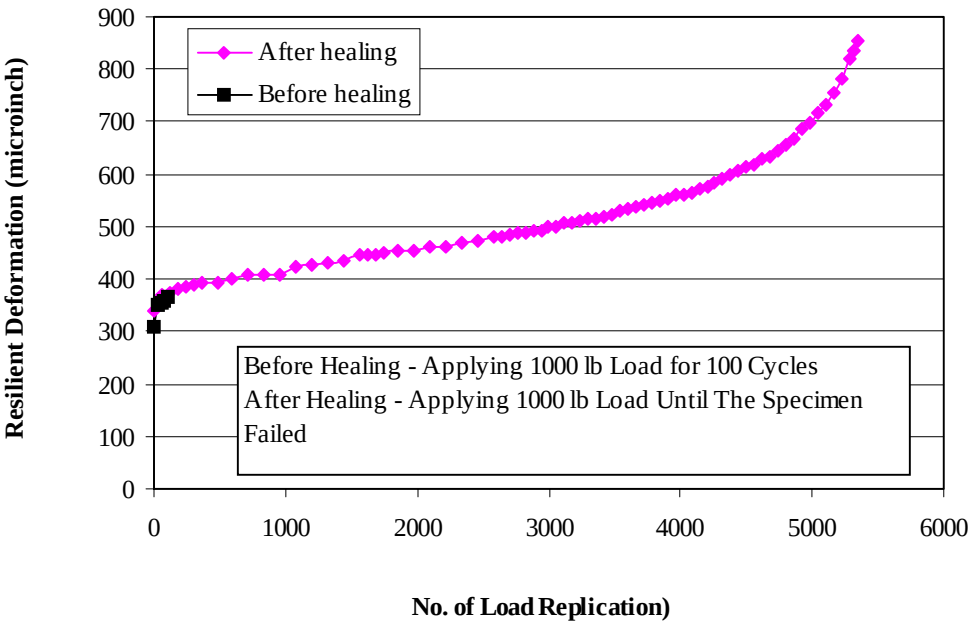

Figure G.4 Resilient Deformation Before and After Healing

APPENDIX H
RESULTS OF DISSIPATED CREEP STRAIN ENERGY FROM FRACTURE TESTS AND STRENGTH TESTS

Table H.1: Fracture Energy Density Obtained from ITLT Program

	Fracture Energy (KJ/m^3)		Fracture Energy (KJ/m^3)
Superpave Coarse1	7408	I10MW	4895
Superpave Coarse2	6086	I95DN	2635
Superpave Fine1	5370	I95SJ	2105
Superpave Fine2	6718	I10DE	1987
Superpave Coarse1 (A)	4463	I10DW	1543
Superpave Coarse2 (A)	3687	I10ME	1536
Superpave Fine1 (A)	3524	US301N	695
Superpave Fine2 (A)	3565	US301S	238

Table H.2: Dissipated Creep Strain Energy Parameters from Fracture Tests Using Method1 Described in Section 5.5.1

	Dissipated Energy (KJ/m^3)		Dissipated Energy (KJ/m^3)
Superpave Coarse1	0.143	I10MW	0.083
Superpave Coarse2	0.130	I95DN	0.066
Superpave Fine1	0.118	I95SJ	0.093
Superpave Fine2	0.126	I10DE	0.091
Superpave Coarse1 (A)	0.093	I10DW	0.088
Superpave Coarse2 (A)	0.072	I10ME	0.121
Superpave Fine1 (A)	0.091	US301N	0.052
Superpave Fine2 (A)	0.077	US301S	0.018

Table H.3: Dissipated Creep Strain Energy Obtained from Strength Tests Described in Section 5.5.2

	Resilient Modulus	Failure Strain	Tensile Strength	Initial Strain	Elastic Energy	Fracture Energy*	Dissipated Energy
	(Gpa)	(microstrain)	(Mpa)	(microstrain)	(KJ/m^3)	(KJ/m^3)	(KJ/m^3)
Superpave Coarse1	7.92	4629	1.64	4423	0.1698	3.7964	3.6266
Superpave Coarse2	7.73	3771	1.70	3551	0.1869	3.2056	3.0186
Superpave Fine1	9.49	2920	2.08	2700	0.2280	3.0364	2.8085
Superpave Fine2	8.62	3714	1.87	3497	0.2028	3.4731	3.2703
Superpave Coarse1 (A)	9.62	2224	2.11	2005	0.2314	2.3467	2.1153
Superpave Coarse2 (A)	11.78	1897	2.06	1721	0.1801	1.9536	1.7735
Superpave Fine1 (A)	9.93	1833	2.06	1625	0.2137	1.8883	1.6746
Superpave Fine2 (A)	12.93	1526	2.56	1328	0.2534	1.9535	1.7000
I10MW	8.93	3284	1.82	3080	0.1855	2.9884	2.8030
I95DN	7.26	2361	1.30	2181	0.1164	1.5347	1.4183
I95SJ	8.00	1020	1.94	777	0.2352	0.9894	0.7542
I10DE	6.66	1920	1.25	1732	0.1173	1.2000	1.0827
I10DW	7.71	1330	1.33	1157	0.1147	0.8845	0.7697
I10ME	6.69	1996	1.18	1820	0.1041	1.1776	1.0736
US301N	8.48	712	1.13	579	0.0753	0.4023	0.3270
US301S	4.74	407	0.93	211	0.0912	0.1893	0.0980

* Note: Fracture energy density was calculated by FE = (1/2)(Tensile Strength)(Failure Strain)

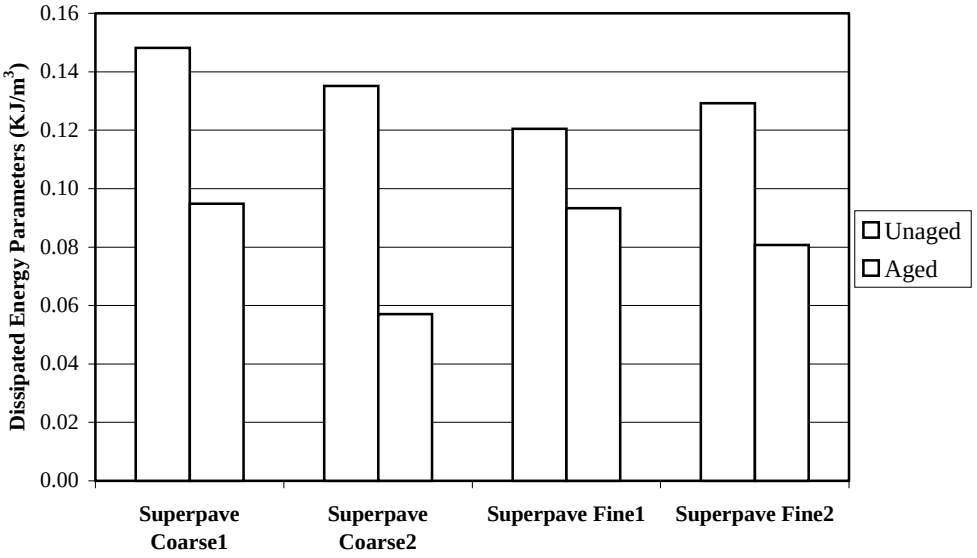

Figure H.1: Fracture Energy Density of Superpve Mixtures @ 10C

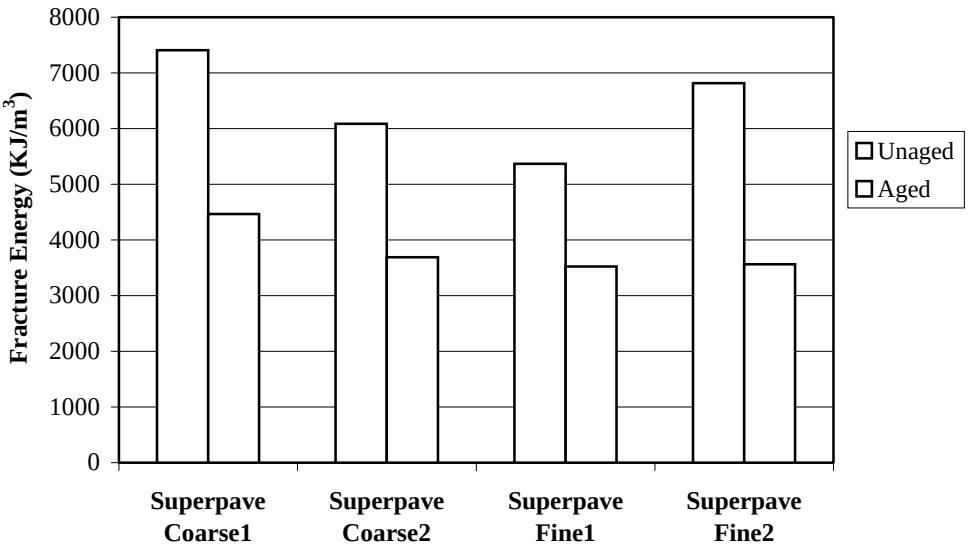

Figure H.2: Dissipated Creep Strain Energy Parameters

of Superpve Mixtures @ 10C

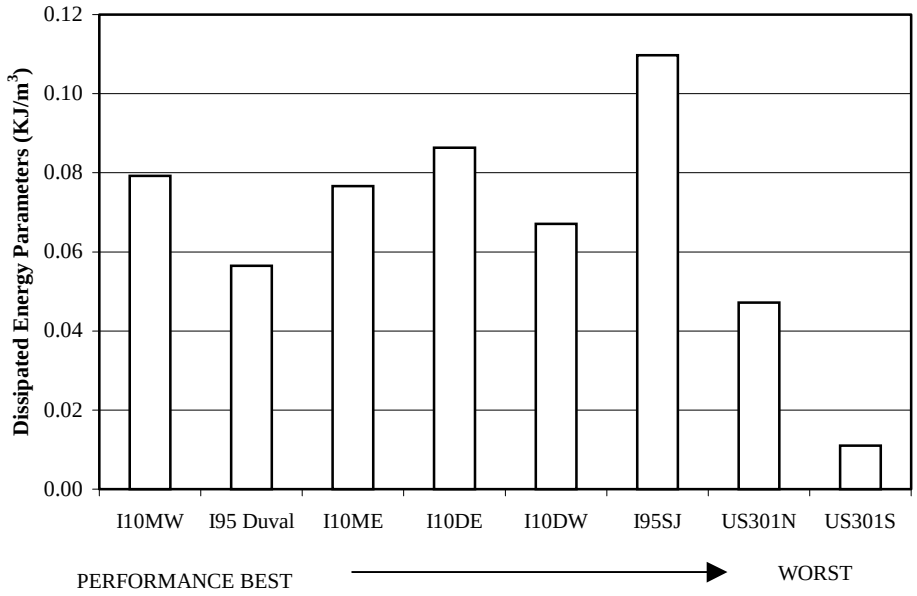

Figure H.3: Fracture Energy Density of Eight Field Sections @ 10C

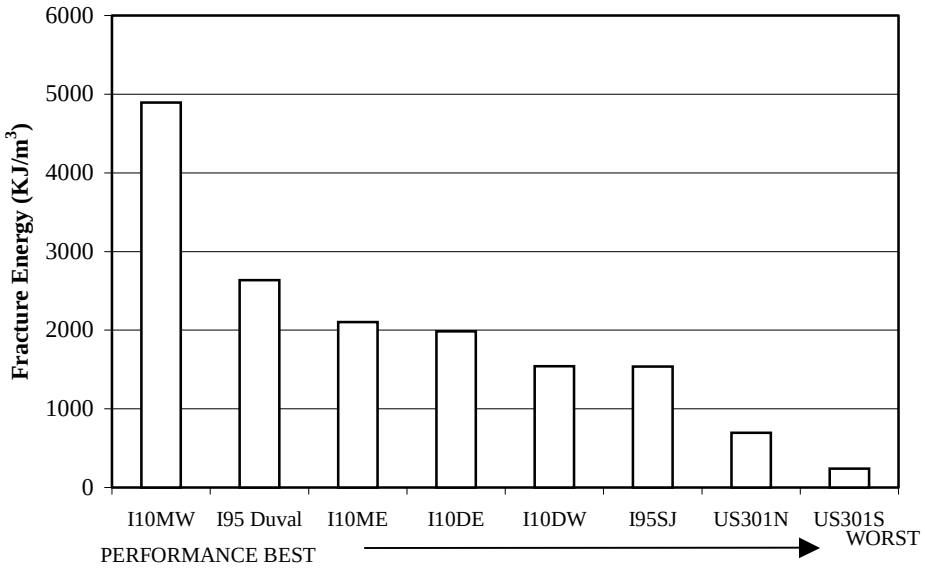

Figure H.4: Dissipated Creep Strain Energy Parameters

of Eight Field Sections @ 10C

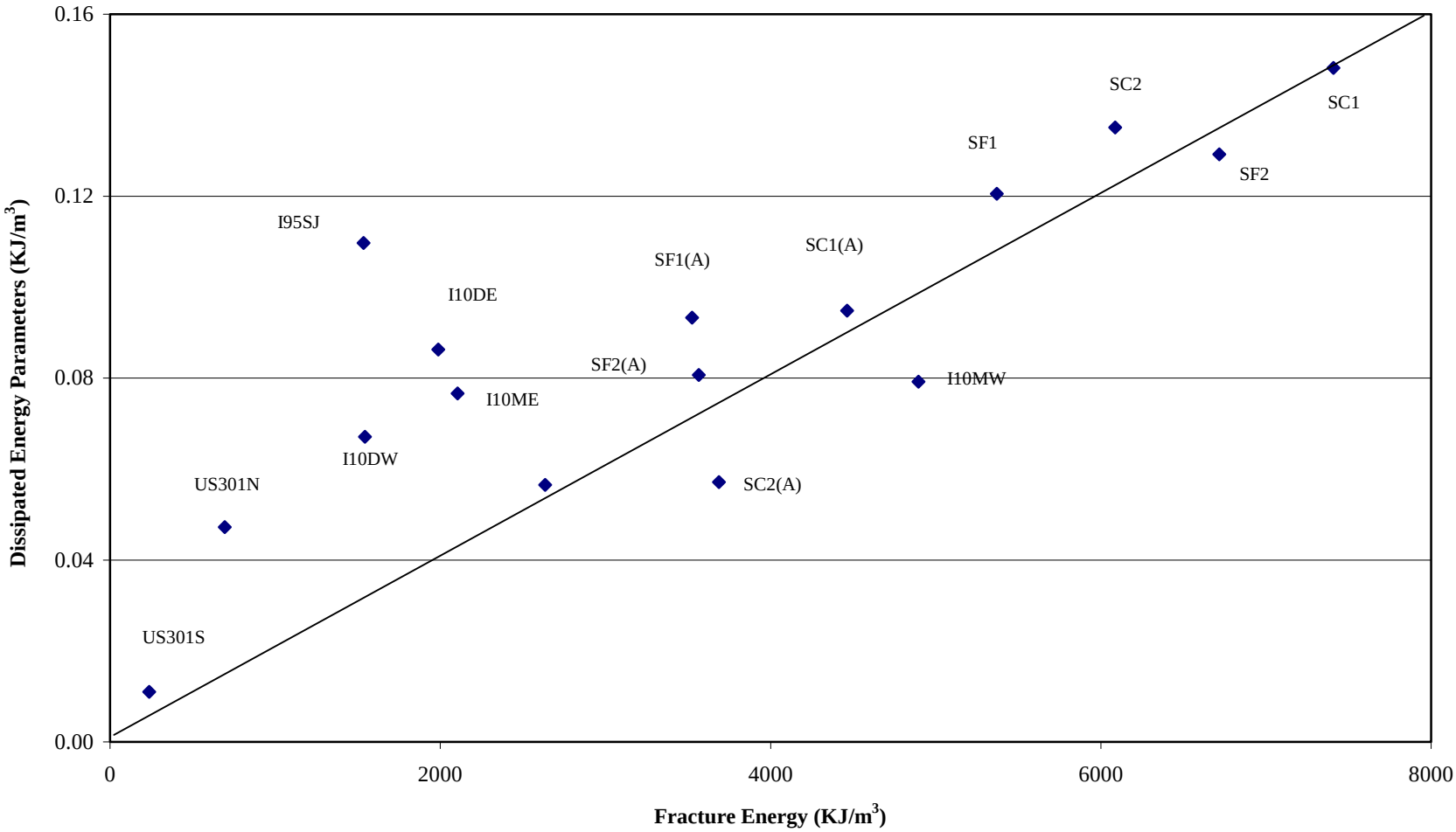

Figure H.5: Relation Between Fracture Energy Density and Dissipated Creep Strain Energy Parameters@10C

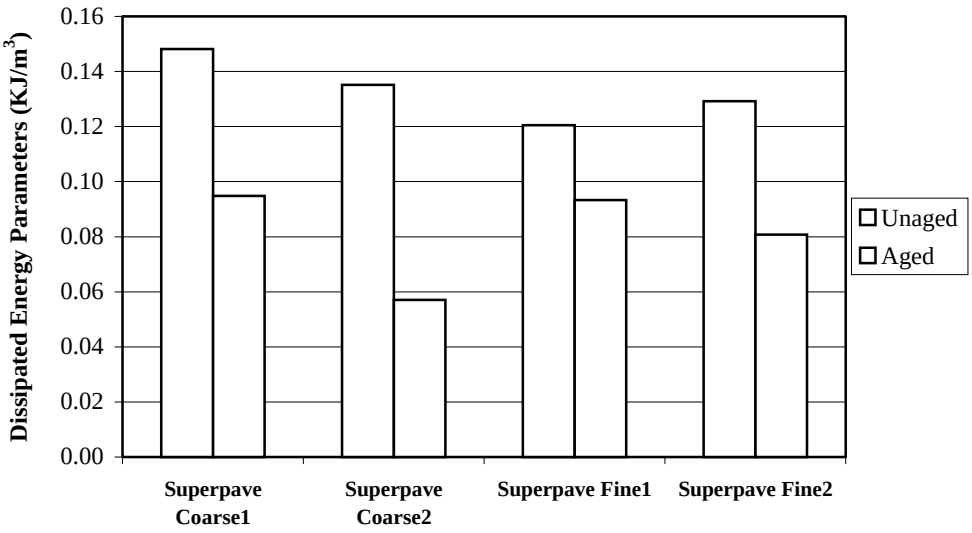

Figure H.6: Dissipated Creep Strain Energy from Strength Tests of Superpave Mixtures @ 10C

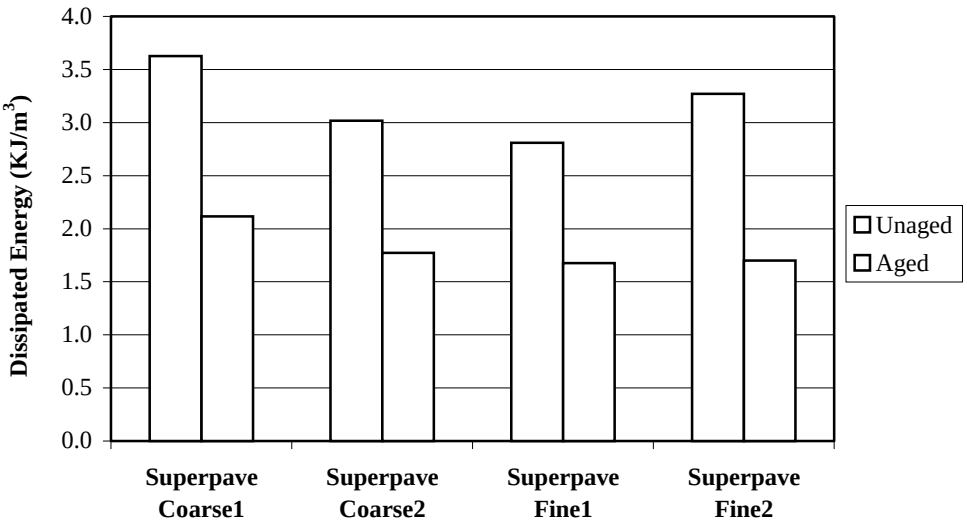

Figure H.2: Dissipated Creep Strain Energy Parameters of Superpave Mixtures @ 10C

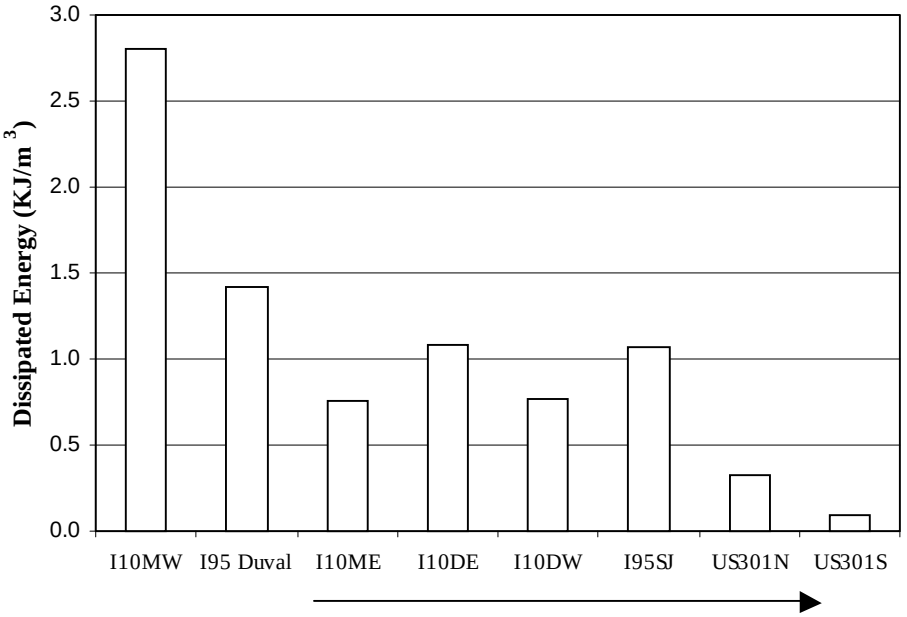

Figure H.7: Dissipated Creep Strain Energy from Strength Tests of Eight Field Sections @ 10C

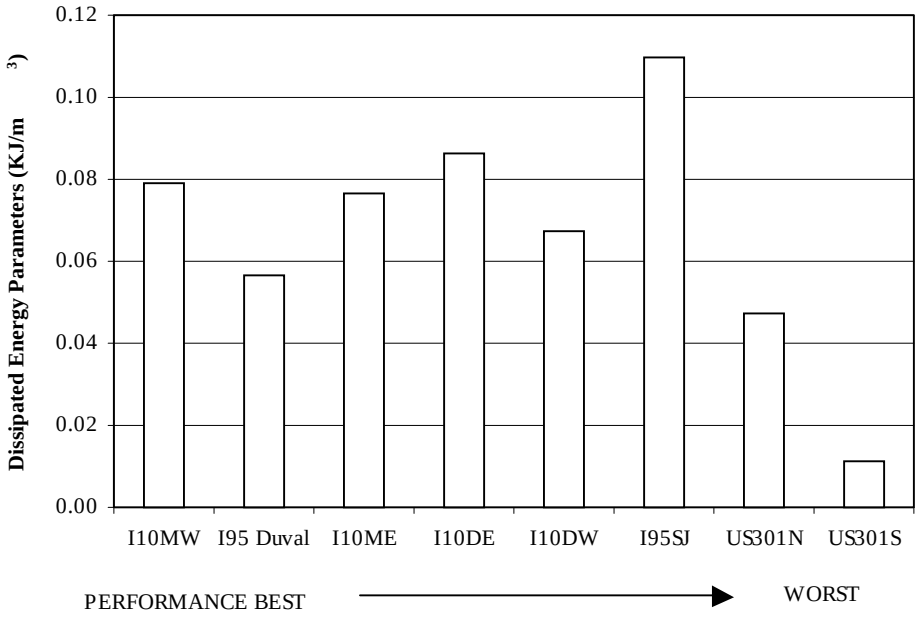

Figure H.4: Dissipated Creep Strain Energy Parameters of Eight Field Sections @ 10C

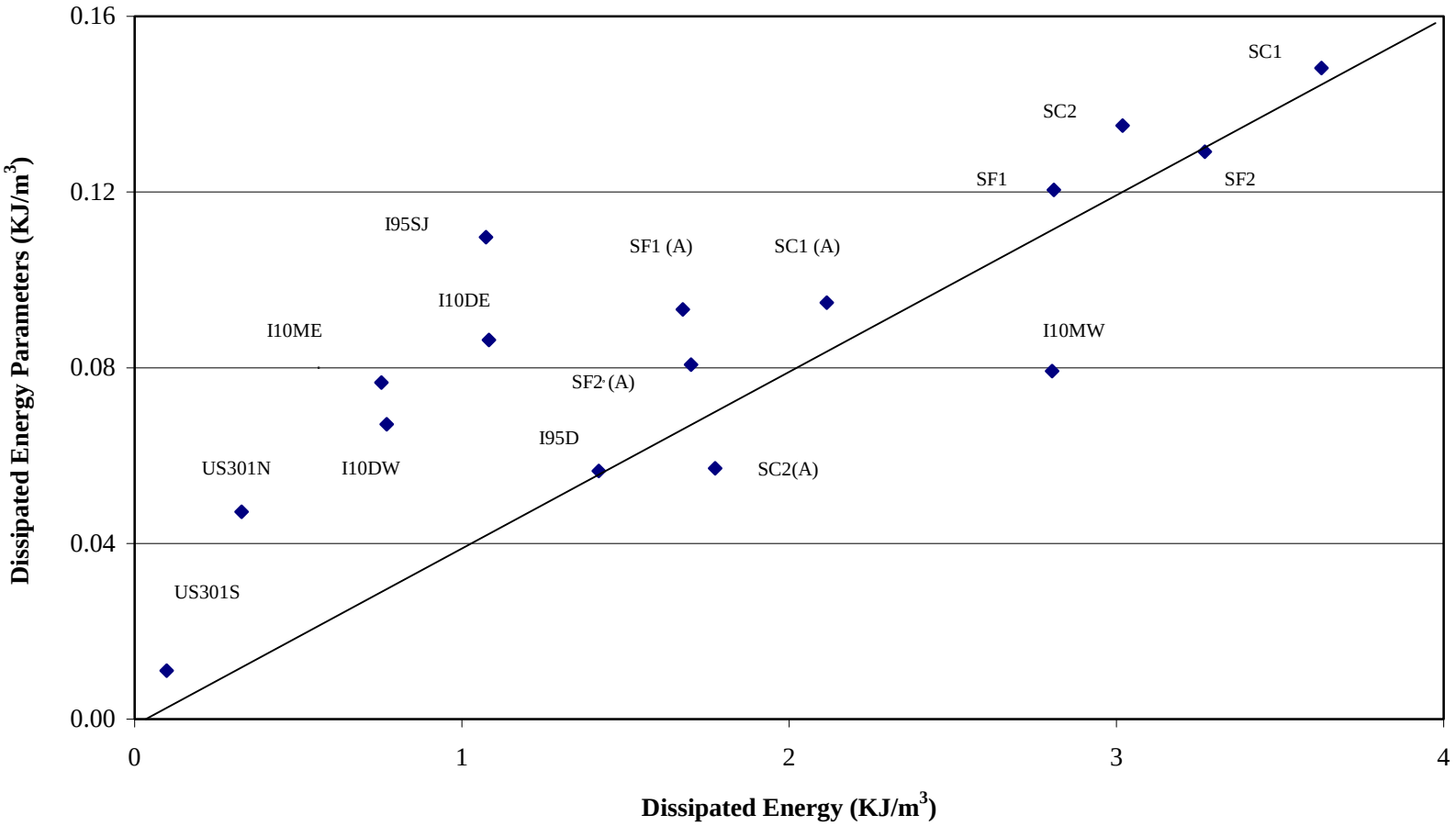

Figure H.8: Relation Between Dissipated Creep Strain Energy and of Dissipated Creep Strain Energy Parameters @10C

Table H.4: Dissipated Creep Strain Energy Parameters from Fracture Tests Using Method2 Described in Section 5.5.1

	Dissipated Energy (KJ/m^3)		Dissipated Energy (KJ/m^3)
Superpave Coarse1	0.148	I10MW	0.079
Superpave Coarse2	0.140	I95DN	0.057
Superpave Fine1	0.121	I95SJ	0.077
Superpave Fine2	0.129	I10DE	0.086
Superpave Coarse1 (A)	0.095	I10DW	0.067
Superpave Coarse2 (A)	0.057	I10ME	0.110
Superpave Fine1 (A)	0.093	US301N	0.047
Superpave Fine2 (A)	0.081	US301S	0.011

APPENDIX I
EVALUATION OF YIELD STRENGTH AND DISSIPATED CREEP STRAIN ENERGY AS A THRESHOLD

Table I.1: Results of Calculated Yield Strength

	Far Away Stress	Dissipated Energy (strength)	D1 Value	m-Value	Calculated Yield Strength	Average Stress	Tensile Strength
	(psi)	(psi)			(psi)	(psi)	(psi)
Superpave Coarse1	142	0.5260	3.81E-7	0.80	370	271	238
Superpave Coarse2	140	0.4378	4.98E-7	0.77	283	222	247
Superpave Fine1	139	0.4073	5.73E-7	0.66	392	282	302
Superpave Fine2	160	0.4743	8.33E-7	0.56	410	302	271
Superpave Coarse1 (A)	149	0.3068	6.96E-7	0.55	615	406	306
Superpave Coarse2 (A)	150	0.2572	4.48E-7	0.58	575	385	299
Superpave Fine1 (A)	138	0.2429	5.91E-7	0.57	337	251	299
Superpave Fine2 (A)	166	0.2466	4.18E-7	0.50	605	410	371
I10MW	223	0.4065	5.96E-7	0.60	795	541	261
I95DN	152	0.2057	9.09E-7	0.49	492	342	189
I95SJ	216	0.1557	4.73E-7	0.47	578	421	276
I10DE	115	0.1570	8.55E-7	0.55	238	185	181
I10DW	115	0.1117	6.58E-7	0.46	282	210	196
I10ME	137	0.1094	7.70E-7	0.61	*	*	181
US301N	162	0.0474	1.37E-6	0.26	240	206	174
US301S	156	0.0142	3.47E-6	0.18	*	*	138

*Note: Negative calculated yield strength values were obtained for I10ME and US301S

Table I.2: Results of Predicted Yield Strength from Seven SAS Models

	Calculated	Predicted Yield Strength From Seven SAS Models						
	Yield Strength	ModelB 5.1	ModelB 5.2	Model B 5.3	Model B 5.4	Model B 5.5	ModelB 5.6	ModelB 5.7
	(psi)	(psi)	(psi)	(psi)	(psi)	(psi)	(psi)	(psi)
Superpave Coarse1	370	372	372	376	389	314	403	394
Superpave Coarse2	283	392	388	370	376	346	391	417
Superpave Fine1	392	506	496	431	515	477	515	540
Superpave Fine2	410	466	449	474	547	531	585	508
Superpave Coarse1 (A)	615	530	515	526	536	544	548	522
Superpave Coarse2 (A)	575	512	498	495	482	526	476	490
Superpave Fine1 (A)	337	513	499	501	482	532	473	487
Superpave Fine2 (A)	605	651	648	693	641	572	611	581
I10MW	795	443	427	441	481	510	514	465
I95DN	492	334	304	370	337	541	375	369
I95SJ	578	489	467	536	464	560	453	442
I10DE	238	311	287	361	269	-	254	364
I10DW	282	351	319	375	323	-	258	242
I10ME	*	*	*	*	*	*	*	*
US301N	240	343	300	264	371	-	357	390
US301S	*	*	*	*	*	*	*	*

*Note: Negative calculated yield strength values were obtained for I10ME and US301S

-Note: Data was not used

```
/*      Model I1.sas

   1.  THE PURPOSE OF THIS PROGRAM IS TO FIND THE MODEL TO DETERMINE
        calculated yield strength = A*m-value + B*tensile strength + C
   2.  IN THIS PROGRAM, DATA INCLUDEED:
       6 FIELD SECTIONS (EXCEPT I10ME AND US301S,
       BECAUSE THE CALCULATED YEILD STRENGTH ARE NEGATIVE),
       SUPERPAVE COARSE (1 AND 2, AGED AND UNAGED) - TOTAL = 4
       SUPERPAVE FINE (1 AND 2, AGED AND UNAGED) - TOTAL = 4
*/

data one;
input YStreng mvalue TStreng;

cards;
370  0.7961  238
283  0.7729  247
392  0.656   302
410  0.5649  271
615  0.548   306
575  0.5837  299
337  0.5726  299
605  0.4955  371
795  0.6     261
492  0.49    189
578  0.47    276
238  0.55    181
282  0.46    196
240  0.26    174


proc print;

proc glm;
model YStreng = mvalue TStreng/p clm;

output out = new predicted = yhat residual = Residual;

proc print data = new;

proc corr;
var YStreng yhat;

run;
```

```
/*      Model I2.sas

   1.  THE PURPOSE OF THIS PROGRAM IS TO FIND THE MODEL TO DETERMINE
        log(calculated yield strength) = A*log(m-value) + B*log(tensile
                                         strength) + C
   2.  IN THIS PROGRAM, DATA INCLUDED:
       6 FIELD SECTIONS (EXCEPT I10ME AND US301S,
       BECAUSE THEIR CALCULATED YEILD STRENGTH ARE NEGATIVE),
       SUPERPAVE COARSE (1 AND 2, AGED AND UNAGED) - TOTAL = 4
       SUPERPAVE FINE (1 AND 2, AGED AND UNAGED) - TOTAL = 4
 */

data one;
input YStreng mvalue TStreng;

cards;
2.568  -0.099  2.376
2.452  -0.112  2.392
2.593  -0.183  2.480
2.613  -0.248  2.433
2.789  -0.261  2.486
2.760  -0.234  2.475
2.528  -0.242  2.475
2.782  -0.305  2.570
2.9   -0.222  2.417
2.692  -0.310  2.275
2.762  -0.328  2.440
2.377  -0.260  2.258
2.450  -0.337  2.292
2.38   -0.585  2.241


proc print;

proc glm;
model YStreng = mvalue TStreng/p clm;

output out = new predicted = yhat residual = Residual;

proc print data = new;

proc corr;
var YStreng yhat;

run;
```

```
/*      Model I3.sas

   1.  THE PURPOSE OF THIS PROGRAM IS TO FIND THE MODEL TO DETERMINE
       calculated yield strength = A*m-value + B*tensile strength +
                                   C*(m-value*tensile) + D
   2.  IN THIS PROGRAM, DATA INCLUDED:
       6 FIELD SECTIONS (EXCEPT I10ME AND US301S,
       BECAUSE THEIR CALCULATED YEILD STRENGTH ARE NEGATIVE),
       SUPERPAVE COARSE (1 AND 2, AGED AND UNAGED) - TOTAL = 4
       SUPERPAVE FINE (1 AND 2, AGED AND UNAGED) - TOTAL = 4
 */

data one;
input YStreng mvalue TStreng mTStreng;

cards;
370  0.7961  238  189
283  0.7729  247  191
392  0.656   302  198
410  0.5649  271  153
615  0.548   306  168
575  0.5837  299  174
337  0.5726  299  171
605  0.4955  371  184
795  0.6     261  157
492  0.49    189  92
578  0.47    276  130
238  0.55    181  100
282  0.46    196  90
240  0.26    174  45


proc print;

proc glm;
model YStreng = mvalue TStreng mTStreng/p clm;

output out = new predicted = yhat residual = Residual;

proc print data = new;

proc corr;
var YStreng yhat;

run;
```

```
/*      Model I4.sas

   1.  THE PURPOSE OF THIS PROGRAM IS TO FIND THE MODEL TO DETERMINE
       calculated yield strength = A*m-value + B*tensile strength +
                                   C*(dissipated energy) + D
   2.  IN THIS PROGRAM, DATA INCLUDED:
       6 FIELD SECTIONS (EXCEPT I10ME AND US301S,
       BECAUSE THEIR CALCULATED YEILD STRENGTH ARE NEGATIVE),
       SUPERPAVE COARSE (1 AND 2, AGED AND UNAGED) - TOTAL = 4
       SUPERPAVE FINE (1 AND 2, AGED AND UNAGED) - TOTAL = 4
 */

data one;
input YStreng mvalue TStreng DEnergy;

cards;
370  0.7961  238  0.526
283  0.7729  247  0.4378
392  0.656   302  0.4073
410  0.5649  271  0.4743
615  0.548   306  0.3068
575  0.5837  299  0.2572
337  0.5726  299  0.2429
605  0.4955  371  0.2466
795  0.6     261  0.4065
492  0.49    189  0.2057
578  0.47    276  0.1557
238  0.55    181  0.1570
282  0.46    196  0.1117
240  0.26    174  0.0474


proc print;

proc glm;
model YStreng = mvalue TStreng DEnergy/p clm;

output out = new predicted = yhat residual = Residual;

proc print data = new;

proc corr;
var YStreng yhat;

run;
```

```
/*      Model I5.sas

   1.  THE PURPOSE OF THIS PROGRAM IS TO FIND THE MODEL TO DETERMINE
        calculated yield strength = A*m-value + B*m-value^2
                         C*tensile strength + D*TensileStrength^2 + E
   2.  IN THIS PROGRAM, DATA INCLUDED:
       3 FIELD SECTIONS (EXCEPT I10ME AND US301S,
       BECAUSE THEIR CALCULATED YEILD STRENGTH ARE NEGATIVE),
       ALSO EXCEPT I10DE/I10DW/US301N, BECAUSE WEAK RELATION IN M-VALUE
AND TSTRENGTH WAS OBTAINED FROM SENSITIVITY ANALYSIS)
       SUPERPAVE COARSE (1 AND 2, AGED AND UNAGED) - TOTAL = 4
       SUPERPAVE FINE (1 AND 2, AGED AND UNAGED) - TOTAL = 4
 */

data one;
input YStreng mvalue mvalue2 TStreng TStren2;

cards;
370  0.7961  0.6338  238  56574
283  0.7729  0.5974  247  60790
392  0.656   0.4303  302  91004
410  0.5649  0.3191  271  73555
615  0.548   0.3003  306  93648
575  0.5837  0.3407  299  89262
337  0.5726  0.3279  299  89262
605  0.4955  0.2455  371  137851
795  0.6     0.3600  261  68152
492  0.49    0.2401  189  35548
578  0.47    0.2209  276  75934


proc print;

proc glm;
model YStreng = mvalue mvalue2 TStreng TStren2/p clm;

output out = new predicted = yhat residual = Residual;

proc print data = new;

proc corr;
var YStreng yhat;

run;
```

```
/*      Model I6.sas

   1.  THE PURPOSE OF THIS PROGRAM IS TO FIND THE MODEL TO DETERMINE
        (calculated yield strength) = A*ln(m-value) + B*ln(tensile
                strength) + C * ln(DISSIPATED ENERGY) + D
   2.  IN THIS PROGRAM, DATA INCLUDED:
       6 FIELD SECTIONS (EXCEPT I10ME AND US301S,
       BECAUSE THEIR CALCULATED YEILD STRENGTH ARE NEGATIVE),
       SUPERPAVE COARSE (1 AND 2, AGED AND UNAGED) - TOTAL = 4
       SUPERPAVE FINE (1 AND 2, AGED AND UNAGED) - TOTAL = 4
 */

data one;
input YStreng mvalue TStreng DEnergy;

cards;
370   -0.2280  5.4717  -0.6425
283   -0.2576  5.5076  -0.8260
392   -0.4216  5.7093  -0.8982
410   -0.5711  5.6029  -0.7459
615   -0.6015  5.7236  -1.1816
575   -0.5384  5.6997  -1.3579
337   -0.5576  5.6997  -1.4151
605   -0.7022  5.9170  -1.4000
795   -0.5108  5.5647  -0.9002
492   -0.7133  5.2393  -1.5813
578   -0.7550  5.6188  -1.8598
238   -0.5978  5.2001  -1.8515
282   -0.7765  5.1593  -2.1919
240   -1.3471  5.1593  -3.0485

proc print;

proc glm;
model YStreng = mvalue TStreng DEnergy/p clm;

output out = new predicted = yhat residual = Residual;

proc print data = new;

proc corr;
var YStreng yhat;

run;
```

```
/*      Model I7.sas

   1.  THE PURPOSE OF THIS PROGRAM IS TO FIND THE MODEL TO DETERMINE
       calculated yield strength = A*(m-value*dissipated energy) +
                                   B*(tensile strength*dissipated energy)
                                   + C*(dissipated energy) + D
   2.  IN THIS PROGRAM, DATA INCLUDED:
       6 FIELD SECTIONS (EXCEPT I10ME AND US301S,
       BECAUSE THEIR CALCULATED YEILD STRENGTH ARE NEGATIVE),
       SUPERPAVE COARSE (1 AND 2, AGED AND UNAGED) - TOTAL = 4
       SUPERPAVE FINE (1 AND 2, AGED AND UNAGED) - TOTAL = 4
 */

data one;
input YStreng mvaluDE TStreDE DEnergy;

cards;
370  0.4187  125  0.526
283  0.3384  108  0.4378
392  0.2672  123  0.4073
410  0.2679  129  0.4743
615  0.1681  94   0.3068
575  0.1501  77   0.2572
337  0.1391  73   0.2429
605  0.1222  92   0.2466
795  0.2439  106  0.4065
492  0.1008  39   0.2057
578  0.0732  43   0.1557
238  0.0864  28   0.1570
282  0.514   22   0.1117
240  0.0123  8    0.0474


proc print;

proc glm;
model YStreng = mvaluDE TStreDE DEnergy/p clm;

output out = new predicted = yhat residual = Residual;

proc print data = new;

proc corr;
var YStreng yhat;

run;
```